UNIVERSITY OF GENOA

PhD in Haemato-oncology and clinical-translational internal medicine

XXXV Cycle

Coordinator: Prof. Edoardo Giannini

Curriculum:

Autoimmune and autoinflammatory diseases: pathophysiological and diagnostic aspects

Development and testing of anti-eNAMPT neutralizing monoclonal antibodies

PhD candidate:
Elise SEMERENA

Supervisor:
Dr. Krzysztof MASTERNAK

Academic year:
2019-2022

Abstract

Nicotinamide phosphoribosyltransferase (NAMPT) is an intracellular enzyme that plays an essential role in mammalian cell metabolism by participating to NAD^+ production. Through a mechanism not yet deciphered, NAMPT is secreted in the extracellular space and is therefore referred to as extracellular NAMPT (eNAMPT). In the extracellular milieu, eNAMPT has been shown to execute multiple functions, from adipokine to pro-inflammatory activities, likely by interacting with cell surface receptors. Circulating eNAMPT levels have been associated with various inflammatory conditions, such as cancer, suggesting a potential for this protein as a diagnostic tool. Furthermore, an active role for eNAMPT in cancer pathogenesis has also been proposed, based on studies demonstrating that eNAMPT supports tumor cell proliferation, stimulates tumor invasion and metastasis and promotes immunosupressive conditions. However, eNAMPT pro-tumoral functions were shown to be independent of enzymatic activity, indicating that they cannot be counteracted by chemical inhibitors. A new approach, using monoclonal antibodies, has therefore been suggested to neutralize eNAMPT extracellular functions.

My PhD project aimed to develop and test novel anti-eNAMPT neutralizing monoclonal antibodies (mAbs). Firstly, I generated 81 specific, fully human anti-eNAMPT mAbs using a phage display platform. Characterization of these antibodies revealed that they exhibited different binding characteristics and targeted different regions on eNAMPT. In addition, several of them showed a high affinity for eNAMPT. Secondly, I sought to assess the neutralizing properties of these anti-eNAMPT mAbs in relevant *in vitro* binding and functional assays. However, I was unable to convincingly demonstrate eNAMPT interaction with its putative receptors, nor the pro-tumoral, pro-chemotactic and pro-inflammatory effects of eNAMPT. As a result, I could not evaluate the blocking abilities of the generated eNAMPT binding antibodies.

Acknowledgements

First of all, I would like to express my deepest gratitude to my PhD supervisor Dr. Krzysztof Masternak. Thank you, Krzysztof, for your availability, your patience and all the sound advice you have provided to me during the past years. This project was not easy, but your support and encouragement allowed me to persevere despite the difficulties. Thank you also for all the knowledge you shared with me, I learned a lot about monoclonal antibody development under your supervision. Finally, I am very grateful for the time and the energy you devoted to the correction of this thesis manuscript.

I would also like to extend my sincere thanks to my thesis evaluators, Professor Silvia Deaglio and Professor Nadia Raffaelli, for accepting and taking the time to assess this work. Also, many thanks to Prof. Silvia Deaglio and her team for their help in the search for an *in vitro* assay demonstrating eNAMPT activity.

I am also very grateful to Professor Alessio Nencioni, my PhD co-supervisor, who kindly welcomed me in his laboratory for three weeks and shared with me his knowledge on eNAMPT. Thank you very much Alessio for your availability, your optimism and the precious help you and your team brought me during this thesis. I would also like to take this opportunity to warmly thank Dr. Irene Caffa et Dr. Giulia Allavena, from Prof. Nencioni's team, who performed a multitude of western blots and other assays for this research project. A special thanks to Irene, for her kindness, her judicious advices and for introducing me to the gastronomy of Genoa.

I would like to sincerely thank Dr. Nicolas Fisher for allowing me to complete my thesis at Novimmune/LCB.

J'aimerais également exprimer ma profonde gratitude envers Ulla Ravn, qui m'a guidée tout au long de mes activités de Phage display. Merci infiniment, Ulla, pour m'avoir fait partager ton expérience, pour ta disponibilité, mais aussi pour ton soutien et ta gentillesse. J'ai beaucoup appris à tes cotés. Un grand merci également à Nicolas Bosson et Sebastien Calloud, qui m'ont formé techniquement et qui ont toujours pris le temps de répondre à mes nombreuses questions. De façon générale, je remercie toute l'équipe Phage Display, dont chaque membre m'a aidé à un moment ou à un autre de cette thèse, de m'avoir chaleureusement accueillie.

Ce projet n'aurait pas pu avancer sans Giovanni Magistrelli et son équipe, qui m'ont formé au reformatting des anticorps et m'ont apporté une aide précieuse durant cette thèse. Merci Giovanni pour ta disponibilité et pour m'avoir fait partager tes nombreuses connaissances sur les protéines recombinantes. Je remercie également Pauline Malinge, pour son support technique et scientifique lors des mesures d'affinité des anticorps, mais aussi pour sa gentillesse et sa sympathie. Enfin, un grand merci à Jeremie Bourguignon, Tereza Bautzova,

Flora Juan et Marie Borlet qui m'ont accompagné lors de la production des anticorps et ont toujours été disponibles pour répondre à mes questions.

Je tiens également à remercier Bruno Daubeuf et Valery Moine pour leur aide technique et scientifique durant cette thèse. Merci beaucoup, Bruno, de m'avoir fait partager ta précieuse expertise sur TLR4 et aidé à interpréter mes résultats inattendus. Merci Valery pour ton aide et tes judicieux conseils concernant les expériences de cytométrie de flux. De manière générale, je remercie tous les membres de l'équipe PHC pour leur disponibilité et leur gentillesse. Plus particulièrement, un grand merci à Margaux Legrand, de m'avoir formé aux essais TDCC dans les dernières semaines de ma thèse.

Je souhaiterais également remercier les Drs. Eric Hatterer et Sara Majocchi, pour leurs conseils avisés et les discussions scientifiques concernant mon projet. Je ne voudrais pas oublier Elise Penarrieta, Lise Nouveau, Julien Montorfani et Lucie Diby. Elise et Lise, merci infiniment d'avoir toujours été là pour me soutenir, m'encourager et pour vos nombreux conseils. Je remercie également, Julien et Lucie, pour leur constante bonne humeur et leur sympathie; bientôt votre tour, courage ! D'une manière générale, un grand merci à tous mes collègues de LCB que je n'ai pas cité ici, mais dont les encouragements et la bienveillance tout au long de ces années ont été d'une grande aide. Ce fut un réel plaisir de travailler à vos côtés.

D'une façon plus personnelle je tiens à exprimer ma gratitude envers mes amis pour leur soutien sans faille tout au long de mes études. Tout d'abord, un grand merci à Louise, Maitena, Laura et Caroline pour votre positivité, vos encouragements et tous les moments partagés depuis maintenant 13ans, milesker neskak ! Merci à Thomas et Etienne, avec qui j'ai quitté le pays basque pour Bordeaux, pour votre amitié et les nombreux fous rires partagés. Merci Camille, Anaïs et Léana, pour votre soutien indéfectible, votre écoute et vos conseils qui m'ont grandement aidé dans les moments de doutes. Je remercie également Maurine, Margaux, Delphine et Elina avec qui j'ai partagé des moments inoubliables durant mes années TBB. Enfin, je remercie Louis, Lucile, Rémi, Lucy, Laure et Vassili pour leur soutien et les merveilleux moments partagés ces trois dernières années. Merci Louis, Lucile et Rémi, d'avoir été des collègues géniaux, de m'avoir aidé pour la relecture de cette thèse, mais aussi de m'avoir fait rire et déstresser lorsque j'en avais besoin. Un petit mot également pour mes deux boxeuses préférées, Laure et Lucy, qui sont des sources d'énergie et de motivation indispensables.

Enfin et surtout, je tiens à remercier mes parents, Beñat et Marie-Jo, de m'avoir donné les moyens d'arriver jusqu'ici et de m'avoir toujours guidé sans me mettre la pression. Merci infiniment pour votre soutien inconditionnel tout au long de mes études, milesker denetako! Je remercie également ma sœur, Marion, qui me comprend sans que j'aie à m'expliquer et qui est toujours présente lorsque j'ai besoin d'elle. Enfin, merci à toi, Antonin, pour ton écoute, ton soutien de chaque instant et de m'avoir permis d'avancer durant ces années de thèse.

Table of contents

1. Review

Tentative title: Extracellular nicotinamide phosphoribosyltransferase (eNAMPT) as a biomarker for inflammatory, metabolic and neoplastic diseases: a comprehensive review

Elise Semerena[1], Alessio Nencioni[2,3] and Krzysztof Masternak[1].

[1]Light Chain Bioscience - Novimmune SA, 15 chemin du Pré-Fleuri, 1228 Plan-les-Ouates, Switzerland.
[2]Department of Internal Medicine and Medical Specialties, University of Genoa, 16132, Genoa, Italy.
[3]Ospedale Policlinico San Martino IRCCS, 16132, Genoa, Italy.

Abstract

Nicotinamide phosphoribosyltransferase (NAMPT) is an enzyme that plays a central role in mammalian cell metabolism by contributing to NAD biosynthesis. Nonetheless, NAMPT activity is not limited to the intracellular compartment, as once secreted, the protein accomplishes diverse functions in the extracellular space. Specifically, extracellular NAMPT (eNAMPT) was shown to possess adipokine, cytokine and pro-angiogenic activities in the extracellular milieu, likely through its binding to a cell surface receptor. Multiple studies reported an association between circulating eNAMPT and various inflammatory conditions, suggesting its involvement in numerous pathological processes, including cancer, metabolic diseases, arthritis, inflammatory bowel disease (IBD) and lung injury. In this review, we will discuss the potential of eNAMPT as a disease biomarker and the emerging therapeutic strategies related to its targeting.

I. Introduction

Nicotinamide phosphoribosyltransferase (NAMPT) is a homodimeric class II phosphoribosyl-transferase (EC 2.4.2.12), ubiquitously expressed in mammalian tissues, that plays a crucial role in nicotinamide adenine dinucleotide (NAD) metabolism [1], [2]. NAMPT is the rate-limiting enzyme of the NAD salvage pathway that catalyses the production of nicotinamide mononucleotide (NMN) from nicotinamide (NAM) and 5'-phosphoribosyl-1-pyrophosphate (PRPP) [3]. Subsequently, NMN molecules are converted to oxidized NAD by NMN adenylyltransferases 1-3 (NMNATs 1-3) [4]. NAD then fuels cellular redox reactions and the

activity of NAD-degrading enzymes, such as the cluster of differentiation(CD) 38 (CD38), poly(ADP-ribose) polymerases (PARPs) and sirtuins (SIRT1-7) [1], [5]. These NAD-dependent enzymes mediate fundamental intracellular processes, including cell signalling, DNA repair and prevention of apoptosis [1], [5]. Thus, by modulating NAD levels, NAMPT plays a pivotal role in cell metabolism and survival [3]. Consistent with this, a high degree of conservation of the *NAMPT* gene is observed between species [6]–[8]. Noteworthy, orthologs of mammalian *NAMPT* gene are found not only in other vertebrates (e.g., birds [8], fish [9]) but also in sponges [9] and bacteria [10]. Interestingly, NAMPT is present both in the nucleus and in the cytosol, at varying levels, depending on the cell cycle phases [11], [12]. In addition, studies suggested that NAMPT may also be localized in the mitochondria, although this remains controversial [13]–[15]. In 2019, Yoshida et al. demonstrated that NAMPT is transported into the systemic circulation via extracellular vesicles (EVs), before being reinternalized to participate in NAD production in recipient cells [16]. As mentioned above, NAMPT is not only found inside cells and EVs, but can also be directly secreted into the extracellular space. Historically, diverse names were attributed to extracellular NAMPT (eNAMPT), as its functions were discovered. eNAMPT was first identified as a cytokine secreted by pre-B cells and named Pre-B-cell colony enhancing factor (PBEF) due to its ability to synergize with interleukin (IL)-7 and stem cell factor (SCF) to promote pre B-cell colony formation [17]. Later on, the protein was baptized “visfatin” based on its adipokine function and the evidence of its secretion from visceral adipose tissue [7], [18]. Although both these names are still found in the literature, the term eNAMPT is preferentially used nowadays. eNAMPT is released by all cellular types [2] and this widespread secretion implies the potential involvement of eNAMPT in different types of disorders. Indeed, a significant association between the circulating levels of eNAMPT and the risks for various diseases has been found [19]–[21]. The present review will discuss the potential of eNAMPT as a disease biomarker and its possible contribution to disease pathogenesis.

II. eNAMPT biology: an unclear mechanism of secretion

eNAMPT is secreted by a wide range of cell types including adipocytes, β-cells, immune cells, neurons, endothelial cells and cardiomyocytes (reviewed in Grolla et al. [2]). eNAMPT release in the extracellular space is an active phenomenon and not the consequence of cell lysis or cell death [18], [22], [23]. In human circulation, eNAMPT secretion follows a diurnal rhythm, peaking in the afternoon [24]; with serum levels ranging from 3 to 68 ng/mL in healthy individuals [25], [26]. In addition, eNAMPT protein is also present in human synovial fluid (SF) [27], follicular fluid [28], bronchoalveolar lavage (BAL) fluid [29], saliva [30], and cerebrospinal fluid [31].

As reviewed in Carbone et al. [3], different stimuli promoting eNAMPT secretion can be grouped into three main categories: cellular stress (e.g. ischemia, oxygen-glucose deprivation

(OGD), oxidative and endoplasmic reticulum (ER) stress, hypoxia [32]), nutritional cues (e.g. glucose or insulin) and inflammatory signals (e.g. lipopolysaccharide (LPS), tumour necrosis factor-α (TNF-α), IL-1β, interferon-γ (IFNγ) [33]). The exact mechanism of eNAMPT release into the extracellular space remains unclear. eNAMPT lacks the peptide signal for a secretion through the classical ER-Golgi secretory pathway [17]. Furthermore, no canonical caspase-1 cleavage site is observed in the *NAMPT* gene sequence [9]. This suggests that eNAMPT is not released via the conventional canonical secretory pathway, which is also supported by the fact that eNAMPT secretion was not affected by inhibitors of the ER-Golgi pathway (brefeldin A or monensin) [18], [34]–[36]. On the other hand, a recent study found that, in the presence of brefeldin A or monensin, IFNγ-induced eNAMPT secretion from macrophages was significantly reduced [33]. Further studies are therefore needed to clarify the mechanisms underlying eNAMPT release.

eNAMPT, which accounts for only 1% of total NAMPT under non-stimulating conditions [32], bears distinctive post-translational modifications. Specifically, differences in acetylation levels were found between eNAMPT and intracellular NAMPT. SIRT-1-mediated deacetylation of NAMPT K53 was shown to predispose the protein to secretion and to increase its release [37]. On the contrary, deacetylation of NAMPT by SIRT-6 was shown to down-regulate eNAMPT release [38].

III. eNAMPT, a protein with pleiotropic functions

The different functions of eNAMPT, namely enzymatic, adipokine, cytokine and pro-angiogenic activities, are summarized in Figure 1 and described in the paragraphs below.

3.1. eNAMPT as an ecto-enzyme

Whether eNAMPT performs its phosphoribosyltransferase activity in the extracellular milieu is not yet fully elucidated. NAMPT dimerization is essential for its enzymatic role, as shown by the reduced activity of non-dimerizing S199D and S200D *NAMPT* mutants [18], [39]. Various studies have reported eNAMPT existence as a dimer in conditioned media of tissues and cells [18], [35], [40], [41], suggesting that eNAMPT may be enzymatically active in the extracellular space. Furthermore, Revollo et al. [18] demonstrated that adipocyte-derived eNAMPT exerts a strong NAD biosynthetic activity, which is even higher than that of intracellular NAMPT. In line with this, they found high levels of NMN in mouse plasma [18]. eNAMPT has also been shown to increase extracellular NMN and NAD levels in vascular smooth muscle cell cultures (VSMC) and MCF7 cell cultured medium [42], [43]. Accordingly, studies show that the extracellular NMN may enter inside cells and contribute to intracellular NAD biosynthesis [43]–[45].

Yet, under physiological conditions, eNAMPT substrates, NAM and PRPP, are present at low concentrations or virtually absent from the extracellular milieu [46]. A similar observation has been made for ATP, which is an activator of NAMPT activity and is required for the conversion of NMN to NAD [46]. This implies that outside the cells, eNAMPT probably lacks the substrates for a sustained enzymatic activity. On the other hand, pathological conditions such as tumour microenvironment (TME), which is characterized by elevated necrosis and acidic pH in hypoxic areas, could offer increased levels of eNAMPT substrates [42]. Thus, eNAMPT enzymatic activity in the extracellular space cannot be excluded, at least in certain (pathological) situations.

3.2. eNAMPT as an adipokine

Adipokines are molecules released from adipose tissues, regulating glucose homeostasis, body weight, inflammation and/or blood pressure [47]. The first description of eNAMPT as an adipokine was made in 2005 by Fukuhara et al. [48]. These authors demonstrated that eNAMPT is secreted by mouse adipocytes *in vitro*. This was subsequently confirmed in rats, where eNAMPT production was reported in perivascular adipose tissues [43]. In addition, eNAMPT was shown to be expressed in human visceral, subcutaneous and epicardial fat tissues [48]–[50]. Fukuhara et al. also suggested that, similar to insulin, eNAMPT exerts a glucose lowering effect in 3T3-L1 adipocyte cells and in mice, by binding to and activating the insulin receptor (IR) [48]. Specifically, within 30 minutes after intravenous administration of eNAMPT, they observed a significant reduction in plasma glucose concentrations in c57BL/6J mice [48]. The latter publication was eventually retracted due to a lack of reproducibility regarding the direct binding to IR [51]. However, other studies have confirmed eNAMPT insulin-mimetic effects on human osteoblasts [52] and glomerular mesangial cells [53]. Consistent with this, eNAMPT-mediated phosphorylation of IR [52], [54] and insulin receptor substrate (IRS)-1 and IRS-2 [52] were observed in human osteoblasts and in mouse pancreatic β-cells. Nevertheless, the adipokine action of eNAMPT through insulin signalling remains controversial, as another group reported the eNAMPT-mediated increase in glucose transport did not involve IRS-1 phosphorylation in skeletal muscle [55].

Evidence suggests that eNAMPT plays a vital role in maintaining the viability and function of pancreatic β-cells. For instance, eNAMPT was shown to prevent apoptosis and free fatty acid (FFA)-induced metabolic dysfunction in MIN6 pancreatic cell line [56]. Furthermore, Revollo et al. demonstrated that eNAMPT mediates the regulation of glucose-induced insulin release by β-cells [18]. Noteworthy, they showed that eNAMPT enzymatic activity is key for this process, rather than its insulin-mimetic activity. Evidence supports that eNAMPT biosynthetic activity and its reaction product, NMN, directly or indirectly maintain β-cell function [57], [58]. Particularly, a study revealed that exogenous administration of NMN in mice receiving a high-fat diet (HFD) improved their glucose intolerance and lipid profiles by restoring normal levels of NAD in white adipose tissue and liver [59].

3.3. eNAMPT as a pro-inflammatory cytokine

The pro-inflammatory activity of eNAMPT is well documented. Numerous studies demonstrated that eNAMPT activates inflammatory signalling pathways, including nuclear factor kappa-light-chain-enhancer of activated B cells (NF-kB) [60]–[62], mitogen-activated protein kinase (MAPK) [62], [63], and signal transducer and activator of transcription-3 (STAT3) [64], [65], leading to the production of pro-inflammatory cytokines (IL-1β, IL-1Ra, IL-6, CXCL8, IL-10 and TNF-α) and chemokines (C-C motif chemokine ligand (CCL)2, CCL3, CCL18 and CCL20) [60], [61], [63]–[68]. In addition, eNAMPT can act as a chemokine and induce the recruitment of human monocytes and B cells *in vitro,* as well as that of murine neutrophils and monocytes in a subcutaneous air pouch *in vivo* model [33], [67]. eNAMPT not only induces immune cell chemotaxis but also promotes their proliferation and differentiation [64], [69]. Strikingly, while several studies have shown that eNAMPT induces monocyte differentiation into M1 macrophages [32], [33], [70], other works show the opposite effect, i.e., eNAMPT driving M2 differentiation [64], [71]. These discrepancies could potentially be explained by the use of cells of different origin, different experimental conditions or different sources of recombinant eNAMPT in these experiments [72]. For instance, M2 polarization was observed in monocytes from leukemic patients [64], whereas M1 polarization was reported with monocytes from healthy donors [32]. As suggested by Travelli et al., this may reflect a versatile effect of eNAMPT in monocyte differentiation, e.g., the induction of an M1 phenotype under physiological conditions and an M2 phenotype in pathological contexts such as cancer [72].

Overall, eNAMPT appears to be a modulator of immune cell pro-inflammatory programs, with a privileged action on monocytes/macrophages. For instance, eNAMPT was shown to support the survival of mouse macrophages by suppressing ER-stress-induced apoptosis of these cells through the activation of STAT3 [65]. Moschen et al. demonstrated that eNAMPT upregulates monocyte co-stimulatory molecules, including CD40, CD54, and CD80, suggesting a contribution of eNAMPT to the activation of monocyte effector functions [67]. In line with this, eNAMPT promoted monocyte-mediated phagocytosis [67]. The pro-inflammatory functions of eNAMPT are not limited to immune cells, as the protein is also involved in vascular inflammation. Particularly, eNAMPT was shown to upregulate endothelial cell adhesion molecules (intercellular adhesion molecule 1 (ICAM-1) and vascular cell adhesion molecule 1 (VCAM-1)) leading to monocyte adhesion to endothelial cells [73], [74]. In agreement with that, another study reported that eNAMPT promoted NLR family pyrin domain containing 3 (NLRP3) inflammasome complex activation and subsequent release of pro-inflammatory IL-1β from endothelial cells [75]. Taken together, these findings point to eNAMPT as a key cytokine mediating inflammation. Interestingly, numerous studies reported that the enzymatic activity is not required for eNAMPT function as a cytokine [32], [33], [64], [65], [76]. Furthermore, one study reported that eNAMPT dimerization is also not needed for its cytokine activities [65].

3.4. eNAMPT as a pro-angiogenic factor

In addition to its pro-inflammatory function, eNAMPT was shown to play a substantial role in angiogenesis. eNAMPT induced human umbilical vein endothelial cells (HUVEC) proliferation, migration and capillary tube formation *in vitro* [77]–[79]. The pro-angiogenic function of eNAMPT was also confirmed in *in vivo* angiogenesis models [77]. Interestingly, eNAMPT also promoted the upregulation of other pro-angiogenic factors that contribute to the formation of new blood vessels [80]. For example, eNAMPT was shown to induce vascular endothelial growth factor (VEGF) production and secretion, as well as VEGF receptor 2 expression, by endothelial and amniotic epithelial cells via the activation of MAPK and phosphatidylinositol-3 kinase/protein kinase B/mammalian target of rapamycin (PI3K/AKT/mTOR) signalling pathways [78], [79], [81], [82]. Other studies suggested that eNAMPT mediates angiogenesis in endothelial cells by eliciting IL-6, CXCL8, fibroblast growth factor 2 (FGF-2) and monocyte chemoattractant protein-1 (MCP-1) release through, respectively, janus kinase 2 (JAK2)/STAT3, thromboxane synthase (TXAS), Notch1 and extracellular signal-regulated kinase 1/2 (ERK1/2), NF-kB and PI3K signalling pathways [83]–[87]. Finally, eNAMPT also indirectly participates in extracellular matrix (ECM) remodelling, a process required for angiogenesis, via the upregulation of proteases involved in vascular basal membrane degradation. Specifically, eNAMPT was shown to increase the expression and the activity of matrix metalloproteinases (MMPs; gelatinases : MMP-2 and -9; collagenases: MMP-1 and -8), which are potent matrix-degrading enzymes; in endothelial cells, macrophages and pre-adipocytes [62], [78], [88]–[90].

IV. Putative eNAMPT receptors

The rapid activation of specific intracellular pathways, occurring within minutes following exposure to eNAMPT, suggests that this protein exerts its functions by binding to one or more cell surface receptor(s) [2], [64]. Over the last years, several cell surface receptors have been proposed as putative eNAMPT receptors. The first one was the C-C chemokine receptor type 5 (CCR5). In 2012, Van den Bergh et al. demonstrated a direct binding of eNAMPT to CCR5, with an affinity in the nM range [91]. Later, Torretta et al. found that eNAMPT shares a common structure conformation with CCL7, a known CCR5 ligand [92]. This study also suggested that eNAMPT, like CCL7, acts as an antagonist of CCR5. These authors demonstrated that pre-treatment of HeLa-CCR5 cells with eNAMPT significantly diminished the percentage of RANTES-PE positive cells [92]. Finally, Currie and colleagues confirmed the interaction between eNAMPT and CCR5 in an ELISA binding assay [93], [94].

More recent studies show the interaction between Toll-like receptor 4 (TLR4) and eNAMPT. In 2015, Camp et al. revealed that eNAMPT activates the NF-kB pathway in mice through interaction with TLR4 [95]. Consistent with this, another study demonstrated that TLR4 gene silencing in macrophages resulted in a significant reduction in eNAMPT-mediated NF-kB

activation [60]. eNAMPT has also been shown to promote vascular dysfunction in mice through a TLR4-mediated pathway [75]. In particular, the authors demonstrated that a specific TLR4 inhibitor, CLI 095, prevented eNAMPT-mediated impairment of the endothelial responses to acetylcholine (ACh) [75]. Gasparrini et al. confirmed the direct binding of eNAMPT to TLR4 with a KD value of 18nM [66]. Using site-directed mutagenesis, these authors identified two regions involved in TLR4 binding in the N-terminal part of eNAMPT (β1-β2 loop: 41-52aa; and α1-α2 loop: 68-77aa). This finding was very recently confirmed by Kim et al. [96], who showed that the 57-65aa region of eNAMPT interacts with TLR4 leucine-rich repeats (LRR) domain. A TLR4 binding site in the C-terminal region of eNAMPT (445-457aa) has also been proposed by another group [97].

On the other hand, Colombo et al. recently demonstrated that eNAMPT promotes the expression of inflammatory M1-related gene expression (e.g. Il6, Il1b, Cox2, Tnf) independent of TLR4 [33]. Furthermore, they reported that a competitive molecular antagonist of CCR5 (maraviroc) did not alter eNAMPT-induced activation of M1 macrophages [33]. Overall, these results suggest the existence of one or more alternative receptors for eNAMPT-mediated M1 macrophage activation, i.e., other than TLR4 or CCR5. Another research group performed an eNAMPT receptor-binding identification screen with a coverage of >2500 known human receptors using Retrogenix cellular microarray platform [98]. They obtained multiple hits (e.g. BDKRB1, CD44, LRP8), suggesting that eNAMPT may pleiotropically interact with several receptors [98]. Last, but not least, Kim et al. [96] recently demonstrated eNAMPT interaction with NADPH oxidase 2 (Nox2 or CYBB) through its N-terminal region (52-56aa). All these alternative interactions still need to be validated. Thus, further investigations are required to fully elucidate the question of the biologically relevant eNAMPT receptor(s).

V. eNAMPT in human disease

5.1. Metabolic and cardiovascular diseases

Over the past years, multiple studies, including a meta-analysis [19], have reported increased circulating eNAMPT concentrations in patients diagnosed with obesity, diabetes or atherosclerosis, suggesting a role for eNAMPT as a biomarker for metabolic and cardiovascular diseases.

5.1.1. Obesity

Experimental evidence

Like for many other adipokines, eNAMPT secretion from adipose tissues is altered in obesity. One experimental study reported that plasma eNAMPT levels are significantly more elevated in obese mice (HFD-fed mice) than in controls [99]. However, whether eNAMPT contributes

to obesity and the mechanisms underlying this possible effect are not clearly deciphered yet. Several studies demonstrated that eNAMPT induces NLRP3 inflammasome complex activation and subsequent secretion of mature IL-1β [75], [99]–[101], which is known to be involved in the development of the chronic low-grade inflammation characteristic of obesity [102]. Specifically, activation of the NLRP3 complex by eNAMPT was shown to promote glomerular injury, as shown by the increased expression of the injury factor desmin in podocytes [100]. Chen et al. [101] reported that eNAMPT-mediated NLRP3 inflammasome activation provoked the disassembly of junction proteins (zonula occludens (ZO)-1, ZO-2, occludin and VE-cadherin) in mouse vascular endothelial cells, suggesting that eNAMPT promotes endothelial dysfunction. Finally, eNAMPT has been shown to enhance the expression of ECM proteins (collagen type C and osteopontin) and MMPs (MMP-2 and -9) in 3T3-L1 pre-adipocyte, leading to ECM accumulation and remodeling and, consequently, to adipose tissue fibrosis [88]. All this evidence points to a role for eNAMPT in the development of obesity-associated pathologies, including glomerular damage, endothelial dysfunction and adipose tissue fibrosis [103].

Clinical data

Various clinical studies reported significantly higher circulating eNAMPT levels in obese patients than in lean controls [reviewed by Carbone et al. [3] and shown in Table 1 ([88], [104]–[111])]. Furthermore, correlations between eNAMPT levels and unfavourable metabolic profiles, including high waist circumference and waist-to-hip ratio and elevated levels of triglycerides, have been observed [105], [107], [110]. eNAMPT was also often positively correlated with body mass index (BMI) [88], [105], [106], although not in all studies [109], [112]. These discrepancies could be explained by differences in the type of study, the type of population recruited, the number of cases per cohort or the methods of sample collection and measurement between clinical studies [113]. Consistent with an association between eNAMPT and adiposity, several studies reported a reduction of circulating eNAMPT levels after weight loss. For instance, exercise has been shown to decrease eNAMPT levels in overweight/obese patients [114]–[116]. Furthermore, Friebe et al. observed that serum eNAMPT concentrations were significantly reduced in obese subjects after bariatric surgery and that this reduction correlated with a decline in white blood cells (WBC) [104]. A link between eNAMPT concentrations and leucocyte counts was also suggested by another group who demonstrated that macrophages accumulate in human visceral white adipose tissues (WAT) in a way that correlates with increasing BMI, and release eNAMPT [117], [118]. In addition, they found that visceral WAT macrophages secreted higher levels of eNAMPT than mature adipocytes [117]. All of this supports a relationship between eNAMPT and inflammation in obesity, which is consistent with the positive correlation of eNAMPT levels with inflammatory (IL-6, TNF-α, c-reactive protein (CRP)) and endothelial markers (VCAM-1, ICAM-1, angiotensin-2 (ang-2), and E-selectin) observed in obese patients [106], [110], [119]. eNAMPT was also positively associated with endotrophin ($r = 0.619$, $P < 0.001$), a marker of

fibrosis worsening and metabolic abnormalities, in obese patients [88]. Finally, a receiver operating characteristic (ROC) analysis showed that plasma eNAMPT concentrations predict visceral adipose tissue accumulation in obese children (sensitivity = 88.9%, specificity = 91.5%, AUC = 0.920) [109]. Overall, this evidence suggests that eNAMPT might be a potential biomarker of the chronic low-grade inflammation occurring in obesity.

5.1.2. Diabetes

Experimental evidence

The role of eNAMPT in the pathophysiology of diabetes is not obvious, as many studies have reported a beneficial effect of eNAMPT on pancreatic function. Indeed, as discussed above, eNAMPT and its product, NMN, were shown to maintain β-cell homeostasis by modulating cellular NAD levels [18]. This is well illustrated by the fact that impaired islet function in fructose rich diet (FRD)-fed mice was associated with reduced plasma eNAMPT levels and was reversed by NMN administration [58]. In line with this, injection of NMN into aged β-cell-specific SIRT-1-overexpressing transgenic mice (BESTO) restored the beneficial effect of SIRT-1 on glucose tolerance, which was lost with mice ageing [57]. However, one study reported that eNAMPT administration for 14 days induced a diabetic phenotype in mice [120]; suggesting, in contrast, a detrimental effect of eNAMPT on β-cell activity. An explanation for this bimodal role of eNAMPT in diabetes was subsequently advanced by the same group, who proposed that physiological concentrations of dimeric eNAMPT maintain pancreatic function, whereas high concentrations of monomeric eNAMPT drive pathological mechanisms [121]. Specifically, they demonstrated that low, physiological levels of eNAMPT (1ng/mL) enhanced static and dynamic glucose-stimulated insulin secretion (GSIS) and intracellular cytosolic calcium levels in mouse islets. On the contrary, high-levels of eNAMPT (5ng/mL) or eNAMPT in its monomeric form caused these favourable effects to be lost and led to eNAMPT-mediated islet inflammation and β-cell failure through p38-MAPK and STAT3 pathways [121]. These findings suggest that eNAMPT functional/structural changes and pro-inflammatory effects play a key role in the pathophysiology of diabetes.

Clinical data

Multiple clinical studies investigated the correlation between eNAMPT and the different types of diabetes. Elevated levels of eNAMPT were measured in type 1 (T1DM) [122], [123], type 2 (T2DM) [121], [123]–[129] and gestational diabetes patients [130], [131] compared to non-diabetic individuals (detailed in Table 1). The clinical association between eNAMPT and diabetes was independent of BMI [124], [125]. No significant differences in circulating eNAMPT concentrations were found between pre-diabetic subjects and healthy controls [126]. In addition, the levels of eNAMPT in newly diagnosed T2DM patients were similar to that of non-diabetic individuals, whereas eNAMPT levels of known T2DM patients were

higher [123]. This suggests that eNAMPT may only play a role in the later stages of the disease. Consistent with this, serum eNAMPT levels were shown to increase with diabetes worsening and particularly with β-cell deterioration progression, a major feature of T2DM, as attested by the positive correlation of eNAMPT with haemoglobin A1c (HbA_{1c}) [121], [123]. T1DM patients with long-lasting disease and more advanced β-cell deterioration than T2DM patients showed increased levels of circulating eNAMPT as compared to type 2 diabetic subjects [123]. The link between eNAMPT and insulin resistance, another main characteristic of T2DM pathophysiology, was also extensively explored. Some studies observed an association between eNAMPT levels and homeostasis model assessment of insulin resistance (HOMA-IR) in diabetic patients, suggesting a relationship between eNAMPT and insulin resistance [19], [128], [129], [132]. Furthermore, serum eNAMPT levels were higher in children with impaired insulin sensitivity compared to normal children [104]. However, others found no correlation between circulating eNAMPT levels and HOMA-IR [133], [134]. It is therefore not possible, at this time, to conclude on a possible association between eNAMPT and insulin resistance. Finally, eNAMPT was shown to predict gestational diabetes with high sensitivity and specificity (sensitivity = 87.1%, specificity = 70%, AUC = 0.799) [131], suggesting, together with previous evidence, that eNAMPT may be a promising biomarker for diabetes detection.

5.1.3. Atherosclerosis

Experimental evidence

Along with serum lipid levels, plasma eNAMPT levels were shown to be significantly elevated in apoE KO atherosclerotic mice [135]. Studies also demonstrated that eNAMPT is highly expressed in human symptomatic atherosclerotic plaques and that this protein localizes to areas where foam cells are present [68],[136]. Pro-atherogenic stimuli (e.g. oxidized low-density lipoprotein, hypoxia and TNF-α) increased eNAMPT expression in THP-1 monocytes [68], [135] and eNAMPT release by RAW264.7 macrophage-like cells [137]. In turn, eNAMPT triggered cholesterol uptake by macrophages *in vitro,* by modulating scavenger receptor (SR-A) and CD36 expressions, and *in vivo,* in atherosclerotic mice [137]. In addition, Dahl et al., reported that the secretion of pro-inflammatory cytokines (TNF-α and CXCL8) by peripheral blood mononuclear cells (PBMCs) from patients with unstable angina was induced by eNAMPT [68]. Thus, through its pro-inflammatory function, eNAMPT may participate in foam cell formation and fatty streak development during atherogenesis. Additional studies indicate that eNAMPT could also contribute to atherosclerosis development by promoting endothelial dysfunction. Specifically, eNAMPT has been shown to alter the migration and adhesion of endothelial progenitor cells (EPC, key cells allowing the regeneration of impaired blood vessels), as well as to induce their apoptosis [138], [139]. As mentioned previously, eNAMPT also directly impaired microvascular endothelium-dependent vasorelaxation by reducing the endothelial response to vasodilators, such as ACh [75], [140]. eNAMPT may also compromise vessel wall integrity and compound plaque vulnerability by promoting MMPs expression in

monocytes/macrophages [68], [89] and endothelial cells [78]. Finally, eNAMPT showed the ability to induce human vascular smooth muscle cell proliferation [43] and to upregulate their nitric oxide synthase (iNOS) levels [141], thereby promoting vascular inflammation.

Clinical data

Consistent with the experimental findings, higher circulating eNAMPT levels were observed in patients with atherosclerotic plaques as compared to controls (see Table 1, [142]–[147]). Increased plasma eNAMPT concentrations were also measured after mechanical induction of plaque rupture [68] or in patients diagnosed with acute myocardial infarction [148], suggesting a relationship between eNAMPT levels and plaque instability. This was confirmed by Kadoglou et al. [143], who reported a negative correlation between eNAMPT concentrations and the gray-scale median (GSM) score, which quantifies plaque vulnerability, in atherosclerotic patients. Circulating eNAMPT concentrations were found to also positively correlate with the extent of atherosclerosis, as measured by intima media thickness (IMT) [144], [146]. A negative association between eNAMPT and flow-mediated vasodilatation (FMD) was observed by Takebayashi et al. [149], supporting a link between eNAMPT and endothelial dysfunction. Finally, circulating eNAMPT was found to be an independent predictor of atherosclerosis and was proposed to be a risk factor for the development of atherosclerotic plaques [145], [147].

5.2. Arthritis

5.2.1. Osteoarthritis (OA)

Experimental evidence

Several studies have suggested that eNAMPT exerts pro-degradative effects in the context of osteoarthritis. For instance, Cheleschi et al. demonstrated eNAMPT contribution to cartilage turnover, showing that eNAMPT promotes OA chondrocytes and synovial fibroblasts (OASFs) apoptosis [150], [151]. Furthermore, they reported that eNAMPT increases mitochondrial superoxide anion production as well as the expression of antioxidant enzymes (e.g. superoxide dismutase (SOD-2), catalase (CAT) and nuclear factor erythroid 2-related factor 2 (NFR2)) in the same cells [150]–[152]. Thus, eNAMPT modulates oxidative stress balance, a process involved in joint degeneration during OA [153]. eNAMPT may also exacerbate OA by promoting the expression of a variety of proteases. Studies show that eNAMPT stimulates the release of sulphated glycosaminoglycans (GAGs) from cartilage and meniscus explants, reflecting an elevated aggrecanase activity and proteoglycan loss [98], [154], [155]. In line with this, Gosset et al., reported that eNAMPT reduces aggrecan mRNA and the levels of high molecular weight aggregated proteoglycan and induces the expression of ADAMTS-4 and ADAMTS-5 aggrecanases in immature mouse articular chondrocytes [156]. eNAMPT was shown to upregulate the expression of MMPs (collagenases: MMP-1, -8, -13; gelatinases:

MMP-2, -9; stromelysins: MMP-3, -10; matrilysin: MMP-7) during OA [98], [150], [151], [156]. Specifically, eNAMPT was found to co-localize with MMP-13 in areas of joint damage in human hip cartilage [98]. Finally, in human and mouse OA chondrocytes, eNAMPT promoted the synthesis of prostaglandin E2 (PGE2), a well-known cartilage catabolic factor [156], [157]. eNAMPT may not only stimulate the activity of catabolic proteins, but also directly alter the expression of cartilage structural proteins, thereby contributing to cartilage homeostasis impairment. Particularly, eNAMPT was shown to reduce the expression of collagen type II and type X in OA chondrocytes and OASFs [151], [158]. Consistent with this, another study demonstrated that eNAMPT prevented insulin like growth factor-1 (IGF-1)-mediated production of collagen type II and proteoglycan [159]. In addition to its pro-degradative effects, the pro-inflammatory and pro-angiogenic functions of eNAMPT have also been suggested to be involved in the pathogenesis of OA. eNAMPT was shown to activate NF-kB and MAPK signalling pathways in OASFs, leading to the downstream expression of pro-inflammatory cytokines (IL-1β, IL-6, IL-17a, TNF-α) and to the subsequent activation of inflammatory processes participating to OA synovitis [151], [160]. Upregulations of pro-inflammatory cytokines and chemokines (e.g. CCL4, MCP-1, IL-6 and CCL20) were also observed after stimulation of OA patients cartilage explants or murine chondrocytes with eNAMPT [41], [98]. Finally, eNAMPT was shown to augment VEGF production by human OASFs, which in turn, induces EPC angiogenesis, a phenomenon involved in structural damage and pain during OA [161], [162]. Consistent with this, Pecchi et al. revealed that eNAMPT induces nerve growth factor (NGF) expression and release by chondrocytes, supporting the idea of a possible involvement of this cytokine in OA pain [163].

Clinical data

Several studies reported significantly higher eNAMPT levels in the serum or synovial fluid of OA patients, compared with controls (see Table 1, [161], [164]–[167]). Furthermore, Chen et al. observed that eNAMPT concentrations were more elevated in the synovial fluid of OA patients than in paired serum samples, suggesting an increased dysregulation of eNAMPT levels, locally, i.e. in the affected joints [167]. In OA patients, eNAMPT was shown to be released from all joint tissues, including synovium, subchondral bone and cartilage, but also from infrapatellar fat pad [41], [167]. In particular, eNAMPT release was significantly higher in synovium than cartilage or subchondral bone [41]. Consistent with previous experimental evidence of eNAMPT-mediated cartilage matrix degradation in OA, SF eNAMPT levels increased with Kellgren-Lawrence grade (a system used to classify the severity of OA) and positively correlated with several biomarkers of cartilage degradation (C-terminal crosslinked telopeptide of type II collagen (CTX-II), AGG1 and AGG2 aggrecan fragments) [166]. In addition, eNAMPT concentrations were positively associated with VEGF and pain score in OA patients [161], [168]. Experimental and clinical studies strongly support a relationship between eNAMPT and OA and suggest that measuring SF eNAMPT levels could be a viable diagnostic approach to detect OA. Nevertheless, eNAMPT use as a biomarker for OA may be

limited by the fact that eNAMPT concentrations are affected by several other conditions, such as cardiovascular diseases and diabetes [169].

5.2.2. Rheumatoid arthritis (RA)

Experimental evidence

As with OA, several studies suggest that eNAMPT may play a role in rheumatoid arthritis, which is also characterized by joint damage, but as a result of an autoimmune process (rather than wear and tear, as in OA). One study reported that eNAMPT levels were significantly higher in serum and paw tissue extracts of collagen-induced arthritic mice than in control mice [170]. eNAMPT expression or secretion by human RA synovial fibroblasts (RASFs) was shown to be upregulated by pro-inflammatory cytokines (IL-1β, TNF-α, IL-6) and TLR ligands (poly(I-C), LPS) that are characteristically present in RA joints [27], [171]. Additional studies revealed that, in turn, eNAMPT was able to induce the expression/production of pro-inflammatory cytokines (IL-6, CXCL8), chemotactic signals (chemokines of the CXC and CC family) and matrix-degrading enzymes (MMP-1 and MMP-3) in fibroblasts, and thus to promote inflammatory and destructive processes in RA joints [27], [172]–[174]. Furthermore, eNAMPT was shown to increase RASF adhesion to endothelial cells [175] and to enhance their motility and migration [173]. This may indicate that eNAMPT also contributes to cartilage invasion by RASFs during RA.

Clinical data

Similar to experimental animals, circulating eNAMPT levels were found to be higher in RA patients than in healthy controls (reviewed by Franco-Trepat et al. [176] and shown in Table 1 ([177]–[185])). Noteworthy, RA patients exhibited higher serum and SF concentrations of eNAMPT than OA patients [27], [171]. In RA patients, eNAMPT was strongly expressed in the synovial lining layer and at sites of RASF invasion in the cartilage [27], [173]. The protein was also detected in lymphoid aggregates and perivascular areas [27], [171], [173]. Further studies demonstrated that eNAMPT positively correlates with disease severity and duration [179], [181], [183], [184] and eNAMPT concentrations were significantly higher in patients with radiographic joint damage [184]. In line with these findings, Rho et al. observed a positive association between eNAMPT and the Larsen score, which determines the extent of radiographic changes [179]. eNAMPT also positively correlated with inflammatory mediators (TNF-α, IL-6, CRP) and immune cells counts (neutrophil and B cells) in serum and synovial fluid of RA patients [27], [179]–[182], supporting a role for eNAMPT in RA-related inflammatory mechanisms. Interestingly, a significant decrease in circulating eNAMPT levels was observed in RA patients after treatment with conventional synthetic disease modifying antirheumatic drugs (csDMARDs) [181], anti-TNF-α treatment [186], anti-CD20 antibody [182] or a combination of methotrexate with anti-IL-6 therapy [187], suggesting a role for eNAMPT as a

biomarker for RA activity. Consistent with this, a reduction in serum eNAMPT levels after three months of csDMARDs treatment predicted an amelioration in disease activity score 28 (DAS28) after 12 months of treatment [181]. However, discrepancies exist as no changes in eNAMPT concentration has been observed in other studies, following treatment with DMARDs, TNF-α blockers, or a combination of both [188], [189]. Overall, clinical findings suggest that eNAMPT may be a predictive factor of RA worsening, although further validations of this use of eNAMPT are required.

5.3. Inflammatory bowel disease (IBD)

Experimental evidence

The experimental studies that investigated NAMPT involvement in the development of IBD mainly focused on the role of the intracellular enzyme, iNAMPT, in these conditions [190]–[192]. Only recently, in 2020, Colombo et al. [193], reported that administration of recombinant eNAMPT to mice suffering from mild colitis, exacerbated mucosal inflammation, indicating a possible contribution of that extracellular protein to IBD. Furthermore, they observed increased expression of TNF-α and IL-1β, and degradation of IkB-α, in colonic tissues of eNAMPT-treated mice. Finally, Colombo et al. showed that eNAMPT neutralization with a monoclonal antibody in dinitrobenzene sulfonic acid (DNBS)-treated mice reduced the recruitment of pro-inflammatory monocytes and neutrophils and the activation of pathogenic Th1 and cytotoxic effector T cells in the colon [193]. They therefore suggested that eNAMPT may participate in colonic inflammation in IBD by activating the pro-inflammatory functions of myeloid cells and by triggering pathogenic Th1/Th17-mediated adaptive immunity.

Clinical data

The majority of clinical studies examining eNAMPT role in IBD, reported that circulating eNAMPT levels were significantly higher in ulcerative colitis (UC) and Crohn's disease (CD) patients compared to healthy individuals (Table 1, [194]–[199]), although two studies failed to find such difference [200], [201]. Interestingly, eNAMPT levels were found to be differently associated with disease activity in UC and CD patients. In CD patients, serum eNAMPT levels were elevated regardless of disease activity, whereas in UC patients, eNAMPT levels were higher in patients with active UC than in patients with inactive disease [67], [195], [196]. Consistent with a role for eNAMPT in intestinal inflammation, positive correlations between eNAMPT and inflammatory markers (IL-6 levels, platelet count, erythrocyte sedimentation rate (ESR) or CRP levels) were observed in IBD patients [195], [198]. In addition, Neubauer et al. reported a strong positive correlation between serum eNAMPT concentrations and NAMPT expression levels in leucocytes of IBD patients [195], suggesting an involvement of immune cells in the elevation of eNAMPT levels. Moschen et al. observed a co-localization of NAMPT with macrophages and dendritic cells in inflamed colonic tissue [67]. Colombo et al. reported

that after 14 weeks of therapy, IBD patients responding to anti-TNF-α treatment exhibited a decrease in circulating eNAMPT, while non-responders maintained elevated serum eNAMPT levels [193]. These results suggest an association between high circulating eNAMPT levels and an increased risk of resistance to IBD treatment and thus, that eNAMPT may be a promising predictor of patient response to therapy. Finally, the potential of eNAMPT as a diagnostic tool was supported by an ROC analysis which showed that serum eNAMPT levels predict active UC with a high sensitivity and specificity (sensitivity = 92.9%, specificity = 86.7%, AUC = 0.911) [198]. In conclusion, accumulating evidence points to eNAMPT as a biomarker of active IBD. Further studies are required to ascertain whether eNAMPT also plays a role in the pathogenesis of IBD, and particularly, in the mucosal inflammation that is a hallmark of these diseases.

5.4. Lung injury

Experimental evidence

Growing evidence indicates the involvement of eNAMPT in the development of different pulmonary conditions, such as acute lung injury (ALI), acute respiratory distress syndrome (ARDS), a severe form of ALI, and ventilator-induced lung injury (VILI). Neutralization of eNAMPT with an antibody was shown to attenuate inflammatory lung injury in preclinical mouse, rat, and porcine ARDS/VILI models [202]–[204]. Of note, Lee et al. reported higher serum eNAMPT levels in ALI mouse models (LPS- and CASP-treated mice) than in control mice [205]. As with most, if not all, of the diseases in which eNAMPT has been suggested to be implicated, eNAMPT appears to contribute to ALI/ARDS and VILI via its pro-inflammatory/cytokine-like function. Specifically, studies observed that eNAMPT act as a leucocyte chemoattractant and increases BAL polymorphonuclear leucocytes (PMN) counts and BAL chemokines levels (keratinocyte-derived chemokine (Kc) and macrophage inflammatory protein (MIP-2)) *in vivo* [95], [206]. Tracheal administration of eNAMPT was shown to augment BAL pro-inflammatory cytokines (IL-6, TNF-α and IL-1β) levels in mice, supporting a possible role for this protein in lung injury-associated inflammatory responses [206]. eNAMPT also exacerbated mechanical VILI features, as evidenced by the greater alveolar wall thickening and neutrophil infiltration observed in VILI mice which also received eNAMPT as compared to mice that were subjected to VILI alone [206]. eNAMPT may also elicit lung injury by promoting endothelial cell barrier disruption. For example, Quijada et al. observed a decrease in transendothelial electrical resistance (TER) in human lung endothelial cells treated with eNAMPT, reflecting a loss of endothelial barrier integrity [203]. In line with this, NAMPT silencing in human pulmonary artery endothelial cells (HPAEC), attenuated thrombin-induced endothelial barrier dysfunction [207]. Finally, eNAMPT was shown to further contribute to pulmonary permeability by dysregulating NF-kB, MAPK and AKT-mTOR-Rictor signalling pathways in human lung endothelial cells [95], [202], [203].

Clinical data

Consistent with the experimental evidence, circulating levels of eNAMPT were significantly increased in patients with ALI, ARDS (see Table 1, [29], [205], [208]) or ARDS-predisposing conditions (e.g. sepsis, acute pancreatitis) [208], [209]. Furthermore, eNAMPT levels were also significantly higher in BAL fluid from ALI patients compared to control individuals [29]. Interestingly, elevated concentrations of eNAMPT seem to be an indicator of poor survival in patients presenting with these conditions. For instance, higher eNAMPT levels were found in non-survivors of sepsis-induced ARDS than in survivors [210]. In addition, the survival rate of ALI patients was shown to negatively correlate with serum eNAMPT concentrations [205]. eNAMPT is also one of a panel of six biomarkers that showed promise in predicting 28-day ARDS mortality [211]. Supporting a link between eNAMPT and pulmonary inflammation, a positive correlation was found between serum eNAMPT and serum IL-6, CXCL8, IL-10 and MCP-1 levels in ALI patients [205], [210]. Importantly, circulating eNAMPT levels discriminated healthy individuals from patients with ARDS (AUC = 0.86, 95% CI:0.82-090, P-value < 0.001) [208] and ARDS-predisposing pathologies [208], [209]. Taken together, these findings indicate that eNAMPT may serve as a novel diagnostic tool for early detection of pulmonary conditions, as a tool for patient stratification for recruitment into clinical trials and, possibly, as a therapeutic target in these disorders.

5.5. Cancer

Experimental evidence

Of all of the pathologies that were investigated, eNAMPT implication in cancer is the best documented and established. eNAMPT was shown to be involved in the development of various cancer types, ranging from solid tumours (e.g. breast, colorectal, gastric, prostate cancers) to haematological malignancies (e.g. chronic lymphocytic leukaemia (CLL) and cutaneous T-cell lymphoma (CTCL)) [212]. Once secreted by the tumour itself [32], [35], [76] or by tumour-associated cells (e.g. leucocytes) [104], eNAMPT is presumed to modulate various hallmarks of cancer and promote tumour progression. Firstly, eNAMPT is thought to directly stimulate cancer cell proliferation. *In vitro* studies shown that eNAMPT induced the proliferation of breast cancer [42], [213]–[215], melanoma [216], hepatocellular carcinoma (HCC) [217], [218], endometrial carcinoma [219] and prostate cancer cells [220], by activating pro-survival signalling pathways such as c-Abl/STAT3, PI3K/AKT, MAPK/ERK, Notch1/NF-kB. Furthermore, eNAMPT was shown to accelerate cell division in MCF-7 breast cancer cells through the upregulation of cyclin D1 and cdk2 [221]. eNAMPT proliferative effect was also confirmed *in vivo,* where eNAMPT administration promoted the growth of endometrial [219] and breast cancer xenografts [213], [222]. eNAMPT was also shown to help cancer cells avoid cell death. For instance, by preventing the reduction in survivin levels, eNAMPT helped MCF-7 cells escape TNF-α induced apoptosis [214]. In addition, eNAMPT was shown to protect Me45 melanoma cells from hydrogen peroxide-induced DNA damage, probably by

augmenting the activity of antioxidant enzymes (CAT, glutathione peroxidase and superoxide dismutase) [216]. Finally, eNAMPT promoted the differentiation of monocytes into nurse-like cells (NLCs) which, in turn, supported CLL cell survival [64].

A critical role of eNAMPT in activating tumour cell invasion *in vitro* and *in vivo* has been reported. eNAMPT promoted breast cancer [213], osteosarcoma [223], ovarian cancer [224], chondrosarcoma [225] and prostate cancer [226] cells migration by inducing intracellular signalling pathways (e.g. c-Abl/STAT3 [213], NF-kB/IL-6 [223], Rho/Rho-associated protein kinase (ROCK) [224], MAPK). In colorectal cancer (CRC) cells, eNAMPT upregulated the expression of stromal-derived factor (SDF)-1, a chemokine known to stimulate CRC cancer cell migration [228]. Consistent with these *in vitro* findings, eNAMPT was shown to increase breast cancer cell invasiveness in a xenograft zebrafish model and to promote lung metastasis in a mouse orthotopic xenograft model [213]. Importantly, a neutralizing anti-eNAMPT antibody was able to inhibit prostate cancer cell invasiveness in a xenograft model [229]. eNAMPT is believed to sustain cancer cell migration and invasion by inducing epithelial to mesenchymal transition (EMT). Soncini et al. demonstrated that eNAMPT induced the EMT program in breast cancer cells via the upregulation of transforming growth factor β (TGFβ) signalling [76]. Similarly, eNAMPT was shown to trigger EMT in gastric and osteosarcoma cancer cells by activating NF-kB/Snail-1 signalling [230], [231]. Another mechanism that might explain the pro-metastatic function of eNAMPT is the induction of the activity of matrix-degrading enzymes. For instance, eNAMPT was shown to upregulate the expression and activity of gelatinases MMP-2 and -9, in various types of cancer cells [213], [217], [220], [221], [225], [226], [232]. Finally, studies demonstrated that eNAMPT stimulates angiogenesis by inducing the secretion of various pro-angiogenic factors in endothelial cells [80] and cancer cells [221].

eNAMPT may also contribute to cancer development by promoting an immunosuppressive tumour micro-environment (TME). Several studies reported that eNAMPT induced the polarization of macrophages into tumour-promoting M2 phenotype [64], [71]. Specifically, increased expression of the M2 markers, CD163 and CD206, was observed in monocytes after exposure to eNAMPT. eNAMPT was also shown to augment the secretion of immunosuppressive molecules and tumour-promoting cytokines (indoleamine 2,3-dioxygenase (IDO), CCL18, IL-10, IL-1β , IL-6 and CXCL8) [64], [67]. Last, but not least, Audrito et al. reported that eNAMPT inhibited autologous T-cell proliferation and increased Treg counts in CLL [64], thus fostering the generation of an immunosuppressive TME. Growing evidence suggests that eNAMPT participates in cancer therapy resistance. A recent study revealed that eNAMPT diminished the sensitivity of colorectal cancer to capecitabine through the upregulation of thymidylate synthase (TYMS) expression [233]. Furthermore, eNAMPT was shown to induce oestrogen receptor α (Erα) Ser167 phosphorylation [234], which is known to contribute to breast cancer resistance to tamoxifen [235]. Finally, eNAMPT-

mediated enhancement of the antioxidant capacity of tumour cells may also contribute to their resilience and drug resistance [216], [236].

Clinical data

Numerous clinical studies investigated the link between circulating eNAMPT levels and cancer development. As reviewed by Dalamaga et al. [212] and summarized in Table 1, higher serum and plasma eNAMPT concentrations were found in cancer patients compared with healthy individuals. In addition, circulating eNAMPT levels were shown to correlate with tumour size and stage of cancer [23], [213], [218], [226], [232], [237]–[243] (the higher eNAMPT levels are the bigger and more advanced the tumour is). Multiple studies reported that eNAMPT levels negatively correlate with disease-free survival and overall patient survival and are positively associated with lymph node invasion and/or metastasis ([213], [232], [242], [244]). In particular, eNAMPT was shown to be an independent risk factor for myometrial invasion in uterus cancer (OR = 1,091, 95%CI = 1.021-1.166, P = 0.010) [245]. Circulating eNAMPT levels also correlated with cancer biomarkers such as CA 15-3 in breast cancer [244], alpha-fetoprotein in hepatocellular carcinoma [239] and lactate dehydrogenase (LDH) in metastatic melanoma [23]. Interestingly, melanoma patients exhibiting PD-L1+ lesions had significantly increased plasma eNAMPT concentrations compared to patients with PD-L1- lesions [23]. This suggests an association between eNAMPT and immunosuppressive conditions. Finally, several ROC analyses demonstrated that eNAMPT has a great potential for predicting cancer [226], [241], [244], [246]. A meta-analysis also revealed that elevated eNAMPT concentrations were associated with an increased risk of cancer (OR = 1.24, 95%CI = 1.14–1.34, P = 0.000) [21]. To conclude, eNAMPT appears as a promising diagnostic biomarker for cancer. In addition, there is evidence to suggest that eNAMPT may also be directly involved in tumour pathogenesis and may thus represent an attractive therapeutic target.

VI. eNAMPT, a potential drug target

Over the years, the development of therapeutic drugs targeting NAMPT mainly focused on inhibiting its enzymatic activity. As reviewed by Ghanem et al. [5], several small molecules have been designed to disrupt NAMPT's NAD-biosynthetic activity in tumour cells. Among these, FK866 (also named APO866, (E)-Daporinad, and WK1) and GMX1778 (also named CHS-828) have been the most studied [5]. Both showed potent anti-cancer activities in preclinical studies [5], and were evaluated in early-phase clinical trials [247]. Unfortunately, these experimental drugs showed limited clinical activity and induced dose-limiting toxicities such as thrombocytopenia and gastrointestinal toxicity [5], [247]. Second-generation inhibitors of NAMPT enzymatic function (NAMPTi), like OT-82, and dual inhibitors, like KPT-9274 which inhibits both P21-activated kinase 4 (PAK4) and NAMPT enzymatic activity, are currently being evaluated in phase I clinical trials in patients with solid and hematologic malignancies; but no

results have been disclosed yet [248]. Thus, to date, the determination of a safe therapeutic window for cancer treatment with NAMPTi has not been achieved.

A not negligible part of the pathological activities of NAMPT in cancer may be carried out by its extracellular form, eNAMPT, whose functions are independent of enzymatic activity and therefore cannot be inhibited by NAMPTi. For this reason, the development of new therapeutic strategies, targeting the eNAMPT protein or both iNAMPT and eNAMPT is becoming increasingly attractive. A promising approach are neutralizing antibodies, blocking eNAMPT interaction with its receptor(s). Several *in vitro* and *in vivo* studies support this therapeutic strategy (summarized in Tables 2 and 3). For instance, Kieswich et al. used a commercial anti-eNAMPT polyclonal antibody to neutralize the monomeric form of eNAMPT in HFD-fed mice [120]. They demonstrated that eNAMPT neutralization improved HFD-fed mice diabetic phenotype by ameliorating their pancreatic islet function, glycaemic control and insulin resistance [120]. Colombo and colleagues developed their own murine anti-eNAMPT monoclonal antibody [193]. They showed that their antibody neutralizes eNAMPT cytokine function *in vitro* and ameliorates acute and chronic colitis in experimental mouse models. In a subsequent study, this antibody was able to abrogate polarization of peritoneal macrophages of healthy mice toward M1-like phenotype [33]. On the other hand, Audrito et al. showed that an anti-eNAMPT pAb prevented eNAMPT-induced STAT3 signalling (a signalling protein known to be an important mediator of immunosuppressive responses in TME) in tumour-infiltrating M2 macrophages [64], [249]. Last but not least, a humanized anti-eNAMPT therapeutic monoclonal antibody, ALT-100, developed by Joe G.N Garcia laboratory and Aqualung Therapeutics is in early clinical development (NCT05426746) [250], [251]. Thanks to a high degree of NAMPT sequence conservation, ALT-100 is cross-reactive with many other mammalian species. ALT-100 was able to reduce the severity of murine and porcine inflammatory lung injury [202]–[204], to attenuate pulmonary hypertension severity in rats [252], to reduce radiation-induced lung fibrosis (RILF) severity in mice [253] and to inhibit prostate cancer cell proliferation, invasion, and metastasis in mice [229]. Recently, ALT-100 also demonstrated therapeutic effects in murine preclinical models of lung vasculitis/hemorrhage and nonalcoholic fatty liver disease (NAFLD) [254], [255]. Taken together, these studies support a rationale for developing neutralizing anti-eNAMPT antibodies for the treatment of diverse inflammatory diseases, such as cancer, lung injury and ulcerative colitis.

Recently, a novel therapeutic approach targeting both eNAMPT and iNAMPT has been proposed. This new strategy consists of inducing the degradation of intracellular NAMPT through the ubiquitin-proteasome pathway using NAMPT-specific PROteolysis-TArgeting Chimera (PROTAC) compounds [256], [257]. As a result, eNAMPT secretion is prevented and both the enzymatic and the non-enzymatic activities of NAMPT are disrupted. Promising preliminary results have been obtained with these molecules *in vitro* and *in vivo* [256], [257]. Zhu et al. [256] reported that PROTACs outperformed FK866 in terms of tumour-killing

activity. Furthermore, they observed that, unlike FK866, their compounds were able to inhibit NF-kB and MAPK/ERK1/2 pathway activation, suggesting that they also block eNAMPT cytokine activity by degrading intracellular NAMPT [256]. Further investigations are required to determine whether these new molecules could be a valid therapeutic approach for cancer treatment.

Concluding remarks

Over the past decade, eNAMPT protein has emerged as a central player in diverse pathologies. Numerous studies have reported a correlation between elevated circulating levels of eNAMPT and pathological conditions such as cancer, obesity, diabetes, atherosclerosis, arthritis, IBD and lung injury. This indicates a great potential for using eNAMPT as a biomarker for inflammatory diseases. Accumulating evidence indicates that eNAMPT not only predicts the onset or the aggravation of disease, but also could contribute to pathogenesis, principally by inducing inflammation. All that said, many aspects of eNAMPT activities remain unclear, including cell surface receptors mediating eNAMPT function, so further investigations are required.

Acknowledgements

This work received funding from the European Union's Horizon 2020 research and innovation programme under the Marie Skłodowska-Curie grant agreement no.813284. In addition, Dr Nencioni acknowledges the support of the Associazione Italiana per la Ricerca sul Cancro (IG#22098).

Figures and tables

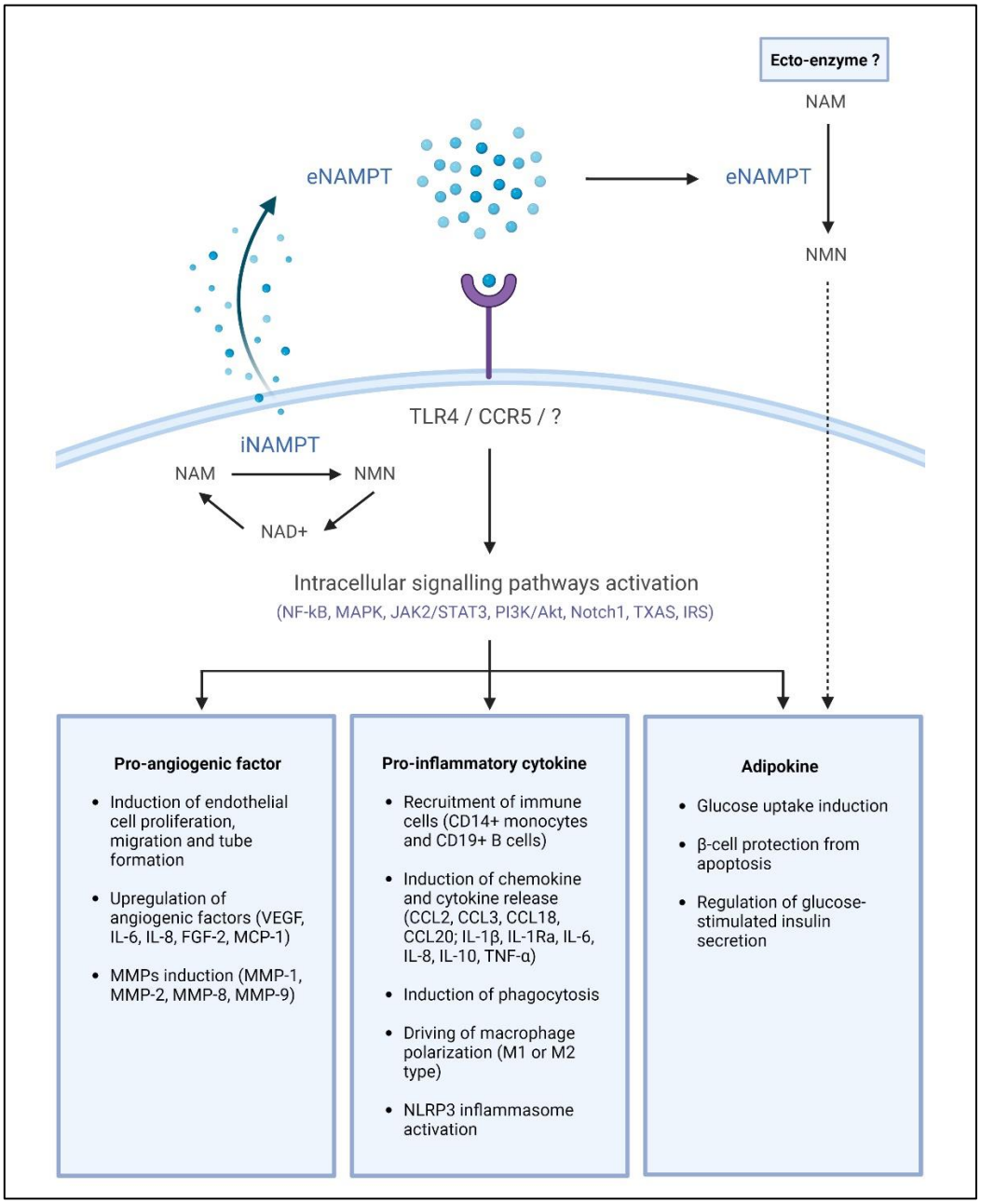

Figure 1: eNAMPT, a pleiotropic protein with multiple functions. eNAMPT protein is secreted in the extracellular space through an unsolved mechanism of secretion. Then, via its binding to one or more undetermined cell surface receptor(s), eNAMPT activates downstream intracellular pathways leading to the induction of a variety of physiological and pathological processes. Furthermore, studies have suggested that eNAMPT acts directly as an ectoenzyme in the extracellular milieu and generates NMN, which is subsequently reinternalized. Abbreviations: Akt, protein kinase B; CD, cluster of differentiation; CCL, chemokine (C-C motif) ligand; FGF, fibroblast growth factor; IL, interleukin; IR, insulin receptor; IRS, insulin receptor substrate; JAK, janus kinase; MAPK, mitogen-activated protein kinases; MCP-1, monocyte chemoattractant protein-1; MMP, matrix metalloproteinase; NAD, nicotinamide adenine dinucleotide; NAM, nicotinamide; NF-kB, nuclear factor kappa-light-chain-enhancer of activated B cells; NMN, nicotinamide mononucleotide; NLRP3, NLR family pyrin domain containing 3; Nocht1, neurogenic locus notch homolog protein 1; PI3K, phosphatidylinositol-3-kinase; STAT3, signal transducer and activator of transcription 3; TXAS, thromboxane synthase; TNF, tumour necrosis factor; VEGF, vascular endothelial growth factor.

Table 1: Clinical studies highlighting eNAMPT potential as a biomarker for various diseases. Also reviewed by Carbone et al. [3], Garten et al. [1], Dalamaga et al. [212] and Audrito et al. [258].

Author	Year	Sample size	Results
Obesity			
Ezzati-Mobaser et al. **[88]**	2020	30 obese children 29 controls	Significantly higher plasma eNAMPT levels were found in obese patients compared to control subjects (P = 0.005). Positive correlations between eNAMPT and BMI z-score (r = 0.356, P = 0.006) and eNAMPT and endotrophin (r = 0.619, P < 0.001) were observed.
Alnowihi et al. **[105]**	2020	35 obese women 15 overweight women 33 controls	The obese group had higher serum eNAMPT levels than the overweight and lean groups (P < 0.001). eNAMPT levels were positively correlated with waist and hip circumferences (r = 0.4, P ≤ 0.001), BMI (r = 0.5, P ≤ 0.001), DBP (r = 0.2, P = 0.02), SBP (r = 0.2, P = 0.02), insulin (r = 0.3, P ≤ 0.01), HOMA-IR (r = 0.2, P = 0.02) and LDL-C (r = 0.3, P ≤ 0.01) and negatively correlated with HDL-C (r = -0.2, P ≤ 0.01), E2 (r = -0.2, P = 0.04), and SHBG (r = -0.26, P ≤ 0.01) values.
Yin et al. **[106]**	2019	160 obese children 84 controls	Serum eNAMPT levels were higher in obese children than in lean children (P < 0.01). Similar plasma eNAMPT concentrations were found in insulin resistance and non-insulin resistance groups of obese children (P > 0.05). Serum eNAMPT levels correlated with SDS-BMI (β(r) = 0.601, P = 0.005), BMI (β(r) = 0.523, P = 0.008), hsCRP (β(r) = 0.633, P = 0.000), IL-6 (β(r) = 0.736, P = 0.000), TNF-α (β(r) = 0.733, P = 0.000), VCAM-1 (β(r) = 0.726, P = 0.000), ICAM-1 (β(r) = 0.953, P = 0.000), Ang-2 (β(r) = 0.933, P = 0.000), and E-selectin (β(r) = 0.896, P = 0.000) levels in obese children.
Ahmadpour et al. **[108]**	2018	35 obese children 35 controls	Serum eNAMPT levels were significantly higher in obese children compared to control children (P < 0.001). A negative correlation between serum eNAMPT and plasma miR-149 levels was found (r = -0.302, P = 0.001).
Nourbakhsh et al. **[111]**	2015	42 obese children 31 controls	Obese children had significantly higher plasma eNAMPT concentrations than lean controls (P < 0.001). In obese subjects, eNAMPT correlated positively with FPG (r = 0.34, P < 0.05), insulin (r = 0.58, P < 0.01) and HOMA-IR (r = 0.57, P < 0.01).
Diabetes			
Mir et al. **[127]**	2022	87 T2DM 85 controls	Male T2DM patients had significantly more elevated serum eNAMPT levels compared to controls (P < 0.01).
Mostafa et al. **[128]**	2021	60 T2DM 60 controls	Circulating levels of eNAMPT were significantly higher in T2DM patients than in control individuals (P < 0.001). Correlations of eNAMPT with FBG (r = 0.621, P < 0.01), insulin (r = 0.416, P < 0.01), HOMA-IR (r = 0.518, P < 0.01), HbA_{1c} (r = 0.388, P < 0.01), IL-34 (r = 0.312, P < 0.01), IRAPe (r = - 0.380, P < 0.01) and irisin (r = -0.494, P < 0.01) were observed.

Sayers et al. **[121]**	2020	27 obese T2DM 15 obese IFG 13 controls	Obese patients with T2DM had significantly higher levels of serum eNAMPT than obese individuals with impaired fasting glucose ($P < 0.05$) and non-diabetic obese controls ($P < 0.05$). Furthermore, increasing eNAMPT levels correlated with increasing HbA_{1c} levels ($r^2 = 0.379$, $P < 0.01$). In non-diabetic individuals, 4.2% of monomeric NAMPT was found, compared with 29% in T2DM patients.
Bawah et al. **[131]**	2019	70 GDM pregnant women 70 controls	During the first trimester, higher serum eNAMPT levels were found in women who subsequently developed GDM ($P < 0.0001$). Increased levels of eNAMPT were associated with GDM [OR = 1.342 (CI = 1.185-1.518), $P < 0.0001$]. Furthermore, an ROC analysis showed that eNAMPT can predict GDM (sensitivity = 87.1%, specificity = 70%, AUC = 0.799).
Hetta et al. **[129]**	2018	80 T2DM 40 controls	T2DM patients had higher levels of serum eNAMPT compared to controls ($P = 0.001$). In the T2DM group, a positive correlation was found between eNAMPT and IL-6 ($r = 0.47$, $P < 0.0001$), TNF-α ($r = 0.62$, $P < 0.0001$), CRP ($r = 0.40$, $P < 0.002$), WC ($r = 0.38$, $P = 0.001$), BMI ($r = 0.40$, $P = 0.008$) and IR ($r = 0.48$, $P = 0.001$).
Atherosclerosis Zheng et al. **[145]**	2019	56 T2DM patients with plaques 41 T2DM patients without plaques	Patients with atherosclerotic plaques had higher serum eNAMPT levels than patients without plaques (male subgroup: $P = 0.005$; female subgroup: $P = 0.008$). Positive correlations were observed between serum eNAMPT levels and WC ($r = 0.226$, $P = 0.029$), waist-hip ratio ($r = 0.221$, $P = 0.032$), TG ($r = 0.222$, $P = 0.030$) and number of plaques ($r = 0.275$, $P = 0.009$). Furthermore, elevated concentrations of serum eNAMPT was shown to be an independent predictor of the presence of atherosclerotic plaques [OR = 3.315 (CI = 1.496–7.349), $P = 0.003$].
Auguet et al. **[142]**	2016	18 patients with unstable carotid atherosclerotic plaques 13 coronary patients with non-atherosclerotic mammary arteries 16 controls	Higher levels of eNAMPT were found in the secretome of patients with atherosclerotic plaques than in those with non-atherosclerotic mammary arteries ($P = 0.021$). Serum eNAMPT levels were increased in patients with unstable carotid atherosclerotic plaques ($P = 0.037$) and non-atherosclerotic mammary arteries ($P = 0.001$) compared to healthy controls.
Kong et al. **[147]**	2014	39 acute ischaemic cerebral infarctions patients with atherosclerosis 21 patients without atherosclerosis 35 healthy controls	Mean serum eNAMPT levels were significantly higher in patients with atherosclerosis than in those without ($P < 0.001$). Positive correlations of eNAMPT with TG ($P = 0.027$) and glucose ($P = 0.004$) were shown. No correlations were observed between eNAMPT and BMI, TC, HDL-C or LDL-C ($P > 0.05$). A logistic regression analysis revealed that eNAMPT levels were a risk factor for atherosclerosis ($\chi 2 = 8.515$, odds ratio = 37.797, $P = 0.004$).
Kadoglou et al. **[143]**	2012	74 patients with carotid atherosclerosis 38 controls	Patients with carotid atherosclerosis had significantly higher serum eNAMPT levels than controls ($P < 0.001$). eNAMPT negatively correlated with GSM score ($r = -0.366$, $P = 0.022$).

			eNAMPT was also significantly correlated with hsCRP (β = 0.499, P < 0.001) and BMI (β = 0.112, P = 0.038).
Zhong et al. **[146]**	2008	40 MetS patients with carotid plaques 99 MetS patients without carotid plaques 105 controls	Serum eNAMPT levels were significantly higher in MetS patients with carotid plaques than in patients without (P < 0.001) or controls (P < 0.001). LogNAMPT in MetS patients correlated with max-IMT (β = 0.293, P = 0.001) and LDL-c (β = 0.219, P = 0.013) in a multiple regression analysis.
Osteoarthritis Askari et al. **[164]**	2020	150 OA patients 300 controls	Higher serum eNAMPT levels were found in OA patients compared to controls (P < 0.001). eNAMPT also correlated positively with OA (β = 24.71, P < 0.001).
Tsai et al. **[161]**	2020	30 OA patients 30 controls	OA patients had significantly increased serum eNAMPT concentrations compared to controls (P < 0.0001). A positive correlation was observed between serum eNAMPT and VEGF levels (r = 0.668, P < 0.0001).
Fioravanti et al. **[165]**	2018	47 erosive hand OA patients 21 controls	Higher serum eNAMPT levels were found in patients with erosive hand OA compared to controls (P < 0.0005).
Duan et al. **[166]**	2012	30 women with OA 12 controls	Higher synovial, but not plasma, eNAMPT levels were found in OA patients compared to healthy individuals (P < 0.001). Patients with a radiological KL grade 4 presented significantly higher SF eNAMPT levels compared to patients with radiological KL grade 3 (P = 0.001). Furthermore, positive correlations were found between SF eNAMPT levels and SF CTX-II (r = 0.497, P = 0.005) and SF aggrecans fragments, AGG1 (r = 0.451, P = 0.012) and AGG2 (r = 0.434, P = 0.017).
Chen et al. **[167]**	2010	23 OA patients 17 controls	OA patients had significantly increased serum eNAMPT levels compared to controls (P < 0.05). Noteworthy, SF eNAMPT levels were more elevated than paired serum eNAMPT levels in OA subjects (P = 0.004). Serum eNAMPT concentrations correlated positively with SF eNAMPT levels (r = 0.79, P < 0.001).
Rheumatoid arthritis Cheleschi et al. **[177]**	2022	50 RA patients 50 controls	Increased serum eNAMPT levels were found in RA patients compared to healthy controls (P < 0.001).
Ali et al. **[178]**	2020	60 RA patients 30 controls	Serum eNAMPT concentrations were significantly more elevated in RA patients compared to controls (P = 0.013). In this study, eNAMPT levels correlated with those of chemerin (r = 0.328, P ≤ 0.01) and with the chemerin/eNAMPT ratio (r = -0.599, P ≤ 0.01).
Sglunda et al. **[181]**	2014	40 RA patients 30 controls	Serum eNAMPT levels were significantly higher in RA patients than in healthy controls (P = 0.034). eNAMPT was positively

			correlated with DAS28 (r = 0.383, P = 0.015) and CRP levels (r = 0.456, P = 0.003) and negatively correlated with anti-CCP levels (r = -0.400, P = 0.011). Noteworthy, serum eNAMPT concentrations decreased significantly after three months of nonsteroidal antirheumatic drugs treatment compared to baseline values (P < 0.0001). This eNAMPT reduction was associated with a decrease in DAS28 (r = 0.378, P = 0.018) and CRP (r = 0.386, P = 0.015) and predicted an amelioration in DAS28 after 12 months of treatment (P = 0.031, R^2 = 10.1%). Finally, in RA patients, the reduction in eNAMPT levels significantly predicted a rise in total cholesterol (P = 0.015).
El-Hini et al. **[183]**	2013	40 RA patients 40 controls	Elevated serum eNAMPT levels were found in RA patients compared to healthy controls (P = 0.000). In addition, eNAMPT concentrations positively correlated with insulin (r = 0.303, P = 0.05), HOMA-IR (r = 0.346, P = 0.029), HOMA-B (r = 0.434, P = 0.005), cholesterol (r = 0.501, P = 0.001), TG (r = 0.471, P = 0.002), LDL-C (r = 0.319, P = 0.045) and disease activity score (DAS moderate: r = 0.329, P = 0.038; DAS severe >5: r = 0.528, P = 0.003). A negative correlation was also found with HDL-C (r = -0.398, P = 0.011) and adiponectin (r = -0.686, P = 0.000).
Šenolt et al. **[182]**	2011	29 RA patients 33 controls	Serum eNAMPT levels were significantly increased in RA patients than in healthy controls (P = 0.026). Noteworthy, eNAMPT levels of RA patients at week 16 of rituximab treatment were close to those of controls (P = 0.086). In addition, serum eNAMPT levels correlated positively with the total number of B cells (rs = 0.417, P = 0.025). However, eNAMPT levels did not correlate with DAS28 (rs = -0.021, P = 0.913), with CRP (rs = 0.091, P = 0.640) or with IgM-RF levels (rs = -0.276, P = 0.147).
Inflammatory bowel disease			
Colombo et al. **[199]**	2023	180 IBD patients (128 CD, 52 UC) 18 controls	Higher serum eNAMPT levels were found in IBD patients compared to controls (P < 0.0001). No differences in eNAMPT concentrations were observed between UC and CD patients (P > 0.05). Serum eNAMPT concentrations correlated positively with hsCRP (r = 0.62, P = 0.0001), severity score (r = 0.40, P = 0.0001), BMI (r = 0.56, P = 0.001) and IL-6 (r = 0.36, P = 0.001) and negatively with IL-10 (r = -0.55, P = 0.001). eNAMPT levels were significantly lower in patients responsive to adalimumab treatment than in non-responsive patients (P < 0.001). Furthermore, an ROC analysis showed that eNAMPT is able to discriminate responsive patients from non-responsive patients (AUC = 0.71, CI = 0.56 - 0.86).
Saadoun et al. **[198]**	2021	85 IBD patients (56 UC, 29 CD) 30 controls	Increased serum eNAMPT levels were found in IBD patients compared to healthy controls (P < 0.001). In UC patients, eNAMPT concentrations correlated with BMI (r = 0.31, P = 0.02), CRP (r = 0.58, P < 0.001), ESR (r = 0.58, P < 0.001), TLC (r = 0.28, P = 0.04), FC (r = 0.69, P<0.001) and serum albumin (r = -0.54, P < 0.001). In CD patients, eNAMPT levels correlated positively with ESR (r = 0.44, P = 0.02), CRP (r = 0.48, P = 0.01)

			and FC (r = 0.64, P < 0.001). An ROC curve analysis demonstrated that eNAMPT could detect active UC with high efficacy (sensitivity = 92.9%, specificity = 86.7%, AUC = 0.911).
Neubauer et al. **[195]**	2019	240 IBD patients (127 UC, 113 CD) 20 IBS-controls 40 controls	Higher serum eNAMPT levels were found in IBD patients than in IBS and healthy controls (P = 0.018). In addition, patients with active UC had significantly higher serum eNAMPT levels than patients with inactive UC (P = 0.001). No difference was found between patients with active and inactive CD. In UC patients, eNAMPT levels correlated positively with Rachmilewitz index (RI) (ρ = 0.28, P = 0.002) and the Mayo endoscopic score (ρ = 0.47, P < 0.0001). eNAMPT levels correlated negatively with iron (UC: r = −0.30, P = 0.006; CD : r = −0.34, P = 0.003), Tf (UC: r = −0.34, P = 0.001; CD: r= −0.28, P = 0.018) and Alb (UC: r = −0.28, P = 0.006; CD: r= −0.35, P = 0.001), and positively with PLT (UC: r = 0.20, P = 0.030), WBC (UC: r = 0.18, P = 0.044; CD: r = 0.27, P = 0.009), ESR (UC: r = 0.41, P < 0.001), and hsCRP (UC: r = 0.37, P = 0.002; CD: r = 0.35, P = 0.013). Serum eNAMPT levels were also positively correlated with NAMPT expression in leucocytes in 16 IBD patients (r = 0.77, P < 0.001).
Dogan et al. **[196]**	2016	31 UC patients 29 controls	Serum eNAMPT levels were significantly higher in patients with active UC than in controls (P < 0.05). In addition, eNAMPT levels were significantly higher in the active disease period compared with the remission period (P = 0.01).
Waluga et al. **[194]**	2014	40 IBD patients (16 UC, 24 CD) 16 controls	Higher serum eNAMPT levels were found in IBD patients compared to healthy controls (P < 0.05) Noteworthy, corticosteroids and/or azathioprine treatment significantly reduced eNAMPT concentrations (P < 0.05) in CD patients, although these levels remained higher than in healthy controls (P < 0.05).
ALI / ARDS Bime et al. **[208]**	2022	Study cohort 1 (248 ARDS patients 70 controls) Study cohort 2 (100 ARDS patients 78 controls)	In patients with ARDS, plasma eNAMPT concentrations were significantly more elevated than in healthy controls (P < 0.01). Furthermore, eNAMPT was able to discriminate ARDS patients from healthy individuals, as shown by an ROC analysis (Cohort 1: AUC = 0.86, 95%CI = 0.82-0.90, P < 0.001; Cohort 2: AUC = 0.85, 95%CI = 0.8-0.9, P < 0.0001).
Lee et al. **[205]**	2019	110 ALI patients 32 controls	Serum eNAMPT levels were higher in ALI patients than in control individuals (P < 0.001). A negative correlation between eNAMPT levels and survival rate of ALI patients was found (P = 0.002). In addition, increased eNAMPT levels positively correlated with IL-6 (ρ = 0.584, P < 0.001), IL-8 (ρ = 0.313, P = 0.001), IL-10 (ρ = 0.319, P = 0.001) and MCP-1 (ρ = 0.242, P = 0.011).
Ye et al. **[29]**	2005	3 ALI patients 3 controls	Higher serum and BAL eNAMPT levels were found in ALI patients compared to healthy controls (P < 0.01).

Cancer Sawicka-Gutaj et al. **[246]**	2022	22 patients with adrenocortical carcinomas 26 patients with benign adrenocortical tumors	Serum eNAMPT levels were significantly higher in patients with adrenocortical carcinomas than in patients with benign adrenocortical tumors (P = 0.003). Furthermore, eNAMPT concentrations were higher in patients with advanced clinical stage with metastases compared with other patients (P = 0.022). Finally, an ROC analysis showed that serum eNAMPT levels were able to distinguish patients with adrenocortical carcinomas from patients with benign tumours (sensitivity = 50%, specificity = 92.3%, AUC = 0.739, P = 0.001).
Pazgan-Simon et al. **[259]**	2020	69 HCC patients 20 controls	Serum eNAMPT concentrations were significantly more elevated in HCC patients compared with healthy controls (P = 0.04).
Sun et al. **[226]**	2020	34 PCa patients 130 high-risk subjects without PCa 105 non-age-matched controls 27 age-matched controls	Plasma eNAMPT levels of PCa patients were significantly higher than those of high-risk subjects without PCa (P < 0.05), non-age-matched controls (P < 0.01) and age-matched controls (P < 0.001). eNAMPT concentrations were significantly more elevated in extraprostatic-invasive PCa than in organ-confined PCa (P = 0.028). In line with this, plasma eNAMPT levels significantly correlated with PCa tumour stages (P = 0.041). An ROC analysis revealed that the measurement of plasma eNAMPT levels could be used to diagnose PCa (sensitivity = 79%, specificity = 82%, AUC = 0.79, P < 0.05).
Audrito et al. **[23]**	2018	163 BRAF-mutated melanoma patients (113 metastatic melanoma, 50 localized melanoma) 38 controls	Higher plasma eNAMPT levels were found in patients with metastatic melanoma compared to patients with localized stages I-II melanoma and controls (P ≤ 0.0001). In addition, eNAMPT correlated positively with LDH, a marker of tumour burden, in 39 patients (r = 0.41, P = 0.008). Melanoma patients exhibiting PD-L1+ lesions had significantly increased plasma levels of eNAMPT compared to patients with PD-L1- lesions (P ≤ 0.01).
Cymbaluk-Ploska et al. **[241]**	2018	78 patients with endometrial cancer 63 controls	In patients with endometrial cancer, serum eNAMPT concentrations were significantly higher than in controls with a normal endometrium (P = 0.002). Furthermore, eNAMPT levels were higher in patients with highly advanced cancer compared to those with less advanced cancers (P = 0.0002), as well as in G3 versus G2 grading cancers (P = 0.002), in patients with >2cm melanoma versus those with <2cm melanoma (P = 0.003) and in patients with deep myometrium infiltration compared to those with superficial infiltration (P = 0.004). In line with this, in patients with endometrial cancer, high levels of eNAMPT correlated with shorter overall survival (P = 0.0001). Finally, an ROC analysis showed that eNAMPT was able to distinguish patients with endometrial cancer from individuals with benign endometrial lesions (AUC = 0.89, 95%CI = 0.74-0.9, P < 0.002).
Sowa et al. **[260]**	2018	59 patients with parotid gland tumour (30 PA, 21 WT, 8 ACC) 30 controls	Significantly higher serum eNAMPT levels were found in patients with parotid gland tumour (PA, WT and ACC) than in healthy controls (P < 0.05).

Abbreviations: ACC, acinic cell carcinoma; Alb, albumin; ALI, acute lung injury; Ang-2, angiotensin-2; ARDS, acute respiratory distress syndrome; AUC, area under the curve; BAL, bronchoalveolar lavage; BMI, body mass index; CCP, cyclic citrullinated peptide; CD, Crohn's disease; CI, confidence interval; CRP, C-reactive protein; CTX-II, C-terminal telopeptide of collagen type II; DAS28, disease activity score-28; DBP, diastolic blood pressure; E2, estradiol; eNAMPT, extracellular nicotinamide phosphoribosyltransferase; ESR, erythrocyte sedimentation; FBG, fasting blood glucose; FC, fecal calprotectin; FPG, fasting plasma glucose; GDM, gestational diabetes mellitus; GSM, gray scale median; HbA_{1c}, hemoglobin A1C; HCC, hepatocellular carcinoma; HDL-C, high-density lipoprotein-cholesterol; hs, high-sensitivity; HOMA-B, homeostatic model assessment of β-cell function; HOMA-IR, homeostatic model assessment of insulin resistance; IBD, inflammatory bowel disease; IBS, irritable bowel syndrome; ICAM-1, intercellular adhesion molecule-1; IFG, impaired fasting glucose; IgM, immunoglobulin M; IL, interleukin; IMT, intima-media thickness; IR, insulin resistance; KL, Kellgren-Lawrence; LDH, lactate dehydrogenase; LDL-C, low-density lipoprotein-cholesterol; MetS, metabolic syndrome; MCP-1, monocyte chemoattractant protein-1; OA, osteoarthritis; PA, pleiomorphic adenoma; PCa, prostate cancer; PD-L1, programmed cell death-ligand 1; PLT, platelet count; RA, rheumatoid arthritis; RF, rheumatoid factor; ROC, receiver operating characteristic; SBP, systolic blood pressure; SDS-BMI, BMI s.d. score; SF, synovial fluid; SHBG, sex hormone-binding globulin; T2DM, type 2 diabetes mellitus; TC, total cholesterol; TLC, total leucocyte count; Tf, transferrin; TG, triglycerides; TNF-α, tumour necrosis factor-α; UC, ulcerative colitis; VEGF, vascular endothelial growth factor; VCAM-1, vascular cell adhesion molecule-1; WBC, white blood cells; WC, waist circumference; WT, Warthin's tumour.

Table 2: Preclinical *in vitro* studies assessing the neutralizing effect of anti-eNAMPT antibodies.

Author	Year	Cells	Treatment	Results
Pillai et al. **[261].**	2013	Neonatal rat cardiomyocytes	Anti-eNAMPT pAb (Lampire Biological Laboratories [206])	Anti-eNAMPT pAb blocked eNAMPT-induced increase in leucine incorporation into cardiomyocyte proteins ($P < 0.001$) and increase in cardiomyocyte size ($P < 0.001$), indicating that the antibody prevented the prohypertrophic effect of eNAMPT.
Audrito et al. **[64]**	2015	Nurse-like cells (NLC)	50µg/mL of anti-eNAMPT pAb (Lampire Biological Laboratories [206])	eNAMPT-induced STAT3 signalling activation was significantly reduced by anti-eNAMPT pAb in NLCs ($P = 0.02$).
Liu et al. **[262]**	2015	NCI-H446 cells	10µg/mL of anti-eNAMPT antibody (Santa Cruz Biotechnology)	Neutralization of eNAMPT significantly prevented NCI-H446 cell transendothelial migration ($P < 0.01$).
Zhang et al. **[263]**	2018	Macrophages isolated from human PBMC, and polarized into M2 phenotype	Anti-eNAMPT antibody (LifeSpan Biosciences)	M2 macrophages treatment with anti-eNAMPT antibody reduced CD206 expression levels as well as IL-1ra and IL-10 release ($P < 0.05$).
Colombo et al. **[193]**	2020	4T1 cells	10 or 50µg/mL of anti-eNAMPT mAb (C269)	C269 antibody dose-dependently reduced eNAMPT-induced STAT3 phosphorylation in 4T1 cells.
Quijada et al. **[203]**	2020	Human lung endothelial cells (ECs)	10µg/mL of anti-eNAMPT pAb or 10µg/mL of ALT-100 anti-eNAMPT mAb	Anti-eNAMPT pAb significantly diminished eNAMPT-induced NF-kB and MAPK signalling pathways activation in human lung ECs ($P < 0.05$). Furthermore, both anti-eNAMPT mAb and pAb reduced eNAMPT-induced decline in EC barrier integrity (determined by measurement of ECs trans-endothelial electrical resistance) ($P < 0.05$).
Sun et al. **[229]**	2021	DU145 and PC3 cells	10µg/mL of ALT-100 anti-eNAMPT mAb	Treatment of PCa cells with ALT-100 significantly reduced eNAMPT-induced NF-kB phosphorylation ($P < 0.05$).
Xiao et al. **[227]**	2021	A549 and H1299 cells	100ng/mL of anti-eNAMPT pAb (A300-778, Invitrogen)	Anti-eNAMPT pAb inhibited radiation-induced migration and invasion of A549 cells ($P < 0.01$). In addition, the antibody reversed the radiation-mediated upregulation of Snail in A549 and H1299 cells ($P < 0.01$).
Colombo et al. **[33]**	2022	Murine peritoneal macrophages (PEC)	10µg/mL of anti-eNAMPT mAb (C269)	C269 antibody reduced eNAMPT-mediated upregulation of inflammatory M1-related gene expression (Cox2, Nos2, IL-1β, Cxcl9, Cxcl10, IL-6) in PECs ($P < 0.05$).

Abbreviations: CD206, cluster of differentiation 206; Cox2, cyclooxygenase-2; Cxcl, chemokine C-X-C motif ligand; EC, endothelial cell; eNAMPT, extracellular nicotinamide phosphoribosyltransferase; IL, interleukin; mAb, monoclonal antibody; MAPK, mitogen-activated protein kinase; NF-kB, nuclear factor kappa-light-chain-enhancer of activated B cells; NLC, nurse-like cells; Nos2, nitric oxide synthase 2; pAb, polyclonal antibody; PBMC, peripheral blood mononuclear cell; PCa, prostate cancer; PEC, peritoneal macrophages; STAT3, signal transducer and activator of transcription 3.

Table 3: Preclinical *in vivo* studies evaluating the therapeutic potential of anti-eNAMPT antibodies.

Author	Year	Disease model	Treatment (dose/administration)	Results
Hong et al. **[206]**	2008	Murine model of VILI	Anti-eNAMPT pAb from Lampire Biological Laboratories (IT, 70µL, 30min before VILI).	Anti-eNAMPT pAb significantly reduced the VILI-mediated BAL PMN accumulation and tissue albumin leakage in mice ($P < 0.05$). eNAMPT-induced accumulation of BAL PMNs was also significantly diminished in the presence of this antibody ($P < 0.05$).
Kieswich et al. **[120]**	2016	Mouse model of diabetes (HFD-fed mice)	Anti-eNAMPT pAb from LifeSpan Biosciences (IP, 2.5µg/mL, four separate doses during weeks 9–10).	Administration of the anti-eNAMPT antibody reversed the diabetic phenotype of HFD-fed mice (serum glucose and HOMA-IR reduction, $P < 0.05$; QUICKI increase, $P < 0.01$). In the same mice, the latter antibody reduced β-cell dysfunction (increased insulinaemia and islet size; $P < 0.05$) and improved tissue and systemic inflammation (reduced expression of IL-1β, TNF-α, CCL2 in isolated islets; $P < 0.01$).
Colombo et al. **[193]**	2020	DNBS- and DSS-induced colitis mouse models	C269 anti-eNAMPT mAb (IP, 2.5mg/kg/mouse, injected at day 0 and 3 post-DNBS induction and at day 0–3–7 days post-DSS induction).	C269 antibody injection reduced body weight loss (DNBS: $P < 0.001$; DSS: $P < 0.01$), colon shortening (DNBS and DSS: $P < 0.001$), transmural necrosis and oedema (assessed by histological analysis, DNBS: $P < 0.01$, DSS: $P < 0.05$), in DNBS- or DSS-treated mice.
Quijada et al. **[203]**	2020	"One-hit" (LPS) and "two-hit" (LPS/VILI) ARDS mouse models	Anti-eNAMPT pAb and ALT-100 anti-eNAMPT mAb (IV, 4mg/kg and 0.4mg/kg respectively, injected concomitantly to LPS challenge and prior to mechanical challenge).	Both anti-eNAMPT pAb and ALT-100 reduced LPS-induced histological evidence of inflammation and injury ($P < 0.05$) as well as BAL protein content ($P < 0.05$) and BAL PMN counts ($P < 0.05$) in preclinical "one-hit" and "two-hit" ARDS mouse models. In addition, ALT-100 decreased plasma IL-6 levels in mice exposed to "one-hit" or "two-hit" challenge ($P < 0.05$).
Sun et al. **[229]**	2021	PCa orthotopic xenograft mouse models	ALT-100 anti-eNAMPT mAb (IP, 0.4mg/kg in PBS, 1time/week for 12 weeks).	ALT-100 antibody significantly elevated the probability of survival of SCID mice bearing orthotopic DU145 or PC3 xenografts compared to control treatment ($P < 0.05$). In addition, ALT-100 induced a significant reduction in DU145 and PC3 tumour size ($P < 0.05$).
Ahmed et al. **[252]**	2021	PAH hypoxia/sugen rat model	ALT-100 anti-eNAMPT mAb (IP, 1mg/kg, injection beginning at week 4, then 2times/week).	ALT-100 significantly diminished vessel wall thickness ($P < 0.01$), RVSP ($P < 0.05$), RV/(S+LV) ratio ($P < 0.05$), plasma eNAMPT levels, plasma IL-6 levels and plasma TNF-α levels ($P < 0.05$) in rats exposed to hypoxia/sugen.
Garcia et al. **[264]**	2021	WTLI murine model of radiation pneumonitis	Anti-eNAMPT pAb or ALT-100 anti-eNAMPT mAb (IP, 4mg/kg and 0.4mg/kg respectively, injection 1day post WTLI, then 1time/week).	Anti-eNAMPT pAb and ALT-100 significantly decreased WTLI-induced histologic inflammatory injury, BAL protein levels, BAL cell counts and RILI severity score in WTLI 20Gy-exposed mice ($P < 0.05$). In addition, ALT-100 reduced plasma levels of eNAMPT, IL-6 and IL-1β in these same mice ($P < 0.05$).

Bermudez et al. **[202]**	2022	"One-hit" (LPS) and "two-hit"(LPS/VILI or blast trauma/VILI) ARDS rat models	Anti-eNAMPT pAb or ALT-100 anti-eNAMPT mAb (IV, 4mg/kg and 0.4mg/kg respectively, concomitantly to LPS challenge or after blast exposure, and prior to mechanical ventilation).	Both anti-eNAMPT pAb and ALT-100 reduced LPS-induced histological evidence of inflammation and injury ($P < 0.05$), BAL protein content ($P < 0.05$) and BAL PMN counts ($P < 0.05$) in preclinical "one-hit" (LPS) and "two-hit" (LPS/VILI) ARDS rat models. In "two-hit" (blast-trauma/VILI) rats, anti-eNAMPT pAb diminished histological evidence of inflammation and injury compared to PBS ($P < 0.05$).
Sammani et al. **[204]**	2022	Porcine ARDS/VILI model	ALT-100 anti-eNAMPT mAb (IV, 0.4mg/kg, delivered either 2h or 6h after initiation of LPS/VILI).	ALT-100 antibody decreased total BAL cell and BAL PMN counts, lung tissue wet/dry weight ratio, plasma levels of IL-6, IL-1Ra, Ang-2; and BAL protein and lung tissue albumin levels in LPS/VILI-challenged pigs ($P < 0.05$). In addition, ALT-100 attenuated acute kidney injury in LPS/VILI-challenged pigs, as evidenced by reductions in histopathologic score, caspase-3 cleavage staining levels and plasma lipocalin levels ($P < 0.05$).
Garcia et al. **[253]**	2022	WTLI murine model of radiation fibrosis	Anti-eNAMPT pAb or ALT-100 anti-eNAMPT mAb (IP, 4mg/kg and 0.4mg/kg respectively, injection 4h post WTLI, then 1time/week).	Both anti-eNAMPT pAb and ALT-100 mAb significantly reduced WTLI-mediated histologic lung injury, BAL protein levels and BAL cell counts compared with the PBS/IgG1 control ($P < 0.05$). In addition, ALT-100 mAb significantly decreased trichrome blue staining, an indicator of lung fibrosis, and plasma IL-1β levels ($P < 0.05$).
Tumurkhuu et al. **[254]**	2022	Murine model of pristane-induced lung vasculitis and diffuse alveolar hemorrhage	ALT-100 anti-eNAMPT mAb (IP, 1mg/kg, delivered on days 1 and 7).	ALT-100 antibody significantly diminished immune cell infiltration in lung perivascular area in pristane-challenged mice ($P < 0.05$). Furthermore, in the same mice, ALT-100 significantly attenuated pristane-induced increase in BAL cell counts and protein levels as well as pristane-induced NF-kB inflammatory signalling activation ($P < 0.05$).
Sun et al. **[255]**	2023	Streptozotocin (STZ)/HFD murine NAFLD model	ALT-100 anti-eNAMPT mAb (IP, 0.4mg/kg, injection 1time/week from week 9 to week 12).	STZ/HFD mice treatment with ALT-100 antibody reduced NASH severity, as evidenced by reductions in steatosis score, hepatic triglyceride levels and NAFLD activity score ($P < 0.05$). In addition, eNAMPT neutralization by ALT-100 also decreased plasma TNF-α levels and hepatic SNAI1 expression levels in the same mice ($P < 0.05$).

Abbreviations: Ang-2, angiopoietin-2; ARDS, acute respiratory distress syndrome; BAL, bronchoalveolar lavage; CCL-2, chemokine (C-C motif) ligand 2; DNBS, dinitrobenzene sulfonic acid; DSS, dextran sulfate sodium; eNAMPT, extracellular nicotinamide phosphoribosyltransferase; HFD, high fat diet; HOMA-IR, homeostatic model assessment of insulin resistance; IL, interleukin; IP, intraperitoneally; IT, intratracheally; IV, intravenously; LPS, lipopolysaccharide; mAb, monoclonal antibody; NAFLD, non-alcoholic fatty liver disease; NASH, non-alcoholic steatohepatitis; pAb, polyclonal antibody; PBS, phosphate-buffered saline; PCa, prostate cancer; PAH, pulmonary arterial hypertension; PMNs, polymorphonuclear neutrophils; QUICKI, Quantitative Insulin Sensitivity Check Index; RILI, radiation-induced lung injury; RVSP, right ventricular systolic pressure, RV/ (S + LV), ratio of the weight of the right ventricle to that of the septum plus left ventricle; SCID, severe combined immunodeficiency; STZ, streptozotocin; TNF-α, tumour necrosis factor α; VILI, ventilator-induced lung injury; WTLI, whole thoracic lung irradiation.

References

[1] A. Garten, S. Schuster, M. Penke, T. Gorski, T. de Giorgis, and W. Kiess, "Physiological and pathophysiological roles of NAMPT and NAD metabolism," *Nat. Rev. Endocrinol.*, vol. 11, no. 9, pp. 535–546, Sep. 2015, doi: 10.1038/nrendo.2015.117.

[2] A. A. Grolla, C. Travelli, A. A. Genazzani, and J. K. Sethi, "Extracellular nicotinamide phosphoribosyltransferase, a new cancer metabokine," *Br. J. Pharmacol.*, vol. 173, no. 14, Art. no. 14, 2016, doi: 10.1111/bph.13505.

[3] F. Carbone *et al.*, "Regulation and Function of Extracellular Nicotinamide Phosphoribosyltransferase/Visfatin," *Compr. Physiol.*, vol. 7, no. 2, Art. no. 2, 16 2017, doi: 10.1002/cphy.c160029.

[4] A. Chiarugi, C. Dölle, R. Felici, and M. Ziegler, "The NAD metabolome — a key determinant of cancer cell biology," *Nat. Rev. Cancer*, vol. 12, no. 11, pp. 741–752, Nov. 2012, doi: 10.1038/nrc3340.

[5] M. S. Ghanem, F. Monacelli, and A. Nencioni, "Advances in NAD-Lowering Agents for Cancer Treatment," *Nutrients*, vol. 13, no. 5, p. 1665, May 2021, doi: 10.3390/nu13051665.

[6] H. Chen *et al.*, "Gene organization, alternate splicing and expression pattern of porcine visfatin gene," *Domest. Anim. Endocrinol.*, vol. 32, no. 3, pp. 235–245, Apr. 2007, doi: 10.1016/j.domaniend.2006.03.004.

[7] J. R. Revollo, A. A. Grimm, and S. Imai, "The regulation of nicotinamide adenine dinucleotide biosynthesis by Nampt/PBEF/visfatin in mammals:," *Curr. Opin. Gastroenterol.*, vol. 23, no. 2, pp. 164–170, Mar. 2007, doi: 10.1097/MOG.0b013e32801b3c8f.

[8] J. Li, F. Meng, C. Song, Y. Wang, and F. C. Leung, "Characterization of chicken visfatin gene: cDNA cloning, tissue distribution, and promoter analysis," *Poult. Sci.*, vol. 91, no. 11, pp. 2885–2894, Nov. 2012, doi: 10.3382/ps.2012-02315.

[9] A. Rongvaux *et al.*, "Pre-B-cell colony-enhancing factor, whose expression is up-regulated in activated lymphocytes, is a nicotinamide phosphoribosyltransferase, a cytosolic enzyme involved in NAD biosynthesis," *Eur. J. Immunol.*, vol. 32, no. 11, pp. 3225–3234, Nov. 2002, doi: 10.1002/1521-4141(200211)32:11<3225::AID-IMMU3225>3.0.CO;2-L.

[10] P. R. Martin, R. J. Shea, and M. H. Mulks, "Identification of a Plasmid-Encoded Gene from *Haemophilus ducreyi* Which Confers NAD Independence," *J. Bacteriol.*, vol. 183, no. 4, pp. 1168–1174, Feb. 2001, doi: 10.1128/JB.183.4.1168-1174.2001.

[11] T. Kitani, S. Okuno, and H. Fujisawa, "Growth phase-dependent changes in the subcellular localization of pre-B-cell colony-enhancing factor [1]," *FEBS Lett.*, vol. 544, no. 1–3, pp. 74–78, Jun. 2003, doi: 10.1016/S0014-5793(03)00476-9.

[12] P. Svoboda *et al.*, "Nuclear transport of nicotinamide phosphoribosyltransferase is cell cycle–dependent in mammalian cells, and its inhibition slows cell growth," *J. Biol. Chem.*, vol. 294, no. 22, pp. 8676–8689, May 2019, doi: 10.1074/jbc.RA118.003505.

[13] X. Wang *et al.*, "Subcellular NAMPT-mediated NAD $^{+}$ salvage pathways and their roles in bioenergetics and neuronal protection after ischemic injury," *J. Neurochem.*, vol. 151, no. 6, pp. 732–748, Dec. 2019, doi: 10.1111/jnc.14878.

[14] M. Pittelli *et al.*, "Inhibition of Nicotinamide Phosphoribosyltransferase," *J. Biol. Chem.*, vol. 285, no. 44, pp. 34106–34114, Oct. 2010, doi: 10.1074/jbc.M110.136739.

[15] H. Yang *et al.*, "Nutrient-Sensitive Mitochondrial NAD+ Levels Dictate Cell Survival," *Cell*, vol. 130, no. 6, pp. 1095–1107, Sep. 2007, doi: 10.1016/j.cell.2007.07.035.

[16] M. Yoshida *et al.*, "Extracellular Vesicle-Contained eNAMPT Delays Aging and Extends Lifespan in Mice," *Cell Metab.*, vol. 30, no. 2, pp. 329-342.e5, Aug. 2019, doi: 10.1016/j.cmet.2019.05.015.

[17] B. Samal, Y. Sun, G. Stearns, C. Xie, S. Suggs, and I. McNiece, “Cloning and characterization of the cDNA encoding a novel human pre-B-cell colony-enhancing factor,” *Mol. Cell. Biol.*, vol. 14, no. 2, pp. 1431–1437, Feb. 1994, doi: 10.1128/mcb.14.2.1431-1437.1994.

[18] J. R. Revollo *et al.*, “Nampt/PBEF/Visfatin Regulates Insulin Secretion in β Cells as a Systemic NAD Biosynthetic Enzyme,” *Cell Metab.*, vol. 6, no. 5, pp. 363–375, Nov. 2007, doi: 10.1016/j.cmet.2007.09.003.

[19] Y.-H. Chang, D.-M. Chang, K.-C. Lin, S.-J. Shin, and Y.-J. Lee, “Visfatin in overweight/obesity, type 2 diabetes mellitus, insulin resistance, metabolic syndrome and cardiovascular diseases: a meta-analysis and systemic review,” *Diabetes Metab. Res. Rev.*, vol. 27, no. 6, pp. 515–527, 2011, doi: 10.1002/dmrr.1201.

[20] P.-L. Yu, C. Wang, W. Li, and F.-X. Zhang, “Visfatin Level and The Risk of Hypertension and Cerebrovascular Accident: A Systematic Review and Meta-Analysis,” *Horm. Metab. Res. Horm. Stoffwechselforschung Horm. Metab.*, vol. 51, no. 4, pp. 220–229, Apr. 2019, doi: 10.1055/a-0867-1333.

[21] M. Mohammadi, F. Mianabadi, and H. Mehrad-Majd, “Circulating visfatin levels and cancers risk: A systematic review and meta-analysis,” *J. Cell. Physiol.*, vol. 234, no. 4, pp. 5011–5022, Apr. 2019, doi: 10.1002/jcp.27302.

[22] Y.-C. Lin, H.-C. Wu, C.-C. Liao, Y.-C. Chou, S.-F. Pan, and C.-M. Chiu, “Secretion of One Adipokine Nampt/Visfatin Suppresses the Inflammatory Stress-Induced NF- *κ* B Activity and Affects Nampt-Dependent Cell Viability in Huh-7 Cells,” *Mediators Inflamm.*, vol. 2015, pp. 1–9, 2015, doi: 10.1155/2015/392471.

[23] V. Audrito *et al.*, “Extracellular nicotinamide phosphoribosyltransferase (eNAMPT) is a novel marker for patients with BRAF-mutated metastatic melanoma,” *Oncotarget*, vol. 9, no. 27, pp. 18997–19005, Apr. 2018, doi: 10.18632/oncotarget.24871.

[24] C. Benedict *et al.*, “Diurnal Rhythm of Circulating Nicotinamide Phosphoribosyltransferase (Nampt/Visfatin/PBEF): Impact of Sleep Loss and Relation to Glucose Metabolism,” *J. Clin. Endocrinol. Metab.*, vol. 97, no. 2, pp. E218–E222, Feb. 2012, doi: 10.1210/jc.2011-2241.

[25] E. Plati, E. Kouskouni, A. Malamitsi-Puchner, M. Boutsikou, G. Kaparos, and S. Baka, “Visfatin and leptin levels in women with polycystic ovaries undergoing ovarian stimulation,” *Fertil. Steril.*, vol. 94, no. 4, pp. 1451–1456, Sep. 2010, doi: 10.1016/j.fertnstert.2009.04.055.

[26] J. J. Kim *et al.*, “Serum visfatin levels in non-obese women with polycystic ovary syndrome and matched controls,” *Obstet. Gynecol. Sci.*, vol. 61, no. 2, p. 253, 2018, doi: 10.5468/ogs.2018.61.2.253.

[27] F. Brentano *et al.*, “Pre–B cell colony-enhancing factor/visfatin, a new marker of inflammation in rheumatoid arthritis with proinflammatory and matrix-degrading activities,” *Arthritis Rheum.*, vol. 56, no. 9, pp. 2829–2839, Sep. 2007, doi: 10.1002/art.22833.

[28] I. Tsouma *et al.*, “Correlation of visfatin levels and lipoprotein lipid profiles in women with polycystic ovary syndrome undergoing ovarian stimulation,” *Gynecol. Endocrinol.*, vol. 30, no. 7, pp. 516–519, Jul. 2014, doi: 10.3109/09513590.2014.896896.

[29] S. Q. Ye *et al.*, “Pre–B-Cell Colony-enhancing Factor as a Potential Novel Biomarker in Acute Lung Injury,” *Am. J. Respir. Crit. Care Med.*, vol. 171, no. 4, pp. 361–370, Feb. 2005, doi: 10.1164/rccm.200404-563OC.

[30] I. Mamali, N. D. Roupas, A. K. Armeni, A. Theodoropoulou, K. B. Markou, and N. A. Georgopoulos, “Measurement of salivary resistin, visfatin and adiponectin levels,” *Peptides*, vol. 33, no. 1, pp. 120–124, Jan. 2012, doi: 10.1016/j.peptides.2011.11.007.

[31] M. Hallschmid, H. Randeva, B. K. Tan, W. Kern, and H. Lehnert, “Relationship Between Cerebrospinal Fluid Visfatin (PBEF/Nampt) Levels and Adiposity in Humans,” *Diabetes*, vol. 58, no. 3, pp. 637–640, Mar. 2009, doi: 10.2337/db08-1176.

[32] A. A. Grolla *et al.*, “Nicotinamide phosphoribosyltransferase (NAMPT/PBEF/visfatin) is a tumoural cytokine released from melanoma,” *Pigment Cell Melanoma Res.*, vol. 28, no. 6, pp. 718–729, Nov. 2015, doi: 10.1111/pcmr.12420.

[33] G. Colombo, C. Travelli, C. Porta, and A. A. Genazzani, “Extracellular nicotinamide phosphoribosyltransferase boosts IFNγ-induced macrophage polarization independently of TLR4,” *iScience*, vol. 25, no. 4, p. 104147, Apr. 2022, doi: 10.1016/j.isci.2022.104147.
[34] Y. Lu *et al.*, “Nicotinamide phosphoribosyltransferase secreted from microglia *via* exosome during ischemic injury,” *J. Neurochem.*, vol. 150, no. 6, pp. 723–737, Sep. 2019, doi: 10.1111/jnc.14811.
[35] A. Garten *et al.*, “Nicotinamide phosphoribosyltransferase (NAMPT/PBEF/visfatin) is constitutively released from human hepatocytes,” *Biochem. Biophys. Res. Commun.*, vol. 391, no. 1, pp. 376–381, Jan. 2010, doi: 10.1016/j.bbrc.2009.11.066.
[36] M. Tanaka *et al.*, “Visfatin is released from 3T3-L1 adipocytes via a non-classical pathway,” *Biochem. Biophys. Res. Commun.*, vol. 359, no. 2, pp. 194–201, Jul. 2007, doi: 10.1016/j.bbrc.2007.05.096.
[37] M. J. Yoon *et al.*, “SIRT1-Mediated eNAMPT Secretion from Adipose Tissue Regulates Hypothalamic NAD+ and Function in Mice,” *Cell Metab.*, vol. 21, no. 5, pp. 706–717, May 2015, doi: 10.1016/j.cmet.2015.04.002.
[38] G. Sociali *et al.*, “SIRT6 deacetylase activity regulates NAMPT activity and NAD(P)(H) pools in cancer cells,” *FASEB J.*, vol. 33, no. 3, pp. 3704–3717, Mar. 2019, doi: 10.1096/fj.201800321R.
[39] M.-K. Kim *et al.*, “Crystal Structure of Visfatin/Pre-B Cell Colony-enhancing Factor 1/Nicotinamide Phosphoribosyltransferase, Free and in Complex with the Anti-cancer Agent FK-866,” *J. Mol. Biol.*, vol. 362, no. 1, pp. 66–77, Sep. 2006, doi: 10.1016/j.jmb.2006.06.082.
[40] C. Kuehnemann *et al.*, “Extracellular Nicotinamide Phosphoribosyltransferase Is a Component of the Senescence-Associated Secretory Phenotype,” *Front. Endocrinol.*, vol. 13, p. 935106, Jul. 2022, doi: 10.3389/fendo.2022.935106.
[41] M.-C. Laiguillon *et al.*, “Expression and function of visfatin (Nampt), an adipokine-enzyme involved in inflammatory pathways of osteoarthritis,” *Arthritis Res. Ther.*, vol. 16, no. 1, p. R38, 2014, doi: 10.1186/ar4467.
[42] K. Behrouzfar, M. Alaee, M. Nourbakhsh, Z. Gholinejad, and A. Golestani, “Extracellular NAMPT/visfatin causes p53 deacetylation via NAD production and SIRT1 activation in breast cancer cells,” *Cell Biochem. Funct.*, vol. 35, no. 6, pp. 327–333, Aug. 2017, doi: 10.1002/cbf.3279.
[43] P. Wang, T.-Y. Xu, Y.-F. Guan, D.-F. Su, G.-R. Fan, and C.-Y. Miao, “Perivascular adipose tissue-derived visfatin is a vascular smooth muscle cell growth factor: role of nicotinamide mononucleotide,” *Cardiovasc. Res.*, vol. 81, no. 2, pp. 370–380, Feb. 2009, doi: 10.1093/cvr/cvn288.
[44] L. Formentini, F. Moroni, and A. Chiarugi, “Detection and pharmacological modulation of nicotinamide mononucleotide (NMN) in vitro and in vivo,” *Biochem. Pharmacol.*, vol. 77, no. 10, pp. 1612–1620, May 2009, doi: 10.1016/j.bcp.2009.02.017.
[45] A. Grozio *et al.*, “Slc12a8 is a nicotinamide mononucleotide transporter,” *Nat. Metab.*, vol. 1, no. 1, pp. 47–57, Jan. 2019, doi: 10.1038/s42255-018-0009-4.
[46] N. Hara, K. Yamada, T. Shibata, H. Osago, and M. Tsuchiya, “Nicotinamide Phosphoribosyltransferase/Visfatin Does Not Catalyze Nicotinamide Mononucleotide Formation in Blood Plasma,” *PLoS ONE*, vol. 6, no. 8, p. e22781, Aug. 2011, doi: 10.1371/journal.pone.0022781.
[47] L. Recinella, G. Orlando, C. Ferrante, A. Chiavaroli, L. Brunetti, and S. Leone, “Adipokines: New Potential Therapeutic Target for Obesity and Metabolic, Rheumatic, and Cardiovascular Diseases,” *Front. Physiol.*, vol. 11, p. 578966, Oct. 2020, doi: 10.3389/fphys.2020.578966.
[48] A. Fukuhara *et al.*, “Visfatin: a protein secreted by visceral fat that mimics the effects of insulin,” *Science*, vol. 307, no. 5708, pp. 426–430, Jan. 2005, doi: 10.1126/science.1097243.
[49] B. K. Tan, J. Chen, J. E. Digby, S. D. Keay, C. R. Kennedy, and H. S. Randeva, “Increased Visfatin Messenger Ribonucleic Acid and Protein Levels in Adipose Tissue and Adipocytes in Women

with Polycystic Ovary Syndrome: Parallel Increase in Plasma Visfatin," *J. Clin. Endocrinol. Metab.*, vol. 91, no. 12, pp. 5022–5028, Dec. 2006, doi: 10.1210/jc.2006-0936.
[50] K.-H. Cheng *et al.*, "Adipocytokines and proinflammatory mediators from abdominal and epicardial adipose tissue in patients with coronary artery disease," *Int. J. Obes.*, vol. 32, no. 2, pp. 268–274, Feb. 2008, doi: 10.1038/sj.ijo.0803726.
[51] A. Fukuhara *et al.*, "Retraction," *Science*, vol. 318, no. 5850, p. 565, Oct. 2007, doi: 10.1126/science.318.5850.565b.
[52] H. Xie *et al.*, "Insulin-like effects of visfatin on human osteoblasts," *Calcif. Tissue Int.*, vol. 80, no. 3, pp. 201–210, Mar. 2007, doi: 10.1007/s00223-006-0155-7.
[53] H. K. Song *et al.*, "Visfatin: a new player in mesangial cell physiology and diabetic nephropathy," *Am. J. Physiol.-Ren. Physiol.*, vol. 295, no. 5, pp. F1485–F1494, Nov. 2008, doi: 10.1152/ajprenal.90231.2008.
[54] J. E. P. Brown *et al.*, "Visfatin regulates insulin secretion, insulin receptor signalling and mRNA expression of diabetes-related genes in mouse pancreatic b-cells," *J. Mol. Endocrinol.*, p. 8, 2010.
[55] E. Harasim, A. Chabowski, and J. Górski, "Lack of downstream insulin-mimetic effects of visfatin/eNAMPT on glucose and fatty acid metabolism in skeletal muscles," *Acta Physiol. Oxf. Engl.*, vol. 202, no. 1, pp. 21–28, May 2011, doi: 10.1111/j.1748-1716.2011.02254.x.
[56] Q. Cheng, W. Dong, L. Qian, J. Wu, and Y. Peng, "Visfatin inhibits apoptosis of pancreatic β-cell line, MIN6, via the mitogen-activated protein kinase/phosphoinositide 3-kinase pathway," *J. Mol. Endocrinol.*, vol. 47, no. 1, pp. 13–21, Aug. 2011, doi: 10.1530/JME-10-0106.
[57] K. M. Ramsey, K. F. Mills, A. Satoh, and S. Imai, "Age-associated loss of Sirt1-mediated enhancement of glucose-stimulated insulin secretion in beta cell-specific Sirt1-overexpressing (BESTO) mice," *Aging Cell*, vol. 7, no. 1, pp. 78–88, Feb. 2008, doi: 10.1111/j.1474-9726.2007.00355.x.
[58] P. W. Caton, J. Kieswich, M. M. Yaqoob, M. J. Holness, and M. C. Sugden, "Nicotinamide mononucleotide protects against pro-inflammatory cytokine-mediated impairment of mouse islet function," *Diabetologia*, vol. 54, no. 12, pp. 3083–3092, Dec. 2011, doi: 10.1007/s00125-011-2288-0.
[59] J. Yoshino, K. F. Mills, M. J. Yoon, and S. Imai, "Nicotinamide Mononucleotide, a Key NAD+ Intermediate, Treats the Pathophysiology of Diet- and Age-Induced Diabetes in Mice," *Cell Metab.*, vol. 14, no. 4, pp. 528–536, Oct. 2011, doi: 10.1016/j.cmet.2011.08.014.
[60] A. Managò *et al.*, "Extracellular nicotinate phosphoribosyltransferase binds Toll like receptor 4 and mediates inflammation," *Nat. Commun.*, vol. 10, no. 1, Art. no. 1, Sep. 2019, doi: 10.1038/s41467-019-12055-2.
[61] M. R. Yun, J. M. Seo, and H. Y. Park, "Visfatin contributes to the differentiation of monocytes into macrophages through the differential regulation of inflammatory cytokines in THP-1 cells," *Cell. Signal.*, vol. 26, no. 4, Art. no. 4, Apr. 2014, doi: 10.1016/j.cellsig.2013.12.010.
[62] Y. Fan et *al*., "Visfatin/PBEF/Nampt induces EMMPRIN and MMP-9 production in macrophages via the NAMPT-MAPK (p38, ERK1/2)-NF-κB signaling pathway," *Int. J. Mol. Med.*, vol. 27, no. 4, Apr. 2011, doi: 10.3892/ijmm.2011.621.
[63] Y. J. Heo *et al.*, "CCL20 induced by visfatin in macrophages via the NF-κB and MKK3/6-p38 signaling pathways contributes to hepatic stellate cell activation," *Mol. Biol. Rep.*, vol. 47, no. 6, pp. 4285–4293, Jun. 2020, doi: 10.1007/s11033-020-05510-7.
[64] V. Audrito *et al.*, "Extracellular nicotinamide phosphoribosyltransferase (NAMPT) promotes M2 macrophage polarization in chronic lymphocytic leukemia," *Blood*, vol. 125, no. 1, pp. 111–123, Jan. 2015, doi: 10.1182/blood-2014-07-589069.
[65] Y. Li *et al.*, "Extracellular Nampt Promotes Macrophage Survival via a Nonenzymatic Interleukin-6/STAT3 Signaling Mechanism," *J. Biol. Chem.*, vol. 283, no. 50, pp. 34833–34843, Dec. 2008, doi: 10.1074/jbc.M805866200.

[66] M. Gasparrini *et al.*, “Molecular insights into the interaction between human nicotinamide phosphoribosyltransferase and Toll-like receptor 4,” *J. Biol. Chem.*, vol. 298, no. 3, p. 101669, Mar. 2022, doi: 10.1016/j.jbc.2022.101669.
[67] A. R. Moschen *et al.*, “Visfatin, an adipocytokine with proinflammatory and immunomodulating properties,” *J. Immunol. Baltim. Md 1950*, vol. 178, no. 3, pp. 1748–1758, Feb. 2007, doi: 10.4049/jimmunol.178.3.1748.
[68] T. B. Dahl *et al.*, “Increased Expression of Visfatin in Macrophages of Human Unstable Carotid and Coronary Atherosclerosis: Possible Role in Inflammation and Plaque Destabilization,” *Circulation*, vol. 115, no. 8, pp. 972–980, Feb. 2007, doi: 10.1161/CIRCULATIONAHA.106.665893.
[69] J. Skokowa *et al.*, “NAMPT is essential for the G-CSF–induced myeloid differentiation via a NAD+–sirtuin-1–dependent pathway,” *Nat. Med.*, vol. 15, no. 2, pp. 151–158, Feb. 2009, doi: 10.1038/nm.1913.
[70] B. Bermudez *et al.*, “Leukocyte Overexpression of Intracellular NAMPT Attenuates Atherosclerosis by Regulating PPARγ-Dependent Monocyte Differentiation and Function,” *Arterioscler. Thromb. Vasc. Biol.*, vol. 37, no. 6, pp. 1157–1167, Jun. 2017, doi: 10.1161/ATVBAHA.116.308187.
[71] Y.-Y. Wang *et al.*, “Visfatin Enhances Breast Cancer Progression through CXCL1 Induction in Tumor-Associated Macrophages,” *Cancers*, vol. 12, no. 12, p. 3526, Nov. 2020, doi: 10.3390/cancers12123526.
[72] C. Travelli, G. Colombo, S. Mola, A. A. Genazzani, and C. Porta, “NAMPT: A pleiotropic modulator of monocytes and macrophages,” *Pharmacol. Res.*, vol. 135, pp. 25–36, 2018, doi: 10.1016/j.phrs.2018.06.022.
[73] YT. Lin et *al*., “Visfatin Promotes Monocyte Adhesion by Upregulating ICAM-1 and VCAM-1 Expression in Endothelial Cells via Activation of p38-PI3K-Akt Signaling and Subsequent ROS Production and IKK/NF-κB Activation,” *Cell. Physiol. Biochem.*, vol. 52, no. 6, pp. 1398–1411, May 2019, doi: 10.33594/000000098.
[74] S.-R. Kim *et al.*, “Visfatin enhances ICAM-1 and VCAM-1 expression through ROS-dependent NF-κB activation in endothelial cells,” *Biochim. Biophys. Acta BBA - Mol. Cell Res.*, vol. 1783, no. 5, pp. 886–895, May 2008, doi: 10.1016/j.bbamcr.2008.01.004.
[75] T. Romacho *et al.*, “Visfatin/eNampt induces endothelial dysfunction in vivo: a role for Toll-Like Receptor 4 and NLRP3 inflammasome,” *Sci. Rep.*, vol. 10, no. 1, p. 5386, Mar. 2020, doi: 10.1038/s41598-020-62190-w.
[76] D. Soncini *et al.*, “Nicotinamide Phosphoribosyltransferase Promotes Epithelial-to-Mesenchymal Transition as a Soluble Factor Independent of Its Enzymatic Activity,” *J. Biol. Chem.*, vol. 289, no. 49, pp. 34189–34204, Dec. 2014, doi: 10.1074/jbc.M114.594721.
[77] S.-R. Kim *et al.*, “Visfatin promotes angiogenesis by activation of extracellular signal-regulated kinase 1/2,” *Biochem. Biophys. Res. Commun.*, vol. 357, no. 1, pp. 150–156, May 2007, doi: 10.1016/j.bbrc.2007.03.105.
[78] R. Adya, B. K. Tan, A. Punn, J. Chen, and H. S. Randeva, “Visfatin induces human endothelial VEGF and MMP-2/9 production via MAPK and PI3K/Akt signalling pathways: novel insights into visfatin-induced angiogenesis,” *Cardiovasc. Res.*, vol. 78, no. 2, Art. no. 2, May 2008, doi: 10.1093/cvr/cvm111.
[79] J. Xiao *et al.*, “Involvement of dimethylarginine dimethylaminohydrolase-2 in visfatin-enhanced angiogenic function of endothelial cells,” *Diabetes Metab. Res. Rev.*, vol. 25, no. 3, pp. 242–249, Mar. 2009, doi: 10.1002/dmrr.939.
[80] A. Dakroub *et al.*, “Visfatin: An emerging adipocytokine bridging the gap in the evolution of cardiovascular diseases,” *J. Cell. Physiol.*, vol. 236, no. 9, pp. 6282–6296, Sep. 2021, doi: 10.1002/jcp.30345.

[81] J.-W. Park *et al.*, “Visfatin exerts angiogenic effects on human umbilical vein endothelial cells through the mTOR signaling pathway,” *Biochim. Biophys. Acta BBA - Mol. Cell Res.*, vol. 1813, no. 5, pp. 763–771, May 2011, doi: 10.1016/j.bbamcr.2011.02.009.
[82] J. M. Astern, A. C. Collier, and C. E. Kendal-Wright, “Pre-B cell colony enhancing factor (PBEF/NAMPT/Visfatin) and vascular endothelial growth factor (VEGF) cooperate to increase the permeability of?the?human placental amnion,” *Placenta*, vol. 34, no. 1, pp. 42–49, Jan. 2013, doi: 10.1016/j.placenta.2012.10.008.
[83] J.-Y. Kim *et al.*, “Visfatin through STAT3 activation enhances IL-6 expression that promotes endothelial angiogenesis,” *Biochim. Biophys. Acta BBA - Mol. Cell Res.*, vol. 1793, no. 11, pp. 1759–1767, Nov. 2009, doi: 10.1016/j.bbamcr.2009.09.006.
[84] S.-R. Kim *et al.*, “Upregulation of thromboxane synthase mediates visfatin-induced interleukin-8 expression and angiogenic activity in endothelial cells,” *Biochem. Biophys. Res. Commun.*, vol. 418, no. 4, pp. 662–668, Feb. 2012, doi: 10.1016/j.bbrc.2012.01.072.
[85] Y.-H. Bae *et al.*, “Notch1 mediates visfatin-induced FGF-2 up-regulation and endothelial angiogenesis,” *Cardiovasc. Res.*, vol. 89, no. 2, pp. 436–445, Feb. 2011, doi: 10.1093/cvr/cvq276.
[86] Y.-H. Bae, M.-K. Bae, S.-R. Kim, J. H. Lee, H.-J. Wee, and S.-K. Bae, “Upregulation of fibroblast growth factor-2 by visfatin that promotes endothelial angiogenesis,” *Biochem. Biophys. Res. Commun.*, vol. 379, no. 2, pp. 206–211, Feb. 2009, doi: 10.1016/j.bbrc.2008.12.042.
[87] R. Adya, B. K. Tan, J. Chen, and H. S. Randeva, “Pre-B cell colony enhancing factor (PBEF)/visfatin induces secretion of MCP-1 in human endothelial cells: Role in visfatin-induced angiogenesis,” *Atherosclerosis*, vol. 205, no. 1, pp. 113–119, Jul. 2009, doi: 10.1016/j.atherosclerosis.2008.11.024.
[88] S. Ezzati-Mobaser *et al.*, “The up-regulation of markers of adipose tissue fibrosis by visfatin in pre-adipocytes as well as obese children and adolescents,” *Cytokine*, vol. 134, p. 155193, Oct. 2020, doi: 10.1016/j.cyto.2020.155193.
[89] B. Li *et al.*, “Visfatin Destabilizes Atherosclerotic Plaques in Apolipoprotein E–Deficient Mice,” *PLOS ONE*, vol. 11, no. 2, p. e0148273, Feb. 2016, doi: 10.1371/journal.pone.0148273.
[90] R. Adya, B. K. Tan, J. Chen, and H. S. Randeva, “Nuclear Factor-κB Induction by Visfatin in Human Vascular Endothelial Cells,” *Diabetes Care*, vol. 31, no. 4, pp. 758–760, Apr. 2008, doi: 10.2337/dc07-1544.
[91] R. Van den Bergh *et al.*, “Monocytes contribute to differential immune pressure on R5 versus X4 HIV through the adipocytokine visfatin/NAMPT,” *PloS One*, vol. 7, no. 4, Art. no. 4, 2012, doi: 10.1371/journal.pone.0035074.
[92] S. Torretta *et al.*, “The Cytokine Nicotinamide Phosphoribosyltransferase (eNAMPT; PBEF; Visfatin) Acts as a Natural Antagonist of C-C Chemokine Receptor Type 5 (CCR5),” *Cells*, vol. 9, no. 2, Art. no. 2, Feb. 2020, doi: 10.3390/cells9020496.
[93] D. Ratnayake *et al.*, “Macrophages provide a transient muscle stem cell niche via NAMPT secretion,” *Nature*, Feb. 2021, doi: 10.1038/s41586-021-03199-7.
[94] Ratnayake Dhanushika, Currie Peter, and MArtino Mikael, “WO 2021212168 CCR5 NAMPT”
[95] S. M. Camp *et al.*, “Unique Toll-Like Receptor 4 Activation by NAMPT/PBEF Induces NFκB Signaling and Inflammatory Lung Injury,” *Sci. Rep.*, vol. 5, p. 13135, Aug. 2015, doi: 10.1038/srep13135.
[96] J.-S. Kim *et al.*, “Colon-Targeted eNAMPT-Specific Peptide Systems for Treatment of DSS-Induced Acute and Chronic Colitis in Mouse,” *Antioxidants*, vol. 11, no. 12, p. 2376, Nov. 2022, doi: 10.3390/antiox11122376.
[97] J. G. N. Garcia, “Compositions and methods for treating pulmonary arterial hypertension,” WO2018191747A1, Oct. 18, 2018 Accessed: Jul. 15, 2022. [Online]. Available: https://patents.google.com/patent/WO2018191747A1/en

[98] A. M. Philp, S. Butterworth, E. T. Davis, and S. W. Jones, “eNAMPT Is Localised to Areas of Cartilage Damage in Patients with Hip Osteoarthritis and Promotes Cartilage Catabolism and Inflammation,” *Int. J. Mol. Sci.*, vol. 22, no. 13, p. 6719, Jun. 2021, doi: 10.3390/ijms22136719.
[99] M. Xia, K. M. Boini, J. M. Abais, M. Xu, Y. Zhang, and P.-L. Li, “Endothelial NLRP3 Inflammasome Activation and Enhanced Neointima Formation in Mice by Adipokine Visfatin,” *Am. J. Pathol.*, vol. 184, no. 5, pp. 1617–1628, May 2014, doi: 10.1016/j.ajpath.2014.01.032.
[100] S. Koka et *al.*, “Podocyte NLRP3 Inflammasome Activation and Formation by Adipokine Visfatin,” *Cell. Physiol. Biochem.*, vol. 53, no. 2, pp. 355–365, Aug. 2019, doi: 10.33594/000000143.
[101] Y. Chen, A. L. Pitzer, X. Li, P.-L. Li, L. Wang, and Y. Zhang, “Instigation of endothelial Nlrp3 inflammasome by adipokine visfatin promotes inter-endothelial junction disruption: role of HMGB1,” *J. Cell. Mol. Med.*, vol. 19, no. 12, pp. 2715–2727, Dec. 2015, doi: 10.1111/jcmm.12657.
[102] K. Wani, H. AlHarthi, A. Alghamdi, S. Sabico, and N. M. Al-Daghri, “Role of NLRP3 Inflammasome Activation in Obesity-Mediated Metabolic Disorders,” *Int. J. Environ. Res. Public. Health*, vol. 18, no. 2, p. 511, Jan. 2021, doi: 10.3390/ijerph18020511.
[103] A. Dakroub *et al.*, “Visfatin: A Possible Role in Cardiovasculo-Metabolic Disorders,” *Cells*, vol. 9, no. 11, p. 2444, Nov. 2020, doi: 10.3390/cells9112444.
[104] D. Friebe *et al.*, “Leucocytes are a major source of circulating nicotinamide phosphoribosyltransferase (NAMPT)/pre-B cell colony (PBEF)/visfatin linking obesity and inflammation in humans,” *Diabetologia*, vol. 54, no. 5, pp. 1200–1211, May 2011, doi: 10.1007/s00125-010-2042-z.
[105] S. M. Alnowihi, H. A. A. Doghaither, and N. N. Osman, “Serum visfatin concentration and its relationship with sex hormones in obese Saudi women,” *Int. J. Health Sci.*, vol. 14, no. 3, p. 5, 2020.
[106] C. Yin, W. Hu, M. Wang, and Y. Xiao, “The role of the adipocytokines vaspin and visfatin in vascular endothelial function and insulin resistance in obese children,” *BMC Endocr. Disord.*, vol. 19, no. 1, p. 127, Dec. 2019, doi: 10.1186/s12902-019-0452-6.
[107] D. Taşkesen, B. Kirel, and T. Us, “Serum Visfatin Levels, Adiposity and Glucose Metabolism in Obese Adolescents,” *J. Clin. Res. Pediatr. Endocrinol.*, vol. 4, no. 2, pp. 76–81, Apr. 2012, doi: 10.4274/Jcrpe.547.
[108] F. Ahmadpour, “The Association of Plasma Levels of Mir-34A and Mir-149 with Obesity and Insulin Resistance in Obese Children and Adolescents,” *Acta Endocrinol. Buchar.*, vol. 14, no. 2, pp. 149–154, 2018, doi: 10.4183/aeb.2018.149.
[109] S. Araki *et al.*, “Plasma Visfatin Concentration as a Surrogate Marker for Visceral Fat Accumulation in Obese Children,” *Obesity*, vol. 16, no. 2, pp. 384–388, Feb. 2008, doi: 10.1038/oby.2007.54.
[110] R.-Z. Li *et al.*, “Elevated visfatin levels in obese children are related to proinflammatory factors,” *J. Pediatr. Endocrinol. Metab.*, vol. 0, no. 0, pp. 1–8, Jan. 2012, doi: 10.1515/jpem-2012-0237.
[111] M. Nourbakhsh, M. Nourbakhsh, Z. Gholinejad, and M. Razzaghy-Azar, “Visfatin in obese children and adolescents and its association with insulin resistance and metabolic syndrome,” *Scand. J. Clin. Lab. Invest.*, vol. 75, no. 2, pp. 183–188, Feb. 2015, doi: 10.3109/00365513.2014.1003594.
[112] H. Jin *et al.*, “Serum visfatin concentrations in obese adolescents and its correlation with age and high-density lipoprotein cholesterol,” *Diabetes Res. Clin. Pract.*, vol. 79, no. 3, pp. 412–418, Mar. 2008, doi: 10.1016/j.diabres.2007.09.019.
[113] A. Körner, A. Garten, M. Blüher, R. Tauscher, J. Kratzsch, and W. Kiess, “Molecular Characteristics of Serum Visfatin and Differential Detection by Immunoassays,” *J. Clin. Endocrinol. Metab.*, vol. 92, no. 12, pp. 4783–4791, Dec. 2007, doi: 10.1210/jc.2007-1304.

[114] A. Makarewicz *et al.*, “Comparison of the Effect of Endurance, Strength, and Endurance-Strength Training on Inflammatory Markers and Adipokines Levels in Overweight and Obese Adults: Systematic Review and Meta-Analysis of Randomised Trials,” *Healthcare*, vol. 10, no. 6, p. 1098, Jun. 2022, doi: 10.3390/healthcare10061098.
[115] A. Saeidi *et al.*, “The effects of physical activity on adipokines in individuals with overweight/obesity across the lifespan: A narrative review,” *Obes. Rev.*, vol. 22, no. 1, Jan. 2021, doi: 10.1111/obr.13090.
[116] M. Kozlowska-Flis et *al*., “Short and long-term effects of high-intensity interval training applied alone or with whole-body cryostimulation on glucose homeostasis and myokine levels in overweight to obese subjects,” *Front. Biosci.-Landmark*, vol. 26, no. 11, p. 1132, 2021, doi: 10.52586/5015.
[117] C. A. Curat *et al.*, “Macrophages in human visceral adipose tissue: increased accumulation in obesity and a source of resistin and visfatin,” *Diabetologia*, vol. 49, no. 4, pp. 744–747, Apr. 2006, doi: 10.1007/s00125-006-0173-z.
[118] S. P. Weisberg, D. McCann, M. Desai, M. Rosenbaum, R. L. Leibel, and A. W. Ferrante, “Obesity is associated with macrophage accumulation in adipose tissue,” *J. Clin. Invest.*, vol. 112, no. 12, pp. 1796–1808, Dec. 2003, doi: 10.1172/JCI200319246.
[119] M. Jurdana, A. Petelin, M. Černelič Bizjak, M. Bizjak, G. Biolo, and Z. Jenko-Pražnikar, “Increased serum visfatin levels in obesity and its association with anthropometric/biochemical parameters, physical inactivity and nutrition,” *E-SPEN J.*, vol. 8, no. 2, pp. e59–e67, Apr. 2013, doi: 10.1016/j.clnme.2013.02.001.
[120] J. Kieswich, S. R. Sayers, M. F. Silvestre, S. M. Harwood, M. M. Yaqoob, and P. W. Caton, “Monomeric eNAMPT in the development of experimental diabetes in mice: a potential target for type 2 diabetes treatment,” *Diabetologia*, vol. 59, no. 11, pp. 2477–2486, Nov. 2016, doi: 10.1007/s00125-016-4076-3.
[121] S. R. Sayers *et al.*, “Structure-functional changes in eNAMPT at high concentrations mediate mouse and human beta cell dysfunction in type 2 diabetes,” *Diabetologia*, vol. 63, no. 2, pp. 313–323, Feb. 2020, doi: 10.1007/s00125-019-05029-y.
[122] D. G. Haider, J. Pleiner, M. Francesconi, G. F. Wiesinger, M. Müller, and M. Wolzt, “Exercise Training Lowers Plasma Visfatin Concentrations in Patients with Type 1 Diabetes,” *J. Clin. Endocrinol. Metab.*, vol. 91, no. 11, pp. 4702–4704, Nov. 2006, doi: 10.1210/jc.2006-1013.
[123] A. López-Bermejo *et al.*, “Serum visfatin increases with progressive beta-cell deterioration,” *Diabetes*, vol. 55, no. 10, pp. 2871–2875, Oct. 2006, doi: 10.2337/db06-0259.
[124] A. Esteghamati *et al.*, “Serum visfatin is associated with type 2 diabetes mellitus independent of insulin resistance and obesity,” *Diabetes Res. Clin. Pract.*, vol. 91, no. 2, pp. 154–158, Feb. 2011, doi: 10.1016/j.diabres.2010.11.003.
[125] M.-P. Chen *et al.*, “Elevated Plasma Level of Visfatin/Pre-B Cell Colony-Enhancing Factor in Patients with Type 2 Diabetes Mellitus,” *J. Clin. Endocrinol. Metab.*, vol. 91, no. 1, pp. 295–299, Jan. 2006, doi: 10.1210/jc.2005-1475.
[126] T. Dogru *et al.*, “Plasma visfatin levels in patients with newly diagnosed and untreated type 2 diabetes mellitus and impaired glucose tolerance,” *Diabetes Res. Clin. Pract.*, vol. 76, no. 1, pp. 24–29, Apr. 2007, doi: 10.1016/j.diabres.2006.07.031.
[127] M. M. Mir *et al.*, “Differential Association of Selected Adipocytokines, Adiponectin, Leptin, Resistin, Visfatin and Chemerin, with the Pathogenesis and Progression of Type 2 Diabetes Mellitus (T2DM) in the Asir Region of Saudi Arabia: A Case Control Study,” *J. Pers. Med.*, vol. 12, no. 5, p. 735, May 2022, doi: 10.3390/jpm12050735.
[128] T. M. Mostafa, N. M. El-Gharbawy, and R. H. Werida, “Circulating IRAPe, Irisin, and IL-34 in Relation to Insulin Resistance in Patients With Type 2 Diabetes,” *Clin. Ther.*, vol. 43, no. 7, pp. e230–e240, Jul. 2021, doi: 10.1016/j.clinthera.2021.05.003.

[129] H. F. Hetta *et al.*, “Visfatin Serum Levels in Obese Type 2 Diabetic Patients: Relation to Proinflammatory Cytokines and Insulin Resistance,” *Egypt. J. Immunol.*, vol. 25, no. 2, pp. 141–151, Jun. 2018.
[130] K. Krzyzanowska *et al.*, “Increased visfatin concentrations in women with gestational diabetes mellitus,” *Clin. Sci.*, vol. 110, no. 5, pp. 605–609, May 2006, doi: 10.1042/CS20050363.
[131] A. T. Bawah, M. M. Seini, A. Abaka-Yawason, H. Alidu, and S. Nanga, “Leptin, resistin and visfatin as useful predictors of gestational diabetes mellitus,” *Lipids Health Dis.*, vol. 18, no. 1, p. 221, Dec. 2019, doi: 10.1186/s12944-019-1169-2.
[132] O. Shaker *et al.*, “Plasma visfatin and retinol binding protein-4 levels in patients with type 2 diabetes mellitus and their relationship to adiposity and fatty liver,” *Clin. Biochem.*, vol. 44, no. 17–18, pp. 1457–1463, Dec. 2011, doi: 10.1016/j.clinbiochem.2011.08.1148.
[133] Z. Hongyan, “Correlation of circulating full-length visfatin (PBEF/NAMPT) with metabolic parameters in subjects with and without diabetes: a cross-sectional study,” *Clin. Endocrinol. (Oxf.)*, p. 9, 2008.
[134] S. Sandeep, K. Velmurugan, R. Deepa, and V. Mohan, “Serum visfatin in relation to visceral fat, obesity, and type 2 diabetes mellitus in Asian Indians,” *Metabolism*, vol. 56, no. 4, pp. 565–570, Apr. 2007, doi: 10.1016/j.metabol.2006.12.005.
[135] T. Dahl, T. Ranheim, S. Holm, R. Berge, P. Aukrust, and B. Halvorsen, “Nicotinamide phosphoribosyltransferase and lipid accumulation in macrophages: NAMPT AND LIPID ACCUMULATION,” *Eur. J. Clin. Invest.*, vol. 41, no. 10, pp. 1098–1104, Oct. 2011, doi: 10.1111/j.1365-2362.2011.02515.x.
[136] C.-A. Chiu *et al.*, “Increased Expression of Visfatin in Monocytes and Macrophages in Male Acute Myocardial Infarction Patients,” *Mediators Inflamm.*, vol. 2012, pp. 1–7, 2012, doi: 10.1155/2012/469852.
[137] F. Zhou *et al.*, “Visfatin induces cholesterol accumulation in macrophages through up-regulation of scavenger receptor-A and CD36,” *Cell Stress Chaperones*, vol. 18, no. 5, pp. 643–652, Sep. 2013, doi: 10.1007/s12192-013-0417-z.
[138] L. Sun, S. Chen, H. Gao, L. Ren, and G. Song, “Visfatin induces the apoptosis of endothelial progenitor cells via the induction of pro-inflammatory mediators through the NF-κB pathway,” *Int. J. Mol. Med.*, vol. 40, no. 3, pp. 637–646, Sep. 2017, doi: 10.3892/ijmm.2017.3048.
[139] Y. Sun *et al.*, “Effect of visfatin on the function of endothelial progenitor cells in high-fat-fed obese rats and investigation of its mechanism of action,” *Int. J. Mol. Med.*, vol. 30, no. 3, pp. 622–628, Sep. 2012, doi: 10.3892/ijmm.2012.1032.
[140] S. Vallejo *et al.*, “Visfatin Impairs Endothelium-Dependent Relaxation in Rat and Human Mesenteric Microvessels through Nicotinamide Phosphoribosyltransferase Activity,” *PLoS ONE*, vol. 6, no. 11, p. e27299, Nov. 2011, doi: 10.1371/journal.pone.0027299.
[141] T. Romacho *et al.*, “Extracellular PBEF/NAMPT/visfatin activates pro-inflammatory signalling in human vascular smooth muscle cells through nicotinamide phosphoribosyltransferase activity,” *Diabetologia*, vol. 52, no. 11, pp. 2455–2463, Nov. 2009, doi: 10.1007/s00125-009-1509-2.
[142] T. Auguet *et al.*, “Adipo/cytokines in atherosclerotic secretomes: increased visfatin levels in unstable carotid plaque,” *BMC Cardiovasc. Disord.*, vol. 16, no. 1, p. 149, Dec. 2016, doi: 10.1186/s12872-016-0320-5.
[143] N. P. E. Kadoglou *et al.*, “Adipokines: a novel link between adiposity and carotid plaque vulnerability: APELIN AND VISFATIN IN CAROTID PLAQUE VULNERABILITY,” *Eur. J. Clin. Invest.*, vol. 42, no. 12, pp. 1278–1286, Dec. 2012, doi: 10.1111/j.1365-2362.2012.02728.x.
[144] N. P. E. Kadoglou *et al.*, “Visfatin (Nampt) and Ghrelin as Novel Markers of Carotid Atherosclerosis in Patients with Type 2 Diabetes,” *Exp. Clin. Endocrinol. Diabetes*, vol. 118, no. 02, pp. 75–80, Oct. 2009, doi: 10.1055/s-0029-1237360.

[145] L.-Y. Zheng, X. Xu, R.-H. Wan, S. Xia, J. Lu, and Q. Huang, “Association between serum visfatin levels and atherosclerotic plaque in patients with type 2 diabetes,” *Diabetol. Metab. Syndr.*, vol. 11, no. 1, p. 60, Dec. 2019, doi: 10.1186/s13098-019-0455-5.
[146] M. Zhong, H. Tan, H. Gong, S. Wang, Y. Zhang, and W. Zhang, “Increased serum visfatin in patients with metabolic syndrome and carotid atherosclerosis,” *Clin. Endocrinol. (Oxf.)*, vol. 69, no. 6, pp. 878–884, Dec. 2008, doi: 10.1111/j.1365-2265.2008.03248.x.
[147] Q. Kong *et al.*, “Increased serum visfatin as a risk factor for atherosclerosis in patients with ischaemic cerebrovascular disease,” *Singapore Med. J.*, vol. 55, no. 7, pp. 383–387, 2014, doi: 10.11622/smedj.2014091.
[148] M. Zheng, N. Lu, M. Ren, and H. Chen, “Visfatin associated with major adverse cardiovascular events in patients with acute myocardial infarction,” *BMC Cardiovasc. Disord.*, vol. 20, no. 1, p. 271, Dec. 2020, doi: 10.1186/s12872-020-01549-3.
[149] K. Takebayashi, M. Suetsugu, S. Wakabayashi, Y. Aso, and T. Inukai, “Association between plasma visfatin and vascular endothelial function in patients with type 2 diabetes mellitus,” *Metabolism*, vol. 56, no. 4, pp. 451–458, Apr. 2007, doi: 10.1016/j.metabol.2006.12.001.
[150] S. Cheleschi *et al.*, “Exploring the Crosstalk between Hydrostatic Pressure and Adipokines: An In Vitro Study on Human Osteoarthritic Chondrocytes,” *Int. J. Mol. Sci.*, vol. 22, no. 5, p. 2745, Mar. 2021, doi: 10.3390/ijms22052745.
[151] S. Cheleschi *et al.*, “MicroRNA Mediate Visfatin and Resistin Induction of Oxidative Stress in Human Osteoarthritic Synovial Fibroblasts Via NF-κB Pathway,” *Int. J. Mol. Sci.*, vol. 20, no. 20, p. E5200, Oct. 2019, doi: 10.3390/ijms20205200.
[152] S. Cheleschi *et al.*, “MicroRNA-34a and MicroRNA-181a Mediate Visfatin-Induced Apoptosis and Oxidative Stress via NF-κB Pathway in Human Osteoarthritic Chondrocytes,” *Cells*, vol. 8, no. 8, p. E874, Aug. 2019, doi: 10.3390/cells8080874.
[153] O.-M. Zahan, O. Serban, C. Gherman, and D. Fodor, “The evaluation of oxidative stress in osteoarthritis,” *Med. Pharm. Rep.*, vol. 93, no. 1, pp. 12–22, Jan. 2020, doi: 10.15386/mpr-1422.
[154] A. L. McNulty, M. R. Miller, S. K. O’Connor, and F. Guilak, “The Effects of Adipokines on Cartilage and Meniscus Catabolism,” *Connect. Tissue Res.*, vol. 52, no. 6, pp. 523–533, Dec. 2011, doi: 10.3109/03008207.2011.597902.
[155] J. F. Nishimuta and M. E. Levenston, “Meniscus is more susceptible than cartilage to catabolic and anti-anabolic effects of adipokines,” *Osteoarthritis Cartilage*, vol. 23, no. 9, pp. 1551–1562, Sep. 2015, doi: 10.1016/j.joca.2015.04.014.
[156] M. Gosset *et al.*, “Crucial role of visfatin/pre–B cell colony-enhancing factor in matrix degradation and prostaglandin E2 synthesis in chondrocytes: Possible influence on osteoarthritis,” *Arthritis Rheum.*, vol. 58, no. 5, pp. 1399–1409, May 2008, doi: 10.1002/art.23431.
[157] C. Jacques *et al.*, “Proinflammatory Actions of Visfatin/Nicotinamide Phosphoribosyltransferase (Nampt) Involve Regulation of Insulin Signaling Pathway and Nampt Enzymatic Activity,” *J. Biol. Chem.*, vol. 287, no. 18, pp. 15100–15108, Apr. 2012, doi: 10.1074/jbc.M112.350215.
[158] S. Junker *et al.*, “Expression of adipokines in osteoarthritis osteophytes and their effect on osteoblasts,” *Matrix Biol.*, vol. 62, pp. 75–91, Oct. 2017, doi: 10.1016/j.matbio.2016.11.005.
[159] R. R. Yammani and R. F. Loeser, “Extracellular nicotinamide phosphoribosyltransferase (NAMPT/visfatin) inhibits insulin-like growth factor-1 signaling and proteoglycan synthesis in human articular chondrocytes,” *Arthritis Res. Ther.*, vol. 14, no. 1, p. R23, 2012, doi: 10.1186/ar3705.
[160] M.-H. Wu, C.-H. Tsai, Y.-L. Huang, Y.-C. Fong, and C.-H. Tang, “Visfatin Promotes IL-6 and TNF-α Production in Human Synovial Fibroblasts by Repressing miR-199a-5p through ERK, p38 and JNK Signaling Pathways,” *Int. J. Mol. Sci.*, vol. 19, no. 1, p. E190, Jan. 2018, doi: 10.3390/ijms19010190.

[161] C.-H. Tsai, S.-C. Liu, W.-H. Chung, S.-W. Wang, M.-H. Wu, and C.-H. Tang, “Visfatin Increases VEGF-Dependent Angiogenesis of Endothelial Progenitor Cells during Osteoarthritis Progression,” *Cells*, vol. 9, no. 5, p. 1315, May 2020, doi: 10.3390/cells9051315.
[162] I. J. MacDonald, S.-C. Liu, C.-M. Su, Y.-H. Wang, C.-H. Tsai, and C.-H. Tang, “Implications of Angiogenesis Involvement in Arthritis,” *Int. J. Mol. Sci.*, vol. 19, no. 7, p. 2012, Jul. 2018, doi: 10.3390/ijms19072012.
[163] E. Pecchi *et al.*, “Induction of nerve growth factor expression and release by mechanical and inflammatory stimuli in chondrocytes: possible involvement in osteoarthritis pain,” *Arthritis Res. Ther.*, vol. 16, no. 1, p. R16, 2014, doi: 10.1186/ar4443.
[164] A. Askari *et al.*, “The role of adipose tissue secretion in the creation and pain level in osteoarthritis,” *Endocr. Regul.*, vol. 54, no. 1, pp. 6–13, Jan. 2020, doi: 10.2478/enr-2020-0002.
[165] A. Fioravanti *et al.*, “Can adipokines serum levels be used as biomarkers of hand osteoarthritis?,” *Biomarkers*, vol. 23, no. 3, pp. 265–270, Apr. 2018, doi: 10.1080/1354750X.2017.1401665.
[166] Y. Duan *et al.*, “Increased synovial fluid visfatin is positively linked to cartilage degradation biomarkers in osteoarthritis,” *Rheumatol. Int.*, vol. 32, no. 4, pp. 985–990, Apr. 2012, doi: 10.1007/s00296-010-1731-8.
[167] W. Chen, J. Bao, J. Feng, P. Hu, Z. Shi, and L. Wu, “Increased serum concentrations of visfatin and its production by different joint tissues in patients with osteoarthritis,” *Clin. Chem. Lab. Med.*, vol. 48, no. 8, Jan. 2010, doi: 10.1515/CCLM.2010.230.
[168] S. Bas *et al.*, “Adipokines correlate with pain in lower limb osteoarthritis: different associations in hip and knee,” *Int. Orthop.*, vol. 38, no. 12, pp. 2577–2583, Dec. 2014, doi: 10.1007/s00264-014-2416-9.
[169] E. Franco-Trepat *et al.*, “Visfatin Connection: Present and Future in Osteoarthritis and Osteoporosis,” *J. Clin. Med.*, vol. 8, no. 8, Aug. 2019, doi: 10.3390/jcm8081178.
[170] N. Busso *et al.*, “Pharmacological Inhibition of Nicotinamide Phosphoribosyltransferase/Visfatin Enzymatic Activity Identifies a New Inflammatory Pathway Linked to NAD,” *PLoS ONE*, vol. 3, no. 5, p. 10, 2008.
[171] M. A. Nowell *et al.*, “Regulation of pre–B cell colony-enhancing factor by STAT-3–dependent interleukin-6trans-signaling: Implications in the pathogenesis of rheumatoid arthritis,” *Arthritis Rheum.*, vol. 54, no. 7, pp. 2084–2095, Jul. 2006, doi: 10.1002/art.21942.
[172] L. C. Huber, O. Distler, I. Tarner, R. E. Gay, S. Gay, and T. Pap, “Synovial fibroblasts: key players in rheumatoid arthritis,” *Rheumatology*, vol. 45, no. 6, pp. 669–675, Jun. 2006, doi: 10.1093/rheumatology/kel065.
[173] F. M. P. Meier *et al.*, “Visfatin/Pre-B-cell Colony-enhancing Factor (PBEF), a Proinflammatory and Cell Motility-changing Factor in Rheumatoid Arthritis,” *J. Biol. Chem.*, vol. 287, no. 34, pp. 28378–28385, Aug. 2012, doi: 10.1074/jbc.M111.312884.
[174] L. Evans, A. S. Williams, A. J. Hayes, S. A. Jones, and M. Nowell, “Suppression of leukocyte infiltration and cartilage degradation by selective inhibition of pre-B cell colony-enhancing factor/visfatin/nicotinamide phosphoribosyltransferase: Apo866-mediated therapy in human fibroblasts and murine collagen-induced arthrit,” *Arthritis Rheum.*, vol. 63, no. 7, pp. 1866–1877, Jul. 2011, doi: 10.1002/art.30338.
[175] R. Hasseli *et al.*, “Adipokines and Inflammation Alter the Interaction Between Rheumatoid Arthritis Synovial Fibroblasts and Endothelial Cells,” *Front. Immunol.*, vol. 11, p. 925, Jun. 2020, doi: 10.3389/fimmu.2020.00925.
[176] E. Franco-Trepat *et al.*, “Visfatin as a therapeutic target for rheumatoid arthritis,” *Expert Opin. Ther. Targets*, vol. 23, no. 7, pp. 607–618, Jul. 2019, doi: 10.1080/14728222.2019.1617274.
[177] S. Cheleschi, S. Tenti, G. Bedogni, and A. Fioravanti, “Circulating Mir-140 and leptin improve the accuracy of the differential diagnosis between psoriatic arthritis and rheumatoid arthritis:

a case-control study," *Transl. Res.*, vol. 239, pp. 18–34, Jan. 2022, doi: 10.1016/j.trsl.2021.08.001.
[178] D. Ali, S. Al-Fadhel, N. Al-Ghuraibawi, and H. Al-Hakeim, "Serum chemerin and visfatin levels and their ratio as possible diagnostic parameters of rheumatoid arthritis," *Reumatologia/Rheumatology*, vol. 58, no. 2, pp. 67–75, 2020, doi: 10.5114/reum.2020.95359.
[179] Y. H. Rho *et al.*, "Adipocytokines are associated with radiographic joint damage in rheumatoid arthritis," *Arthritis Rheum.*, vol. 60, no. 7, pp. 1906–1914, Jul. 2009, doi: 10.1002/art.24626.
[180] M. Otero *et al.*, "Changes in plasma levels of fat-derived hormones adiponectin, leptin, resistin and visfatin in patients with rheumatoid arthritis," *Ann. Rheum. Dis.*, vol. 65, no. 9, pp. 1198–1201, Sep. 2006, doi: 10.1136/ard.2005.046540.
[181] O. Sglunda *et al.*, "Decreased Circulating Visfatin Is Associated with Improved Disease Activity in Early Rheumatoid Arthritis: Data from the PERAC Cohort," *PLoS ONE*, vol. 9, no. 7, p. e103495, Jul. 2014, doi: 10.1371/journal.pone.0103495.
[182] L. Šenolt *et al.*, "The level of serum visfatin (PBEF) is associated with total number of B cells in patients with rheumatoid arthritis and decreases following B cell depletion therapy," *Cytokine*, vol. 55, no. 1, pp. 116–121, Jul. 2011, doi: 10.1016/j.cyto.2011.04.004.
[183] S. H. El-Hini, F. I. Mohamed, A. A. Hassan, F. Ali, A. Mahmoud, and H. M. Ibraheem, "Visfatin and adiponectin as novel markers for evaluation of metabolic disturbance in recently diagnosed rheumatoid arthritis patients," *Rheumatol. Int.*, vol. 33, no. 9, pp. 2283–2289, Sep. 2013, doi: 10.1007/s00296-013-2714-3.
[184] Z. Mirfeizi, Z. Noubakht, A. E. Rezaie, M. H. Jokar, and S. Sarabi, "Plasma levels of leptin and visfatin in rheumatoid arthritis patients; is there any relationship with joint damage?," *Iran J Basic Med Sci*, vol. 17, no. 9, p. 5, 2014.
[185] Y. H. Lee and S.-C. Bae, "Circulating adiponectin and visfatin levels in rheumatoid arthritis and their correlation with disease activity: A meta-analysis," *Int. J. Rheum. Dis.*, vol. 21, no. 3, pp. 664–672, Mar. 2018, doi: 10.1111/1756-185X.13038.
[186] R. Klaasen *et al.*, "Treatment-specific changes in circulating adipocytokines: a comparison between tumour necrosis factor blockade and glucocorticoid treatment for rheumatoid arthritis," *Ann. Rheum. Dis.*, vol. 71, no. 9, pp. 1510–1516, Sep. 2012, doi: 10.1136/annrheumdis-2011-200646.
[187] A. Fioravanti *et al.*, "Tocilizumab modulates serum levels of adiponectin and chemerin in patients with rheumatoid arthritis: potential cardiovascular protective role of IL-6 inhibition," *Clin. Exp. Rheumatol.*, p. 8, 2019.
[188] K. S. Kim *et al.*, "Serum adipokine levels in rheumatoid arthritis patients and their contributions to the resistance to treatment," *Mol. Med. Rep.*, vol. 9, no. 1, pp. 255–260, Jan. 2014, doi: 10.3892/mmr.2013.1764.
[189] M. A. Gonzalez-Gay *et al.*, "Visfatin is not associated with inflammation or metabolic syndrome in patients with severe rheumatoid arthritis undergoing anti-TNF-alpha therapy," *Clin. Exp. Rheumatol.*, vol. 28, no. 1, pp. 56–62, 2010.
[190] R. R. Gerner *et al.*, "NAD metabolism fuels human and mouse intestinal inflammation," *Gut*, vol. 67, no. 10, pp. 1813–1823, Oct. 2018, doi: 10.1136/gutjnl-2017-314241.
[191] C. Travelli *et al.*, "Identification of Novel Triazole-Based Nicotinamide Phosphoribosyltransferase (NAMPT) Inhibitors Endowed with Antiproliferative and Antiinflammatory Activity," *J. Med. Chem.*, vol. 60, no. 5, pp. 1768–1792, Mar. 2017, doi: 10.1021/acs.jmedchem.6b01392.
[192] A. Wnorowski, S. Wnorowska, J. Kurzepa, and J. Parada-Turska, "Alterations in Kynurenine and NAD+ Salvage Pathways during the Successful Treatment of Inflammatory Bowel Disease Suggest HCAR3 and NNMT as Potential Drug Targets," *Int. J. Mol. Sci.*, vol. 22, no. 24, p. 13497, Dec. 2021, doi: 10.3390/ijms222413497.

[193] G. Colombo *et al.*, "Neutralization of extracellular NAMPT (nicotinamide phosphoribosyltransferase) ameliorates experimental murine colitis," *J. Mol. Med.*, vol. 98, no. 4, pp. 595–612, Apr. 2020, doi: 10.1007/s00109-020-01892-0.
[194] M. Waluga, "Serum adipokines in inflammatory bowel disease," *World J. Gastroenterol.*, vol. 20, no. 22, p. 6912, 2014, doi: 10.3748/wjg.v20.i22.6912.
[195] K. Neubauer *et al.*, "Oversecretion and Overexpression of Nicotinamide Phosphoribosyltransferase/Pre-B Colony-Enhancing Factor/Visfatin in Inflammatory Bowel Disease Reflects the Disease Activity, Severity of Inflammatory Response and Hypoxia," *Int. J. Mol. Sci.*, vol. 20, no. 1, p. 166, Jan. 2019, doi: 10.3390/ijms20010166.
[196] S. Dogan, K. Guven, M. Celikbilek, K. Deniz, B. Saraymen, and S. Gursoy, "Serum Visfatin Levels in Ulcerative Colitis: Visfatin and Ulcerative Colitis," *J. Clin. Lab. Anal.*, vol. 30, no. 5, pp. 552–556, Sep. 2016, doi: 10.1002/jcla.21901.
[197] L. Valentini *et al.*, "Circulating adipokines and the protective effects of hyperinsulinemia in inflammatory bowel disease," *Nutrition*, vol. 25, no. 2, pp. 172–181, Feb. 2009, doi: 10.1016/j.nut.2008.07.020.
[198] M. M. Saadoun, N. A. el-Aziz Nosair, H. A.-H. Abdel-Azeez, S. M. Sharaf, and M. H. Ahmed, "Serum Visfatin as a Diagnostic Marker of Active Inflammatory Bowel Disease," *J. Gastrointestin. Liver Dis.*, vol. 30, no. 3, pp. 339–345, Sep. 2021, doi: 10.15403/jgld-3504.
[199] G. Colombo *et al.*, "NAMPT and NAPRT serum levels predict response to anti-TNF therapy in inflammatory bowel disease," *Front. Med.*, vol. 10, p. 1116862, 2023, doi: 10.3389/fmed.2023.1116862.
[200] F. Trejo-Vazquez *et al.*, "Positive association between leptin serum levels and disease activity on endoscopy in inflammatory bowel disease: A case-control study," *Exp. Ther. Med.*, Feb. 2018, doi: 10.3892/etm.2018.5835.
[201] S. Terzoudis, N. Malliaraki, J. Damilakis, D. A. Dimitriadou, C. Zavos, and I. E. Koutroubakis, "Chemerin, visfatin, and vaspin serum levels in relation to bone mineral density in patients with inflammatory bowel disease:," *Eur. J. Gastroenterol. Hepatol.*, vol. 28, no. 7, pp. 814–819, Jul. 2016, doi: 10.1097/MEG.0000000000000617.
[202] T. Bermudez *et al.*, "eNAMPT neutralization reduces preclinical ARDS severity via rectified NFkB and Akt/mTORC2 signaling," *Sci. Rep.*, vol. 12, no. 1, p. 696, Dec. 2022, doi: 10.1038/s41598-021-04444-9.
[203] H. Quijada *et al.*, "Endothelial eNAMPT Amplifies Preclinical Acute Lung Injury: Efficacy of an eNAMPT-Neutralising mAb," *Eur. Respir. J.*, Nov. 2020, doi: 10.1183/13993003.02536-2020.
[204] S. Sammani *et al.*, "eNAMPT Neutralization Preserves Lung Fluid Balance and Reduces Acute Renal Injury in Porcine Sepsis/VILI-Induced Inflammatory Lung Injury," *Front. Physiol.*, vol. 13, p. 916159, Jun. 2022, doi: 10.3389/fphys.2022.916159.
[205] Y.-C. Lee *et al.*, "Essential Role of Visfatin in Lipopolysaccharide and Colon Ascendens Stent Peritonitis-Induced Acute Lung Injury," *Int. J. Mol. Sci.*, vol. 20, no. 7, p. 1678, Apr. 2019, doi: 10.3390/ijms20071678.
[206] S.-B. Hong *et al.*, "Essential role of pre-B-cell colony enhancing factor in ventilator-induced lung injury," *Am. J. Respir. Crit. Care Med.*, vol. 178, no. 6, pp. 605–617, Sep. 2008, doi: 10.1164/rccm.200712-1822OC.
[207] S. Q. Ye *et al.*, "Pre-B-cell-colony-enhancing factor is critically involved in thrombin-induced lung endothelial cell barrier dysregulation," *Microvasc. Res.*, vol. 70, no. 3, pp. 142–151, Nov. 2005, doi: 10.1016/j.mvr.2005.08.003.
[208] C. Bime *et al.*, "Circulating eNAMPT as a biomarker in the critically ill: acute pancreatitis, sepsis, trauma, and acute respiratory distress syndrome," *BMC Anesthesiol.*, vol. 22, no. 1, p. 182, Dec. 2022, doi: 10.1186/s12871-022-01718-1.
[209] I. Karampela *et al.*, "Circulating eNampt and resistin as a proinflammatory duet predicting independently mortality in critically ill patients with sepsis: A prospective observational study," *Cytokine*, vol. 119, pp. 62–70, Jul. 2019, doi: 10.1016/j.cyto.2019.03.002.

[210] K. Lee, J. W. Huh, C.-M. Lim, Y. Koh, and S.-B. Hong, “Clinical role of serum pre-B cell colony-enhancing factor in ventilated patients with sepsis and acute respiratory distress syndrome,” *Scand. J. Infect. Dis.*, vol. 45, no. 10, pp. 760–765, Oct. 2013, doi: 10.3109/00365548.2013.797600.
[211] C. Bime *et al.*, “Development of a biomarker mortality risk model in acute respiratory distress syndrome,” *Crit. Care*, vol. 23, no. 1, p. 410, Dec. 2019, doi: 10.1186/s13054-019-2697-x.
[212] M. Dalamaga, G. S. Christodoulatos, and C. S. Mantzoros, “The role of extracellular and intracellular Nicotinamide phosphoribosyl-transferase in cancer: Diagnostic and therapeutic perspectives and challenges,” *Metabolism*, vol. 82, pp. 72–87, May 2018, doi: 10.1016/j.metabol.2018.01.001.
[213] A. C. Hung *et al.*, “Extracellular Visfatin-Promoted Malignant Behavior in Breast Cancer Is Mediated Through c-Abl and STAT3 Activation,” *Clin. Cancer Res.*, vol. 22, no. 17, pp. 4478–4490, Sep. 2016, doi: 10.1158/1078-0432.CCR-15-2704.
[214] Z. Gholinejad *et al.*, “Extracellular NAMPT/Visfatin induces proliferation through ERK1/2 and AKT and inhibits apoptosis in breast cancer cells,” *Peptides*, vol. 92, pp. 9–15, Jun. 2017, doi: 10.1016/j.peptides.2017.04.007.
[215] H.-J. Park *et al.*, “Visfatin promotes cell and tumor growth by upregulating Notch1 in breast cancer,” *Oncotarget*, vol. 5, no. 13, Art. no. 13, Jul. 2014, doi: 10.18632/oncotarget.2086.
[216] R. J. Bułdak *et al.*, “Visfatin affects redox adaptative responses and proliferation in Me45 human malignant melanoma cells: An in vitro study,” *Oncol. Rep.*, vol. 29, no. 2, pp. 771–778, Feb. 2013, doi: 10.3892/or.2012.2175.
[217] C. Miethe, M. Zamora, L. Torres, K. G. Raign, C. J. Groll, and R. S. Price, “Characterizing the differential physiological effects of adipocytokines visfatin and resistin in liver cancer cells,” *Horm. Mol. Biol. Clin. Investig.*, vol. 38, no. 2, May 2019, doi: 10.1515/hmbci-2018-0068.
[218] S. Ninomiya *et al.*, “Possible role of visfatin in hepatoma progression and the effects of branched-chain amino acids on visfatin-induced proliferation in human hepatoma cells,” *Cancer Prev. Res. Phila. Pa*, vol. 4, no. 12, pp. 2092–2100, Dec. 2011, doi: 10.1158/1940-6207.CAPR-11-0340.
[219] Y. Wang *et al.*, “Visfatin stimulates endometrial cancer cell proliferation via activation of PI3K/Akt and MAPK/ERK1/2 signalling pathways,” *Gynecol. Oncol.*, vol. 143, no. 1, pp. 168–178, Oct. 2016, doi: 10.1016/j.ygyno.2016.07.109.
[220] S. T. Patel *et al.*, “A novel role for the adipokine visfatin/pre-B cell colony-enhancing factor 1 in prostate carcinogenesis,” *Peptides*, vol. 31, no. 1, pp. 51–57, Jan. 2010, doi: 10.1016/j.peptides.2009.10.001.
[221] J. G. Kim *et al.*, “Visfatin stimulates proliferation of MCF-7 human breast cancer cells,” *Mol. Cells*, vol. 30, no. 4, pp. 341–345, Oct. 2010, doi: 10.1007/s10059-010-0124-x.
[222] Y.-F. Chiang, H.-Y. Chen, K.-C. Huang, P.-H. Lin, and S.-M. Hsia, “Dietary Antioxidant Trans-Cinnamaldehyde Reduced Visfatin-Induced Breast Cancer Progression: In Vivo and In Vitro Study,” *Antioxidants*, vol. 8, no. 12, p. 625, Dec. 2019, doi: 10.3390/antiox8120625.
[223] G.-J. Wang, N.-J. Shen, L. Cheng, Yehan Fang, H. Huang, and K.-H. Li, “Visfatin triggers the in vitro migration of osteosarcoma cells via activation of NF-κB/IL-6 signals,” *Eur. J. Pharmacol.*, vol. 791, pp. 322–330, Nov. 2016, doi: 10.1016/j.ejphar.2016.08.029.
[224] Y. Li, X. Li, K.-R. Liu, J.-N. Zhang, Y. Liu, and Y. Zhu, “Visfatin derived from ascites promotes ovarian cancer cell migration through Rho/ROCK signaling-mediated actin polymerization,” *Eur. J. Cancer Prev.*, vol. 24, no. 3, pp. 231–239, May 2015, doi: 10.1097/CEJ.0000000000000064.
[225] S.-Y. Hung *et al.*, “Visfatin Promotes the Metastatic Potential of Chondrosarcoma Cells by Stimulating AP-1-Dependent MMP-2 Production in the MAPK Pathway,” *Int. J. Mol. Sci.*, vol. 22, no. 16, p. 8642, Aug. 2021, doi: 10.3390/ijms22168642.

[226] B. L. Sun *et al.*, “Role of secreted extracellular nicotinamide phosphoribosyltransferase (eNAMPT) in prostate cancer progression: Novel biomarker and therapeutic target,” *EBioMedicine*, vol. 61, p. 103059, Nov. 2020, doi: 10.1016/j.ebiom.2020.103059.
[227] L. Xiao, Y. Mao, Z. Tong, Y. Zhao, H. Hong, and F. Wang, “Radiation exposure triggers the malignancy of non-small cell lung cancer cells through the activation of visfatin/Snail signaling,” *Oncol. Rep.*, vol. 45, no. 3, pp. 1153–1161, Mar. 2021, doi: 10.3892/or.2021.7929.
[228] W.-S. Huang, C.-N. Chen, C.-I. Sze, and C.-C. Teng, “Visfatin induces stromal cell-derived factor-1 expression by β1 integrin signaling in colorectal cancer cells,” *J. Cell. Physiol.*, vol. 228, no. 5, Art. no. 5, May 2013, doi: 10.1002/jcp.24248.
[229] B. L. Sun *et al.*, “A Humanized Monoclonal Antibody Targeting Extracellular Nicotinamide Phosphoribosyltransferase Prevents Aggressive Prostate Cancer Progression,” *Pharmaceuticals*, vol. 14, no. 12, p. 1322, Dec. 2021, doi: 10.3390/ph14121322.
[230] D. Cao *et al.*, “Visfatin facilitates gastric cancer malignancy by targeting snai1 via the NF-κB signaling,” *Hum. Exp. Toxicol.*, vol. 40, no. 10, pp. 1646–1655, Oct. 2021, doi: 10.1177/09603271211006168.
[231] G. Cheng *et al.*, “Visfatin promotes osteosarcoma cell migration and invasion via induction of epithelial-mesenchymal transition,” *Oncol. Rep.*, vol. 34, no. 2, pp. 987–994, Aug. 2015, doi: 10.3892/or.2015.4053.
[232] G. Wang *et al.*, “Visfatin Triggers the Cell Motility of Non-Small Cell Lung Cancer via Up-Regulation of Matrix Metalloproteinases,” *Basic Clin. Pharmacol. Toxicol.*, vol. 119, no. 6, pp. 548–554, Dec. 2016, doi: 10.1111/bcpt.12623.
[233] K.-L. Wu, K.-C. Lee, C.-K. Yen, C.-N. Chen, S.-F. Chang, and W.-S. Huang, “Visfatin and Resveratrol Differentially Regulate the Expression of Thymidylate Synthase to Control the Sensitivity of Human Colorectal Cancer Cells to Capecitabine Cytotoxicity,” *Life*, vol. 11, no. 12, p. 1371, Dec. 2021, doi: 10.3390/life11121371.
[234] M. Zangooei *et al.*, “Investigating the effect of visfatin on ERα phosphorylation (Ser118 and Ser167) and ERE-dependent transcriptional activity,” *EXCLI J. 17Doc516 ISSN 1611-2156*, 2018, doi: 10.17179/EXCLI2018-1299.
[235] R. de Leeuw, J. Neefjes, and R. Michalides, “A Role for Estrogen Receptor Phosphorylation in the Resistance to Tamoxifen,” *Int. J. Breast Cancer*, vol. 2011, pp. 1–10, 2011, doi: 10.4061/2011/232435.
[236] Y. Liu *et al.*, “Cancer drug resistance: redox resetting renders a way,” *Oncotarget*, vol. 7, no. 27, pp. 42740–42761, Apr. 2016, doi: 10.18632/oncotarget.8600.
[237] T. Motawi, N. Zakhary, H. Darwish, H. Abdullah, and S. Tadros, “Significance of Some Non-Invasive Biomarkers in the Early Diagnosis and Staging of Egyptian Breast Cancer Patients,” *Asian Pac. J. Cancer Prev.*, vol. 21, no. 11, pp. 3279–3284, Nov. 2020, doi: 10.31557/APJCP.2020.21.11.3279.
[238] L.-J. Zhang *et al.*, “The Correlation of Visfatin and Its Gene Polymorphism with Non-Small Cell Lung Cancer,” *Cancer Biother. Radiopharm.*, vol. 33, no. 10, pp. 460–465, Dec. 2018, doi: 10.1089/cbr.2018.2526.
[239] Y. Sun *et al.*, “Elevated serum visfatin levels are associated with poor prognosis of hepatocellular carcinoma,” *Oncotarget*, vol. 8, no. 14, pp. 23427–23435, Apr. 2017, doi: 10.18632/oncotarget.15080.
[240] J. Yang *et al.*, “Visfatin is involved in promotion of colorectal carcinoma malignancy through an inducing EMT mechanism,” *Oncotarget*, vol. 7, no. 22, pp. 32306–32317, May 2016, doi: 10.18632/oncotarget.8615.
[241] A. Cymbaluk-Płoska, A. Chudecka-Głaz, E. Pius-Sadowska, A. Sompolska-Rzechuła, B. Machaliński, and J. Menkiszak, “Circulating Serum Level of Visfatin in Patients with Endometrial Cancer,” *BioMed Res. Int.*, vol. 2018, pp. 1–9, 2018, doi: 10.1155/2018/8576179.

[242] G.-W. Lu, Q.-J. Wang, M.-M. Xia, and J. Qian, “Elevated plasma visfatin levels correlate with poor prognosis of gastric cancer patients,” *Peptides*, vol. 58, pp. 60–64, Aug. 2014, doi: 10.1016/j.peptides.2014.05.016.
[243] T. E. Nakajima *et al.*, “Adipocytokine levels in gastric cancer patients: resistin and visfatin as biomarkers of gastric cancer,” *J. Gastroenterol.*, vol. 44, no. 7, pp. 685–690, Jul. 2009, doi: 10.1007/s00535-009-0063-5.
[244] M. Dalamaga *et al.*, “Could serum visfatin be a potential biomarker for postmenopausal breast cancer?,” *Maturitas*, vol. 71, no. 3, pp. 301–308, Mar. 2012, doi: 10.1016/j.maturitas.2011.12.013.
[245] T. T. Ilhan *et al.*, “Relations of Serum Visfatin and Resistin Levels with Endometrial Cancer and Factors Associated with its Prognosis,” *Asian Pac. J. Cancer Prev.*, vol. 16, no. 11, pp. 4503–4508, Jun. 2015, doi: 10.7314/APJCP.2015.16.11.4503.
[246] N. Sawicka-Gutaj, H. Komarowska, D. Gruszczyński, A. Derwich, A. Klimont, and M. Ruchała, “Serum Visfatin/NAMPT as a Potential Risk Predictor for Malignancy of Adrenal Tumors,” *J. Clin. Med.*, vol. 11, no. 19, p. 5563, Sep. 2022, doi: 10.3390/jcm11195563.
[247] U. Galli, G. Colombo, C. Travelli, G. C. Tron, A. A. Genazzani, and A. A. Grolla, “Recent Advances in NAMPT Inhibitors: A Novel Immunotherapic Strategy,” *Front. Pharmacol.*, vol. 11, p. 656, May 2020, doi: 10.3389/fphar.2020.00656.
[248] Y. Wei, H. Xiang, and W. Zhang, “Review of various NAMPT inhibitors for the treatment of cancer,” *Front. Pharmacol.*, vol. 13, p. 970553, Sep. 2022, doi: 10.3389/fphar.2022.970553.
[249] S. Grivennikov and M. Karin, “Dangerous liaisons: STAT3 and NF-κB collaboration and crosstalk in cancer,” *Cytokine Growth Factor Rev.*, vol. 21, no. 1, pp. 11–19, Feb. 2010, doi: 10.1016/j.cytogfr.2009.11.005.
[250] J. Garcia and M. Ahmed, “Single Nucleotide Polymorphisms and Treatment of Inflammatory Conditions,” Feb. 10, 2022 Accessed: Jul. 22, 2022. [Online]. Available: https://patentscope.wipo.int/search/en/detail.jsf?docId=WO2022032135&docAn=US2021045005
[251] J. G. N. Garcia and D. Maccann, “Anti-Nampt Antibodies and Uses Thereof,” Feb. 11, 2021 Accessed: Aug. 10, 2022. [Online]. Available: https://patentscope.wipo.int/search/en/detail.jsf?docId=WO2021026508
[252] M. Ahmed *et al.*, “Endothelial eNAMPT drives EndMT and preclinical PH: rescue by an eNAMPT-neutralizing mAb,” *Pulm. Circ.*, vol. 11, no. 4, p. 204589402110597, Oct. 2021, doi: 10.1177/20458940211059712.
[253] A. N. Garcia *et al.*, “eNAMPT Is a Novel Damage-associated Molecular Pattern Protein That Contributes to the Severity of Radiation-induced Lung Fibrosis,” *Am. J. Respir. Cell Mol. Biol.*, vol. 66, no. 5, pp. 497–509, May 2022, doi: 10.1165/rcmb.2021-0357OC.
[254] G. Tumurkhuu *et al.*, “eNAMPT/TLR4 inflammatory cascade activation is a key contributor to SLE Lung vasculitis and alveolar hemorrhage,” *J. Transl. Autoimmun.*, vol. 6, p. 100181, 2023, doi: 10.1016/j.jtauto.2022.100181.
[255] B. L. Sun *et al.*, “Involvement of eNAMPT/TLR4 inflammatory signaling in progression of non-alcoholic fatty liver disease, steatohepatitis, and fibrosis,” *FASEB J. Off. Publ. Fed. Am. Soc. Exp. Biol.*, vol. 37, no. 3, p. e22825, Mar. 2023, doi: 10.1096/fj.202201972RR.
[256] X. Zhu *et al.*, “Addressing the Enzyme-independent tumor-promoting function of NAMPT via PROTAC-mediated degradation,” *Cell Chem. Biol.*, vol. 29, no. 11, pp. 1616-1629.e12, Nov. 2022, doi: 10.1016/j.chembiol.2022.10.007.
[257] Y. Wu, C. Pu, Y. Fu, G. Dong, M. Huang, and C. Sheng, “NAMPT-targeting PROTAC promotes antitumor immunity via suppressing myeloid-derived suppressor cell expansion,” *Acta Pharm. Sin. B*, vol. 12, no. 6, pp. 2859–2868, Jun. 2022, doi: 10.1016/j.apsb.2021.12.017.
[258] V. Audrito and S. Deaglio, “NAMPT and NAPRT: Two Metabolic Enzymes With Key Roles in Inflammation,” *Front. Oncol.*, vol. 10, p. 17, 2020.

[259] M. Pazgan-Simon *et al.*, “Serum visfatin and vaspin levels in hepatocellular carcinoma (HCC),” *PLOS ONE*, vol. 15, no. 1, p. e0227459, Jan. 2020, doi: 10.1371/journal.pone.0227459.
[260] P. Sowa, M. Misiolek, B. Orecka, E. Czecior, and M. Adamczyk-Sowa, “Serum levels of selected adipocytokines in benign and malignant parotid gland tumor patients,” *Cytokine*, vol. 106, pp. 40–44, Jun. 2018, doi: 10.1016/j.cyto.2018.03.004.
[261] V. B. Pillai *et al.*, “Nampt secreted from cardiomyocytes promotes development of cardiac hypertrophy and adverse ventricular remodeling,” *Am. J. Physiol.-Heart Circ. Physiol.*, vol. 304, no. 3, pp. H415–H426, Feb. 2013, doi: 10.1152/ajpheart.00468.2012.
[262] T. Liu *et al.*, “Visfatin Mediates SCLC Cells Migration across Brain Endothelial Cells through Upregulation of CCL2,” *Int. J. Mol. Sci.*, vol. 16, no. 12, pp. 11439–11451, May 2015, doi: 10.3390/ijms160511439.
[263] C. Zhang *et al.*, “Nicotinamide Phosphate Transferase (NAMPT) Increases in Plasma in Patients with Acute Coronary Syndromes, and Promotes Macrophages to M2 Polarization,” *Int. Heart. J.*, vol. 59, no. 5, pp. 1116–1122, Sep. 2018, doi: 10.1536/ihj.17-363.
[264] A. N. Garcia *et al.*, “Involvement of eNAMPT/TLR4 signaling in murine radiation pneumonitis: protection by eNAMPT neutralization,” *Transl. Res.*, p. S1931524421001419, Jun. 2021, doi: 10.1016/j.trsl.2021.06.002.

2. Introduction

Nicotinamide phosphoribosyltransferase (NAMPT) is a homodimeric protein detectable both intracellularly and extracellularly [1]. NAMPT is a key enzyme in the nicotinamide adenine dinucleotide (NAD^+) salvage pathway, which catalyzes the production of nicotinamide mononucleotide (NMN) from nicotinamide (NAM) [1]. Furthermore, this protein also accomplishes multiple functions in the extracellular space; including adipokine, cytokine and pro-angiogenic activities [2]. In the following introduction, I will focus on extracellular NAMPT (eNAMPT). eNAMPT biology (secretion, functions, receptors) and its role in cancer are treated in detail in the associated review (section 1).

2.1. NAMPT biology

2.1.1. *NAMPT* gene and protein structure

NAMPT gene was first isolated in 1994 by Samal et al., from human peripheral blood lymphocytes [3]. The *NAMPT* gene is located at the 7q22.3 locus on human chromosome 7 and consists of 11 exons and 10 introns [4], [5]. The *NAMPT* gene is ubiquitously expressed [6] and its sequence is highly conserved among species [7]. This indicates that NAMPT plays an important role in organisms physiology, which is supported by the fact that deletion of *NAMPT* gene is embryonically lethal in mice [8].

Once translated, the 2.4kb NAMPT transcript produces a 491 amino acids (aa) monomer with a molecular mass of 55kDa [9]. The two NAMPT monomers then dimerize to form a homodimeric type II protein [10]. Specifically, each NAMPT monomer is organized into two structural domains and is constituted of 13 α-helices and 19 β-strands (Figure 1) [9]. NAMPT protein is detectable in both the nucleus and the cytosol and its localization varies according to the phases of the cell cycle [11], [12]. Its potential localization in mitochondria is still under debate [13]–[15]. Furthermore, NAMPT can also be released into the systemic circulation in extracellular vesicles (EVs) [16], [17].

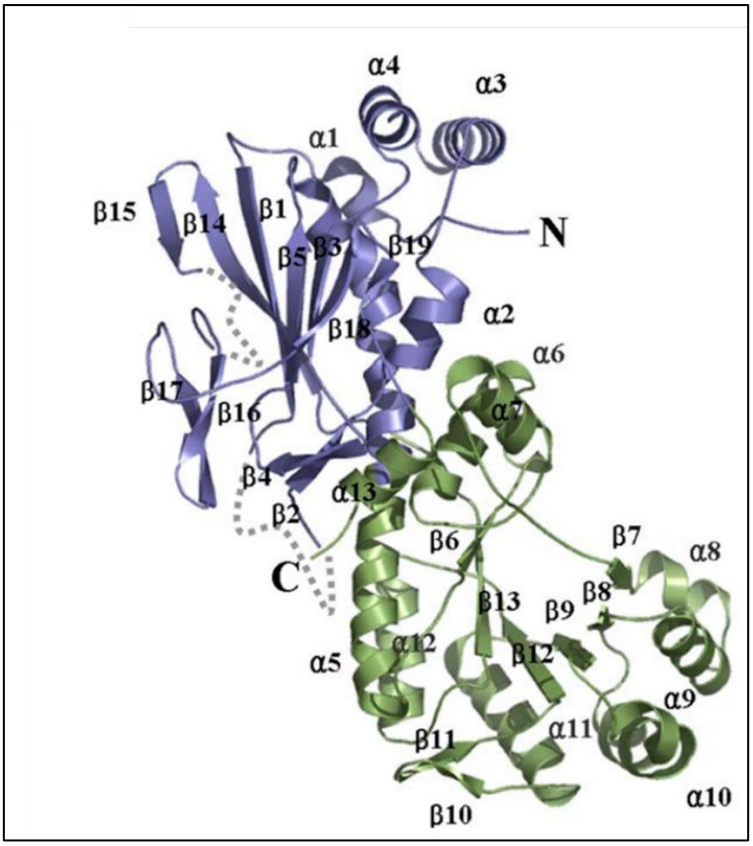

Figure 1: NAMPT monomer crystal structure. Sourced from Kim et al. [9].

2.1.2. eNAMPT secretion

NAMPT can also be directly secreted into the extracellular space through an active mechanism not deciphered yet. eNAMPT is released in the extracellular space by a large variety of cell types upon different kinds of stimuli [1], [10]. There is evidence to suggest that eNAMPT is not secreted through the classical ER-Golgi secretory pathway and that its release is regulated by sirtuin-1 and sirtuin-6 (SIRT1 and SIRT6) enzymes [8], [17]–[21].

2.2. NAMPT functions

2.2.1. NAMPT enzymatic activity

NAMPT is a phosphoribosyltransferase (EC 2.4.2.12) that participates in the production of NAD^+, an essential co-factor for cellular metabolism [6], [10]. Specifically, NAMPT is the rate-limiting enzyme of the NAD^+ salvage pathway in mammals [1]. NAMPT uses NAM and 5'-phosphoribosyl-1-pyrophosphate (PRPP) to produce NMN [1], as illustrated in Figure 2. This NMN is subsequently transformed by NMN adenylyltransferases 1-3 (NMNATs 1-3) to NAD^+, which will be consumed in cellular redox reactions or by NAD^+-dependent enzymes [1], [6]. These NAD^+-consuming enzymes; such as sirtuins, cluster of differentiation 38 (CD38) or

poly(ADP-ribose) polymerases (PARPs), have been shown to modulate various biological processes including mitochondrial biogenesis, DNA repair or apoptosis [22]. Thus, through its NAD-biosynthetic activity, NAMPT contributes to the metabolism and survival of mammalian cells [1].

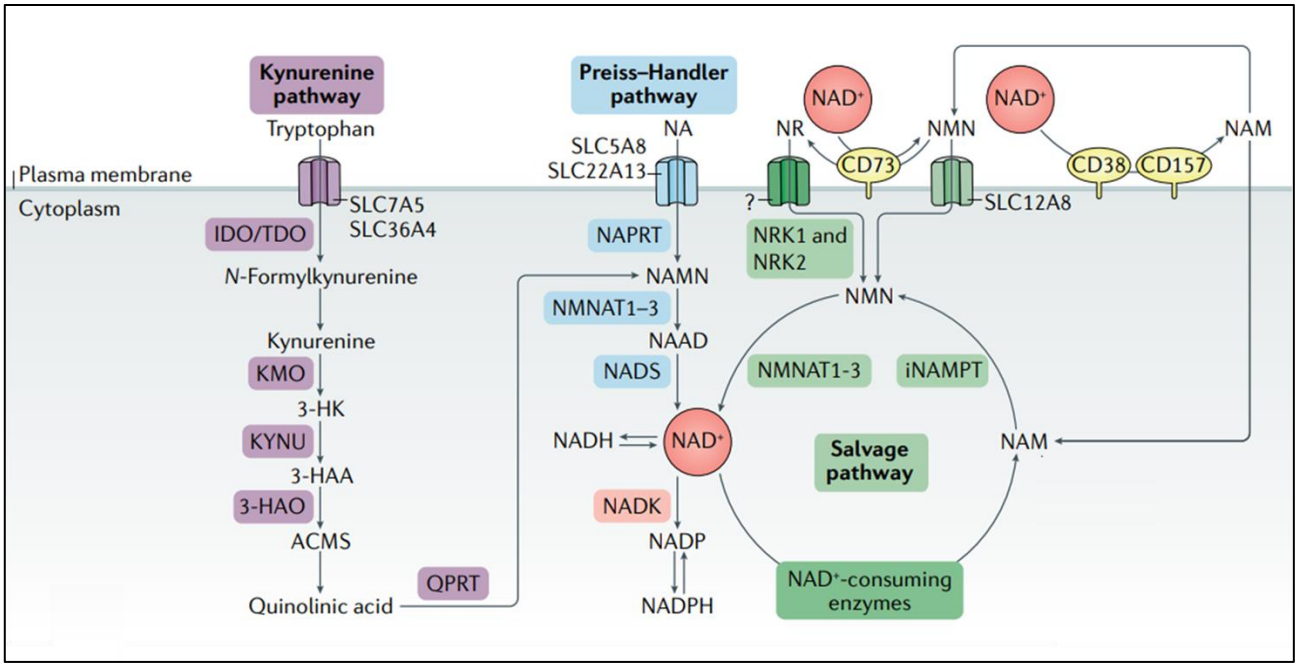

Figure 2: NAD⁺ biosynthetic pathways. Nicotinamide adenine dinucleotide (NAD⁺) can be produced by three different pathways. In the kynurenine pathway, two rate limiting enzymes, indoleamine 2,3-dioxygenase (IDO) or tryptophan 2,3-dioxygenase (TDO) convert the amino acid tryptophan into *N*-Formylkynurenine. After successive enzymatic reactions, *N*-Formylkynurenine is transformed into nicotinic acid mononucleotide (NAMN) which joins the Preiss-Handler pathway. In the latter, NAMN is also generated from nicotinic acid (NA) by the enzyme nicotinic acid phosphoribosyltransferase (NAPRT). NAMN is then converted to NAD⁺ by the action of nicotinamide mononucleotide adenylyltransferases (NMNAT1, NMNAT2 and NMNAT3) followed by NAD⁺ synthetase (NADS). In the salvage pathway, NAMPT rate-limiting enzyme generates nicotinamide mononucleotide (NMN) from nicotinamide (NAM). NMN is subsequently transformed into NAD⁺ by NMNAT1-3. Finally, NAD⁺ fuels the activity of NAD⁺-degrading enzymes. Modified from Covarrubias et al. [23].

2.2.2. eNAMPT extracellular functions

eNAMPT is a pleiotropic protein that has been shown to act as an adipokine, a pro-inflammatory cytokine or a pro-angiogenic mediator in the extracellular space [2]. Whether or not eNAMPT exerts a NAD-biosynthetic activity in the extracellular milieu is controversial [10].

2.3. Putative receptors of eNAMPT

Over the years, several cell surface proteins have been envisioned as putative eNAMPT receptors. In 2005, Fukuhara et al. [24], were the first to propose a receptor for eNAMPT, namely the insulin receptor (IR). However, their publication was retracted due to lack of reproducibility [25]. Later, TLR4 and CCR5 were suggested as eNAMPT receptors [26], [27].

2.3.1. CC-chemokine receptor type 5 (CCR5)

CCR5 is a seven-transmembrane, G-protein coupled receptor (GPCR) that binds with high affinity to the CC family chemokines: CCL3, CCL4, CCL5 (also known as RANTES) and CCL8 [28]–[31]. CCR5 is expressed by a variety of immune cells, including T cells, macrophages and natural killers (NK); and plays an important role in triggering the adaptive immune response by recruiting immune effector cells to inflamed and damaged tissues [30]–[32]. Furthermore, CCR5 may participate in inflammation resolution as it also induces the recruitment of regulatory T cells (Treg) [32]. Engagement of the CCR5 receptor by its ligands induces the activation of G proteins (Gαi, Gαq, and Gβγ) and downstream signalling pathways, such as phosphatidylinositol 3-kinase/protein kinase B (PI3K/AKT) and nuclear factor kappa-light-chain-enhancer of activated B cells (NF-kB) pathways, leading to cytoskeleton rearrangement, adhesion and chemotactic cell migration (Figure 3) [31], [33]. Most importantly, CCR5 has been identified as one of the main co-receptors of human immunodeficiency virus (HIV), allowing the virus to enter and infect host cells [32], [34]. In addition, CCL5/CCR5 axis has been shown to promote tumor growth and invasion, induce angiogenesis and mediate tumor cell resistance to anti-cancer drugs, among several other mechanisms [31].

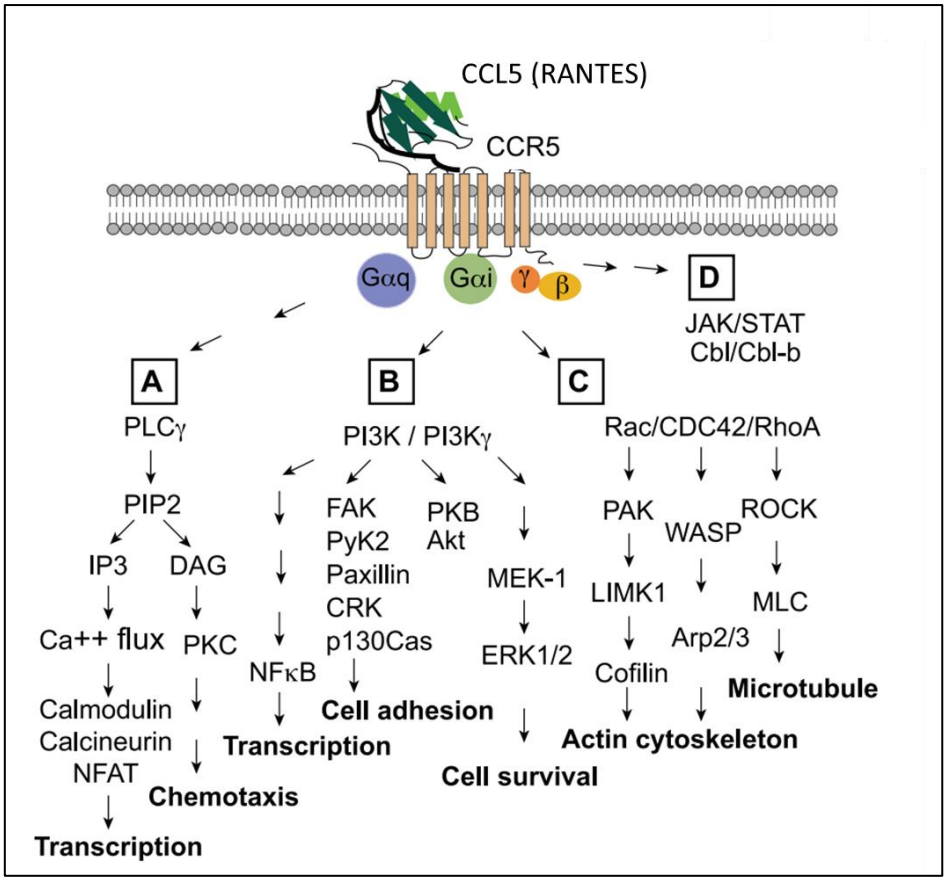

Figure 3: Signalling pathways downstream of CCR5. CCR5 receptor engagement activates heterodimeric G proteins that in turn trigger downstream signalling cascades including phospholipase C-γ (PLC-γ)**(A)**, PI3K/PI3Kγ **(B)**, Rac/CDC42/RhoA (Rho family GTPases)**(C)** and janus kinase/signal transducer and activator of transcription (JAK/STAT) pathways **(D)**. These signalling transduction pathways then mediate cell transcription, chemotaxis, adhesion, survival and cytoskeleton rearrangement. Sourced from Wu and Yoder. [33].

2.3.2. Toll-like receptor 4 (TLR4)

TLR4 is a type-I transmembrane pattern recognition receptor (PRR) belonging to the toll-like receptor (TLR) family [35]. TLRs play a crucial role in innate immunity [35]. They are characterized by an extracellular leucine-rich repeat (LRR) domain allowing the recognition of conserved microbial molecular motifs called pathogen-associated molecular patterns (PAMPs); and an intracellular toll/interleukin-1 receptor-like (TIR) domain, involved in signal transduction [35], [36]. TLR4 binds specifically lipopolysaccharide (LPS), produced by gram-negative bacteria, and is the most studied member of the TLR family [37]. The recognition of LPS by TLR4 follows several sequential steps. First, LPS is extracted from bacterial membranes by LPS binding protein (LBP) and delivered to the protein CD14 [35], [38]. Then, CD14 divides LPS aggregates into monomeric molecules and transfers them to TLR4, associated with the myeloid differentiation factor 2 (MD-2) co-receptor [38]. The binding of two molecules of LPS to TLR4-MD-2 complexes induces their dimerization and subsequent activation of two major downstream signalling pathways, the myeloid differentiation factor 88 (MyD88)- and TIR-

domain-containing adapter inducing interferon-β (TRIF)-dependent pathways (Figure 4) [35]–[37]. Finally, the signalling cascade results in the activation of NF-kB and interferon regulatory factors (IRFs), leading to the synthesis of pro-inflammatory cytokines and chemokines [35]–[37].

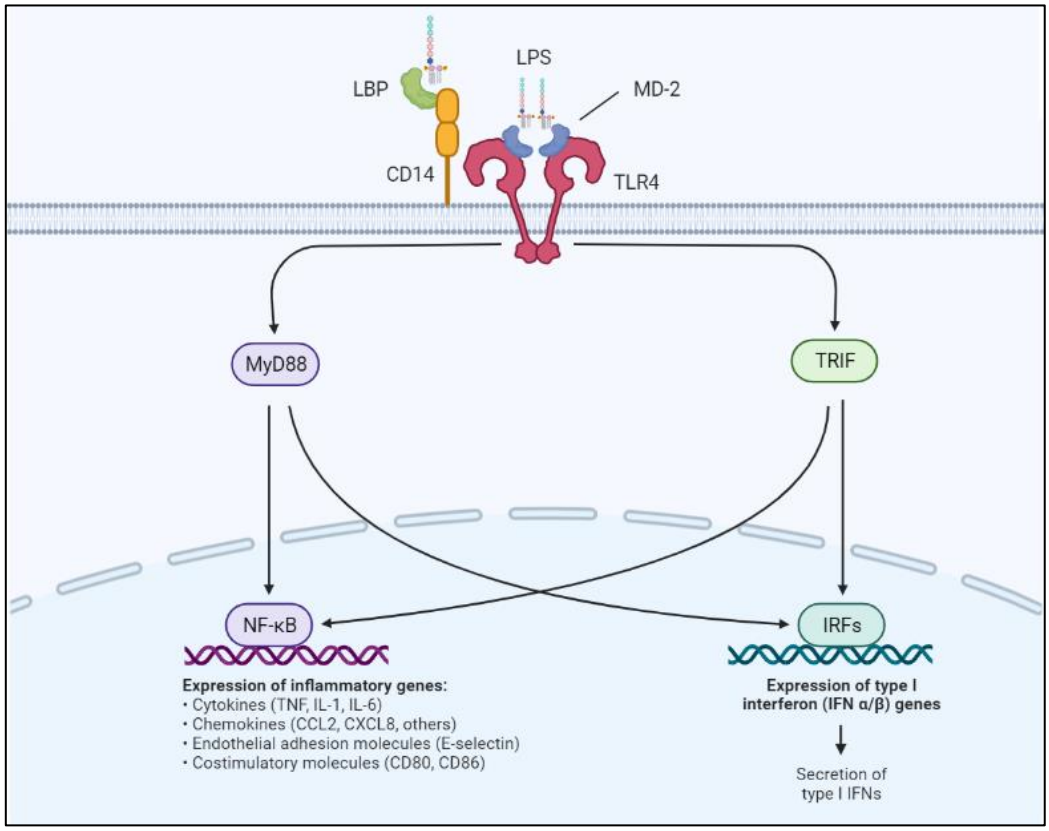

Figure 4: Schematic representation of the LPS/TLR4 signalling pathway. After binding to LBP, LPS is transferred to CD14, which then presents two molecules of LPS to MD-2/TLR4 complexes. LPS association with TLR4/MD-2 induces TLR4 dimerization and the activation of the downstream MyD88 or TRIF-dependent signalling pathways, leading to the expression of inflammatory genes. Inspired from Lu et al. [39] and Vaure and Liu. [35].

2.4. eNAMPT role in cancer

Numerous studies investigated the relationship between eNAMPT and cancer. Elevated concentrations of circulating eNAMPT have been associated with various types of cancer, from solid tumors to hematological malignancies [40]. Furthermore, it has been suggested that eNAMPT modulates several hallmarks of cancer to support tumor development and progression (Figure 5) [10].

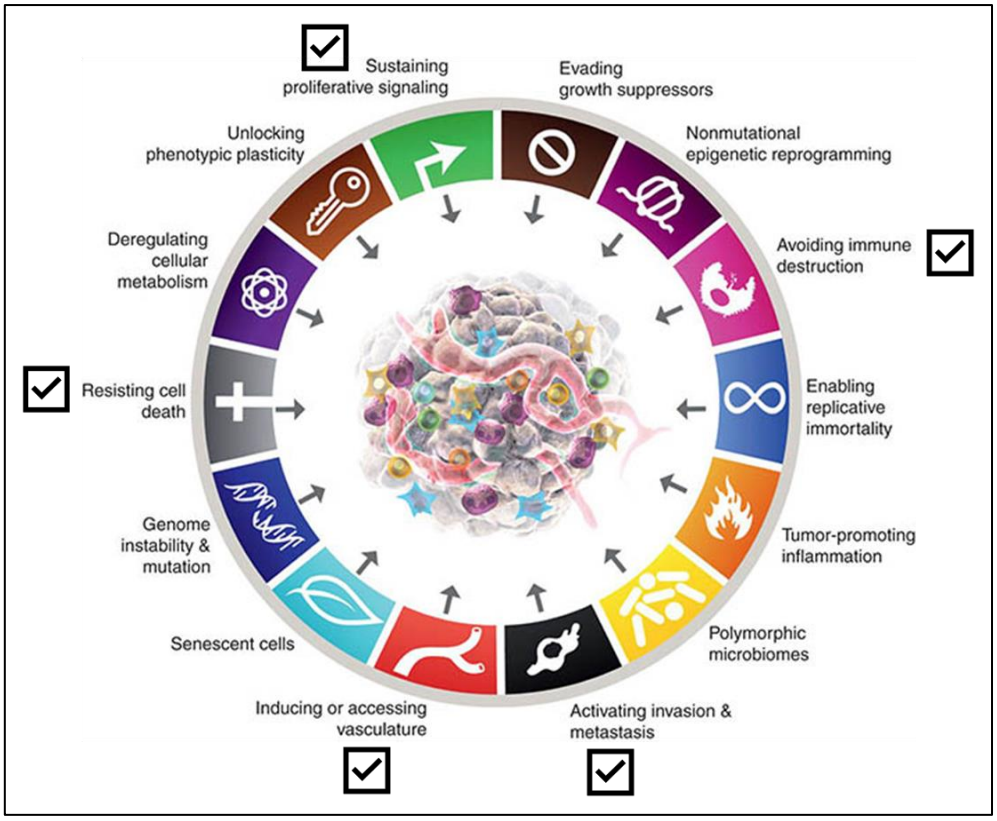

Figure 5: Hallmarks of cancer modulated by eNAMPT. eNAMPT contributes to cancer progression by sustaining tumor cell proliferation, protecting cancer cells from cell death, inducing angiogenesis and metastasis formation, as well as by promoting immunosupressive conditions. Adapted from Hanahan [41].

2.5. Monoclonal antibodies as therapeutics

Antibodies, also known as immunoglobulins (Ig), are proteins secreted by B cells in response to the presence of foreign molecules in the organism [42]. Antibodies recognize a unique antigenic determinant called epitope [42]. In the context of adaptive immune response, antibodies recognize specific antigens on pathogens and allow their elimination, through direct neutralization, recruitment of effector immune cells or activation of the complement [42], [43]. Inspired by this highly specific natural mechanism, researchers have proposed using antibodies to selectively target tumors. This therapeutic approach moved from theory to practice with the advent of hybridoma technology in 1975, which allowed the production of monoclonal antibodies (mAbs) in large quantities [44]. The following section summarizes the structural and functional features of antibodies and the methods of production of monoclonal antibodies.

2.5.1. Antibody structure

Antibodies are heterodimeric Y-shaped proteins, consisting in two identical heavy chains (H) and two identical light chains (L), linked together by disulfide bonds [45]. Based on the sequence and structure of their heavy chains, immunoglobulins are categorized into five classes: IgA, IgD, IgE, IgG and IgM [46]. Among them, IgGs are the most commonly used for therapeutic purposes due to their long half-life and relative ease of production [45]. IgGs can be further divided into four subtypes: IgG1, IgG2, IgG3 and IgG4, which differ in their hinge region (flexible amino acid stretch in heavy chains central part) structure and their functions [42], [47]–[49]. IgG1 is the most abundant IgG subclass [47]. IgG heavy chains contain three constant domains (CH1, CH2 and CH3) and one variable domain (VH), while IgG light chains consist of one constant domain (CL) and one variable domain (VL) (Figure 6) [47]. IgG is organized into three functional units: two antigen-binding fragments (Fabs, corresponding to antibody "arms", see Figure 6), composed of the VH, VL, CL and CH1 domains; and a "stalk" named crystallizable fragment (Fc) comprising the CH2 and CH3 domains [47], [48]. Fabs are responsible for antigen recognition [50]. Fab's variable domains (VL and VH domains) contain, three complementarity-determining regions (CDRs), each; all six forming the paratope (or the antigen-binding site) [46], [50]. On the other hand, the Fc region mediates the effector functions through its interaction with Fc gamma receptors (FcγRs) or the complement system [46], [51]. In addition, antibody Fc portion also binds to neonatal Fc receptor (FcRn) expressed by endothelial cells and macrophages [42], [52]. FcRn binding protects the antibody from lysosomal degradation, thereby contributing to its prolonged half-life [42], [52].

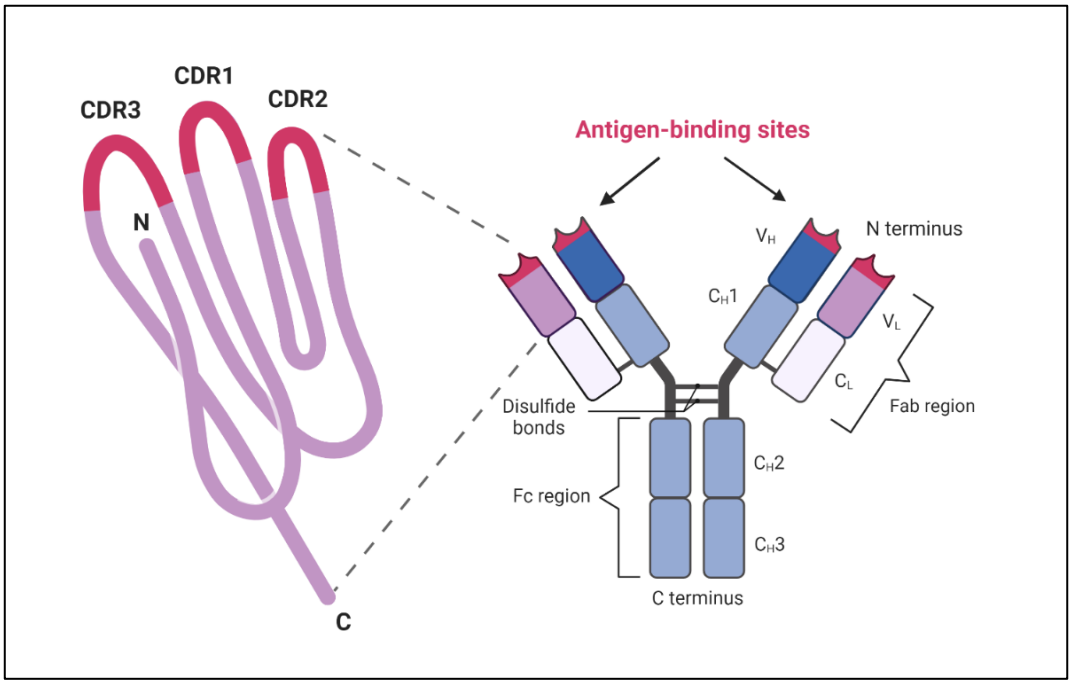

Figure 6: Structure of an IgG1. Cartoon depicting a secreted IgG1 molecule. The heavy and light chains are coloured in blue and pink, respectively. The two antigen-binding sites or paratopes are coloured in red. Inspired from Abbas et al. [42].

2.5.2. Antibody functions

2.5.2.1. Neutralization

Antibodies can directly neutralize the infective or the pathogenic agent (e.g. molecules, bacteria, virus or fungi) by binding to it and blocking its function [42], [43]. In particular, through binding to its target, antibodies can interfere with the ability of the pathogenic agent to interact with cell surface receptors [42], [43].

2.5.2.2. Fc-mediated effector functions

Antibodies can also promote the elimination of microbial pathogens, infected cells or tumor cells, by activating effector mechanisms of the immune system via their Fc region [43]. The IgG1 and IgG3 subtypes are able to activate the complement system [46]. The complement cascade ends with the generation of a membrane attack complex (MAC) that perforates the membrane of the targeted cells or bacteria, leading to their lysis [53]. This mechanism is referred to as complement-dependent cytotoxicity (CDC) [46]. Furthermore, the IgG Fc portion is able to interact with various Fc gamma receptors (FcγRs) expressed on immune cells [54]. The human FcγR family contains six members expressed on myeloid and lymphoid cells, which exhibit immune activating or inhibitory functions [55]. FcγRI (CD64), FcγRIIa (CD32a), FcγRIIc (CD32c), FcγRIIIa (CD16a) and FcγRIIIb (CD16b) are activating FcγR, while FcγRIIb (CD32b) functions as an inhibitory receptor (Figure 7) [54]–[56]. Via engagement of their Fc domain with FcγRs expressed at the surface of effector immune cells, IgGs can initiate target cell killing through antibody-dependent cell-mediated cytotoxicity (ADCC) or antibody-dependent cellular phagocytosis (ADCP) mechanisms [42], [57]. During ADCC, IgGs bind to target cells expressing tumor, viral or bacterial antigens and direct FcγR-bearing effector immune cells, such as NK cells, to eliminate them [58]. During ADCP, IgGs both opsonize target cells and engage the FcγR of phagocytes (e.g. macrophages), leading to target cells engulfment by the latter [42], [59].

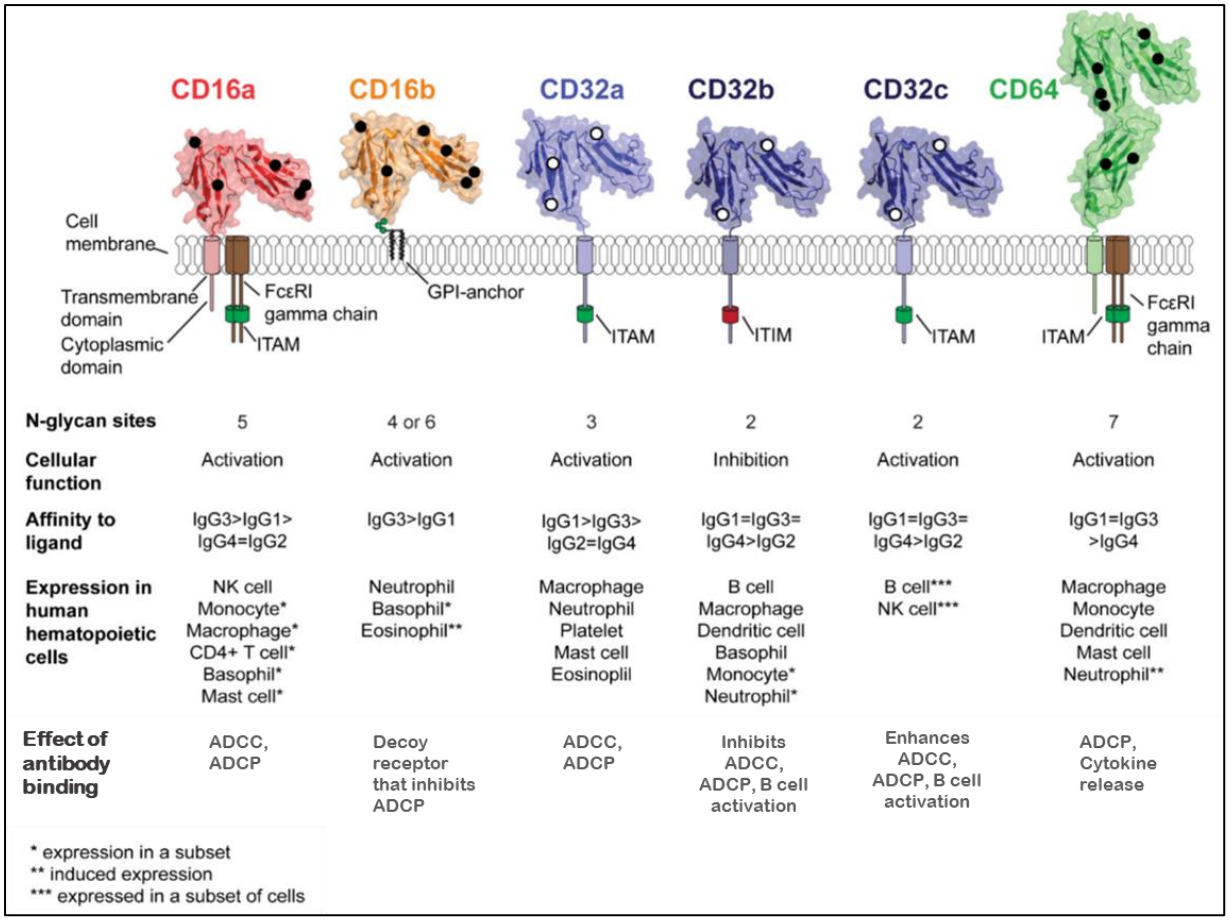

Figure 7: Summary of human FcγR characteristics. The human FcγR family contains six members that can be distinguished by their activating or inhibitory function and their differential affinity for IgG subtypes. Furthermore, human FcγRs are differentially expressed on lymphoid and myeloid immune cells. Adapted from Patel et al. and Musolino et al. [55], [60].

Each IgG subtype binds to individual FcγRs with different affinities (Figure 7) and thereby exhibits a differential ability to trigger effector functions (Table 1) [42], [47]. Human IgG1 and IgG3 isotypes interact efficiently with most FcγRs and are therefore potent activator of Fc-mediated cellular cytotoxicity mechanisms [47]. In contrast, IgG2 and IgG4 display reduced affinity for a number of FcγRs and are hence poor inducers of Fc-mediated effector functions [47], [61].

Table 1: Human IgG subclass Fc-mediated effector functions. Table adapted from Almagro et al. [62]. Abbreviations: CDC, complement-dependent cytotoxicity; ADCC, antibody-dependent cell-mediated cytotoxicity; ADCP, antibody-dependent cellular phagocytosis; IgG, immunoglobulin G.

Subclass	IgG1	IgG2	IgG3	IgG4
CDC	++	+ / -	++	-
ADCC	+++	+ / - -	++	+ / - -
ADCP	+	+	+	+ / - -

2.5.3. Development of therapeutic monoclonal antibodies

2.5.3.1. History of mAbs development

The development of monoclonal antibodies began in 1975 with the introduction of the hybridoma technology by Köhler and Milstein [45], a discovery recognized by the Nobel prize in physiology or medicine in 1984 [63]. The hybridoma technology involves isolating B cells from mice after immunization with a specific antigen and fusing these antibody-producing B-lymphocytes with an immortalized myeloma cell line [64], [65]. This results in the generation of immortalized hybridoma clones that secrete antibodies unlimitedly [65]. Ultimately, clones specific to the antigen of interest are selected to produce high-affinity mAbs in large quantities [63]. This groundbreaking technology was the starting point for the use of monoclonal antibodies for therapeutic and diagnostic purposes and has led to significant improvements in medicine.

The first mAb approved for use in humans was muromonab-CD3 (also named Orthoclone OKT3®), a murine antibody targeting CD3 receptor on T cells, developed in 1986 to prevent kidney transplant rejection [66] (Figure 8). Nevertheless, its use has been limited due to the development of human anti-murine antibodies (HAMA) by treated patients, which has dampened antibody effectiveness and caused the appearance of side effects [45], [64]. To overcome these issues, researchers developed strategies to approximate the structure of human antibodies in order to reduce immunogenicity. For instance, they developed chimeric antibodies, which are antibodies combining murine variable domains with human constant domains, or humanized antibodies, in which only the CDRs are of murine origin [66]. In 1997, the US Food and Drug Administration (FDA) approved the first humanized mAb, an anti-IL-2 receptor named daclizumab (Zenapax®), also indicated for the prevention of kidney transplant rejection [66], [67]. The humanization of murine antibodies greatly improved their tolerability and their use for the treatment of diseases requiring long-term administration, such as cancer [66], [68]. Finally, the advent of phage display, a technology introduced by George P. Smith and Sir Gregory P. Winter, enabled the production of fully human antibodies [66], [69]. The first fully human monoclonal antibody generated with phage display technology, adalimumab (Humira®), was approved by the FDA in 2002 for the treatment of rheumatoid arthritis [67], [68].

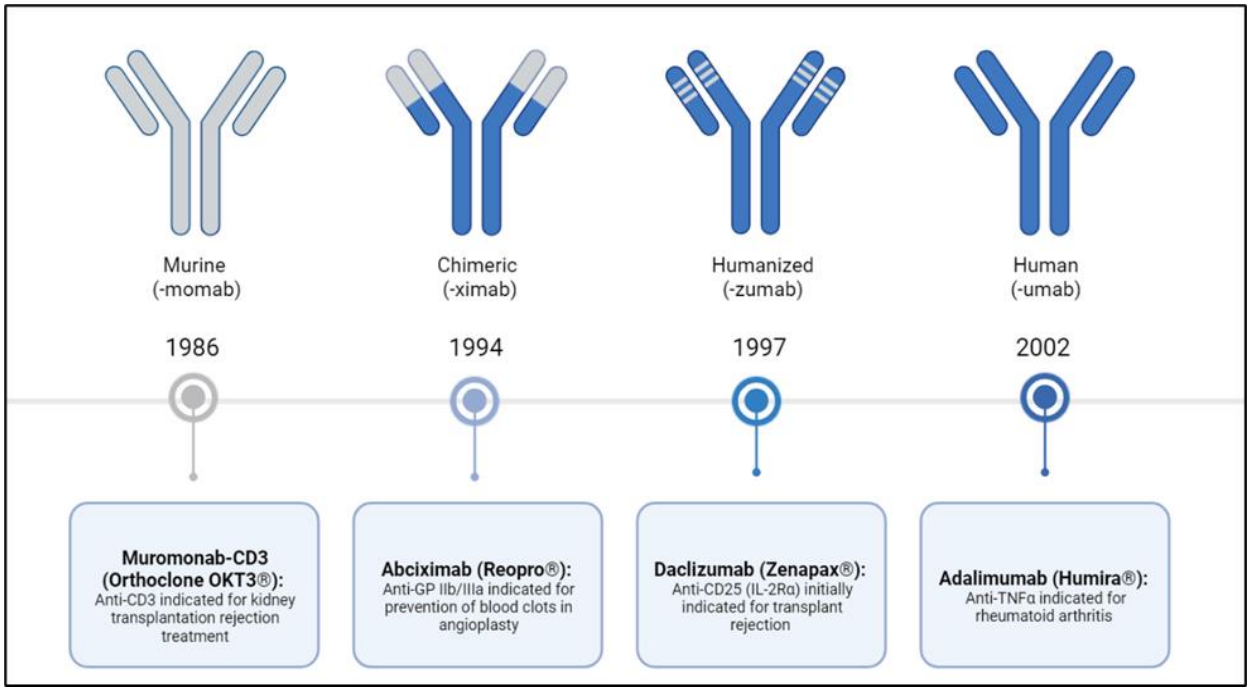

Figure 8: Humanization of monoclonal antibodies from murine to fully human mAbs. The first monoclonal antibody developed for each type of monoclonal antibody is indicated with the date of its approval by the FDA. Adapted from Lu et al. [66].

2.5.3.2. Phage display technology

Phage display is the most widely used technique for the generation of monoclonal antibodies *in vitro* [70]. In 1985, George P. Smith showed that the insertion of a foreign DNA fragment into the coat protein gene of filamentous phage allowed the presentation of a peptide of interest to the phage surface [71], resulting in a direct link between genotype and phenotype [72]. Based on this principle, McCafferty et al. [73] then described the antibody phage display technology which consists of screening, against a desired immobilized antigen, a large antibody fragment repertoire displayed on the surface of filamentous bacteriophages (e.g. M13 bacteriophage) [71], [74]. The antibody fragments displayed are Fab or typically single-chain variable fragments (scFvs) [70], [72]. Specifically, scFvs are composed of the VH and VL domains of an antibody linked by a short peptide linker [74]. ScFvs which are smaller than Fabs, are preferentially used for the generation of monoclonal antibodies by phage display, due to their better expression in *Escherichia coli* (*E.Coli*) [72].

The generation of monoclonal antibodies by phage display starts with the construction of phage display libraries. Four main types of phage display libraries can be generated: immune, naïve, synthetic and semisynthetic libraries [71], [72]. Immune and naïve libraries are generated from mRNA extracted from B cells of immunized and naïve donors respectively [71]. After a reverse transcription polymerase chain reaction (RT-qPCR), the VL and VH gene repertoires of these donors are amplified by PCR and cloned into phagemid vectors [71]. In contrast, synthetic libraries construction involves inserting random CDRs into fully synthetic framework sequences, before cloning the resulting artificial VH and VL gene repertoires into phagemids [72]. Semisynthetic libraries combine synthetic frameworks with natural CDRs [75]. Library construction leads to the generation of large and highly diverse phagemid repertoires [71]. *E.Coli* cells are then transformed with the generated phagemid libraries and infected with helper phages to produce phage display libraries with a size ranging from 10^6 to 10^{11} (Figure 9) [72], [76].

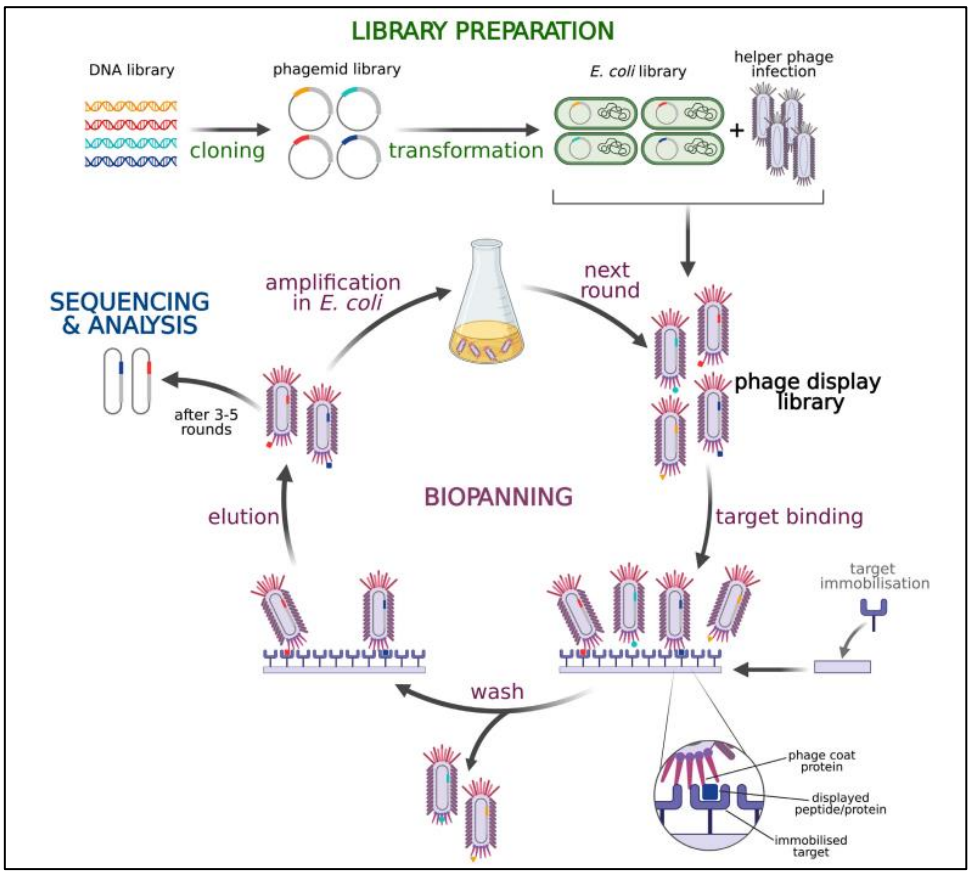

Figure 9: Overview of libraries preparation and selection procedures. Human VH and VL gene repertoires are cloned into phagemids. The phagemid libraries generated are used to transform *E.coli* cells, which are also infected with helper phages. This results in the production of phage display libraries with a diversity ranging from 10^6 to 10^{11} pfu. These phage libraries are then affinity-screened against a target of interest, immobilized on a solid surface. Following a washing procedure allowing to eliminate unbound phages, the target-specific phages are eluted and amplified in *E.coli*. After three rounds of selection (or biopanning), the binders are sequenced and analysed. Sourced from Jaroszewicz et al. [72].

To select for target binding, phage libraries are exposed to immobilized target in a procedure called biopanning or selection [72]. The target protein can be presented on solid surfaces such as immunotubes, magnetics beads, microplates or columns matrices [71]. Successive washing steps are performed to remove unbound phages and weak binders [72]. Afterwards, the bound antibody phages are eluted and amplified in *E.Coli* [71], [77]. This amplification step allows the production of an enriched pool of phages that will constitute the library for the next round of affinity selection [72]. The selection cycle is repeated three to five times. Each repetition significantly increases the proportion of phages specific to the target [72]. At the end of the selection/biopanning cycle, selected antibody phage variants are screened to identify the specific binders and to assess their affinity to the target antigen [72], [77]. Various methods can be used for this screening step, such as enzyme-linked immunosorbent assay (ELISA), immunocytochemistry techniques, flow cytometry or surface plasmon resonance (SPR) [72], [77]. Finally, antibody fragment genes are subcloned to produce monoclonal antibodies [77]. A comprehensive description of the process of generating monoclonal antibody by phage display is presented in the Materials and Methods section.

2.6. NAMPT as therapeutic target

2.6.1. Therapeutics targeting intracellular NAMPT (iNAMPT)

2.6.1.1. NAMPT inhibitors

In the past decade, numerous small molecules inhibiting NAMPT's NAD biosynthetic activity have been designed for the treatment of cancer. The first NAMPT inhibitor (NAMPTi) presenting anti-cancer effects, (E)-N-[4-(1-benzoylpiperidin-4-yl)butyl]-3-(pyridin-3-yl) acrylamide or FK866 (also named APO866), was reported by Hasmann and Schemainda in 2003 [78], [79]. They observed that this compound was able to induce the elimination of HepG2 liver cancer cells by inducing their apoptosis, with a one-digit nanomolar potency [78]. Furthermore, the co-crystallization of NAMPT with FK866 performed by Khan et al. revealed that FK866 inhibits NAMPT activity by binding to the tunnel cavity at the interface of NAMPT dimer and by competing with NAM for the binding site [80]. In 2008, the pyridyl cyanoguanidine CHS-828 (also named GMX1778), which had already shown antitumor activity in the literature [81], was suggested as a NAMPT inhibitor by Olesen et al. [82]. FK866 and CHS-828 chemical structures are presented in Figure 10. FK866, CHS-828 and its prodrug GMX1777, were evaluated in early-phase clinical trials in patients with solid tumors or hematologic malignancies [79]. However, progression of these compounds in clinic was halted due to a lack of objective response and the development of adverse side effects, including thrombocytopenia, gastrointestinal bleeding and skin rash [22], [79]. Since the failure of FK866 and CHS-828 in the clinic, a second wave of NAMPTi as well as dual inhibitors have been developed [22], [83]. Two of them, OT-82 and KPT-9274, are currently being evaluated in phase I clinical trials in patients with solid tumors, leukemia or lymphoma [83].

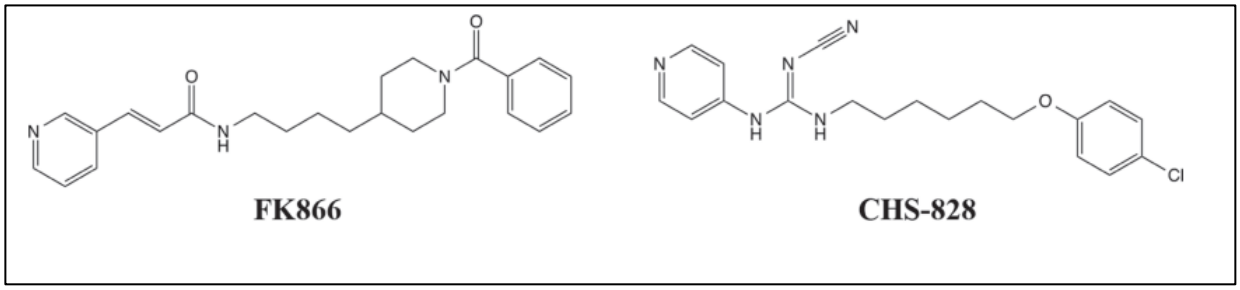

Figure 10: Chemical structure of the NAMPT inhibitors FK866 and CHS-828. Sourced from Ogino et al. [84].

2.6.1.2. NAMPTi-Antibody-drug-conjugate

Antibody-drug-conjugates (ADCs) are therapeutics combining a monoclonal antibody, a chemical linker and a cytotoxic agent [85]. The monoclonal antibody recognizes tumor-associated antigens and allows the delivery of the cytotoxic payload to the tumor site where it will induce cancer cell death [83], [86]. Five years ago, researchers proposed to use NAMPTi as payload for tumor-targeting ADCs, due to their chemical simplicity and their unique mechanism of action [87], [88]. In contrast to NAMPTi, the highly specific targeting of tumor-associated antigens (TAAs) with NAMPTi-ADCs is expected to avoid damage to healthy tissues and limit adverse side effects [83], [89]. Thus, an improved therapeutic window is awaited with NAMPTi-ADCs for cancer treatment [83]. Karpov et al. were the first to demonstrate the potential of using a NAMPT inhibitor as an ADC payload [85]. Similarly, Neumann et al., developed three anti-CD30-NAMPTi-ADCs capable of depleting NAD and ATP in a model of CD30-positive Hodgkin lymphoma (L540cy cells) [87]. Finally, Böhnke et al., recently produced NAMPTi-ADCs targeting various solid TAAs [88]. These conjugates showed high cytotoxic activities *in vitro,* as well as potent antitumour efficacies in THP-1 acute myeloid leukemia and MDA-MB-453 breast cancer xenograft mouse models. Overall, these findings indicate that NAMPTi may constitute promising new payloads for cancer treatment with ADC.

2.6.2. Therapeutics targeting iNAMPT and eNAMPT: PROTACs

A novel therapeutic strategy, allowing the disruption of both iNAMPT and eNAMPT activities, has recently been suggested. This new approach is based on NAMPT-specific PROteolysis-TArgeting Chimera (PROTAC) compounds, inducing intracellular NAMPT protein degradation via the ubiquitin-proteasome pathway [90], [91]. PROTAC molecules are composed of a ligand binding the protein of interest and another ligand recruiting E3 ubiquitin ligase, connected by a linker (Figure 11) [92]. Through its two ligands, PROTAC compound recruits the E3 ubiquitin ligase to the vicinity of iNAMPT and causes proximity-induced ubiquitination and degradation of iNAMPT by the ubiquitin proteasome system [92]. Consequently, eNAMPT secretion and its extracellular activities are abrogated. Zhu et al. [90] reported promising anti-cancer effects of NAMPT-targeted PROTACs: their compounds both potently inhibited iNAMPT activity and

inactivated pro-survival intracellular signalling pathways (NF-kB and mitogen-activated protein kinase-extracellular signal-regulated kinase 1/2 (MAPK-ERK 1/2)) in hematological tumor cells [90]. Wu et al., for their part, developed a NAMPT-specific PROTAC capable of depleting NAD^+ intracellular level *in vitro* and inhibiting tumor infiltration by myeloid-derived suppressive cells in CT26 tumor-bearing mice [91].

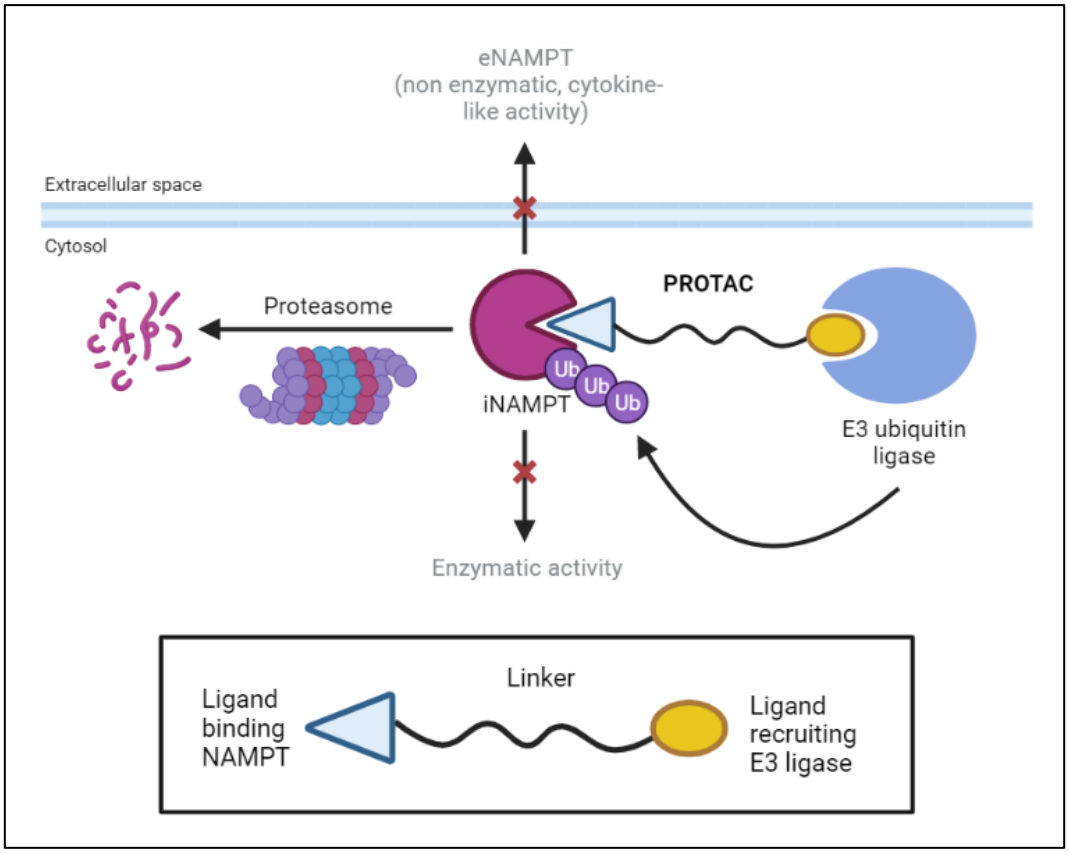

Figure 11: Principle of the PROTAC technology. PROTAC compound consists of a ligand binding the protein of interest (blue triangle) and a ligand recruiting E3 ubiquitin ligase (yellow circle), connected by a linker. NAMPT-specific PROTAC brings E3 ubiquitin ligase into close proximity to NAMPT, leading to NAMPT ubiquitination and degradation by the proteasome. Adapted from Zhu et al. [90].

2.6.3. Therapeutics targeting eNAMPT: anti-eNAMPT antibodies

The use of eNAMPT-specific monoclonal antibodies has been proposed to block eNAMPT extracellular functions [1], [93]. As discussed in detail in the review, various experimental findings suggest that neutralizing eNAMPT with antibodies might be a valuable therapeutic approach for the treatment of inflammatory disorders, such as cancer. For instance, Pillai et al. [94] first showed that eNAMPT blocking with a polyclonal antibody inhibited eNAMPT pro-hypertrophic effect on rat cardiomyocytes, as evidenced by reduced protein synthesis and cardiomyocyte size. Subsequent studies demonstrated that eNAMPT-specific antibodies were able to neutralize eNAMPT-mediated activation of intracellular signalling pathways. For

example, Audrito et al. [95] and Colombo et al. [96] reported a reduction of eNAMPT-induced STAT3 phosphorylation in nurse-like cells (differentiated monocytes obtained from chronic lymphocytic leukemia patients) and 4T1 cells, respectively, in the presence of an eNAMPT-blocking antibody. On the other hand, Quijada et al. [97], demonstrated that an anti-eNAMPT pAb was able to diminish eNAMPT-mediated phosphorylation of NF-kB, p42/44 ERK, p38 and JNK signalling proteins in human lung endothelial cells. A significant reduction in eNAMPT-induced NF-kB activation was also observed by the same group after exposure of prostate cancer cells to an anti-eNAMPT mAb [98]. Interestingly, anti-eNAMPT antibodies were shown to inhibit cancer cell migration *in vitro* (NCI-H446 cell transendothelial migration and A549 cell radiation-induced migration) [99], [100], suggesting that eNAMPT-targeting antibodies could be used to block eNAMPT pro-chemotactic function.

Beside *in vitro* evidence, numerous *in vivo* studies proposed that eNAMPT neutralization with antibodies could be a valid therapeutic approach for the treatment of inflammatory diseases. For instance, Kieswich et al. [101] showed that intraperitoneal administration of an anti-eNAMPT pAb to high fat diet (HFD)-fed mice reverted their diabetic phenotype, as evidenced by reduced serum glucose and insulin levels and increased quantitative insulin sensitivity check index (QUICKI). This polyclonal antibody also improved β-cell function and partially resolved tissue and systemic inflammation. Furthermore, Colombo et al. [96] observed a reduction in intestinal inflammation in mice suffering from colitis (dinitrobenzene sulfonic acid (DNBS)- and dextran sulfate sodium (DSS)- treated mice), after injection of an anti-eNAMPT monoclonal antibody, C269. Specifically, they reported that C269 treatment ameliorated acute colitis by restraining body weight loss, colon shortening and transmural necrosis [96].

Most importantly, the group of Joe G. N. Garcia (University of Arizona) demonstrated therapeutic effects of a humanized therapeutic eNAMPT mAb, ALT-100, currently in a Phase I clinical trial (NCT05426746), in several pre-clinical disease models. This antibody is derived from P-1076 antibody described in WO/2021/026508 patent [102]. First, they reported that ALT-100 was able to reduce the severity of inflammatory lung injury in murine and porcine models [97], [103], [104]. ALT-100 antibody significantly diminished LPS-induced histologic evidence of lung injury and LPS-induced increase in bronchoalveolar lavage (BAL) polymorphonuclear neutrophil (PMN) counts, BAL protein levels and plasma cytokine (IL-6, IL-1Ra) levels. They also showed that ALT-100 treatment reduced tumor size and inhibited tumor cell invasion and metastasis in prostate cancer (PCa) orthotopic xenograft mouse models [98]. Finally, they observed that the antibody attenuated pulmonary hypertension severity in rats [105] and decreased radiation-induced lung fibrosis (RILF) severity in mice [106]. All this evidence (see Tables 2 and 3 of the accompanying review in section 1), supports a rationale for generating eNAMPT-blocking antibodies to treat inflammatory conditions such as cancer.

3. Aim of the study

Ubiquitous intracellular enzyme nicotinamide phosphoribosyltransferase (NAMPT), plays an essential role in cell metabolism and survival by regulating NAD^+ levels [6]. NAMPT is also found in the extracellular space where it has been proposed to exert pathological effects in diverse inflammatory disorders, including cancer [1]. Numerous studies demonstrated that extracellular NAMPT (eNAMPT) sustains tumor cell proliferation, promotes tumor invasion and metastasis and contributes to the establishment of an immunosuppressive micro-environment [10], [95]. eNAMPT also acts as a pro-angiogenic mediator and a pro-inflammatory cytokine [2]. Evidence suggests that eNAMPT performs these extracellular functions by binding to cell surface receptors [10]. Two putative receptors have been identified so far, TLR4 and CCR5 [26], [27].

Importantly, multiple studies reported that eNAMPT functions are independent of enzymatic activity [95], [107]–[109] and thus cannot be addressed with inhibitors of NAMPT enzymatic function [79]. The development of new classes of therapeutics neutralizing eNAMPT biological activity has therefore become a key priority, with eNAMPT blocking antibodies representing the most obvious option [95], [96], [98], [107]. As of today, there are no approved antibody drug candidates targeting eNAMPT, but there is one anti-eNAMPT neutralizing antibody, ALT-100, being evaluated in a Phase I clinical trial in healthy volunteers (NCT05426746).

Within the framework of the INTEGRATA European project, which aimed at developing new chemical and biological approaches to target NAD production and signalling in cancer, this thesis project consisted in developing and testing new anti-eNAMPT neutralizing monoclonal antibodies (mAbs). The first objective was to generate fully human anti-huNAMPT mAbs using a phage display platform. This objective has been accomplished, as a number of high-affinity eNAMPT binders were generated. In the next step, eNAMPT blocking activity of these mAbs was to be investigated in relevant binding and functional assays *in vitro*, and then, eventually in an *in vivo* model of breast cancer. Unfortunately, in spite of huge efforts devoted to reproducing published data and to developing new *in vitro* assays, the eNAMPT blocking properties of the antibodies generated could not eventually be addressed. The reason of this failure lies in our inability to monitor or otherwise demonstrate of any kind eNAMPT function, in any kind of assay, ranging from simple binding assays to more complex cell-based assays. The objective of this study has therefore not been attained, or has been attained partially, as some high-affinity eNAMPT binders have indeed been generated.

4. Materials and methods

4.1. Recombinant NAMPT proteins

4.1.1. In house NAMPT protein

The DNA sequence of NAMPT has been described [3] and is available at GenBank under the accession number NM_005746. An optimized NAMPT DNA sequence, adapted for production in mammalian cells and containing the N-terminal Biotin AviTag (Avidity, Aurora, CO, USA) and Hexahistidine Tag was first ordered for synthesis by Eurofins Genomics (Germany). NAMPT sequence was then cloned into the episomal expression vector pEAK8 (HindIII/EcoRI) and expressed in Transformed Human Embryo Kidney monolayer epithelial cells (PEAK cells, Edge Bio). Six days after transfection, cell culture supernatant was harvested and NAMPT protein was purified by his-tag affinity chromatography with Ni-NTA resin (Qiagen, Hanbrechtikon, Switzerland). Correct size and dimerization of the protein was verified by SDS-PAGE under reducing and non-reducing conditions. To facilitate NAMPT immobilization for phage display selection, the protein was also biotinylated by Avi-Tag-mediating single-site biotinylation, via a method previously described in [110]. The correct biotinylation of NAMPT was controlled by pull-down analysis. Briefly, magnetic streptabeads (Dynabeads M280, Dynal, ThermoFisher Scientific, Waltham, MA, USA) were incubated with PBS (Phosphate-Buffered Saline; Sigma-Aldrich, St Louis, MO, USA), 2.5ug or 1ug of NAMPT-biot protein for 30 minutes at room temperature. The supernatants were then separated from the streptabeads using a magnetic stand and both were analysed by SDS-PAGE under reducing conditions. Non incubated NAMPT protein samples were also loaded into the gel as controls.

4.1.2. Commercial NAMPT proteins

In addition to the in-house recombinant NAMPT protein, several commercial human NAMPT proteins were also used throughout this research project (Table 2). The recognition of the recombinant NAMPT proteins by a specific anti-NAMPT antibody was verified by ELISA (Figure S1A). Furthermore, the enzymatic activity of NAMPT proteins was tested with NAMPT activity colorimetric assay kit (Abcam, Cambridge, UK) following manufacturer's recommendation (Figure S1B).

Table 2: Commercial recombinant NAMPT proteins.

Recombinant protein	Manufacturer	Reference	Tag
Human NAMPT	MyBiosource	MBS203137	His Tag
	SinoBiological	10990-H20B	His and GST Tag
	Adipogen	AG-40A-0031Y-3010	FLAG Tag
	R&D systems	8424-VF	His Tag
	Peprotech	130-09	
	Abcam	ab198090	
	MBL International	CY-E1251	His Tag

4.2. Anti-eNAMPT monoclonal antibody generation

All anti-eNAMPT mAbs generated during this thesis project are human IgG1. The mAbs were produced with an active Fc domain or a silenced Fc domain. The P-1076 antibody, from patent application WO/2021/026508 [102], and from which ALT-100 antibody is derived (P-1076-mod1 in WO/2021/026508 patent) [97], [98], [111], was also produced. ALT-100 and P-1076, differ by only two amino acids: one in the light chain framework region (L-to-V mutation) and one in the heavy chain CDR2 (D-to-E mutation). These mutations were introduced to remove a potential T-cell epitope and a potential cleavage/fragmentation site, respectively [102].

4.2.1. Phage display

4.2.1.1. Phage display libraries

Proprietary synthetic or semi-synthetic phage libraries (diversity: 10^{11}-10^{12} pfu) were used for phage display selections. Novimmune libraries are of two types: in A libraries, both VH and VL genes are diversified while in B libraries, only VL genes are diversified and the VH is fixed ("Novimmune VH"). Noteworthy, in the A libraries, diversity is mainly carried out by the CDR3 of the VH (CDRH3). In B libraries, since the VH is fixed, diversity is provided by the VL CDR3 (CDRL3).

Two lead optimization (LO) and five round optimization (RO) libraries were also constructed as described in [112], [113]. Typically, a lead optimization consists of introducing diversity into the sequence of a candidate antibody, while a round optimization involves introducing diversity into a set of original sequences. In my case, LO libraries were generated by combining the VH sequence of an scFv candidate obtained from an A library, IgG_AE_1D2, with diversified VL sequences of different germlines. Regarding the RO libraries, the CDRL3 of several candidates obtained from B libraries, were extracted and introduced into their corresponding VL germlines, diversified in CDRL1 and CDRL2. The newly obtained VL sequences were then combined with "Novimmune VH". In these LO and RO libraries, diversity is provided only by the VL, the VH being fixed. The LO and RO libraries generated had a diversity of 10^9 pfu.

4.2.1.2. Selections

E. coli TG1 cells were grown in 2xTY medium at 37°C (240 rpm). Aliquots of scFv phage libraries were first blocked with PBS containing 1.5% (w/v) BSA (bovine serum albumin; Sigma-Aldrich), 1.5% (w/v) skimmed milk (Sigma-Aldrich) and 0.05% Tween 20 (Sigma-Aldrich) for one hour at room temperature. In the case of phage selection with immunotubes (for non-biotinylated target), the blocked scFv phage libraries were deselected for one hour at room temperature on immunotubes (ThermoFisher Scientific, Waltham, MA, USA) previously

coated overnight with 3% (w/v) BSA. Then, the deselected phages were incubated for two hours at room temperature on immunotubes previously coated overnight with recombinant NAMPT protein. In the case of phage selection with magnetic beads (for biotinylated target), the blocked scFv phage libraries were deselected either on streptavidin (Dynabeads M280, Dynal, ThermoFisher Scientific) or neutravidin (Sera-Mag SpeedBeads Neutravidin coated magnetic beads, ThermoFisher Scientific) beads. Afterward, in house NAMPT-biot protein was coated on magnetic streptavidin or neutravidin beads and incubated with the deselected phage for two hours at room temperature, 20 rpm. As described in [113], for both strategies, unbound phages were subsequently removed by several washes of PBS/0.1% Tween 20 and PBS. Specific phages were eluted with 100mM triethylamine (TEA, Sigma-Aldrich). After a neutralisation step, TG1 growing cells were infected with the selected phages for one hour at 37°C (100 rpm). The selection output was determined by serial dilution of an infected TG1 sample. An example of output/input ratio obtained is presented in the supplementary Figure S2. Finally, infected TG1 cells were plated on 2xTYAG agar Bioassay plates (100µg/mL ampicillin, 4% glucose (w/v), both from Sigma-Aldrich) and scraped off with 2×TY medium after an overnight incubation at 30°C. TG1 aliquots were stored at -80 °C in glycerol (17%) for further use.

4.2.1.3. Phage rescue

TG1 containing the previously selected phagemids (diversity: 10^9-10^{10} pfu) were inoculated in 2xTYAG medium (100µg/mL ampicillin, 4% glucose (w/v)) and incubated at 37°C (240 rpm) until mid-log growth phase. A superinfection with M13KO7 helper phage was performed for one hour at 37°C (90 rpm) to rescue the libraries. TG1 cells were then grown overnight at 30°C (280 rpm) in a new medium (2xTYAK medium; 100µg/mL ampicillin and 50µg/mL kanamycin (Sigma-Aldrich)). The following day, the bacterial cultures were centrifugated for five minutes at 2400g and the supernatants, containing the phages, were used for a new round of selection.

4.2.1.4. Master plates

After three rounds of selection, individual TG1 clones were randomly picked and grown in 2xTYAG medium (100µg/mL ampicillin, 2% glucose (w/v)) in 96-well round bottom plates (Nunc MicroWell Plates, ThermoFisher Scientific), called Master plates, for six hours at 37°C (120 rpm) or overnight at 30°C (120 rpm). TG1 clones were then stored at -80 °C in glycerol (17%).

4.2.1.5. ScFvs screening

scFv periplasmic preparation

Individual clones were replica plated from the master plates into 96-well deepwell plates (Nunc™ 96-Well Polypropylene DeepWell, ThermoFisher Scientific) containing 2xTYAG medium (100µg/mL ampicillin, 0.1% glucose (w/v)) and grown for six hours at 37°C, 240 rpm. scFvs expression was induced overnight at 30 °C (250 rpm) with 0.02mM isopropyl-β-D-thiogalactopyranoside (IPTG, Applichem, Darmstadt, Germany). The day after, TG1 pellets were recovered and resuspended in TES buffer (50 mM Tris/HCl, pH8, 1 mM EDTA, 20% (w/v) sucrose, all from Sigma-Aldrich) by vortexing. Addition of diluted TES buffer (1:5), followed by incubation of the mixture on ice for 30 minutes, were then performed, allowing the release of bacterial periplasmic content (osmotic shock). After centrifugation, supernatants containing scFvs were recovered and used for screening by enzyme-linked immunosorbent assay (ELISA) or with CellInsight™ CX5 High Content Screening (HCS) platform (ThermoFisher Scientific).

Screening in ELISA

Black 96-well immuno plates (maxisorp plate, ThermoFisher Scientific) were incubated overnight at 4°C with recombinant proteins (1ug/mL). The following day, the plates were blocked for one hour at room temperature with PBS containing 2% BSA and 0.05% Tween 20. After three washes of the assay plates with PBS/0.05% Tween 20, 50µL of periplasmic supernatants were added to the protein-coated wells and incubated for one hour at room temperature. Binding scFvs were detected with mouse anti-c-myc (1 µg/mL, generated in house) and anti-mouse IgG Fcγ-HRP (dilution 1:5000; Jackson Immunoresearch, West Grove, PA, USA) antibodies. The assay was developed with Amplex ultrared reagent (Invitrogen) and the fluorescence was read at 590nm with BioTek Gen 5 microplate reader (Agilent Technologies, Basel, Switzerland).

Screening with CellInsight platform

Streptavidin beads (6.0µm, Polysciences, Warrington, PA, USA) previously coated with NAMPT-biot protein or an irrelevant-biot protein (both at 10ug/mL) were resuspended in filtered PBS containing 2% BSA and dispensed into 384-well clear-bottom plates (Corning, Glendale, AZ, USA) at 3000 beads per well (30uL/well). 70uL of periplasmic preparation mixed with a detection solution containing human anti-c-myc (0.2 µg/mL, generated in house) and anti-human Fc AF647 (dilution 1:5000, Jackson Immunoresearch) antibodies were added to the beads. The assay plates were incubated for three hours at room temperature and binding scFvs were detected using the CellInsight platform and HCS Studio™ Cell Analysis Software.

scFvs expression quantification with CellInsight platform

For screenings involving scFvs generated from LO libraries, scFvs expression was also quantified. Streptavidin beads (6.0 µm, Polysciences) previously coated with 10ug/mL of His Tag Biotinylated antibody (R&D Systems, Minneapolis, MN, USA) were resuspended in filtered PBS containing 2% BSA and dispensed into 384-well clear-bottom plates at 3000 beads per

well (30uL/well). 70uL of periplasmic preparation mixed with a detection solution containing human anti-c-myc (0.2ug/mL) and anti-human Fc AF647 (dilution 1:5000) antibodies were added to the beads. The assay plates were incubated for three hours at room temperature and binding scFvs were detected using the CellInsight platform and HCS Studio™ Cell Analysis Software. A binding / quantification ratio was then calculated for each scFvs.

scFvs sequencing

Finally, TG1 clones containing NAMPT-specific scFvs with high/moderate affinities for the protein were picked from the master plates and transferred in Ecoli NightSeq 96 well plates (Microsynth AG, Balgach, Switzerland) for sequencing by Microsynth company. The obtained sequences were analyzed with Scaligner software. According to their sequence and their binding affinity, several scFvs were selected for reformatting into IgG1 format.

4.2.2. scFv reformatting into IgG

The first step in reformatting scFvs into IgGs was to isolate the variable domains (VL and VH) of the scFvs and subclone them into vectors containing the remaining part of the IgG1 chains (e.g. constant domains CH1, CH2 and CH3 for the heavy chain). Specifically, the VL domain was cloned into kappa or lambda light chain vectors and the VH domain was cloned into a heavy chain vector encoding either an active Fc domain or a silenced Fc domain.

4.2.2.1. Miniprep preparation

Selected scFvs were picked and grown overnight at 37°C (240 rpm) in 2xTYAG medium (100µg/mL ampicillin, 2% glucose (w/v)). The following day, plasmids containing scFv sequences were isolated with ZR Plasmid Miniprep kit (Zymo research, CA, USA) following supplier's procedure. DNA concentration was measured with NanoDrop instrument (ThermoFisher Scientific), and the sequences were controlled by sequencing (Microsynth or Fasteris company, Switzerland) and alignment on scaligner to ensure the absence of any undesirable mutations.

4.2.2.2. Variable domains amplification by PCR

The variable domains of the scFvs were amplified by polymerase chain reaction (PCR) using AccuPrime Pfx DNA polymerase kit (Invitrogen). PCR primers binding to framework 1 (primer 5') or framework 4 (primer 3') of the variable domains and containing BrsDI or BspMI enzyme restriction sites were used. The amplification was performed during 30 cycles with the Matercycler EP Gradient S thermocycler (Eppendorf, Hambourg, Germany). PCR products were then purified using the QIAquick Gel Extraction Microcentrifuge kit (Qiagen) following supplier's procedure.

4.2.2.3. Digestion

Heavy and light chain vectors and purified PCR products were digested with BsrDI or BspMI restriction enzymes in Buffer R (1X final) for 1h30 at 55°C or 37°C (all from ThermoFisher Scientific). Vectors were then dephosphorylated 20 minutes at 37°C with 1µL of phosphatase alkaline (20 units, Roche Pharma**,** Mannheim, Germany). All digested products were purified using QIAquick Gel Extraction Microcentrifuge kit (Qiagen) following supplier's procedure. Their concentration was measured with NanoDrop instrument.

4.2.2.4. Ligation and transformation

The purified variable domains were ligated 15 minutes at room temperature with their corresponding vectors using Rapid DNA ligation kit (Roche Pharma). Ligation samples were then transformed into XL1 Blue competent cells (Zymo Research), and the bacteria were plated on LB-kanamycin (final concentration: 25µg/mL) agar plates and incubated overnight at 37°C. Three colonies for each candidate (3 clones/VL and 3 clones/ VH) were then picked, inoculated into LB-kanamycin medium and allowed to grow overnight for miniprep preparation the following day. The same three clones were also spread on LB-kanamycin agar plates, called master plates, and stored at 4°C for further use.

4.2.2.5. Miniprep preparation and sequencing

Plasmids were isolated with QIAprep Spin Miniprep kit (Qiagen) following supplier's procedure. DNA concentration was measured with NanoDrop instrument. Correct ligation was controlled by sequencing (Fasteris company) the minipreps and by performing an alignment of the resulting sequences on the Sequencher software. For a given antibody candidate, one clone for the light chain and one clone for the heavy chain were chosen for the next steps.

4.2.2.6. Midiprep preparation

Selected clones were picked from the master plates and grown overnight at 37°C (240 rpm) in LB-kanamycin medium. The day after, plasmids were purified with PureLink HiPure Plasmid Filter Midiprep Kit (Invitrogen) and their concentration was measured with NanoDrop instrument. Again, the sequence of the antibodies was checked by sequencing and alignment of the resulting sequences on the Sequencher software.

4.2.2.7. Transfection in PEAK cells

PEAK cells were maintained in Dulbecco's Modified Eagle's Medium (DMEM, Invitrogen), supplemented with 10% heat-inactivated fetal bovine serum (FBS, Sigma-Aldrich), 2mM glutamine (Sigma-Aldrich) and antibiotics at 37°C and 5% CO_2 in humidified atmosphere. Transient co-transfections of the PEAK cells were performed using a mix of DMEM containing Lipofectamine 2000 (Invitrogen) and 18µg of DNA composed 1:1 (w/w) of the heavy chain plasmid and the light chain plasmid. The transfected cells were then incubated at 37°C.

4.2.2.8. Purification

After six days of production, cells supernatant was harvested and clarified by centrifugation (10 minutes at 1300g). IgGs were purified by affinity chromatography using CaptureSelect FcXL affinity resin (ThermoFisher Scientific). Specifically, an appropriate amount of FcXL resin was first washed three times with PBS and resuspended in this same buffer. The resin was then added to cells supernatant and the mix was incubated overnight at 4°C (15 rpm). The next day, samples were centrifuged at 1300g for 10 minutes to collect the resin. The resin was washed two times with PBS and transferred to the Amicon Pro Purification System (Merck Millipore, Burlington, MA). Elution was performed with 50mM glycine (Sigma-Aldrich) at pH 3.5, followed by neutralization of the eluates with Tris-HCl at pH 7.5. Finally, IgGs were formulated in buffer containing 25mM histidine (Sigma-Aldrich), 125mM NaCl (Sigma-Aldrich) at pH 6.0. Antibodies concentration was measured with NanoDrop instrument.

4.2.2.9. Analytics

Purified IgGs were analysed by electrophoresis under denaturing and reducing conditions using the Agilent 2100 Bioanalyzer (Agilent Technologies) and the Protein 80 kit, according to the manufacturer's procedure. Aggregate and fragment levels were determined by SEC-HPLC. The MCS-LAL kit (Charles River Laboratories, Wilmington, MA, USA) was used to assess endotoxin levels. Antibodies were stored at -80°C until use.

4.3. Characterization of the anti-eNAMPT mAbs

4.3.1. ELISA

4.3.1.1. Indirect ELISA

Black 96-well immuno plates (Maxisorp plates) were incubated overnight at 4°C with recombinant proteins (1ug/mL). The following day, the plates were blocked for one hour at room temperature with PBS containing 2% BSA and 0.05% Tween 20. In the case of biotinylated proteins, the coating was performed in black pre-blocked 96-well streptavidin-coated plates (Streptawell plates, Greiner Bio One, Frickenhausen, Germany) for 30 minutes at room temperature. After three washes of the assay plates with PBS/0.05% Tween 20, 50µL of different IgG dilutions were transferred to the wells and incubated for one hour at room temperature. Binding antibodies were detected with an anti-human IgG Fcγ-HRP antibody (dilution 1:5000, Jackson Immunoresearch). Commercial antibodies were detected with an anti-mouse IgG Fcγ-HRP antibody or an anti-rat IgG Fcγ-HRP antibody (dilution 1:5000, both from Jackson Immunoresearch). The assay was developed with Amplex ultrared reagent and the fluorescence was read at 590nm with BioTek Gen 5 microplate reader.

4.3.1.2. Sandwich ELISA

Black 96-well immuno plates (Maxisorp plates) were incubated overnight at 4°C with 10µg/mL of goat anti-human IgG Fcγ antibody (Jackson Immunoresearch). The following day, the plates were blocked for one hour at room temperature with PBS containing 2% BSA and 0.05% Tween 20. After three washes of the assay plates with PBS/0.05% Tween 20, 50µL of IgGs (5ug/mL) were transferred to the wells and incubated for one hour at room temperature. After a new washing step, the plates were incubated with 50µL of different dilutions of recombinant proteins for one hour at room temperature. The recombinant proteins were then detected with streptavidin-HRP (dilution 1:15000, Jackson Immunoresearch) or anti-FLAG tag-HRP antibody (dilution 1:1000, ThermoFisher Scientific) depending on whether or not they were biotinylated. The assay was developed, and the fluorescence measured as previously described.

4.3.1.3. Competitive ELISA

IgG versus scFv

Black 96-well immuno plates (Maxisorp plates) were incubated overnight at 4°C with recombinant NAMPT protein (1µg/mL). The day after, the plates were blocked for one hour at room temperature with PBS containing 2% BSA and 0.05% Tween 20. For biotinylated NAMPT, black pre-blocked 96-well streptavidin-coated plates (Streptawell plates) were used as described before. After three washes of the assay plates with PBS/0.05% Tween 20, 50µL of different IgG dilutions were transferred to the wells and incubated for one hour at room temperature. 50µL of the periplasmic supernatants containing the scFvs (see section 4.2.1.5 for periplasmic preparation) were then added to the wells and the mixtures were incubated for one hour at room temperature. scFvs were then detected with mouse anti-c-myc (1µg/mL) and anti-mouse IgG Fcγ-HRP (dilution 1:5000) antibodies. The assay was developed, and the fluorescence measured as previously described.

λ IgG versus κ IgG

Lambda IgG versus kappa IgG competitive ELISAs were performed following the same principle. The secondary antibodies, anti-human λ light chain-HRP (dilution 1:1000, Sigma-Aldrich) and anti-human κ light chain-HRP (dilution 1:5000, ThermoFisher Scientific) antibodies were used for the detection.

4.3.2. Bio-layer interferometry (BLI) analysis

Anti-eNAMPT mAbs affinity was determined with the Octet RED96 instrument (Fortebio, Pall Corporation, NY, USA). Two types of experiments were performed: a preliminary experiment to confirm the specificity of the generated antibodies for NAMPT and a second experiment to measure the KD of the antibodies. Protein A or AHC2 (anti-human Fc) capture biosensor tips (Pall, Basel, Switzerland) were first hydrated in 1X kinetics buffer (KB 1X, ForteBio, Pall) for 10 minutes. Biosensor tips were then preconditioned with a regeneration cycle in 10mM glycin pH 1.7, according to supplier's recommendation. Following a 60s baseline step in KB 1X, mAbs were loaded to the biosensor tips at 10µg/mL (preliminary experiment) or 0.5µg/mL (affinity determination experiment) for 300s. The signal was then stabilized with another 60s baseline step. The association step was performed by incubating antibody-loaded biosensor tips with recombinant proteins for 600s. For preliminary experiments, 150nM of NAMPT protein or 150nM of an irrelevant protein, diluted in KB 1X, were used. For affinity determination experiments, NAMPT protein was serially diluted to seven concentrations. Following association, a dissociation step was achieved by incubating biosensor tips in KB 1X for 600s. Finally, a regeneration cycle was run to strip biosensor tips for further use. All experiments were performed at 30°C. Data were analysed with Octet analysis studio software. A 1:1 global fitting model was applied to calculate antibodies' KD.

4.4. Antibody neutralizing activity testing

4.4.1. Cell lines

CHO TLR4/MD-2 and CHO CCR5 cells were generated in our laboratory. CHO-TLR4/MD-2 and CHO-CCR5 cells were cultured in DMEM/Nutrient Mixture F-12 Ham (DMEM/F12) supplemented with 10% heat-inactivated FBS and 2mM L-glutamine (all from Sigma-Aldrich). The CHO-TLR4/MD-2 cell clone used was stable. In CHO-CCR5 cells, selection was maintained by adding 500µg/mL of Geneticin (ThermoFisher Scientific) and 250µg/mL of Hygromycine B (ThermoFisher Scientific).

THP1-Blue-CD14 (THP1-Blue™ NF-kB) and HEK-Blue-TLR4/MD-2/CD14 (HEK-Blue™ hTLR4) cells were purchased from InvivoGen (San Diego, CA, USA). Both cell lines stably express an NF-kB-inducible secreted embryonic alkaline phosphatase (SEAP) reporter gene. Furthermore, THP-1-Blue™-CD14 cells were transfected with human CD14 co-receptor, while HEK-Blue-TLR4/MD-2/CD14 were obtained by co-transfection of human TLR4, MD-2 and CD14 proteins. THP-1-Blue™-CD14 cells were cultured in RPMI 1640 (Sigma-Aldrich) supplemented with 10% heat-inactivated FBS, 2mM L-glutamine, 10µg/mL of Blasticidin S Hcl (ThermoFisher Scientific), 200µg/mL of Zeocin (ThermoFisher Scientific) and 250µg/mL of Gentamicin (Sigma-Aldrich). HEK-Blue™-TLR4/MD-2/CD14 cells were maintained in DMEM high glucose (Sigma-Aldrich) supplemented with 10% heat-inactivated FBS, 2mM of L-

glutamine, 100µg/mL of Normocin (InvivoGen), 1X of HEK Blue selection (InvivoGen) and 250µg/mL of Gentamicin.

MCF10A, MDA-MB-231, MCF-7 and PC-3 cells were purchased from the ATCC. MCF10A cells were cultured in DMEM/F12 (ThermoFisher Scientific) supplemented with 5% horse serum, 10µg/mL of insulin, 500ng/mL of hydrocortisone, 20ng/mL of epidermal growth factor, 100ng/mL of cholera toxin (all from Sigma Aldrich) and penicillin-streptomycin (ThermoFisher Scientific). MDA-MB-231, MCF-7 and PC-3 cells were cultured in RPMI 1640 supplemented with 10% heat-inactivated FBS and penicillin-streptomycin. All cells were maintained at 37°C in a humidified atmosphere containing 5% CO_2.

4.4.2. Ligand-receptor binding assay

4.4.2.1. Reagents

Recombinant human TLR4 proteins were purchased from SinoBiological (#10146-H08B), R&D (#1478-TR), Peprotech (#160-06) or Abcam (ab233665). Recombinant huTLR4/huMD-2 complex was purchased from R&D (#3146-TM). Recombinant human CCR5 protein was purchased from AccroBiosystems (#CC5-H52D1). All irrelevant proteins were produced in-house, except PD-L1-Fc, PD1-Fc and MSLN-Fc which were purchased from SinoBiological. All commercial antibodies targeting NAMPT, TLR4 or CCR5 used for ligand/receptor binding assays are listed in Table 3.

Table 3: Commercial antibodies used in the ligand/receptor binding assays.

Antibody	Manufacturer	Reference	Features
Anti-huNAMPT	R&D systems	#MAB4044	mAb
		#BAF4335	pAb, biotinylated
	Adipogen	#AG-20A-0034	mAb
		#AG-25A-0025	pAb
	ThermoFisher Scientific	#MA5-15388	mAb
		#PA5-34858	pAb
	Sigma	#SAB5300038	mAb
Anti-huTLR4	ThermoFisher Scientific	#14-9917-82	mAb
	Biolegend	#312804	mAb, biotinylated
Anti-huCCR5	R&D systems	#MAB182	mAb
	ThermoFisher Scientific	#14-1957-82	mAb

4.4.2.2. ELISA

NAMPT/TLR4 binding assay

Black 96-well immuno plates (Maxisorp plates) were incubated overnight at 4°C with 60nM of recombinant protein (NAMPT protein or an irrelevant protein). The day after, the plates were blocked for one hour at room temperature with PBS containing 2% BSA and 0.05% Tween 20. After three washes of the assay plates with PBS/0.05% Tween 20, 50 µL of different concentrations of TLR4, TLR4/MD-2 or an irrelevant protein were transferred to the wells and incubated for one or two hours at room temperature. His-tagged proteins were detected with an anti-PentaHis-HRP antibody (dilution 1:2000, Qiagen) or with a biotinylated anti-TLR4 antibody (Biolegend, San Diego, CA, USA) and streptavidin-HRP (dilution 1:15000). Other ELISA configurations, with immobilized TLR4 and soluble NAMPT, were performed according to the same principle. NAMPT proteins were detected with an anti-PentaHis-HRP antibody (dilution 1:2000), with a mouse anti-NAMPT mAb (Adipogen) and an anti-mouse IgG Fcγ-HRP antibody (dilution 1:5000) or with a rabbit anti-NAMPT pAb (ThermoFisher Scientific) and an anti-rabbit IgG Fcγ-HRP antibody (dilution 1:5000, Jackson Immunoresearch).

Regarding sandwich ELISAs, a biotinylated anti-His Tag antibody (R&D systems) or a biotinylated anti-TLR4 antibody, was first immobilized overnight at 4°C or one hour at room temperature on streptawell plates. The plates were subsequently incubated with TLR4 protein or an irrelevant protein and incubated with increasing concentrations of NAMPT protein (Adipogen). FLAG-tagged NAMPT protein was finally detected with an anti-FLAG tag-HRP antibody (dilution 1:1000, ThermoFisher Scientific). Between each step, washes with PBS/0.05% Tween 20 were performed. All ELISA assays were developed as described above.

NAMPT/TLR4 blocking assay

Black 96-well immuno plates (Maxisorp plates) were incubated overnight at 4°C with 60nM of NAMPT protein. The following day, the plates were blocked for one hour at room temperature with PBS containing 2% BSA and 0.05% Tween 20. After three washes of the assay plates with PBS/0.05% Tween 20, 50µL of different dilutions of anti-eNAMPT mAbs were transferred to the wells and incubated for one hour at room temperature. 50µL of a fixed concentration of TLR4 protein were then added to the wells and the mixtures were incubated for one or two hours at room temperature. Recombinant His-Tagged TLR4 proteins were detected with an anti-PentaHis-HRP antibody (dilution 1:2000). The assay was developed, and the fluorescence measured as previously described.

4.4.2.3. Bio-layer interferometry

Octet RED96 instrument and its associated software were used to study NAMPT/TLR4 association. Anti-penta-HIS (HIS1K) or streptavidin (SA) capture biosensor tips were first hydrated in KB 1X for 10 minutes. Biosensor tips were then preconditioned with a regeneration cycle in 10mM glycin pH 1.7, according to supplier's recommendation. Following

a baseline step in KB 1X for 60s, NAMPT-biot protein or TLR4 protein was loaded to biosensor tips for 300s. After signal stabilization with two 60s baseline steps, an association step was performed by incubating TLR4, NAMPT or an irrelevant protein with protein-loaded biosensor tips for 600s. Then, a dissociation step was achieved by incubating biosensor tips in KB 1X for 240s. In another type of experiment, AMC (anti-mouse Fc) or protein A capture biosensor tips were used for the loading of an anti-NAMPT antibody (ThermoFisher mAb and Adipogen pAb, respectively). The association was performed with NAMPT protein, TLR4 protein or a combination of NAMPT and TLR4 proteins all diluted in KB 1X. At the end of each BLI experiment, a regeneration cycle was performed to strip biosensor tips. All experiments were performed at 37°C.

4.4.2.4. Flow cytometry

CHO-WT, CHO-TLR4/MD-2 and CHO-CCR5 cells were detached and resuspended in FACS buffer (PBS / 2% BSA / 0.1% azide). 1×10^5 cells suspension was dispensed in V bottom 96-well plate (ThermoFisher Scientific) and incubated with recombinant NAMPT proteins for two hours at 4°C. Following a wash step in FACS buffer, cells were incubated with an anti-NAMPT antibody (biotinylated or not) for 20 minutes at 4°C. Cells were then washed and stained for 20 minutes at 4°C with appropriate detection: streptavidin-Cy5 (ThermoFisher Scientific), anti-mouse IgG(H+L)-PE antibody (ThermoFisher Scientific), anti-rat IgG(H+L)-PE antibody (ThermoFisher Scientific) or anti-rabbit IgG(H+L)-PE antibody (ThermoFisher Scientific). In another experiment, His-tagged NAMPT proteins were directly detected with an anti-PentaHis-AF647 antibody (Qiagen). After a final wash, cells were resuspended in FACS buffer and sytox blue (ThermoFisher Scientific) was added before acquisition, to exclude dead cells from analysis. Cells were acquired on the CytoFLEX S flow cytometer (Beckman Coulter, Nyon, Switzerland) and data analyses were performed using FlowJo software (Tree Star Inc., OR, USA).

4.4.2.5. CellInsight homogeneous assay

For binding assays with beads, polybead microspheres (6.0 µm, Polysciences, Warrington, PA, USA) or streptavidin microspheres (6.0 µm, Polysciences) previously coated with 10µg/mL of TLR4, CCR5, NAMPT-biot or an irrelevant protein were resuspended in filtered PBS containing 2% BSA. For binding assays with cells, CHO-TLR4/MD-2, CHO-CCR5 and CHO-WT cell suspensions were prepared and resuspended in PBS at a concentration of $1x10^6$ cells/mL. Cells were stained with cell trace violet (ThermoFischer Scientific) and incubated for 20 minutes at 37 °C, protected from light. Cell concentration was then adjusted at $1x10^5$ cells/mL in filtered PBS containing 2% BSA. Beads or cells were dispensed into 384-well clear-bottom plates at 3000beads/cells per well (30µL/well). 50µL of increasing concentrations of recombinant NAMPT proteins or anti-TLR4 and anti-CCR5 antibodies were added to the

beads/cells and incubated for 30 minutes at room temperature. Finally, 20µL of appropriate detection (anti-mouse IgG Fcγ-AF647 antibody (Jackson Immunoresearch), streptavidin-Cy5, anti-PentaHis-AF647 antibody or a biotinylated anti-NAMPT pAb (R&D) and streptavidin-Cy5) were added and the incubation continued for three hours at room temperature, protected from light. Bindings were detected using the CellInsight™ CX5 HCS imaging platform associated with the HCS Studio™ Cell Analysis Software.

4.4.3. Intracellular signalling pathway activation assays

4.4.3.1. NF-kB reporter assay

THP1-Blue-CD14 or HEK-Blue-TLR4/MD2/CD14 cells were seeded into flat-bottom 96-well plates (ThermoFisher Scientific) at 1×10^5 cells/well and 2.5×10^4 cells/well, respectively. In parallel, LPS (Sigma-Aldrich) and NAMPT proteins were incubated for one hour at 37°C with 10, 50 or 100µg/mL of polymyxin B (InvivoGen) or medium. Cells were then incubated overnight at 37°C with the different mixtures. The following day, 40µL of supernatants were removed from each well and transferred to a new 96-well plate containing 160µL of QUANTI-Blue™ reagent (InvivoGen). As an alternative of QUANTI-Blue™, cells could also be incubated directly with HEK-Blue™ Detection medium. Reactions were developed at 37°C and SEAP activity was determined by measuring optical density (OD) at 630nm using BioTek Gen 5 microplate reader. In another experiment, NAMPT protein (Peprotech) was incubated for one hour at room temperature with increasing concentrations of P-1076 (with a silenced Fc domain), in presence of an antibody stuffer saturating Fcγ receptors. The mixtures were then added to THP1-Blue-CD14 cells previously seeded in flat-bottom 96-well plates at 1×10^5 cells/well. After overnight incubation at 37°C, NF-kB activation was measured as described above.

4.4.3.2. Western blot

Cells were plated in 100mm Petri dishes and allowed to adhere overnight. The day after, cells were treated for one hour, 24 hours or for different incubation times at 37°C with NAMPT protein (100, 500 or 1000ng/mL, Adipogen), 9µg/mL P-1076 or their combination. Subsequently, cells were lysed in lysis buffer (25mM Tris-phosphate, pH 7.8; 2mM DTT; 2mM 1,2-diaminocyclohexane-N,N,N´,N´-tetraacetic acid; 10% glycerol; 1% Triton X-100 and protease and phosphatase inhibitor mixture), and protein quantification was performed with Bradford protein assay (Bio-Rad Laboratories, Hercules, CA, USA). Proteins (20µg) were resolved on SDS-PAGE, transferred to a polyvinylidene fluoride (PVDF) membrane (ThermoFisher Scientific), and detected with the antibodies listed in Table 4, using standard enhanced chemiluminescence (ECL). Band intensities were quantified with ChemiDoc imaging system (Bio-Rad) and quantity One software (Bio-Rad).

Table 4: Antibodies used for immunoblotting analyses.

Antibody	Manufacturer	Reference
Anti-phospho-p38 (Thr180/Tyr182)	Cell Signaling Technology	#4631
Anti-p38	Cell Signaling Technology	#8690
Anti-phospho-SMAD2 (Ser465/467)	Cell signalling technology	#3108
Anti-SMAD2	Cell signalling technology	#3122
Anti-phospho-IkB-α (Ser32/36)	Cell Signaling Technology	#9246
Anti-IkB-α	Santa Cruz Biotechnology	#sc847
Anti-phospho-NF-kB p65 (Ser536)	Cell Signaling Technology	#3033
Anti-NF-kB p65	Cell Signaling Technology	#6956
Anti-phospho-Akt (Ser 473)	Cell Signaling Technology	#4058
Anti-Akt	Cell Signaling Technology	#4691
Anti-phospho-STAT3 (Tyr705)	Santa Cruz Biotechnology	#sc-8059
Anti-STAT3	Santa Cruz Biotechnology	#sc-482
Anti-vinculin	Santa Cruz Biotechnology	#sc-5573
Anti-vimentin	Santa Cruz Biotechnology	#sc-6260
Goat anti-mouse IgG-HRP	Santa Cruz Biotechnology	#sc-2005
Mouse anti-rabbit IgG-HRP	Santa Cruz Biotechnology	#sc-2357

4.4.4. Proliferation assay

2-2.8x10^3 cells/well were plated in 96-well plates and allowed to adhere overnight. The day after, increasing concentrations of recombinant NAMPT protein (0-100ng/mL, Adipogen) were added to the cells. After 72 hours of incubation at 37°C, cells were fixed with 50% of cold trichloroacetic acid (TCA, Sigma-Aldrich) for 30 minutes at 4°C. Plates were then rinsed with cold water and air-dried overnight. The following day, cells were stained for 10 minutes with 0.4% sulforhodamine B (SRB, Sigma-Aldrich) in 1% glacial acetic acid (Carlo Erba reagents, Cornaredo, Italy) under gentle agitation. Thereafter, cells were rinsed three times with 1% glacial acetic acid, before being air-dried overnight. Finally, 10mM Tris Base (Sigma-Aldrich) were used to extract SRB stain. The OD was measured at 560nm with a Tecan Infinite F200 Pro plate reader (Tecan, Männedorf, Switzerland).

4.4.5. Quantitative reverse transcription PCR

MCF10A cells were plated in 6well-plates and grown for 14 days in medium supplemented or not with 100ng/mL of recombinant NAMPT protein (Adipogen). Cells were recovered and total RNA was extracted with RNeasy mini kit (Qiagen) following supplier's procedure. Subsequently, the isolated RNAs were reverse transcribed using High-Capacity cDNA reverse transcription kit (ThermoFisher Scientific) and a quantitative PCR was performed using SYBR Green GoTaq® QPCR Master Mix (Promega, Milan, Italy), on the 7900 HT Fast Real-Time PCR

instrument (Applied Biosystems by ThermoFisher Scientific). The primer sequences are listed in Table 5. The $2^{-\Delta\Delta Ct}$ method was used to calculate comparisons in gene expression. β-actin gene was used as housekeeping gene.

Table 5: Primer sequences for qPCR analysis

	Sequence primers (5'-3')	
	Forward	**Reverse**
E-cadherin	TGCCCAGAAAATGAAAAAGG	GTGTATGTGGCAATGCGTTC
N-cadherin	ACAGTGGCCACCTACAAAGG	CCGAGATGGGGTTGATAATG
Vimentin	GAGAACTTTGCCGTTGAAGC	GCTTCCTGTAGGTGGCAATC
ZEB1	GAAAATGAGCAAAACCATGATCCTA	CAGGTGCCTCAGGAAAAATGA
β-actin	CACCATTGGCAATGAGCGGTTC	AGGTCTTTGCGGATGTCCACGT

4.5. Statistics

GraphPad Prism (GraphPad Software, CA, USA) was used for all statistical analyses. The EC50 of anti-eNAMPT mAbs was calculated with the "Nonlinear Regression – log(agonist) vs. response -- variable slope" analysis of GraphPad software. One-way ANOVA with Dunnett's multiple comparisons test or two-way ANOVA with Tukey's multiple comparisons test were used for statistical comparison.

4.6. Illustrations

The illustrations in the figures were created with BioRender.com.

5. Results

5.1. Characterization of recombinant NAMPT protein

Human NAMPT protein was produced in house and biotinylated by Avi-Tag-mediating single-site biotinylation.

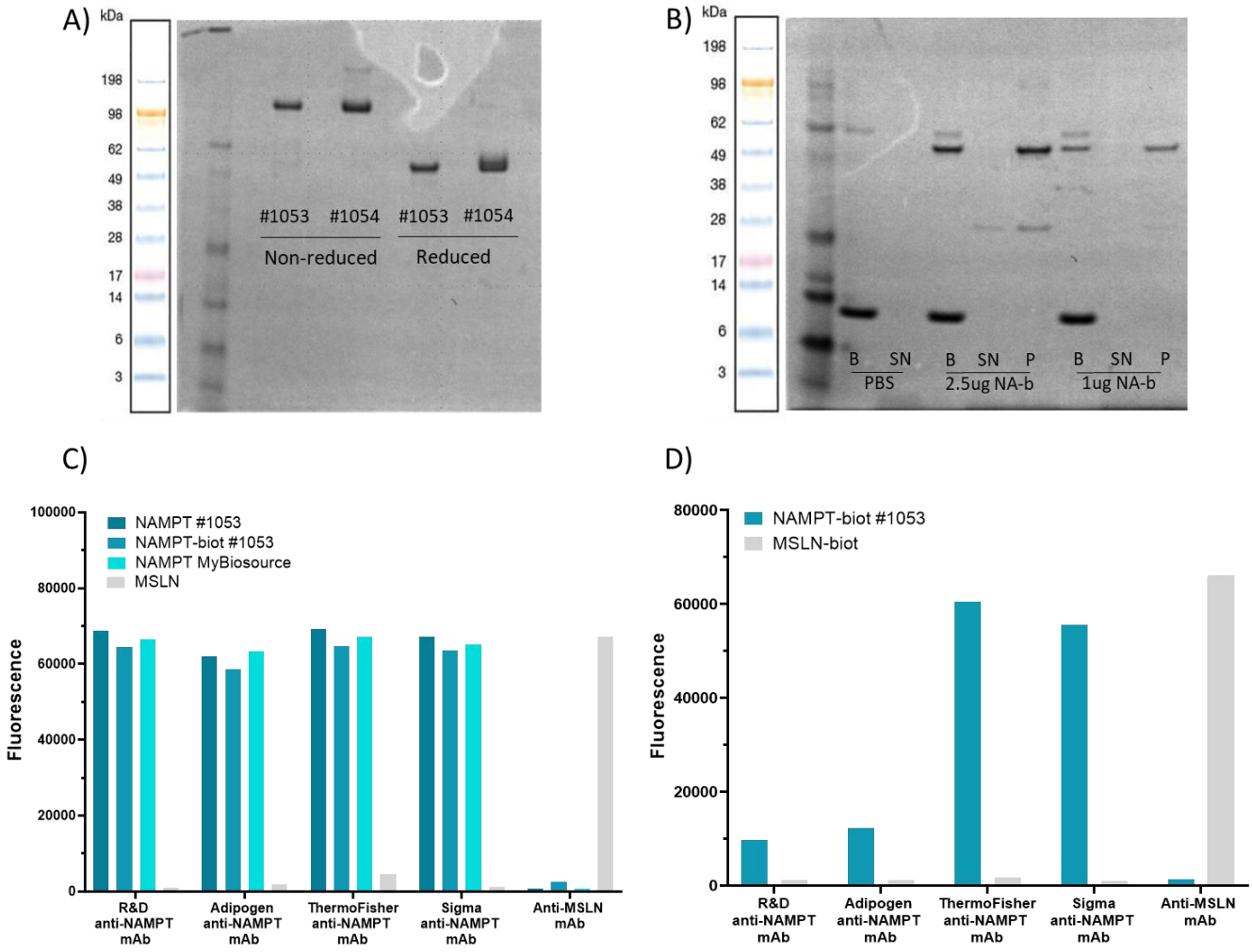

Figure 12: Characterization of NAMPT protein. (A) SDS-PAGE of in house produced NAMPT protein (batches #1053 and #1054) under reducing and non-reducing conditions. One representative experiment of two independent experiments. **(B)** In house NAMPT protein biotinylation level assessment with a pull-down analysis. Streptabeads were incubated with PBS, 2.5ug or 1ug of NAMPT-biot protein (NA-b, #1053) for 30 minutes. The supernatant (SN) was then separated from the streptabeads (B) and both were analyzed by SDS-PAGE under reducing condition. Non incubated NAMPT protein samples (P) were also loaded into the gel as controls. The 10kDa and 62kDa bands correspond to the beads. The 35kDa band corresponds to the BirA enzyme remaining in the NAMPT protein preparation. **(C-D)** In house NAMPT protein detection in ELISA. NAMPT proteins were immobilized on a maxisorp plate **(C)** or a streptawell plate **(D)** and detected with commercial anti-NAMPT antibodies. In house NAMPT protein detection by commercial antibodies was repeated several times.

The correct size (kDa) and dimerization of NAMPT protein were verified by SDS-PAGE (Fig. 12A and Fig. S3). Under reducing condition, a band was observed around 55kDa for the two different batches of NAMPT protein generated (#1053 and #1054), which corresponds to the described molecular weight of NAMPT monomer in the literature [9]. Under non-reducing condition, a dimer was observed. The level of biotinylation of NAMPT protein was evaluated by pull-down analysis (Fig. 12B). The presence of 55kDa bands in NAMPT-coated bead conditions (B), with similar intensities as the corresponding controls (P), suggests that the streptabeads had totally captured NAMPT-biot molecules. This was confirmed by the fact that no NAMPT-biot was apparent in the supernatant fractions (SN). Finally, the binding of commercial anti-NAMPT antibodies to in house produced NAMPT was tested in ELISA. The in house produced NAMPT protein was recognized by all commercial anti-NAMPT antibodies, when the protein was immobilized on a maxisorp plate, as shown in Fig. 12C. Given that passive adsorption on a maxisorp plate could result in protein denaturation (at least to some degree), NAMPT-biot recognition by antibodies was also assessed using a streptawell plate, which allows the immobilization of the protein via its biotin part and maintenance of its conformation. Strikingly, R&D and adipogen anti-NAMPT antibodies poorly detected NAMPT with this ELISA format (Fig. 12D). This suggests that these antibodies require, at least, a partial unfolding of NAMPT protein to bind to their epitopes. In house NAMPT protein batch #1053 was selected for further use in phage display and throughout the research project.

5.2. Anti-eNAMPT antibody generation

5.2.1. Selection and screening

Single chain fragment variable (scFv) constructs were selected by phage display from LCB proprietary synthetic and semi-synthetic phage libraries using different panning strategies and NAMPT protein sources. After three rounds of selection, selected scFv clones were picked randomly and screened by ELISA or homogeneous binding assay using the CellInsight™ CX5 HCS imaging platform. NAMPT-specific scFvs presenting high to moderate binding signal were sequenced. In total, 266 anti-eNAMPT scFvs with unique sequences were obtained. Several scFvs, from different screening campaigns, with the highest binding signals and with diverse sequences were reformatted into human IgG1s. Examples of screening results are presented in Fig. S4.

5.2.2. Anti-eNAMPT monoclonal antibody expression

Of the 56 scFvs reformatted, 54 IgGs were successfully produced. In addition, the anti-eNAMPT mAb, P-1076 [102], from which ALT-100 experimental drug is derived [111], was also produced. P-1076 antibody was described as having an eNAMPT-neutralizing activity *in vitro* and *in vivo* (in mouse and rat models of lung injury) [102]. IgG expression was analyzed by gel electrophoresis. Two bands corresponding to the heavy chain and the light chain were observed (Fig. S5). The slight differences in light chain molecular weight are due to differences in light chain isotype (kappa versus lambda light chains) as well as the presence of glycosylations.

5.2.3. Anti-eNAMPT antibody binding profile

IgGs specificity and binding were assessed by indirect and sandwich ELISA (using maxisorp plates). In sandwich ELISA, recombinant NAMPT in solution binds an anti-eNAMPT antibody immobilized via the Fc part, while in indirect ELISA, NAMPT protein is passively adsorbed (Fig. 13A). Of the 54 IgGs produced, four IgGs were eliminated due to lack of binding or binding specificity (data not shown). The remaining IgGs exhibited different binding characteristics and were categorized accordingly into three groups (A, B and C). Antibodies in group A bound strongly NAMPT in indirect ELISA and weakly or not at all in sandwich ELISA (Fig. 13B and 14 additional IgGs, Figs. S6 and S7). This suggests that these antibodies recognize epitopes that become more exposed in (at least partially) unfolded NAMPT protein. In contrast, antibodies in group B recognized NAMPT in sandwich ELISA, but less so in indirect ELISA (Fig. 13B and 25 additional IgGs, Figs. S8 and S9). The majority of IgGs in group B were able to bind biotinylated NAMPT captured on a streptawell plate (data not shown). This suggests that group B antibodies require proper folding of NAMPT for binding, and may therefore recognize conformational epitopes. Finally, IgGs in group C (Fig. 13B and 8 additional IgGs, Fig. S10) bound NAMPT in both ELISA configurations, similar to the P-1076 antibody. Heterogeneous binding pattern was observed in this group, with some antibodies binding similarly in sandwich and in indirect ELISA, and others binding much better in one ELISA format (principally, indirect ELISA). The EC50s calculated from binding curves of Figures S6, S8 and S10 are presented in Table S1. Three antibodies in group C, IgG_AE_1G9, IgG_AE_1H9, and IgG_AE_1G2 bound NAMPT with high affinity, higher or comparable to P-1076.

In addition, anti-eNAMPT mAbs were evaluated by bio-layer interferometry analysis with anti-eNAMPT antibodies immobilized on protein A coated sensors. As shown in Fig. S11, binding of anti-eNAMPT mAbs correlated with sandwich ELISA results: group B and C antibodies, but not (or weakly) group A antibodies bound the NAMPT protein in the BLI assay.

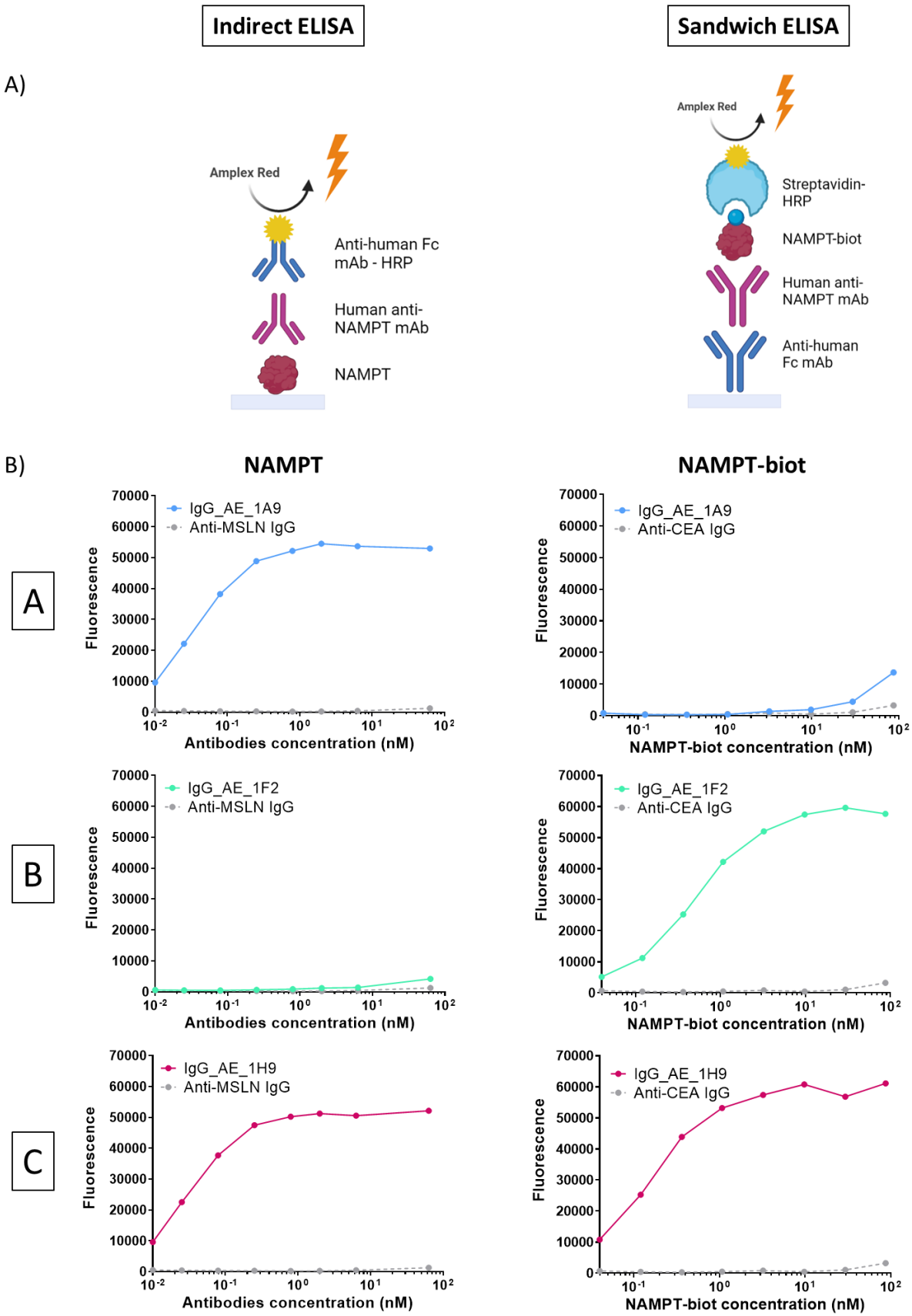

Figure 13: Characterization of anti-eNAMPT antibodies by ELISA. (A) Schematic representation of the ELISA assays. **(B)** The binding of the antibodies was analyzed by indirect ELISA with a commercial NAMPT protein and by sandwich ELISA with in-house NAMPT-biot protein. Maxisorp plates were used for both ELISA assays.

5.2.4. Sorting of the anti-eNAMPT antibodies into epitope bins

- **Epitope binning on NAMPT**

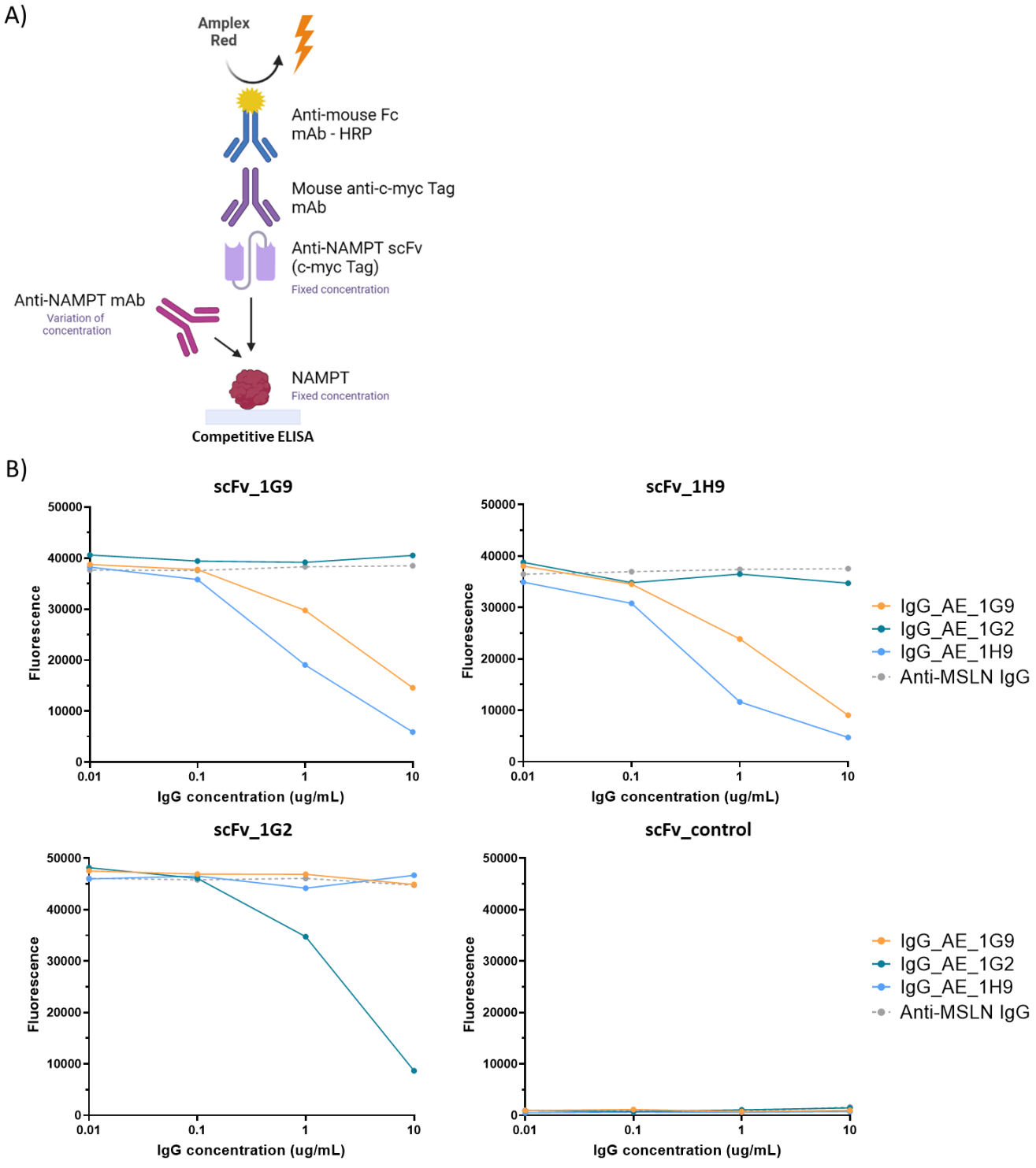

Figure 14: Sorting of the anti-eNAMPT antibodies into epitope bins. (A) Cartoon showing the principle of the competitive ELISA assay. **(B)** Example epitope binning experiments performed with three anti-eNAMPT antibodies. Maxisorp plates were coated with a commercial NAMPT protein and incubated with increasing concentrations of anti-eNAMPT mAbs (0.01 to 10µg/mL) and a neat periplasmic preparation of scFv. C-myc-tagged scFvs were then detected with a mouse anti-c-myc tag antibody and an anti-mouse IgG Fcγ-HRP antibody.

A dose-response binding competition assay (Fig. 14A) was performed, allowing to group the anti-eNAMPT antibodies into several epitope bins. If a competitor antibody was able to block completely the binding of a test scFv, both were categorised into the same epitope bin. If the blocking was nil or incomplete (reflecting steric hindrance, rather than binding to the same epitope/region), then the two antibodies were considered to be in distinct epitope bins. 37 antibodies were analyzed either on NAMPT-coated maxisorp plates or streptawell plates coated with biotinylated NAMPT, depending on their binding profile (A, B or C). The results of dose-response binding competition assays are shown in Fig. 14B and Figs. S12 and S13. The ensuing epitope bin categorization is summarized in Fig. 15. eNAMPT antibodies in group A and C were clustered into five distinct epitope bins (1 to 5), while antibodies in group B and C, into three epitope bins (groups I, II and III). The P-1076 benchmark antibody was analyzed using another ELISA approach and appeared to bind to the same region as group I antibodies (Fig. S14).

- **Epitope binning on NAMPT (Maxisorp plate)**

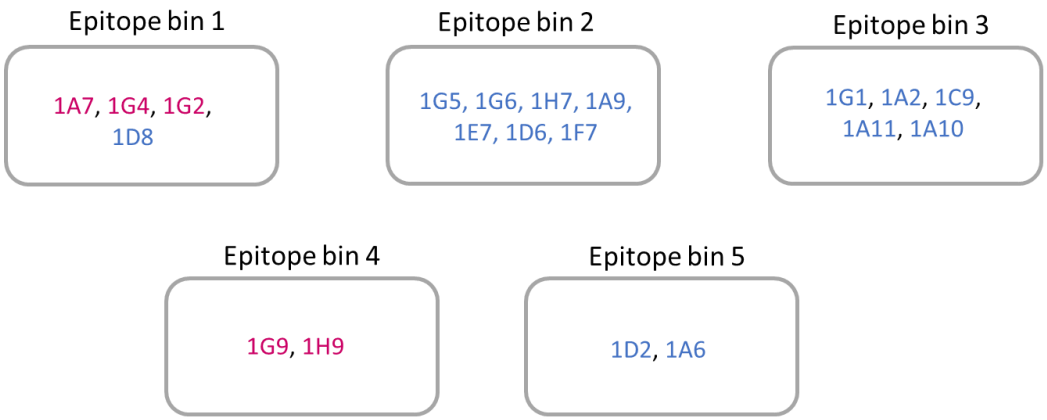

- **Epitope binning on NAMPT-biot (Streptawell plate)**

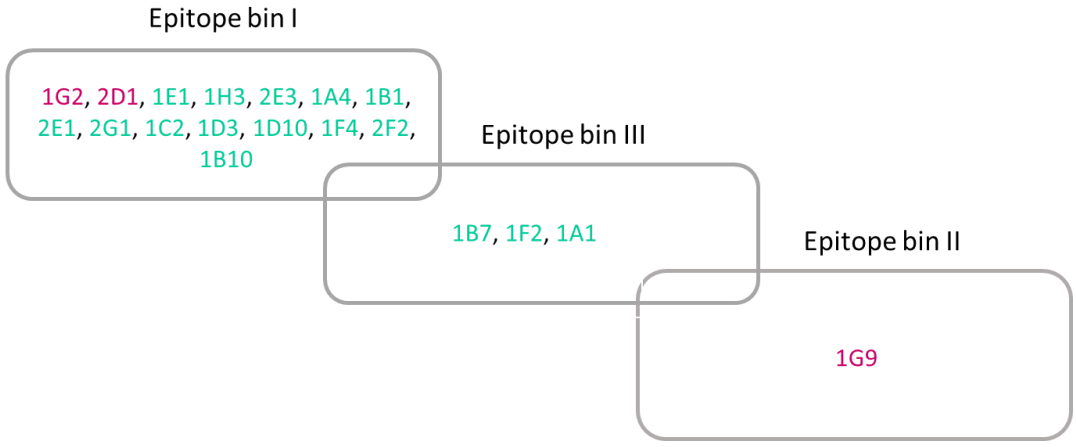

Figure 15: Anti-eNAMPT antibodies sorted into epitope bins. Sorting was based on competitive ELISA using maxisorp or streptawell plates depending on antibody binding attributes. Group A, B and C antibodies are colored in blue, green and purple respectively.

5.2.5. Affinity of the anti-eNAMPT antibodies

Table 6: Anti-eNAMPT antibody affinities. Affinity was measured using bio-layer interferometry (Octet, Forte Bio) and is shown as the KD ± SD. Results are representative of two independent experiments. P-1076 was measured for comparison.

IgG	P-1076	2E1	1G9	1A1	1G2	1G6	1G1	1H9	1D2
Targeted epitope bin	I	I	II	III	1	2	3	4	5
KD (nM)	0.8±0.43	0.5±0.05	0.7±0.14	2.6±0.09	2.7±0.28	7.9±2.3	4.4±0.04	1.0±0.2	19.1±0.95

Binding kinetics and affinities (expressed as KDs) of one candidate from each binning group were assessed by bio-layer interferometry analysis. KDs were calculated from the association/dissociation curves on Fig. S15. As shown in Table 6, all the antibodies tested, except IgG_AE_1D2, showed a high affinity for NAMPT (KDs < 10nM).

5.2.6. Lead optimization of IgG_AE_1D2

A lead optimization (LO) step was performed on IgG_AE_1D2. Mutations in CDRs were introduced in order to increase sequence diversity. Two phage display libraries were built and used for LO. Examples of the results obtained during the screening campaigns are shown in Fig 16. scFv expression and binding signals were measured by ELISA analysis. Some scFvs presented high binding signals for NAMPT but also high expression levels (e.g. scFvd2-A1-1_1D8, Fig. 16A), suggesting that their affinity for NAMPT is actually low. Thus, to determine the best binders a binding/quantification ratio was calculated (Fig. 16B). The specificity of binding was also confirmed (Fig. S16). The scFvs with a higher binding/quantification ratio than scFv-AP1-5_1D2 (parental scFv) were selected for sequencing. A high percentage of diversity was obtained (Fig. 16C). As before, the scFvs with the highest binding signals and with diverse sequences were chosen to be reformatted into IgG1s. LO IgGs specificity and affinity were then assessed by ELISA and BLI analysis. Unfortunately, the LO anti-eNAMPT IgGs did not showed improved affinities compared to IgG_AE_1D2 (Fig. S17). These LO antibodies were therefore not characterized further.

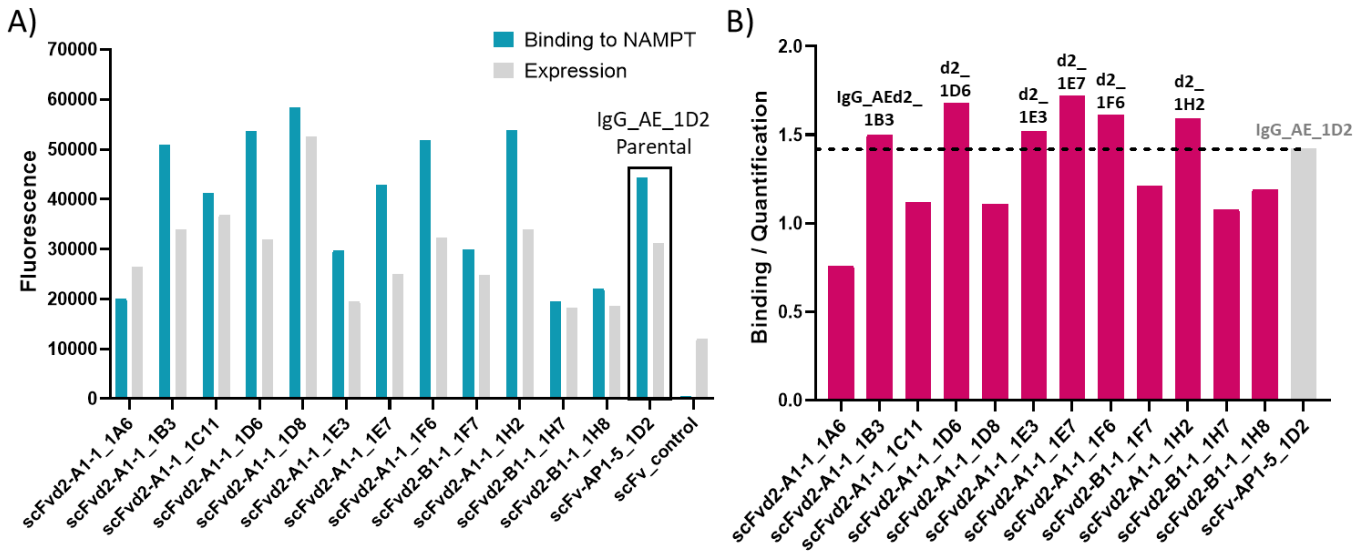

C)

1D2 parental identical sequence	Unique binders sequence	Diversity (%)
0/85	83/85	98

Figure 16: Example of screening results of LO of IgG_AE_1D2. (A) scFvs binding and expression signals were measured by ELISA. **(B)** scFvs binding / quantification ratio was used to determine which scFvs to reformat. Once reformatted into IgGs, scFvs were renamed according to IgG_AEd2_X nomenclature for simplification (e.g. scFvd2-A1-1_**1B3** became IgG_AEd2_**1B3**). **(C)** Sequence diversity obtained for the pool of scFvs sequenced.

Finally, a "round" optimization (RO) was also performed, in the hope of finding new high-affinity antibodies. The principle is the same as for LO, but here the phage libraries are based on a pool of original sequences instead of a single original sequence. 12 anti-eNAMPT antibodies generated from five RO libraries were characterized by ELISA. According to their binding profile, they were catalogued into group B or C (Fig. S18). Antibodies of both groups showed strong binding in sandwich ELISA (Table S2). In indirect ELISA, only group C antibodies bound NAMPT, with low affinity. A BLI analysis of two RO antibodies (IgG_AE_2F4 and IgG_AE_3G4, showing the most robust binding in sandwich ELISA) was performed, but their affinities were not higher than for the previously characterized antibodies (IgG_AE_2F4 KD = 23nM; IgG_AE_3G4 KD = 32nM). The RO antibodies were therefore not characterized further. Thus, overall, the lead and round optimizations did not lead to any affinity improvement. A summary of phage display and reformatting activities is presented in Fig. 17.

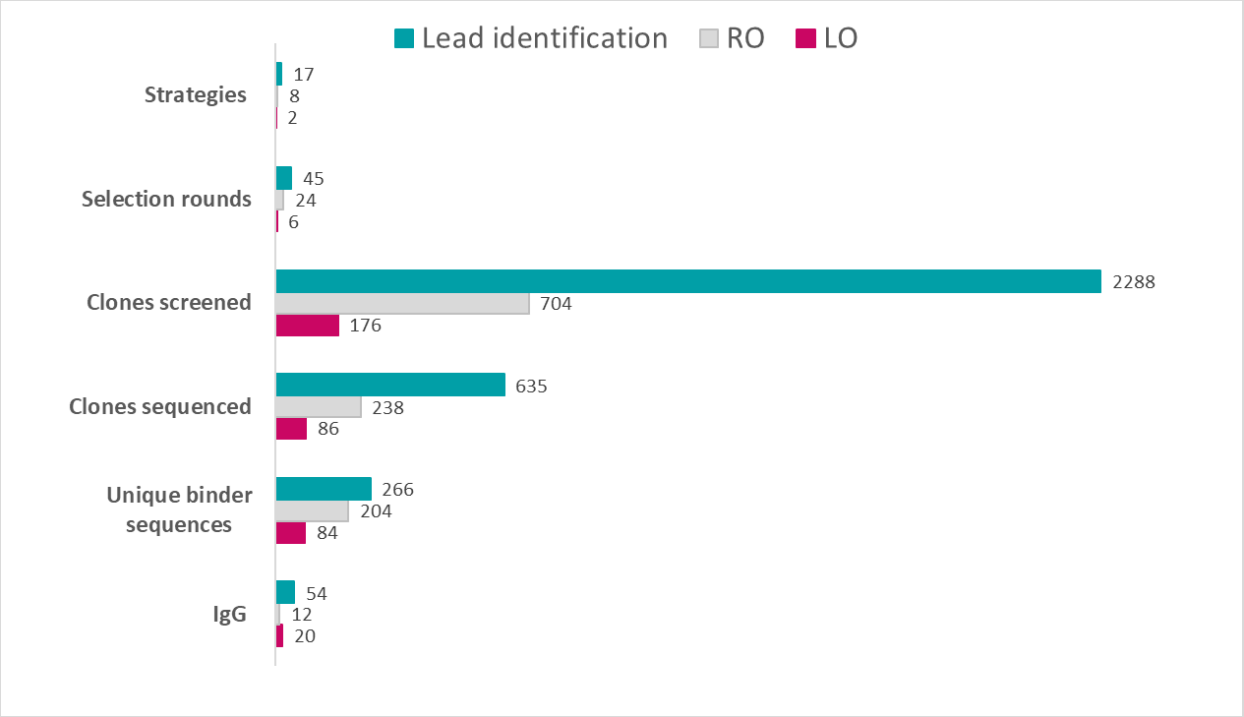

Figure 17: Summary of phage display activities.

5.3. Ligand/receptor binding assays for antibody testing

Based on publications showing the interaction of eNAMPT with CCR5 or TLR4 ([26], [27], [114], [115]), various approaches were used to develop an assay for the testing of the neutralizing activity of anti-eNAMPT mAbs.

5.3.1. eNAMPT binding to cells expressing TLR4 or CCR5

To test the binding of eNAMPT to its putative receptors, in-house generated CHO cell lines expressing either human TLR4/MD-2 or human CCR5 were used. The expression of TLR4 and CCR5 was verified with QIFIKIT® (Fig. 18), confirming high level of receptor expression. We tested eNAMPT from eight different sources (in-house, commercial, produced in *E.Coli*, Baculovirus or mammalian cells – see M&M for details).

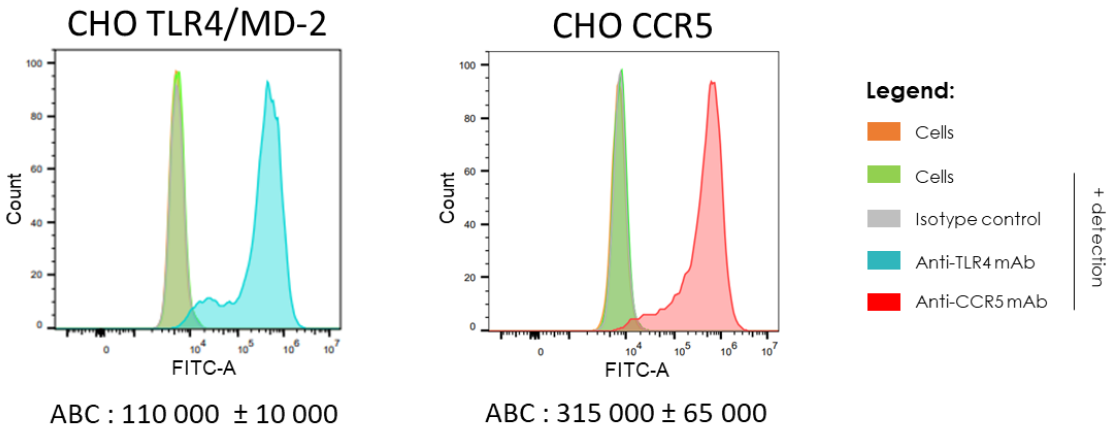

Figure 18: Receptor expression on CHO-TLR4/MD-2 and CHO-CCR5 cell lines. The levels of expression of TLR4 and CCR5 receptors by CHO-TLR4/MD-2 and CHO-CCR5 cells lines respectively were measured by flow cytometry with QIFIKIT® (Dako). Results of one of two independent experiments are shown. Antibody binding capacities (ABC) of 110 000 ± 10 000 and 315 000 ± 65 000 were obtained for CHO-TLR4/MD-2 and CHO-CCR5 cells respectively.

eNAMPT binding to TLR4 or CCR5 receptors was assessed by flow cytometry. Unfortunately, none of the six recombinant NAMPT proteins tested could be demonstrated to interact specifically with cell surface-expressed TLR4 or CCR5 (Fig. 19). Additional analyses with different NAMPT concentrations led to a similar conclusion (Fig. S19).

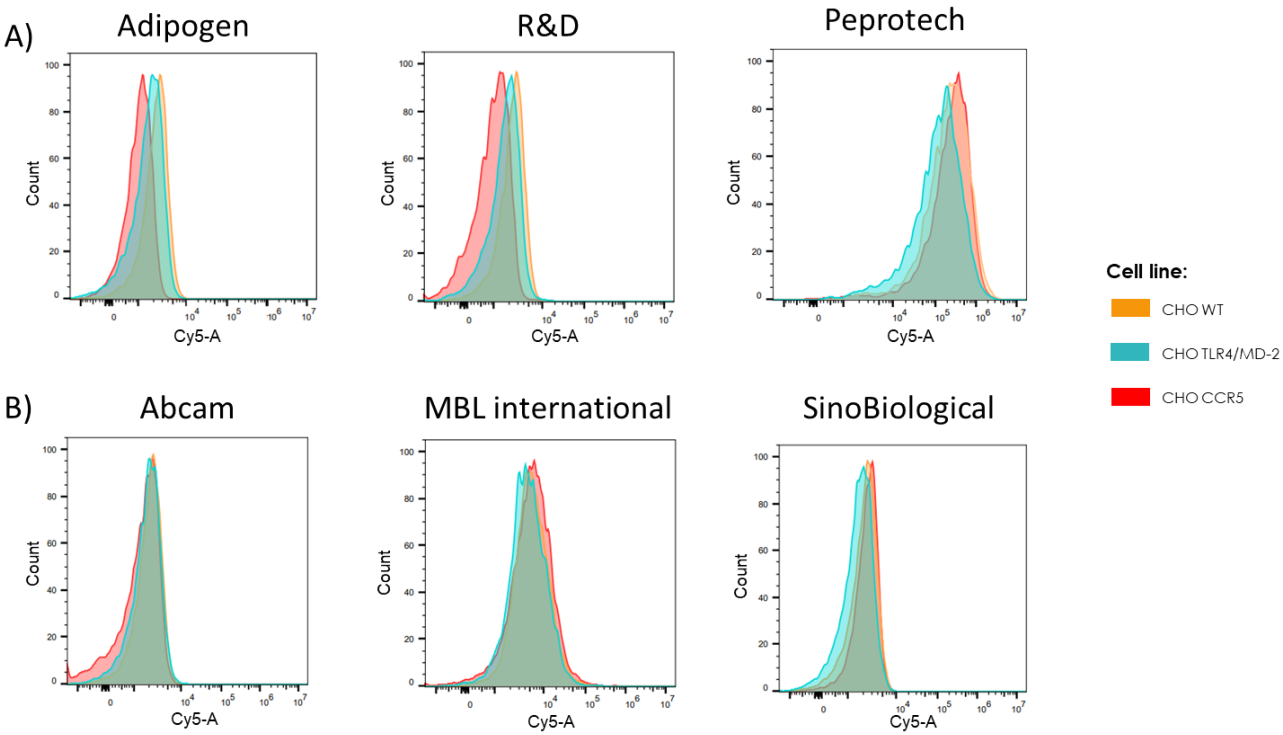

Figure 19: Analysis of eNAMPT binding to CHO-CCR5 and CHO-TLR4/MD-2 cells by flow cytometry. (A-B) NAMPT proteins (50ug/mL) were incubated for two hours with CHO-CCR5, CHO-TLR4/MD-2 or CHO-WT cells. NAMPT proteins were then detected with a biotinylated anti-NAMPT antibody (R&D), which was in turn detected with streptavidin coupled to cy5.

I speculated that eNAMPT/TLR4 or eNAMPT/CCR5 interaction could potentially be blocked by the anti-NAMPT antibody used for detection. I therefore tested alternative detection methods, but without success. Neither anti-NAMPT monoclonal / polyclonal antibodies (Fig. 20 and Fig. S20-21) nor an anti-His-Tag antibody (Fig. 20) were able to detect eNAMPT bound to cell surface CCR5 or TLR4. The slight shift of fluorescence peak observed with in house NAMPT protein at high concentration (50ug/mL) and CHO-CCR5 (see Fig. 20, R&D and ThermoFisher detection and Fig S20, Adipogen detection) or CHO-TLR4 cells (see Fig. S20, Adipogen detection) could not be reproduced in subsequent experiments (see Fig. S21). Overall, I conclude that I was unable to confirm the eNAMPT/TLR4 and eNAMPT/CCR5 direct interactions described in the literature with the approach delineated above.

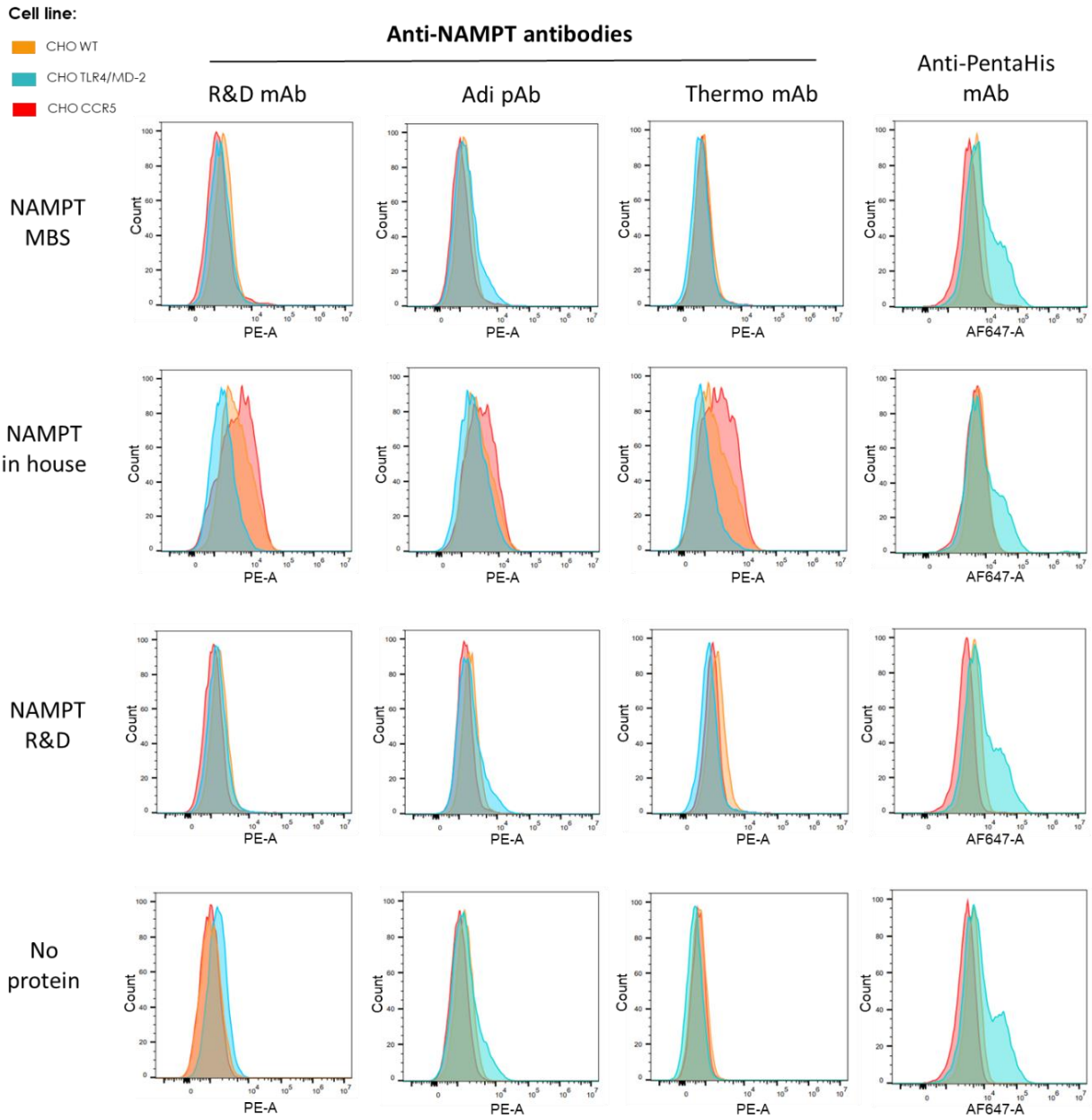

Figure 20: Analysis of eNAMPT binding to CHO-CCR5 and CHO-TLR4/MD-2 cells by flow cytometry. NAMPT proteins (50ug/mL; MBS, MyBiosource; R&D or in house protein) were incubated for two hours with CHO-CCR5, CHO-TLR4/MD-2 or CHO-WT cells. NAMPT proteins were detected either with mouse/rat/rabbit anti-NAMPT antibodies (R&D; Adi, Adipogen; Thermo, ThermoFisher Scientific) and a secondary anti-mouse/rat/rabbit IgG antibody coupled to PE, or an anti-PentaHis antibody coupled to AF647 (right panels).

The reported KDs of the interactions between eNAMPT and TLR4 or CCR5 are in the nM range [27], [114], they should therefore be fairly easily detectable by flow cytometry. Notwithstanding in an attempt to corroborate the published results, I tried in addition an alternative assay format. Using the same recombinant cell lines and different detection reagents, I run a homogeneous binding assay (using CellInsight™ CX5 HCS imaging platform), but, once again, I was unable to observe any specific interaction between recombinant NAMPT proteins and cell surface expressed CCR5 or TLR4 (Fig. 21, Fig. S22).

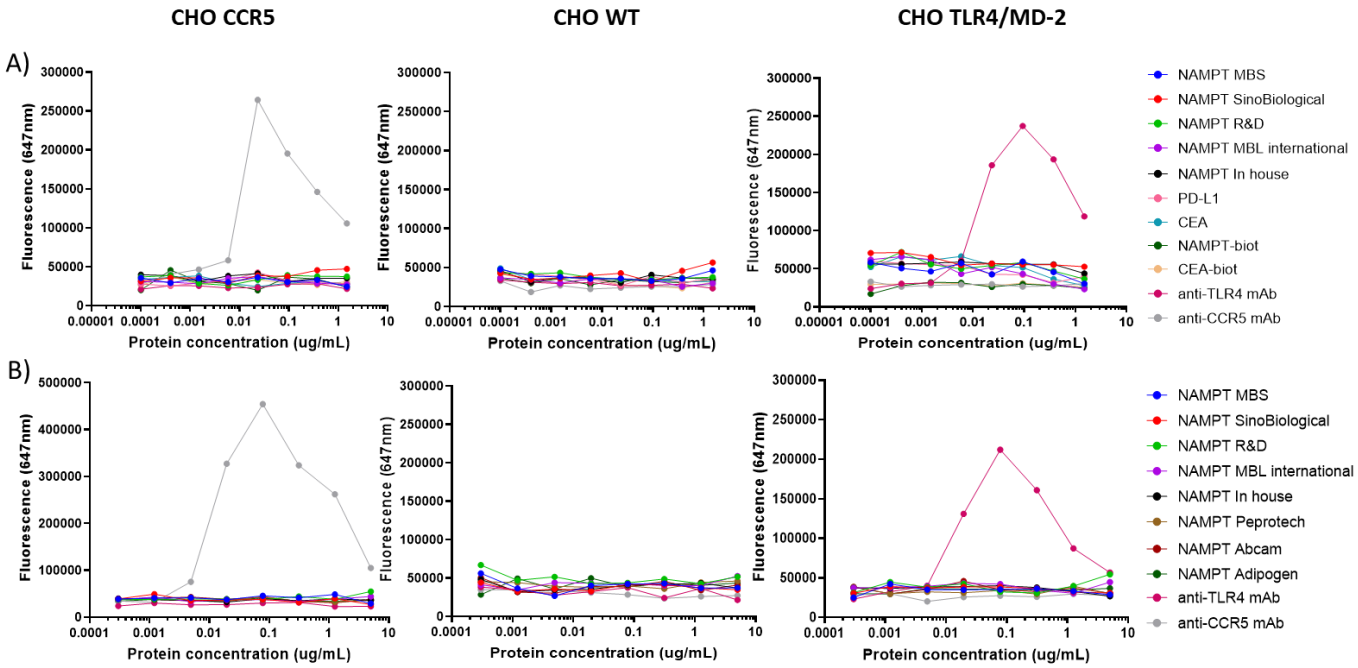

Figure 21: Analysis of eNAMPT binding to CHO-CCR5 and CHO-TLR4/MD-2 cells with the CellInsight™ CX5 HCS imaging platform. (A-B) Increasing concentrations of NAMPT proteins were incubated with CHO-CCR5, CHO-TLR4/MD-2 or CHO-WT cells for three hours. **(A)** Bound NAMPT was detected with an anti-PentaHis mAb coupled to AF647 or with streptavidin coupled to Cy5. **(B)** Bound NAMPT was detected with a biotinylated anti-NAMPT pAb (R&D) and streptavidin coupled to Cy5. In order to control the correct expression of the receptors, cells were also incubated with anti-TLR4 and anti-CCR5 mAbs, detected with an anti-mouse IgG Fcγ antibody coupled to AF647.

One hypothesis for the absence of eNAMPT/TLR4 interaction could be that eNAMPT is not able to interact with TLR4, when MD-2 and TLR4 are associated, as suggested in Gasparrini et al. publication [114]. Based on *in silico* modeling analyses, Camp et al. [26] speculated that, unlike LPS, NAMPT is able to bind directly to TLR4, without the requirement for MD-2/TLR4 association. Physiologically, in macrophages, the presence of MD-2 does not appear to block eNAMPT-mediated NF-kB signalling via TLR4 [116]. However, we cannot formally exclude that in the cell-based binding assays, MD-2 impeded the binding of eNAMPT to TLR4. As proposed by Gasparrini et al. [114], a competition for TLR4 binding could potentially occur *in vivo* between eNAMPT and MD-2. It would have been interesting to perform the flow cytometry and the CellInsight binding experiments with a CHO cell line expressing solely TLR4. However, this option is limited by the fact that the MD-2 protein present in cell culture serum could probably bind to TLR4, as human MD-2 and bovine MD-2 have a sequence homology of 79% (determined by BLAST analysis). Thus, to be completely free of MD-2, the cells would have to be cultured in absence of serum, conditions that can greatly impact TLR4 expression.

Currently, little is known about the modalities of interaction of eNAMPT with its receptors. Eventually, further research to decipher the mechanism of eNAMPT/TLR4 or eNAMPT/CCR5 interactions may help with the development of cell-based binding assays that would, in turn, allow assessing the blocking activity of eNAMPT binding mAbs.

5.3.2. eNAMPT binding to recombinant TLR4 and CCR5 proteins

eNAMPT-receptor interactions were also assessed using recombinant human TLR4 and CCR5 proteins. TLR4- and CCR5-coated beads or NAMPT-biot-coated streptabeads were tested in the CellInsight homogeneous binding assay. Same as with the cell-based assays, no eNAMPT/TLR4 or eNAMPT/CCR5 interaction was observed, despite using different NAMPT sources or detections (Fig. 22).

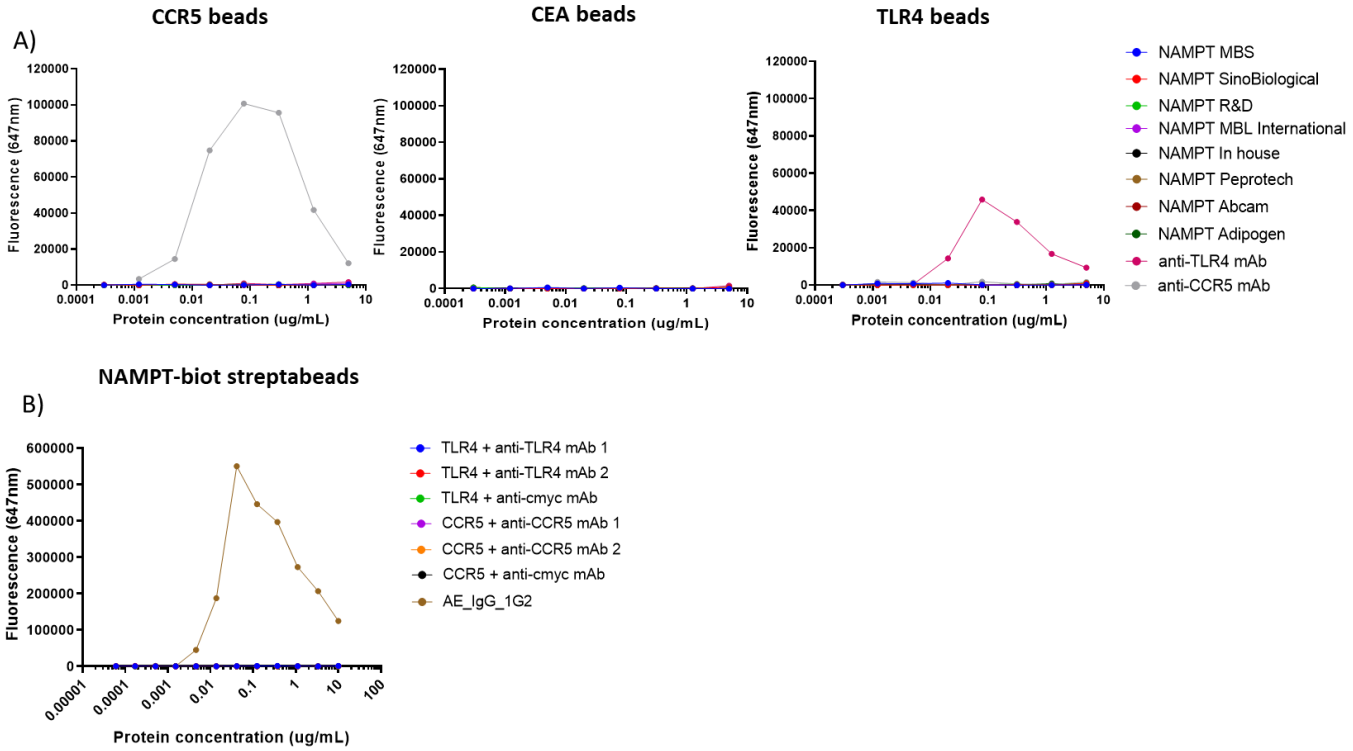

Figure 22: Analysis of eNAMPT binding to CCR5 and TLR4 proteins with CellInsight™ CX5 HCS imaging platform. **(A)** Increasing concentrations of NAMPT were incubated with TLR4- or CCR5-coated beads for three hours. Bound NAMPT proteins was detected with a biotinylated anti-NAMPT pAb (R&D) and streptavidin coupled to Cy5. **(B)** Increasing concentrations of TLR4 or CCR5 proteins were incubated with NAMPT-biot-coated streptabeads for three hours. TLR4 and CCR5 proteins were detected with specific antibodies and an anti-mouse IgG Fcγ antibody coupled to AF647. To control the coating of NAMPT-biot protein, streptabeads were also incubated with IgG_AE_1G2 antibody.

eNAMPT interaction with TLR4 receptor was also assessed with BLI technology using the Octet platform (ForteBio). The first experiment was inspired by the SPR assay of Camp et al. [26]: an anti-NAMPT pAb immobilized on protein A biosensors was incubated with recombinant NAMPT, TLR4 or a mix of NAMPT-TLR4 proteins. However, unlike Camp et al., the pre-mix of NAMPT and TLR4 did not result in increased binding response over NAMPT alone (Fig. 23A). I also tried another configuration with NAMPT-biot protein bound to streptavidin (SA) biosensors and incubated with recombinant TLR4 protein, however, no specific binding could be detected (Fig. 23B). Other strategies using HIS1K (anti-PentaHis tag) or AMC (anti-mouse Fc) biosensors were unsuccessful as well (Fig. S23 and S24).

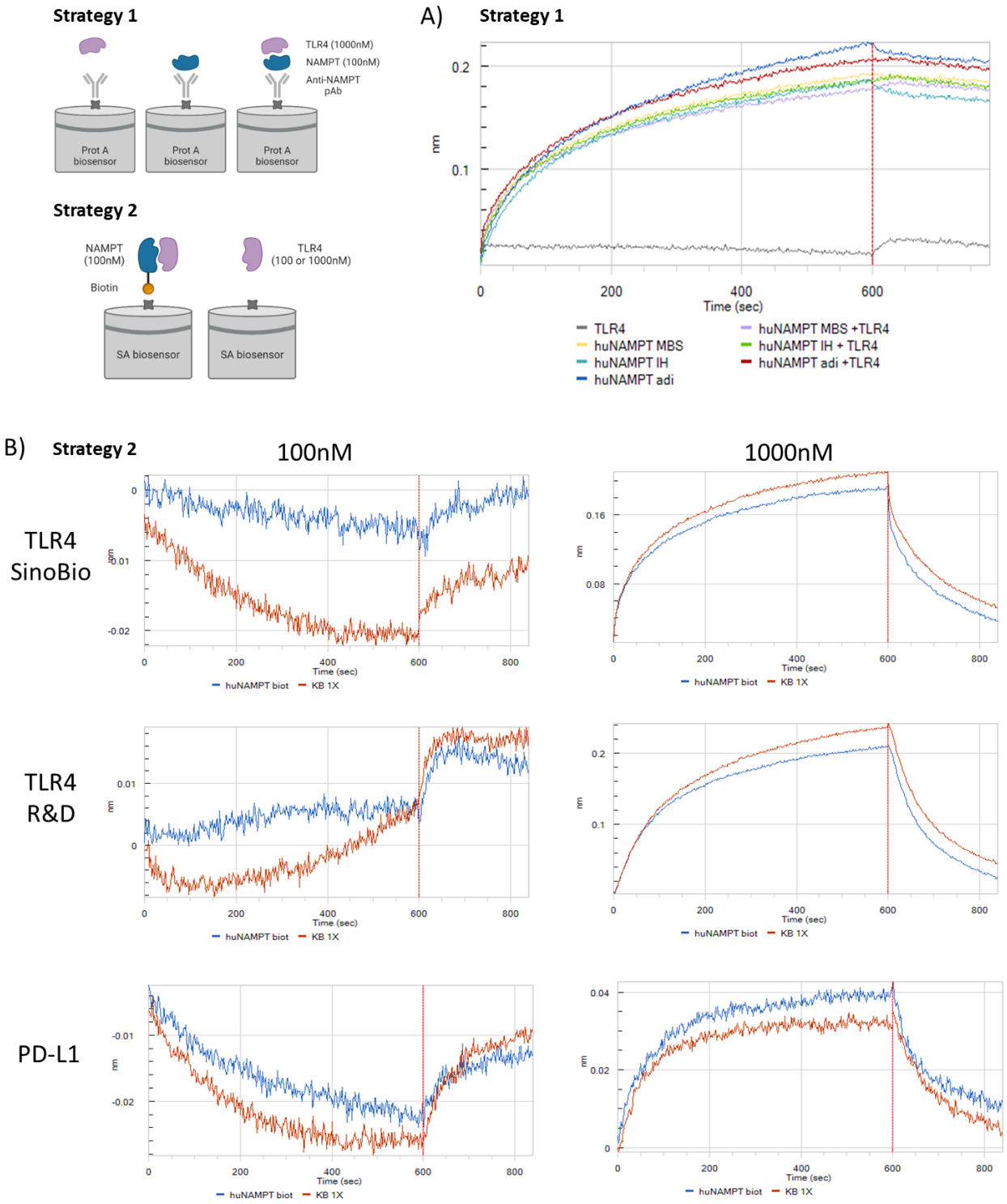

Figure 23: Analysis of eNAMPT binding to TLR4 with bio-layer interferometry (BLI). (A) An anti-NAMPT pAb (Adipogen) was loaded onto protein A biosensors and incubated for 600sec with NAMPT (100nM), TLR4 (1000nM) or a mix of NAMPT-TLR4 proteins. The anti-NAMPT pAb was then incubated with KB 1X buffer to allow protein dissociation. The sensorgram is representative of two independent experiments. Adi, adipogen; MBS, MyBiosource; IH, in house. **(B)** In house produced NAMPT-biot protein (blue) or nothing (rust, KB 1X) was loaded onto streptavidin biosensors and incubated for 600sec with TLR4 or PD-L1 proteins (100 or 1000nM). NAMPT-biot was then incubated with KB 1X buffer to allow protein dissociation.

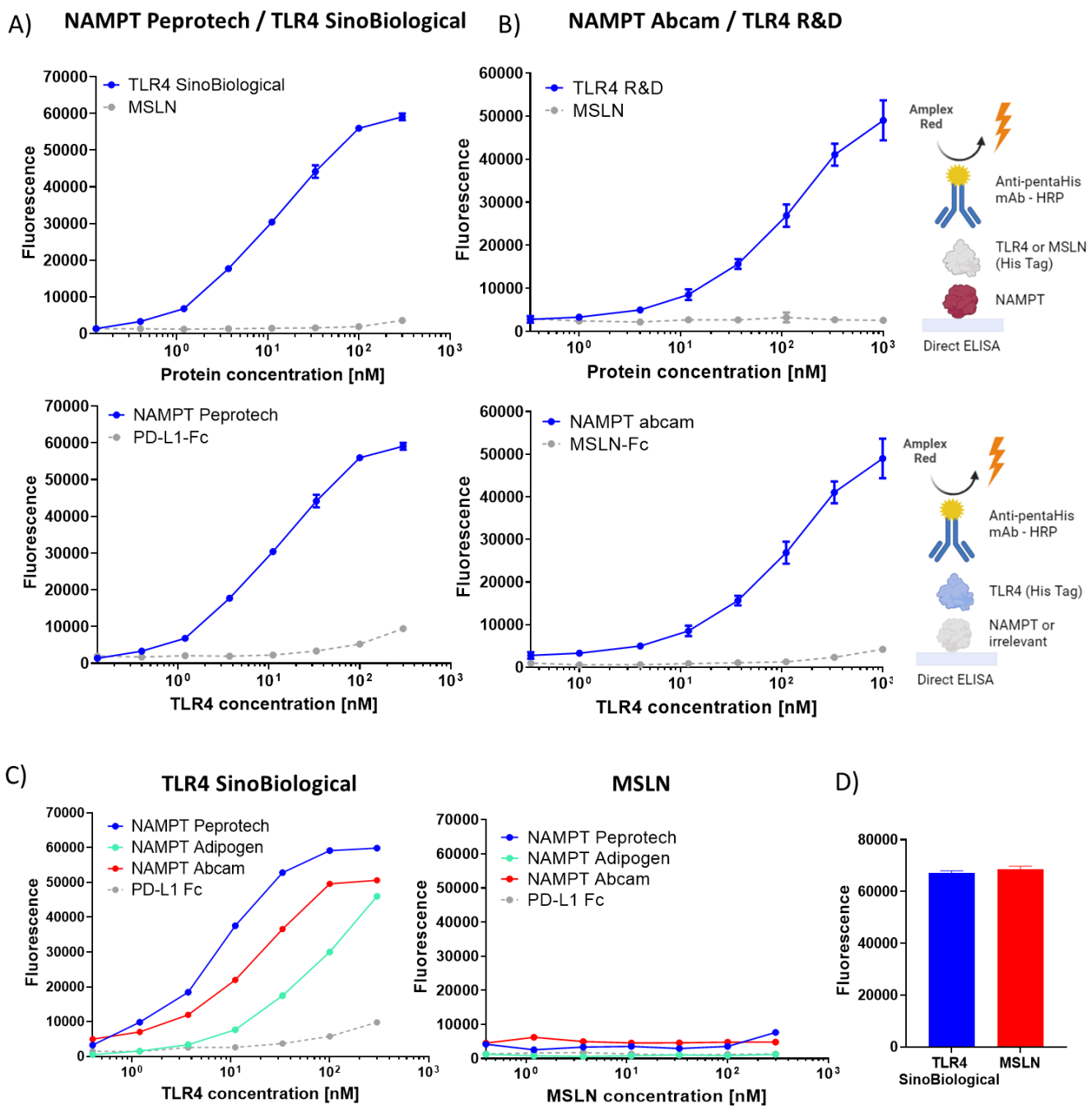

Figure 24: TLR4 binds to eNAMPT in direct ELISA. (A-C) Maxisorp plates were coated with NAMPT and incubated with increasing concentrations of TLR4 or MSLN (negative control). His-tagged proteins were then detected with an anti-PentaHis tag antibody coupled to HRP. **(D)** Correct detection of the tag His was controlled by incubating coated his-tagged proteins with an anti-PentaHis tag antibody coupled to HRP. **(A)**, **(B)**, **(C)** correspond to three independent experiments.

Finally, the binding of TLR4 to eNAMPT was assessed by direct ELISA (with passive adsorption of recombinant NAMPT). As shown in Fig. 24, a dose-dependent and apparently specific binding of TLR4 to NAMPT protein was indeed observed with recombinant proteins of different origins (two TLR4 and three NAMPT). Furthermore, we also detected an eNAMPT/TLR4 interaction in the presence of MD-2 protein (Fig. S25).

Alternative ELISA configurations were also tested (Fig. 25). Unfortunately, neither the ELISAs in a reverse configuration, with TLR4 coated on the plate, nor sandwich ELISAs (in any format) showed any specific binding between recombinant TLR4 and NAMPT proteins (example experiments are shown in Fig. S26).

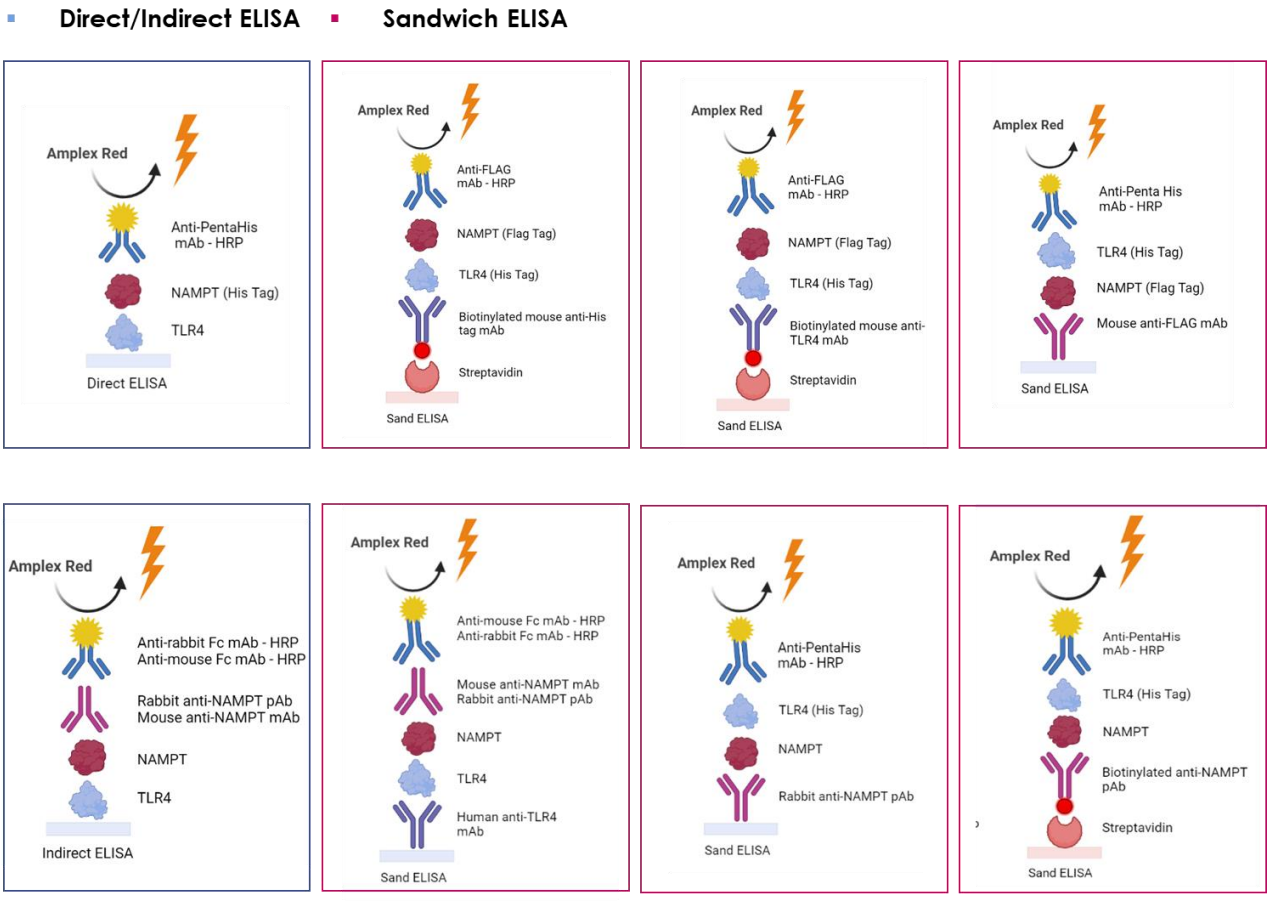

Figure 25: Alternative ELISA configurations tested.

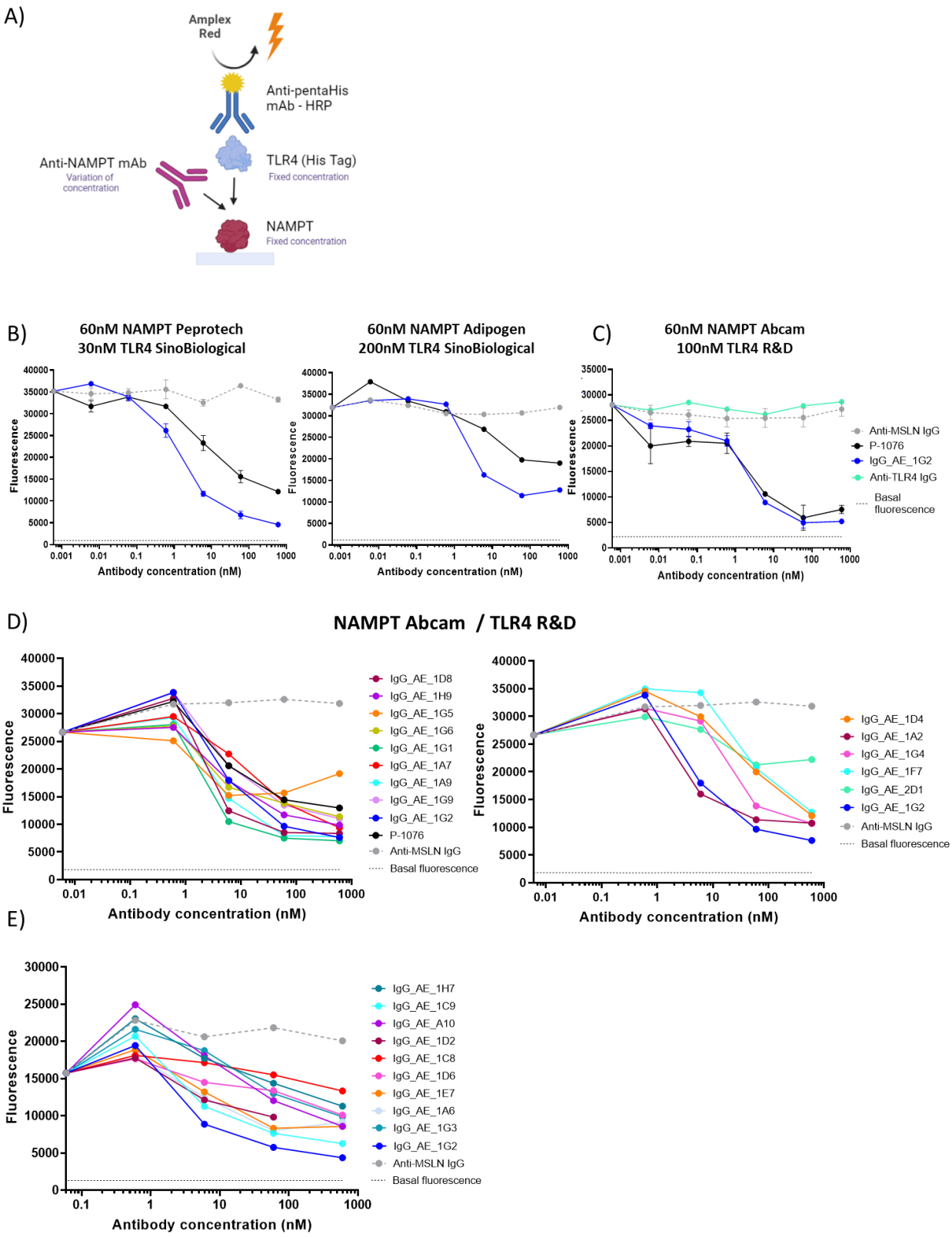

Figure 26: Anti-eNAMPT mAbs block TLR4/eNAMPT interaction. **(A)** Schematic representation of the assay. **(B-E)** Maxisorp plates were coated with 60nM NAMPT protein and incubated with increasing concentrations of anti-eNAMPT mAbs and a fixed concentration of TLR4 (30, 50, 100 or 200nM). His-tagged TLR4 was then detected with an anti-PentaHis tag antibody coupled to HRP. Four independent experiments are presented in **(B)**, **(C)**, **(D)**, and **(E)**.

In view of the results of the binding assays described above, I set out to evaluate the blocking potential of anti-eNAMPT mAbs using the unique ELISA assay configuration that displayed a (apparently) specific interaction between recombinant eNAMPT and its purported cell surface receptor, TLR4. Preliminary blocking ELISA experiments were performed with P-1076 and IgG_AE_1G2 antibodies, in order to validate the assay. As shown in Fig. 26B and C, P-1076 and IgG_AE_1G2 antibodies blocked eNAMPT/TLR4 interaction in a dose-dependent manner. The eNAMPT/TLR4 binding was not affected by an anti-TLR4 antibody neutralizing TLR4 dimerization (Fig. 26C). All group A and C antibodies were then tested in this blocking assay (Fig. 26D-E). Group B antibodies, which showed low or no binding to NAMPT passively adsorbed on maxisorp plates, could not be tested. Unexpectedly, all the group A and C mAbs tested inhibited TLR4 binding to immobilized recombinant NAMPT irrespectively of their corresponding epitope bins (epitope bins 1, 2, 3, 4 or 5). Several commercial anti-NAMPT antibodies were also tested and all were able to prevent eNAMPT/TLR4 binding (data not shown). In other words, I have not identified any antibody that binds NAMPT with high affinity, yet doesn't block recombinant TLR4 binding. Group A and C antibodies were tested once again in subsequent experiments, either with the same recombinant proteins pair or with an alternative (NAMPT Peprotech / TLR4 SinoBiological) pair (Fig. S27). As shown in Fig. 27, six antibodies blocked more potently than the P-1076 benchmark. Their characteristics are presented in Table 7.

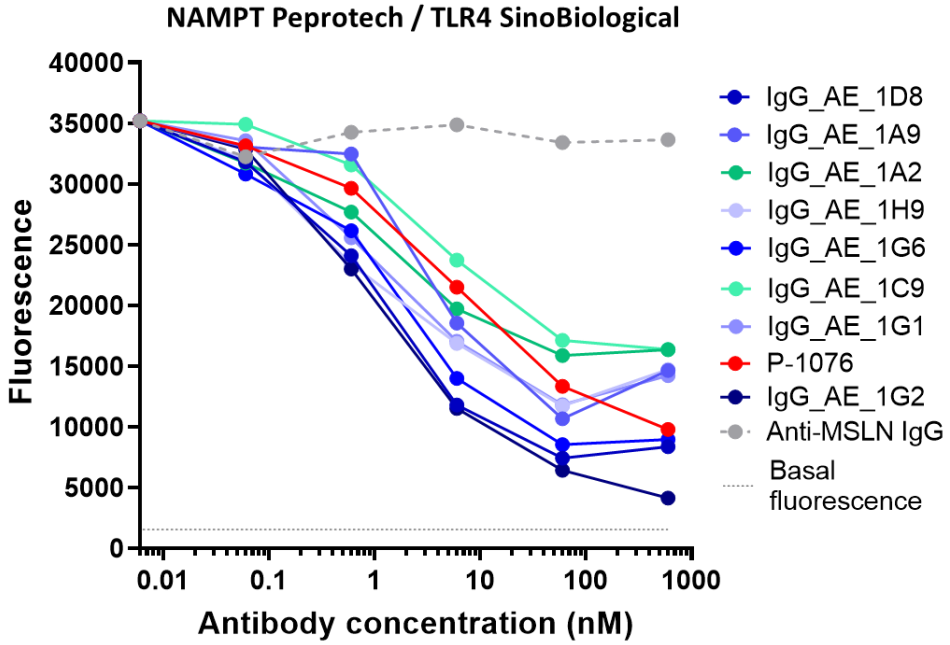

Figure 27: Blocking eNAMPT-TLR4 binding with anti-eNAMPT IgGs. Maxisorp plates were coated with 60nM NAMPT protein and incubated with increasing concentrations of anti-eNAMPT mAbs and a fixed concentration of TLR4 (30nM). His-tagged TLR4 was then detected with an anti-PentaHis tag antibody coupled to HRP.

Table 7: Summary of the characteristics of the most potent neutralizing anti-eNAMPT IgGs identified in the blocking ELISA assay. Affinity was measured using bio-layer interferometry (Octet, Forte Bio) and is shown as the KD ± SD. Results are representative of two independent experiments. P-1076 was measured for comparison. The KD of the other blocking antibodies were not measured.

Name	Binding Profile	KD (nM)	Epitope bin	IgG with a close sequence
P-1076	C	0.8 ± 0.43	I	
IgG_AE_1G2	C	2.7 ± 0.28	I, 1	
IgG_AE_1D8	A	9.3 ± 2.34	1	
IgG_AE_1G6	A	7.9 ± 2.3	2	IgG_AE_1G5
IgG_AE_1A9	A	24.7 ± 0.2	2	
IgG_AE_1H9	C	1.0 ± 0.2	4	IgG_AE_1G9
IgG_AE_1G1	A	4.4 ± 0.04	3	

5.4. Functional cell-based assays

eNAMPT has been described to act as a pro-inflammatory cytokine in various pathological conditions [1], [2]. Furthermore, eNAMPT was shown to contribute to cancer cell proliferation and migration [10]. We have therefore used various approaches to develop a functional assay allowing to determine how the anti-eNAMPT mAbs affect these functions, and particularly, whether they can neutralize them.

5.4.1. Induction of intracellular signalling pathways by eNAMPT

5.4.1.1. NF-kB pathway activation in reporter cell lines

Multiple studies reported that eNAMPT participates in disease pathogenesis by activating inflammatory signalling pathways, leading to the release of pro-inflammatory cytokines [2], [93]. NF-kB pathway, which is downstream of TLR4, was shown to be activated by eNAMPT in immune and endothelial cells [26], [95], [116], [117].

I first assessed eNAMPT ability to activate the NF-kB pathway through TLR4 receptor using HEK-Blue™ and THP1-Blue ™ NF-kB reporter cell lines (InvivoGen). HEK-Blue™ cells were co-transfected with human TLR4, MD-2 and CD14 co-receptors genes for LPS recognition and binding, whereas THP-1-Blue ™ cells were only transfected with human CD14, as these cells naturally express TLRs and MD-2. As shown in Fig. 28, TLR4 natural ligand, LPS, induced a robust activation of NF-kB in HEK-Blue-TLR4/MD-2/CD14 cells, which was abrogated when LPS was pre-incubated with its inhibitor (polymyxin B). Recombinant NAMPT proteins from different suppliers or generated in house were then tested on the same cells. The NAMPT proteins either did not induce NF-kB pathway activation (Adipogen, in house, R&D and SinoBiological NAMPT proteins) or were contaminated with endotoxins (MBL international and MyBiosource NAMPT proteins) (Fig. 28). Adipogen, in house and R&D NAMPT proteins also did not induce NF-kB pathway in THP1-Blue-CD14 cells (Fig. S28). SinoBiological, MBL international and MyBiosource NAMPT proteins were not tested in THP1-Blue-CD14 cells.

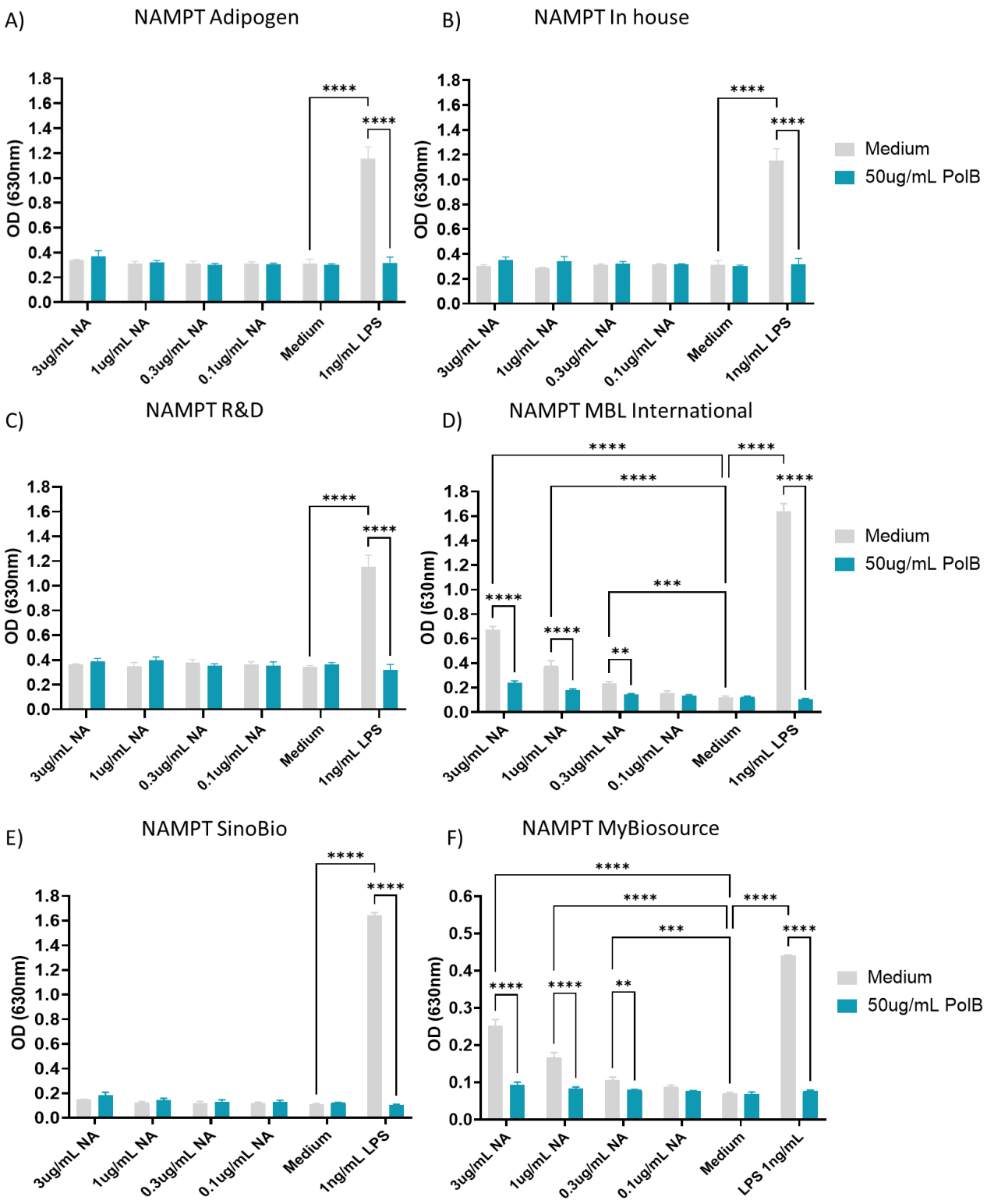

Figure 28: NF-kB pathway induction in HEK-Blue-TLR4/MD-2/CD14 reporter cells. (A-F) HEK-Blue-TLR4/MD-2/CD14 cells (InvivoGen) were stimulated with NAMPT proteins (NA, 0.1-3ug/mL) or with LPS (1ng/mL), preincubated or not with polymyxin B (PolB, 50ug/mL) as indicated. NF-kB activation was quantified by determining the activity of SEAP using QUANTI-Blue™ detection reagent **(A-E)** or HEK-Blue™ Detection medium **(F)**. **(A-D)** Results are representative of two independent experiments and are represented as mean OD ± SD of three replicates. **(E-F)** Results are represented as mean OD ± SD of three replicates. *, $p < 0.05$; **, $p < 0.01$; ***, $p < 0.001$; ****, $p < 0.0001$; ns, not statistically significant; were obtained using a two-way ANOVA with Tukey's multiple comparisons test.

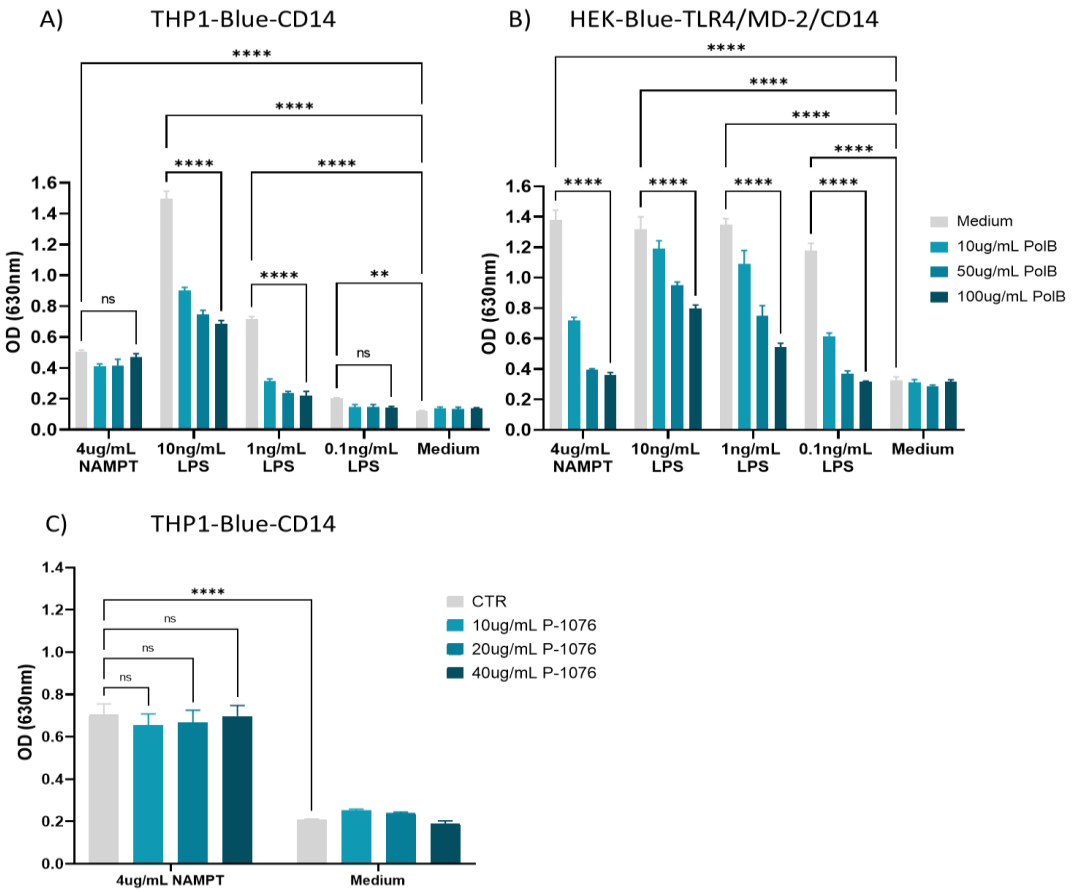

Figure 29: NF-kB pathway induction by Peprotech NAMPT protein in THP1-Blue-CD14 and HEK-Blue-TLR4/MD-2/CD14 reporter cells. **(A)** THP1-Blue-CD14 cells (InvivoGen) and **(B)** HEK-Blue-TLR4/MD-2/CD14 cells (InvivoGen) were stimulated with 4ug/mL of NAMPT (Peprotech) or LPS preincubated with polymyxin B (PolB, at 0, 10, 50 or 100ug/mL). **(C)** THP1-Blue-CD14 cells were stimulated with 4ug/mL of NAMPT preincubated with increasing concentrations of P-1076 antibody (0-40ug/mL). **(A-C)** NF-kB activation was quantified by determining the activity of SEAP using QUANTI-Blue™ detection reagent. Results are representative of two independent experiments and are represented as mean OD ± SD of three replicates. *, $p < 0.05$; **, $p < 0.01$; ***, $p < 0.001$; ****, $p < 0.0001$; ns, not statistically significant; were obtained using a two-way ANOVA with Tukey's multiple comparisons test.

Surprisingly, Peprotech recombinant NAMPT protein activated the two NF-kB reporter cell lines differently. In THP1-Blue-CD14 cells, the protein induced a weak activation of NF-kB pathway, which was not due to residual LPS present in the protein preparation (Fig. 29A). Nevertheless, as THP1-Blue-CD14 cells naturally express other TLRs through which NF-kB signalling can also be activated, a contamination by another TLR ligand cannot be excluded. Thus, we cannot be sure that the observed residual NF-kB activation is induced by eNAMPT. Furthermore, as shown in Fig. 29C, this eNAMPT-mediated NF-kB activation was not blocked by P-1076 antibody. In HEK-Blue-TLR4/MD-2/CD14 cells, eNAMPT-induced activation of NF-kB was strong, but was actually elicited by contaminating endotoxins (Fig. 29B). The fact that the endotoxins present in Peprotech NAMPT preparation activate NF-kB in HEK-Blue but not in THP1-Blue cells can be explained by the increased sensitivity of HEK-Blue cells. Indeed, 0.1ng/mL of LPS were sufficient to trigger a strong NF-kB signalling in HEK-Blue, whereas 1ng/mL of LPS were required for THP1-Blue cells (Fig. 29A-B).

5.4.1.2. Activation of other intracellular pathways

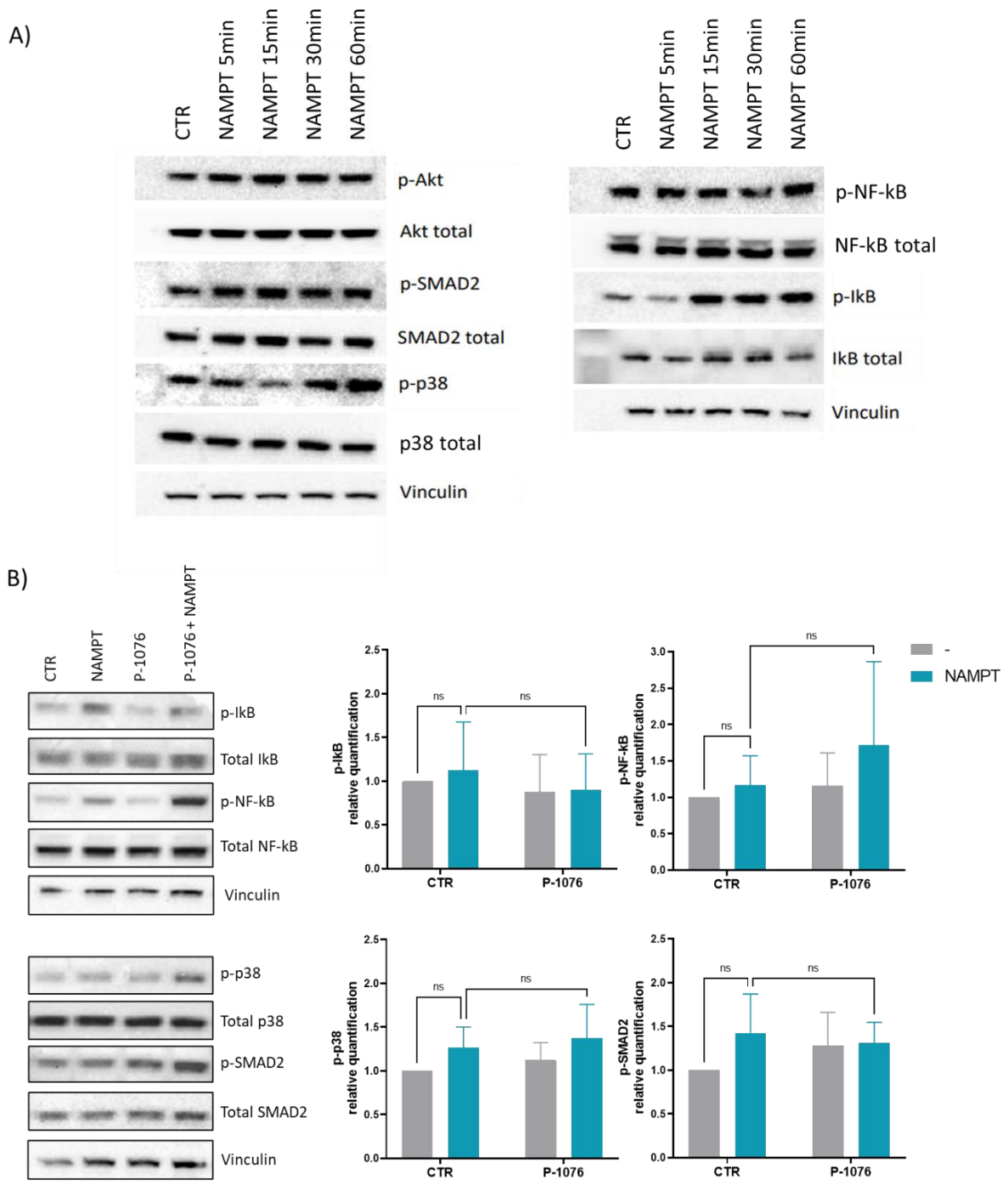

Figure 30: Intracellular pathways activation in MCF10A cells. (A) MCF10A cells were stimulated with NAMPT (100ng/mL) or not (CTR, control) for the indicated times. Cell extracts were immunoblotted for total and phosphorylated AKT, SMAD2, p38, NF-kB and IkB. **(B)** MCF10A cells were stimulated with NAMPT (100ng/mL) in the presence of P-1076 (9ug/mL) or not (CTR) for one hour. Cell extracts were immunoblotted for total and phosphorylated SMAD2, p38, NF-kB and IkB. Results are representative of two (for SMAD-2) or four (for the other signalling proteins) independent experiments. *, $p < 0.05$; **, $p < 0.01$; ***, $p < 0.001$; ****, $p < 0.0001$; ns, not statistically significant; were obtained using a two-way ANOVA with Tukey's multiple comparisons test.

eNAMPT was shown to induce the activation of intracellular signalling pathways in MCF10A mammary epithelial cells [108], [118]. In order to reproduce these results, I therefore performed western blots using the same eNAMPT preparation than Soncini et al. [108] (Adipogen NAMPT protein). This recombinant NAMPT protein was used in all the western blot analyses presented hereafter. In a preliminary experiment, treatment of MCF10A cells with eNAMPT induced a slight p38 and IkB phosphorylation (Fig. 30A). However, these preliminary results could not be reproduced as exemplified in Fig. 30B.

Similar analyses were performed with breast cancer cell lines MCF-7 and MDA-MB-231, in which eNAMPT was also shown to activate signalling pathways [119], [120]. In one experiment, stimulation of MCF-7 cells with eNAMPT slightly induced IkB, NF-kB, p38 and AKT activation (with a 1.2-fold, 1.6-fold and 1.8-fold increase respectively (Fig. 31A)). However, as shown in Fig. 31B, this was not observed in a second analysis.

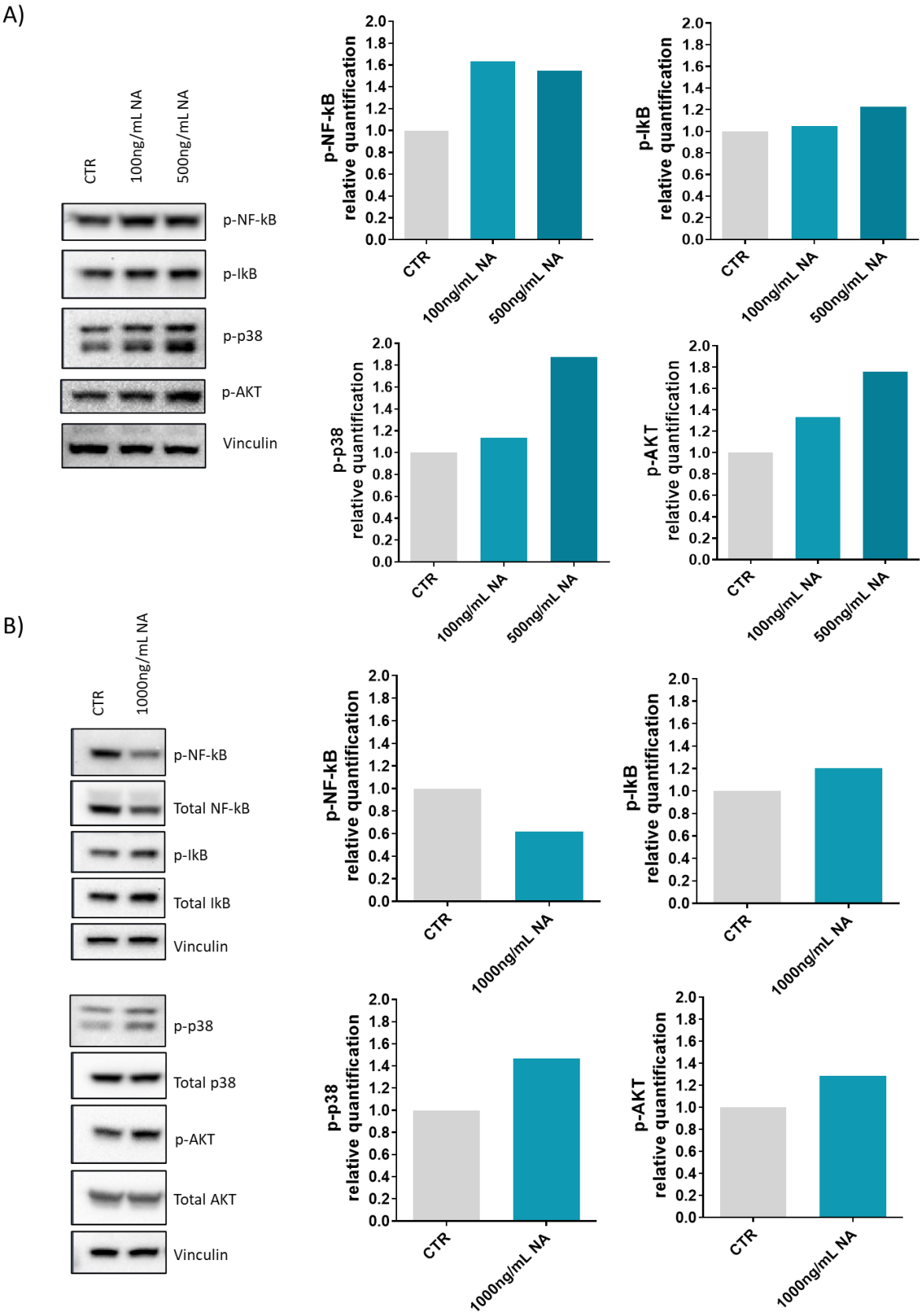

Figure 31: Intracellular pathways activation in MCF-7 cells. (A-B) MCF-7 cells were stimulated with NAMPT (NA; 100, 500 or 1000ng/mL) or not (CTR, control) for 24h. Cell extracts were then immunoblotted for total and phosphorylated NF-kB, IkB, p38 and AKT. **(A)** and **(B)** correspond to two independent experiments.

Similarly, treatment of MDA-MB-231 cells with recombinant NAMPT protein failed to induce the activation of AKT, p38, NF-kB/IkB and STAT3 signalling pathways (Fig. 32). A dose-dependent reduction of IkB activation was observed in the presence of eNAMPT. This decrease was not reproduced in a second analysis (data not shown).

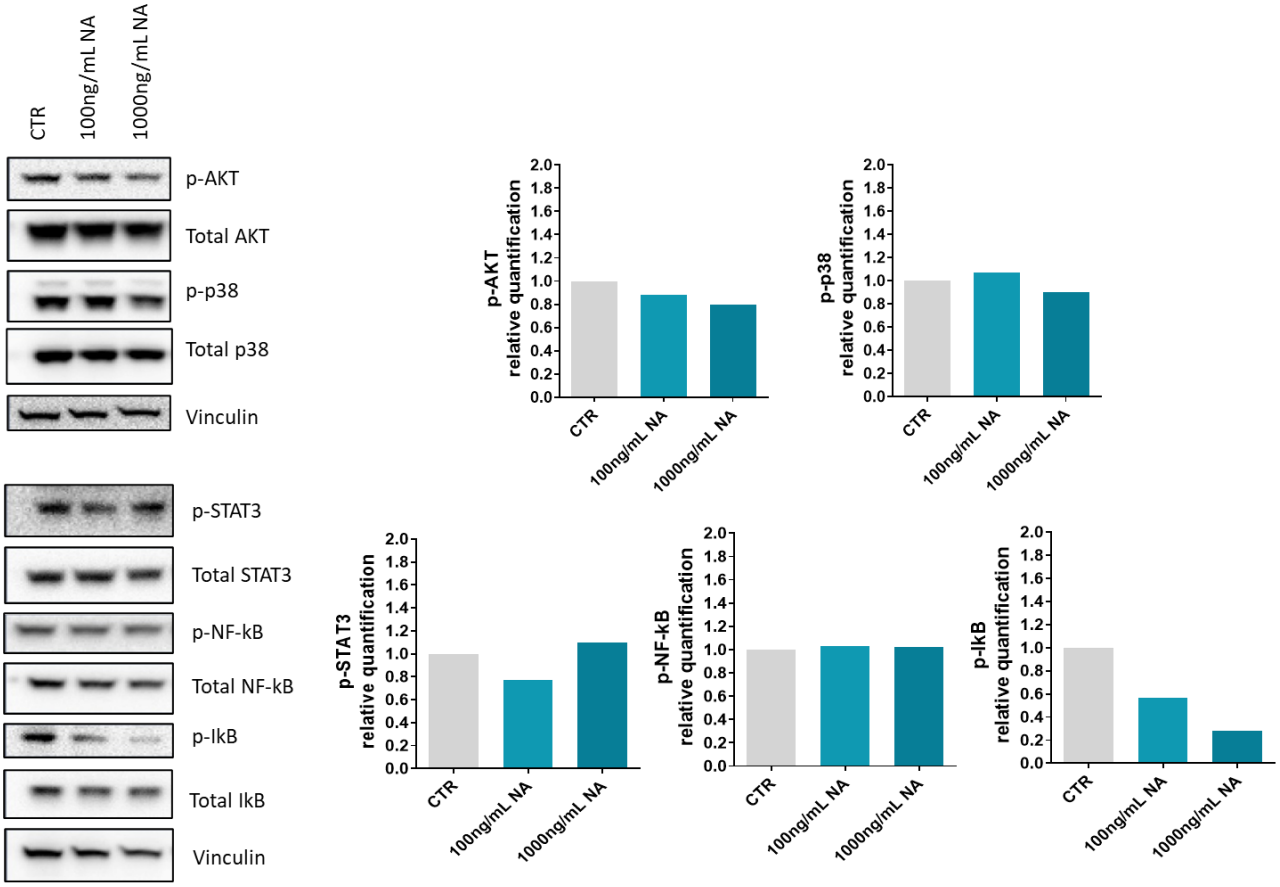

Figure 32: Intracellular pathways activation in MDA-MB-231 cells. MDA-MB-231 cells were stimulated with NAMPT (NA, 100 or 1000ng/mL) or not (CTR, control) for one hour. Cell extracts were then immunoblotted for total and phosphorylated AKT, p38, STAT3, NF-kB and IkB.

Finally, NF-kB/IkB signalling pathway activation by eNAMPT in prostate cancer cells (PC-3) was assessed, based on the publication of Sun et al. [98]. The activation of other signalling proteins such as AKT and p38 was also evaluated at the same time. As shown in Fig. 33, stimulation of PC-3 cells with eNAMPT did not significantly induce p38, AKT, NF-kB and IkB phosphorylation. Overall, activation of signalling pathways by eNAMPT in various cell lines could not be demonstrated or otherwise confirmed. These results highlight the difficulty of reproducing data and obtaining reliable results with western blots. Indeed, western blot analysis is subjected to inherent variability and poor reproducibility [121], [122].

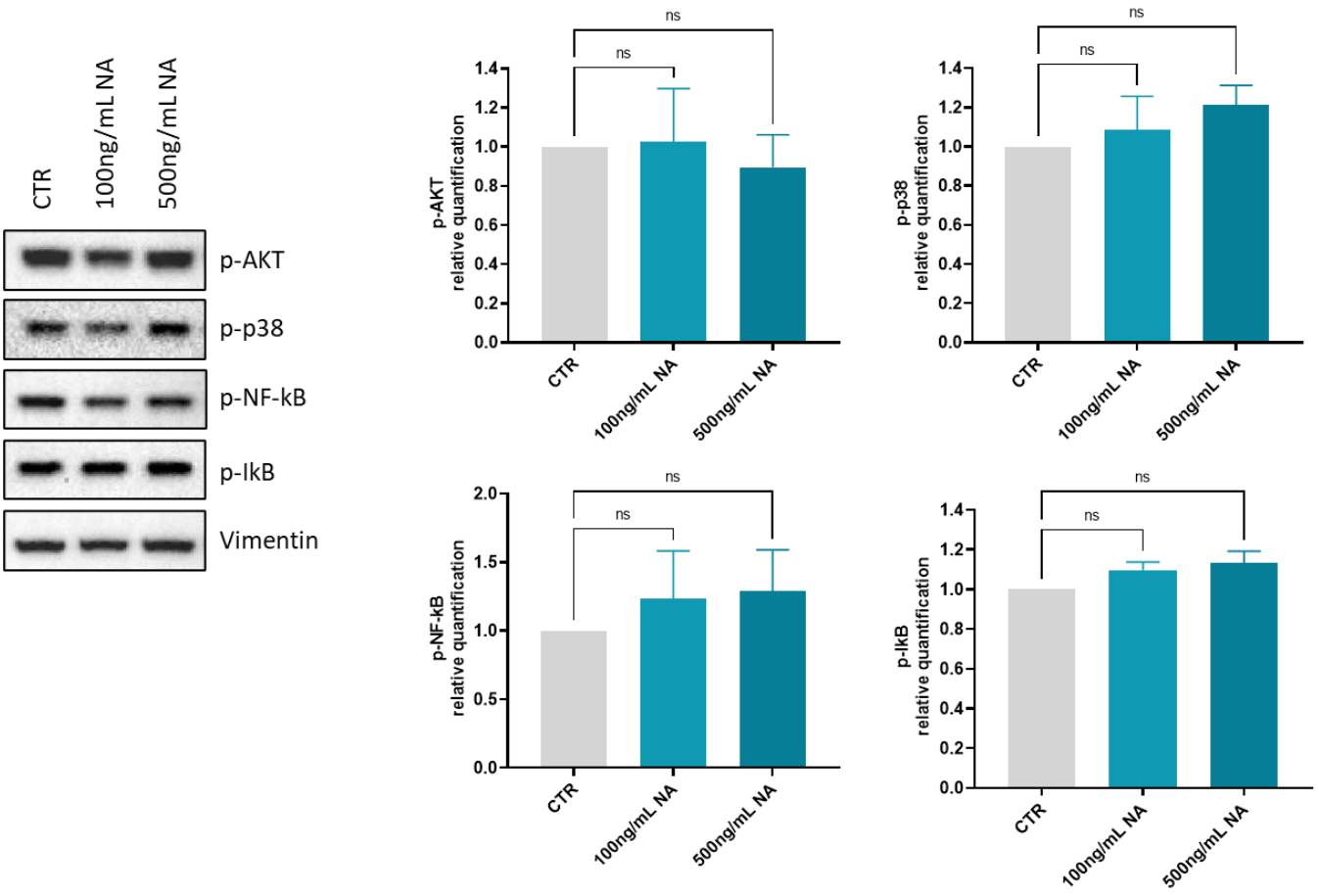

Figure 33: Intracellular pathways activation in PC-3 cells. PC-3 cells were stimulated with NAMPT (100 or 500ng/mL) or not (CTR, control) for 24h. Cell extracts were then immunoblotted for p-AKT, p-p38, p-NF-kB and p-IkB. Results are representative of two independent experiments. ns, not statistically significant; was obtained using a one-way ANOVA with Dunnett's multiple comparisons test.

5.4.2. Proliferative effect of eNAMPT

Hung et al. and Gholinejad et al. [119], [120] demonstrated that eNAMPT contributes to tumor development by sustaining cancer cell proliferation. Based on these publications, I assessed the induction of breast cancer cell (MCF-7 and MDA-MB-231) proliferation by eNAMPT (Fig. 34). Unfortunately, in this and in further experiments (data not shown) recombinant NAMPT protein failed to induce cancer cell proliferation.

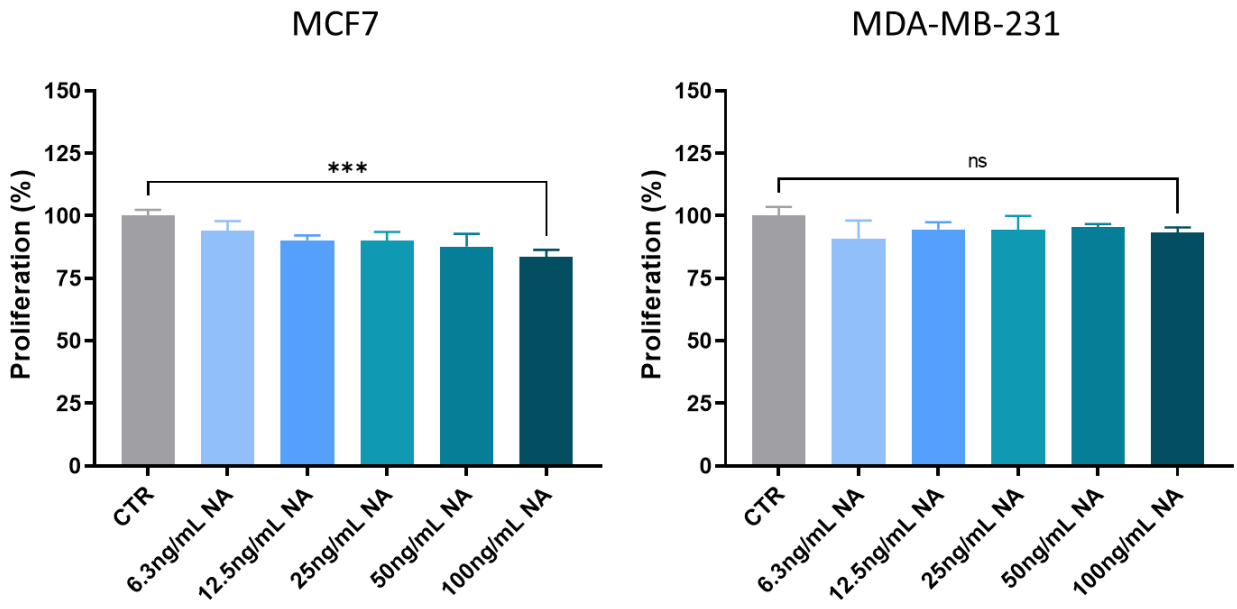

Figure 34: The effect of eNAMPT on breast cancer cell proliferation. Proliferation of MDA-MB-231 and MCF-7 cells treated with NAMPT (NA, 0–100ng/mL) for 72 hours was measured with SRB colorimetric assay. *, $p < 0.05$; **, $p < 0.01$; ***, $p < 0.001$; ****, $p < 0.0001$; ns, not statistically significant; were obtained using a one-way ANOVA with Dunnett's multiple comparisons test.

5.4.3. Epithelial-to-mesenchymal transition of MCF10A cells

Based on Soncini et al. publication [108], eNAMPT-induced epithelial-to-mesenchymal transition (EMT) of MCF10A mammary epithelial cells was assessed. Specifically, the expression of epithelial (E-cadherin) and mesenchymal (N-cadherin, vimentin and ZEB1) genes, which are respectively down-regulated and up-regulated during this biological process, was assessed by RT-qPCR after 14 days of incubation with eNAMPT. Unfortunately, no significant changes in the expression of these genes could be observed (Fig. 35). Thus, the eNAMPT induction of EMT in MCF10A cells could not be confirmed.

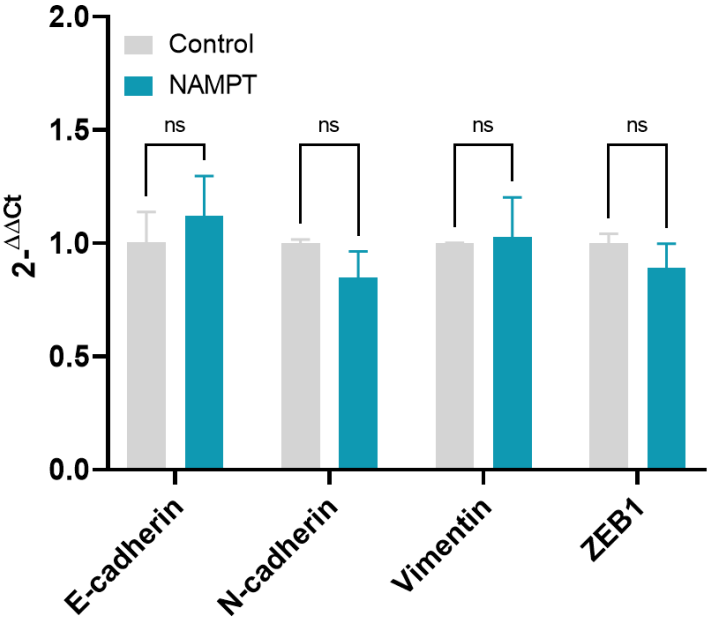

Figure 35: Induction of epithelial-to-mesenchymal transition in mammary epithelial cells. MCF10A cells were incubated for 14 days with 100ng/mL of recombinant NAMPT protein (Adipogen). Cells RNA was extracted and E-cadherin, N-cadherin, vimentin and ZEB1 mRNA levels were quantified by qPCR. Results are representative of two independent experiments. ns, not statistically significant, was obtained using a two-way ANOVA with Tukey's multiple comparisons test.

6. Discussion

6.1. Development of anti-eNAMPT antibodies

Over the course of my thesis, I produced 554 anti-eNAMPT single-chain fragment variables (scFvs) with unique sequences. 86 of them, which presented high binding affinity for NAMPT, were reformatted into IgGs and produced at small scale for subsequent analyses. In addition, the eNAMPT-blocking P-1076 antibody [102], from which the experimental drug ALT-100 is derived, was also produced, with the intention of using it as a benchmark/comparator in binding and functional assays.

Of the 86 monoclonal antibodies (mAbs) I generated, 81 were specific to NAMPT. Furthermore, they presented different binding characteristics, targeting different regions on NAMPT, as demonstrated in a series of binding competition experiments. As a consequence, they were grouped into distinct epitope bins (as a reminder, mAbs sorted into the same epitope bin bind to the same region of the target and compete for binding, but do not necessarily recognize the same epitope).

6.2. Neutralizing activity of the anti-eNAMPT antibodies

6.2.1. Ligand/receptor binding assays

The affinity of the interaction between eNAMPT and its cell surface receptors TLR4 and CCR5 has been published [27], [114] and their respective KD values are in the nM range. Of note, several mAbs (identified by phage display, as well as the P-1076 benchmark), falling into different epitope bins, presented a sufficiently high affinity for eNAMPT to be able, at least in theory, to efficiently compete with TLR4 and/or CCR5 for ligand binding.

I therefore wanted to assess in the first place whether anti-eNAMPT mAbs were able to block eNAMPT/receptor interactions. To this end, we used recombinant proteins and cells expressing TLR4 or CCR5, which I tested in a variety of eNAMPT/receptor binding assays using different technologies, such as ELISA, bio-layer interferometry, CellInsight platform and flow cytometry. Given that protein structural integrity and stability are critical for ligand/receptor binding, and can vary considerably depending on protein mode of production [123], [124], we tested recombinant NAMPT proteins produced in different expression systems (*E.coli*, insects or mammalian cells) and purchased from different suppliers.

Dose-dependent and specific binding of TLR4 to NAMPT could be demonstrated in one distinctive ELISA configuration, with recombinant NAMPT protein immobilized by passive coating on maxisorp plates and recombinant TLR4 protein in solution. We therefore used this assay to assess the blocking ability of anti-eNAMPT antibodies. All the mAbs tested, including

the P-1076 benchmark, turned out to be neutralizing, i.e., they were competing with soluble TLR4 for NAMPT binding. The fact that all these mAbs efficiently blocked TLR4 binding was unexpected and difficult to explain mechanistically, given that these different mAbs fall into five distinct epitope bins, which means that they are targeting remote, or perhaps even opposite surfaces of the NAMPT protein.

Unfortunately, I failed to confirm the eNAMPT/TLR4 interaction in other binding assays, either in alternative ELISA configurations or cell-based assays with engineered cells expressing high levels of TLR4 at the cell surface. This fact, along with the inexplicable results of the mAb-TLR4 competition ELISA, brought me to a conclusion that I do not have a reliable TLR4-based binding assay for testing the neutralizing activity of my anti-eNAMPT mAbs. By the same token, I failed to demonstrate the interaction between eNAMPT and its alternative putative receptor CCR5; this, in spite of numerous attempts, and different assay types tried, with recombinant CCR5 and with cells expressing high cell surface levels of CCR5. To my knowledge, no one has been able so far to demonstrate a direct interaction between eNAMPT and its proposed receptors CCR5 and TLR4 expressed on cells (under native conditions).

6.2.2. Functional cell-based assays

Having failed to demonstrate a direct interaction between eNAMPT and TLR4 or CCR5, I set out to test the effect of recombinant NAMPT in "receptor-agonistic" functional cell-based assays. Based on published results [26], [95], [108], [117], [119], [120], I tried to replicate the induction of diverse intracellular signal transduction pathways (MAPK/ERK, TGF-β/SMAD2/3, PI3K/Akt, JAK/STAT, NF-kB) by recombinant NAMPT.

Using a monocytic reporter cell line transfected with CD14 (THP1-Blue-CD14), I could observe a low-level induction of NF-kB-driven reporter gene expression with one recombinant NAMPT preparation (Peprotech). That residual reporter gene signal was rather variable and could not be inhibited by P-1076 benchmark or any other eNAMPT mAbs tested (neither was it caused by contaminating LPS, as it was not blocked by polymyxin B). I therefore concluded that the observed reporter gene induction could be due to another (trace) contaminant present in the Peprotech preparation. THP-1 are human leukemia monocytic cells, and human monocytes are known to naturally express other TLRs (e.g. TLR1, TLR2, TLR7)[125], which, like TLR4, are upstream of the NF-kB pathway. I therefore tested another reporter cell line, in which NF-kB activation is almost exclusively mediated by TLR4 (HEK-Blue-TLR4/MD-2/CD14 cells). Alas, none of the seven recombinant NAMPT proteins tested activated reporter gene expression in these cells. Of note, Gasparrini et al. [114], tested the same HEK-Blue-TLR4/MD-2/CD14 cell line and, like my case, were not able to induce NF-kB activation with recombinant NAMPT proteins. They hypothesized, that MD-2 and TLR4 association may have prevented the binding of NAMPT to TLR4 on these cells, which remains to be demonstrated by further analysis.

eNAMPT was shown to activate additional intracellular signalling pathways in various type of cancer cells, such as breast and prostate cancer cell lines [98], [119], [120], [126]. We therefore set out to assess eNAMPT-induced phosphorylation of p38, SMAD2, AKT, NF-kB/IkB or STAT3 by western blotting. Unfortunately, we did not observe any strong, consistent or reproducible phosphorylation events in this series of experiments.

Also, multiple *in vitro* and *in viv*o studies reported that eNAMPT contributes to cancer progression by supporting tumor cell proliferation [119], [120], [127], [128]. In a further attempt to find a functional assay for eNAMPT biological activity, we evaluated its pro-proliferative effect on MCF-7 and MDA-MB-231 breast cancer cell lines. Unfortunately, and once again, these attempts failed – eNAMPT treatment did not result in any increase of cancer cell proliferation.

Lastly, we have also tried a more sophisticated and elaborated functional assay. In the context of cancer, eNAMPT has been shown to exert pro-metastatic functions, notably by promoting tumor cell epithelial-to-mesenchymal transition (EMT) [108]. We therefore performed a series of experiments trying to faithfully reproduce the experimental conditions from Soncini et al. [108], but, once again, without success.

Taken all together, I have generated a panel of mAbs binding different regions of NAMPT with moderate to high affinities. These features suggest that at least some of these mAbs may be able to efficiently neutralize pathological functions of eNAMPT. Nonetheless, as I was unable to reproduce eNAMPT binding to TLR4 and CCR5, eNAMPT-induced activation of intracellular signalling pathways, or, finally, eNAMPT pro-tumoral and pro-chemotactic functions; I had no means of testing the neutralizing potential of eNAMPT mAbs I have generated.

6.3. Conclusion and perspectives

The INTEGRATA European project focused on the discovery of new biological and chemical approaches to target NAD production and signalling in cancer. Within this framework, my PhD research project aimed to develop and test anti-eNAMPT neutralizing monoclonal antibodies (mAbs). During my thesis, I successfully generated a total of 81 specific anti-eNAMPT mAbs targeting different regions on NAMPT. Among these, several showed moderate or even high affinity for NAMPT, with values close to that of P-1076 benchmark. However, as explained above, I was unable to test their neutralizing potential.

To attain this goal, it would be necessary to have a reliable *in vitro* assay that monitors some of the numerous biological activities that have been ascribed to this adipokine/cytokine. During my thesis, I have unsuccessfully tried a limited number of such functional assays, but there are still plenty of other assays described in the literature which I could not explore because of time and resource limitations. For instance, eNAMPT has been shown to promote endothelial cell migration, invasion and capillary tube formation *in vitro* [129]–[131]. Additionally, eNAMPT was described to contribute to the formation of new blood vessels, by upregulating the expression of pro-angiogenic factors, such as VEGF, IL-6, IL-8, FGF-2 and MCP-1 [132]–[134]. Other studies reported that eNAMPT promotes the expression, production and activity of matrix metalloproteinases in endothelial cells, macrophages and cancer cells [126], [130], [135]–[140]. The above biological functions of eNAMPT (as well as others that I did not mention here) were revealed by experiments that could potentially provide useful *in vitro* assays for monitoring eNAMPT biological activities, and ultimately, the neutralizing potential of eNAMPT-binding mAbs.

It may also be interesting to determine the epitopes targeted by eNAMPT mAbs. For that sake, Gasparrini et al. and Kim et al. [114], [141] proposed that the TLR4-binding regions of eNAMPT are localized in its N-terminal region, while another group suggested that eNAMPT C-terminal region might contribute to the interaction with TLR4 [26], [142]. Thus, it would be of particular interest to know whether our anti-eNAMPT antibodies recognize these regions.

Recent publications from Dr. Garcia's laboratory describe the therapeutic effects of eNAMPT blocking antibodies P-1076 and/or ALT-100 in various animal models of disease [98], [102], [103], [105], [143]. An alternative, unorthodox option would therefore consist on testing the antibodies I generated *in vivo*, directly, without any previous functional *in vitro* characterization (in particular the mAbs that compete with P-1076 for binding to the target). However, this would require a large-scale production of antibodies and considerable time and resources, typically necessary to run *in vivo* experiments.

7. Appendices

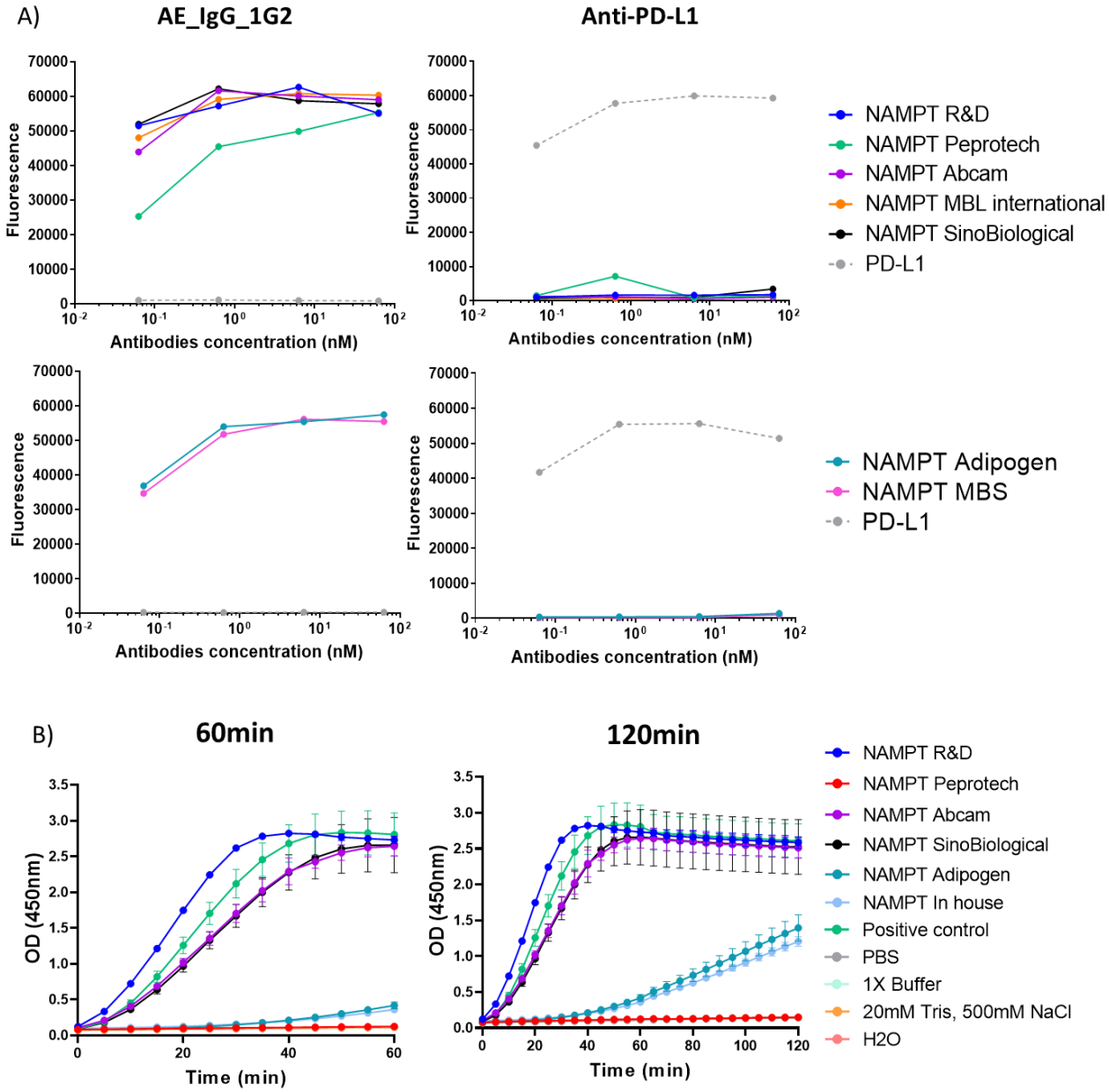

Supplementary Figure S1: Characterization of recombinant NAMPT proteins. (A) Detection of recombinant NAMPT proteins by ELISA. NAMPT proteins were immobilized on a maxisorp plate and detected with an anti-NAMPT or an anti-PD-L1 (irrelevant) antibody. **(B)** The enzymatic activity of NAMPT proteins was assessed using Abcam colorimetric assay following supplier's procedure. Results are representative of two independent experiments.

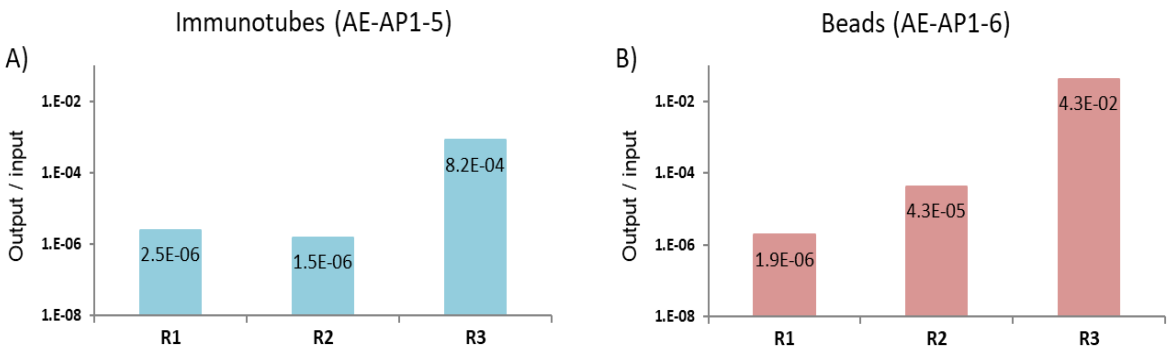

Supplementary Figure S2: Example of output/input ratios obtained during phage display selections against NAMPT. (A-B) scFv-displaying phages output/input ratios obtained with selection strategies using either commercial NAMPT-coated immunotubes **(A)** or in house NAMPT-biot-coated streptavidin/neutravidin beads **(B)**. Both selection strategies were performed on the same phage library (AP1).

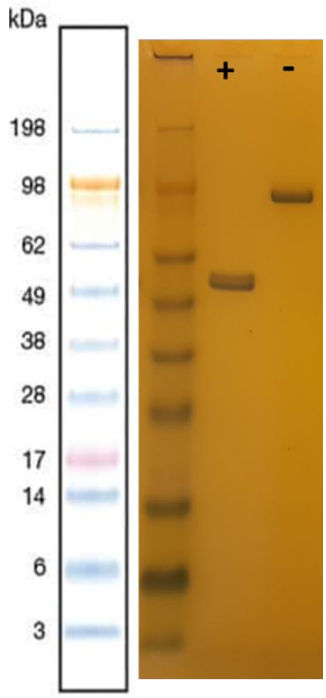

Supplementary Figure S3: Analysis of Adipogen recombinant NAMPT protein by SDS-PAGE. Commercial NAMPT protein (Adipogen) was analyzed by SDS-PAGE under reducing (+) and non-reducing (-) conditions.

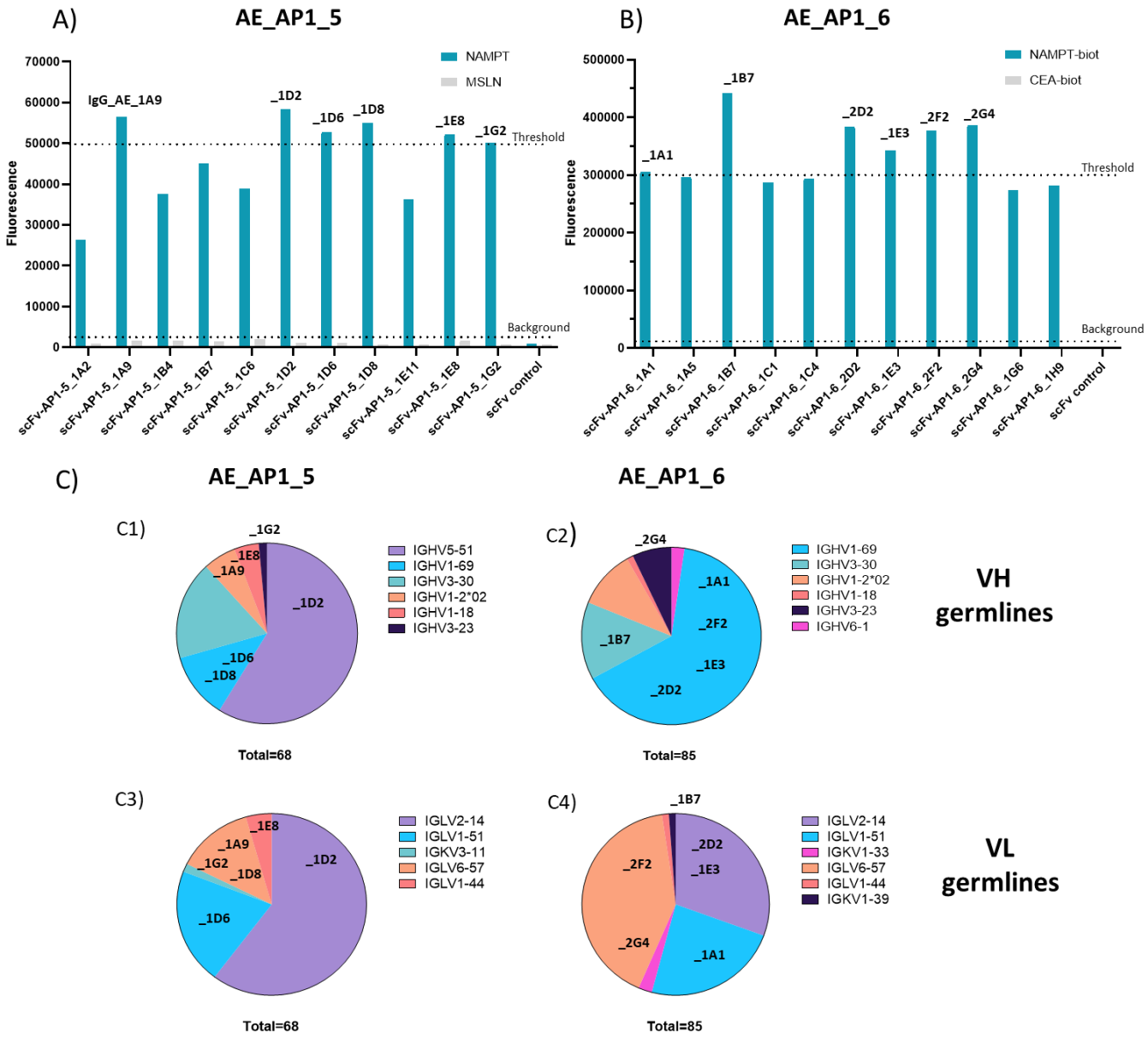

Selection	AE_AP1_5	AE_AP1_6
Unique binders sequence	28/68	32/85
Diversity (%)	41	38

Supplementary Figure S4: Example of phage display screening results. (A-B) scFvs binding signals measured by ELISA **(A)** or homogeneous binding assay (cellInsight platform) **(B)** for AE_AP1_5 and AE_AP1_6 selections respectively. Specific high/moderate affinity binders were selected for sequencing. A more stringent threshold (dashed line) was applied to select scFvs for reformatting. **(C)** Germline proportion and sequence diversity obtained for the pool of scFvs sequenced. No overlapping sequences were found between the two strategies. scFvs with dissimilar sequences were selected for reformatting and are indicated in bold. Once reformatted into IgGs, scFvs were renamed according to IgG_AE_X nomenclature for simplification (e.g. scFv-AP1-5_**1A9** became IgG_AE_**1A9**).

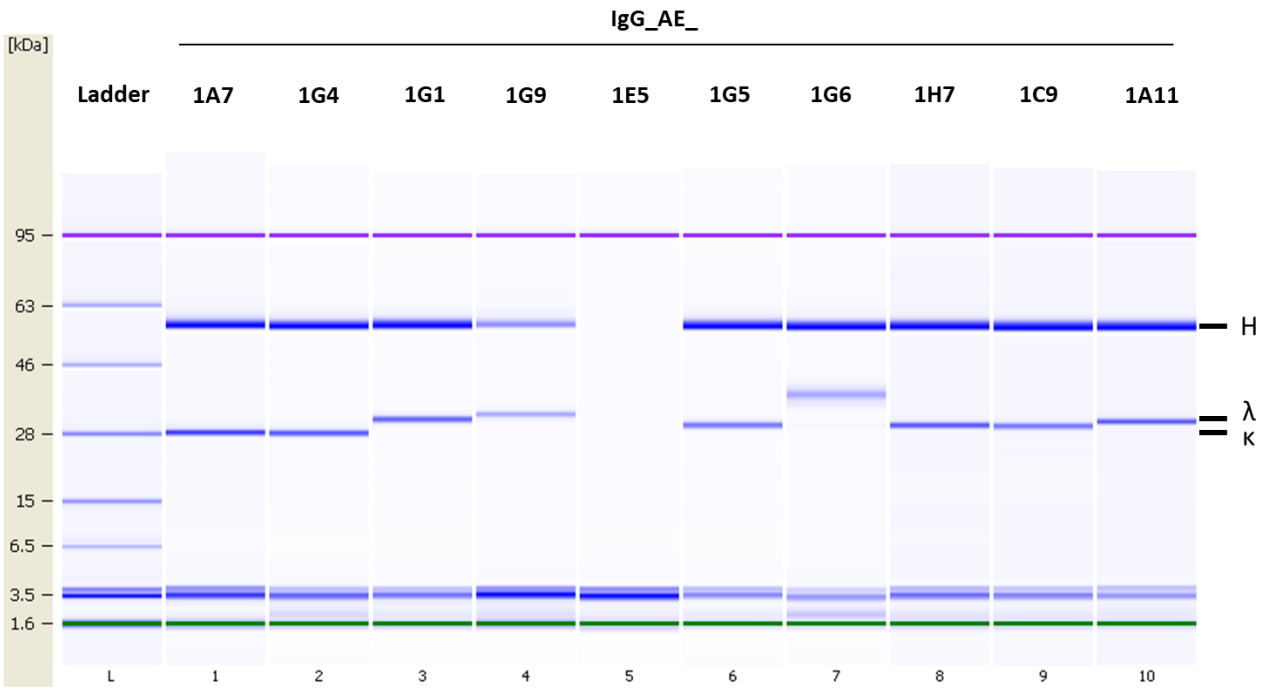

Supplementary Figure S5: Expression of anti-eNAMPT antibodies analyzed by SDS-PAGE. Gel electrophoresis analysis of the IgGs in reducing conditions using Agilent Bioanalyzer 2100 Protein 80. The bands corresponding to the common heavy chain (H) and the κ and λ light chains are indicated.

GROUP A

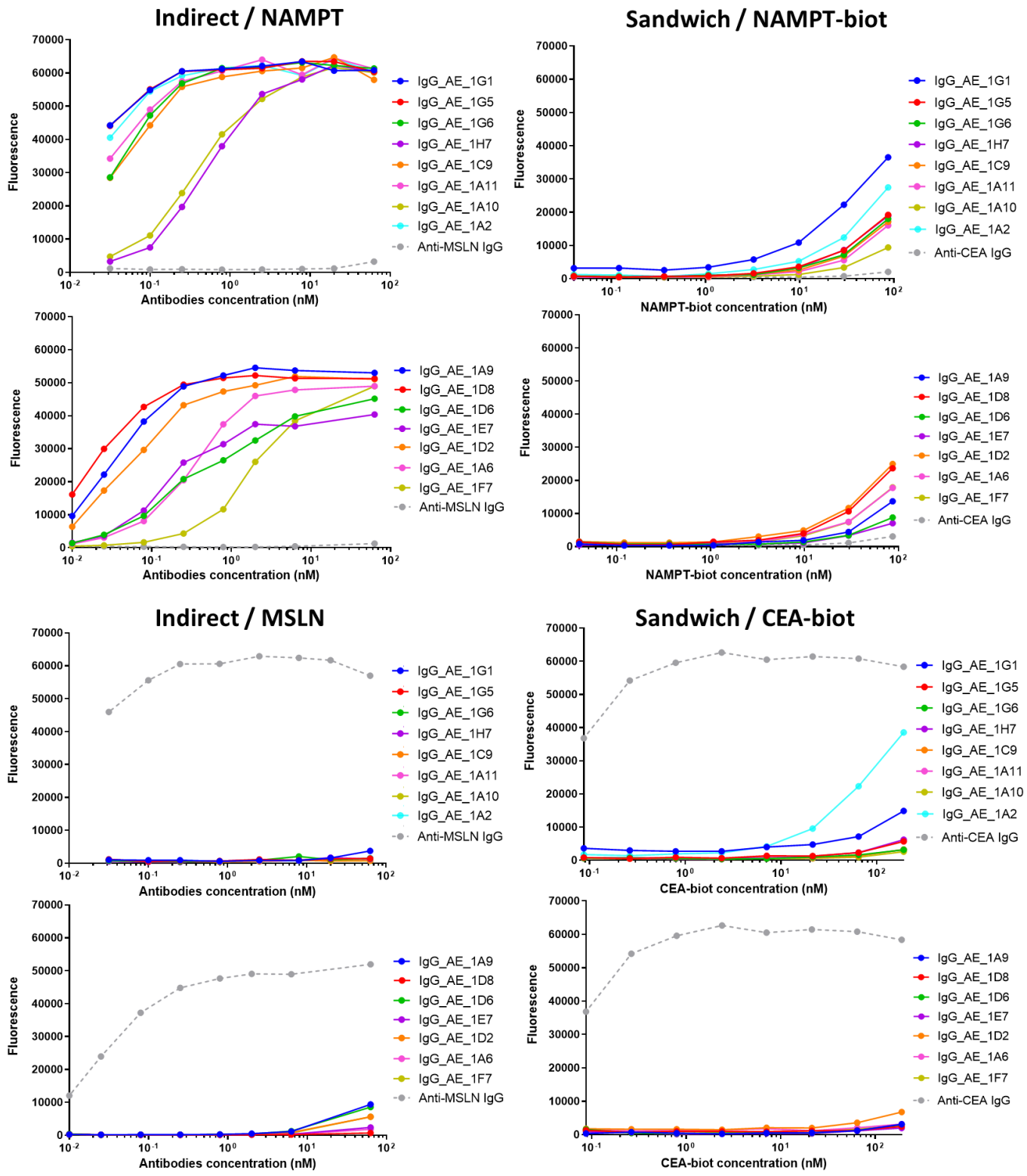

Supplementary Figure S6: Characterization of group A anti-eNAMPT antibody binding by ELISA. The binding of group A antibodies to NAMPT was analyzed by indirect ELISA with a commercial NAMPT protein or by sandwich ELISA with in house NAMPT-biot protein. Maxisorp plates were used for both ELISA assays.

GROUP A

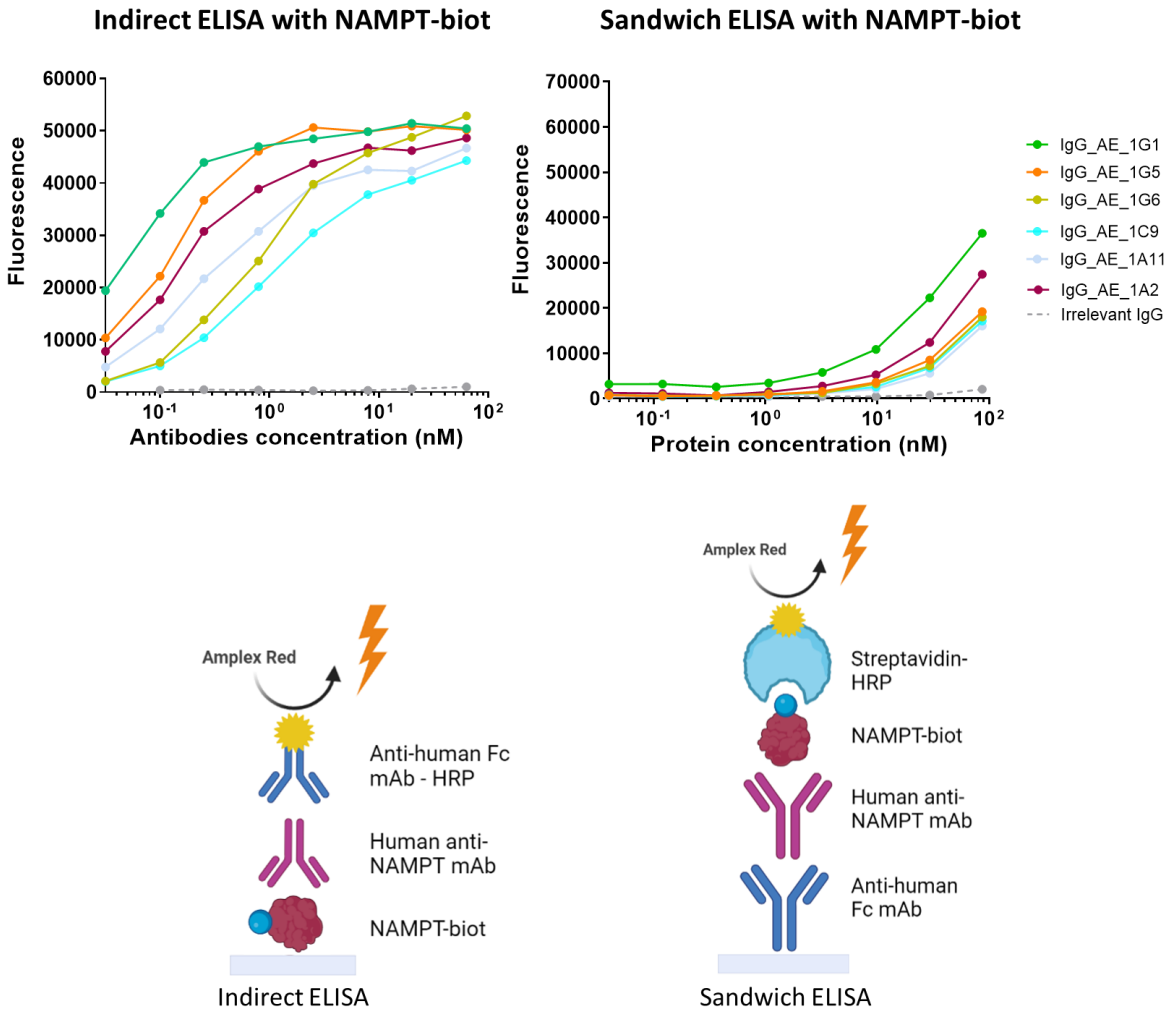

Supplementary Figure S7: Binding of selected group A anti-eNAMPT antibodies. The binding of selected group A antibodies was compared in indirect ELISA and sandwich ELISA using the same target protein (in house NAMPT-biot). Maxisorp plates were used for both ELISA assays.

GROUP B

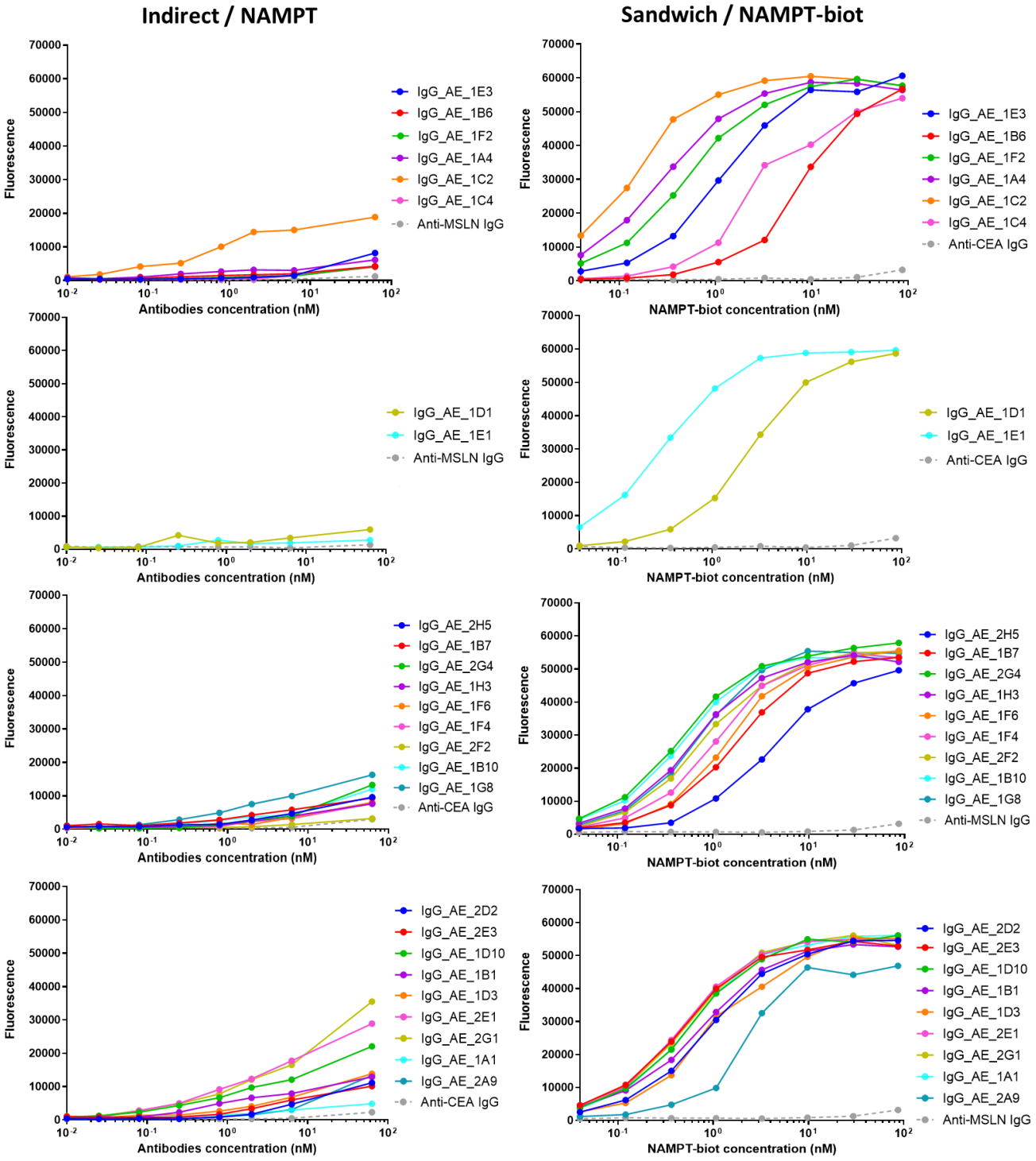
Indirect / NAMPT
Sandwich / NAMPT-biot
Fluorescence
Antibodies concentration (nM)
NAMPT-biot concentration (nM)
IgG_AE_1E3
IgG_AE_1B6
IgG_AE_1F2
IgG_AE_1A4
IgG_AE_1C2
IgG_AE_1C4
Anti-MSLN IgG
Anti-CEA IgG
IgG_AE_1D1
IgG_AE_1E1
IgG_AE_2H5
IgG_AE_1B7
IgG_AE_2G4
IgG_AE_1H3
IgG_AE_1F6
IgG_AE_1F4
IgG_AE_2F2
IgG_AE_1B10
IgG_AE_1G8
IgG_AE_2D2
IgG_AE_2E3
IgG_AE_1D10
IgG_AE_1B1
IgG_AE_1D3
IgG_AE_2E1
IgG_AE_2G1
IgG_AE_1A1
IgG_AE_2A9

GROUP B

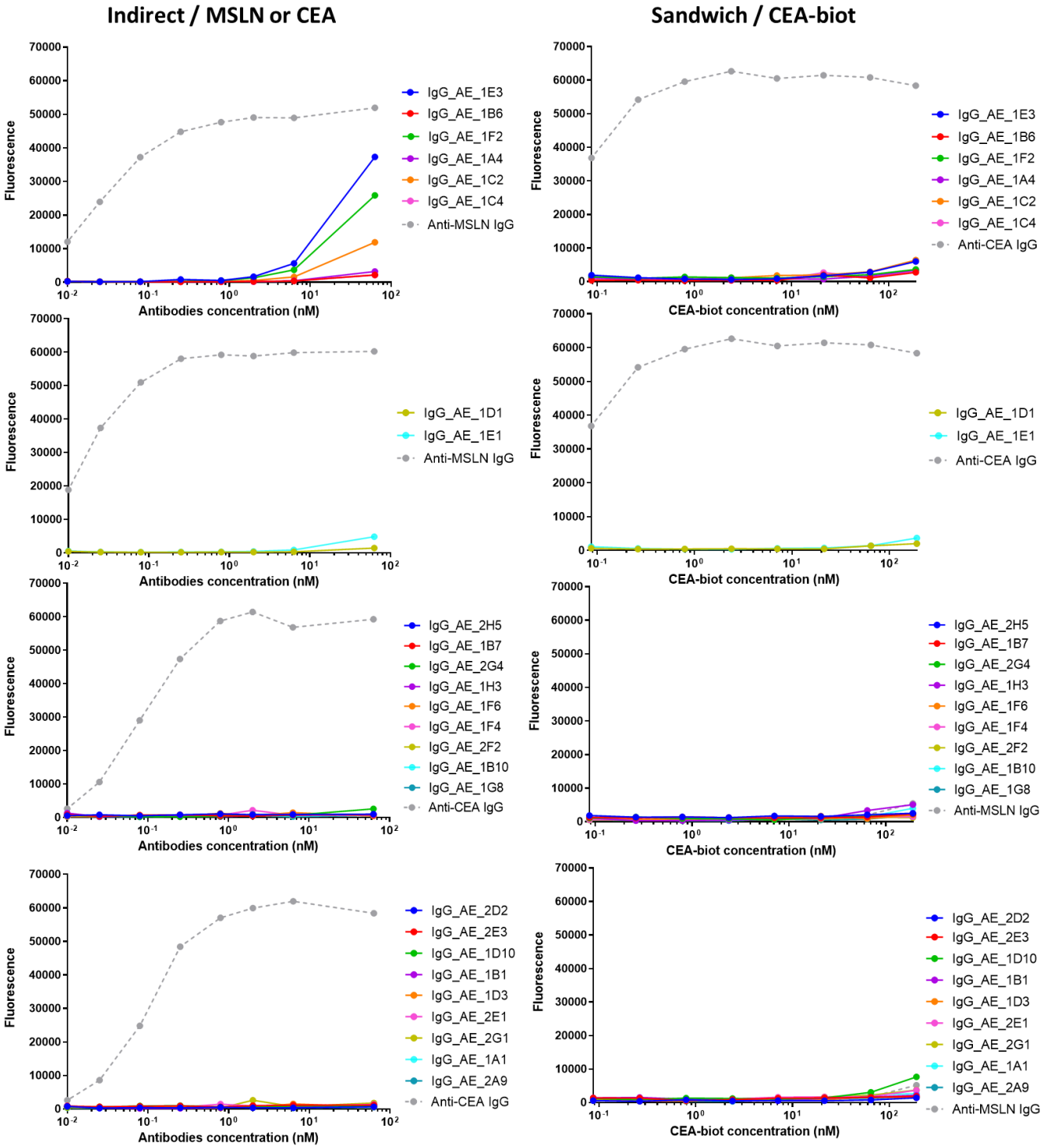

Supplementary Figure S8: Characterization of group B anti-eNAMPT antibody binding by ELISA. The binding of group B antibodies to NAMPT was analyzed by indirect ELISA with a commercial NAMPT protein or by sandwich ELISA with in house NAMPT-biot protein. Maxisorp plates were used for both ELISA assays.

GROUP B

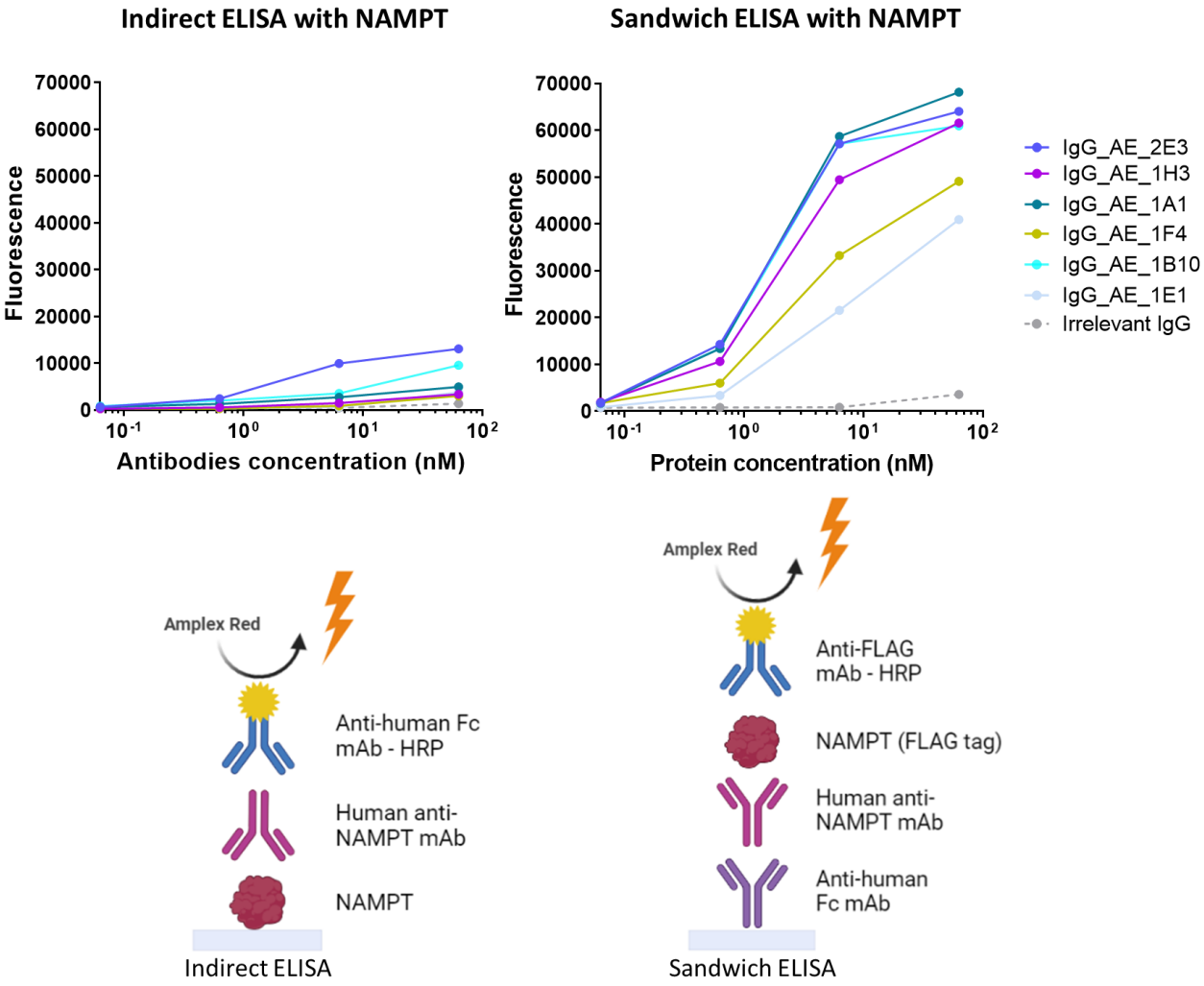

Supplementary Figure S9: Binding of selected group B anti-eNAMPT antibodies. The binding of selected group B antibodies to commercial NAMPT protein was compared in indirect ELISA and sandwich ELISA. Maxisorp plates were used for both ELISA assays.

GROUP C

Indirect / NAMPT

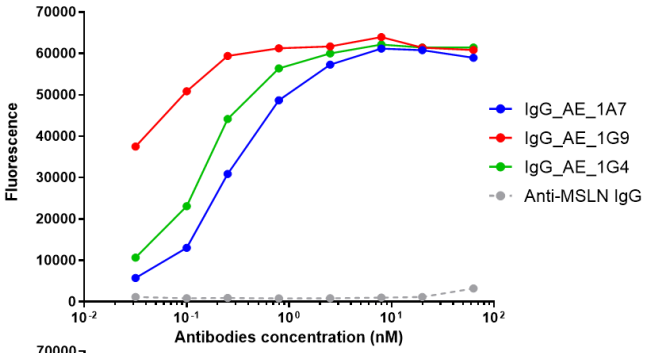

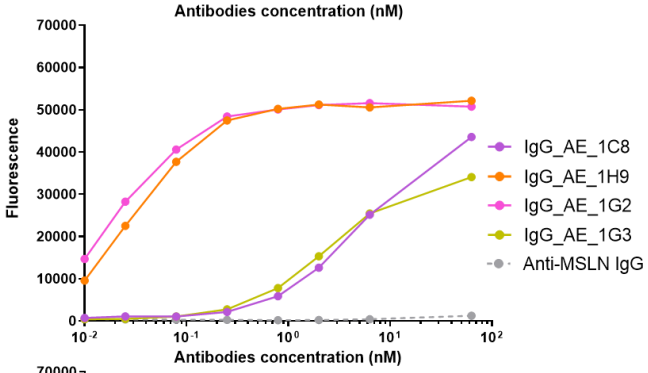

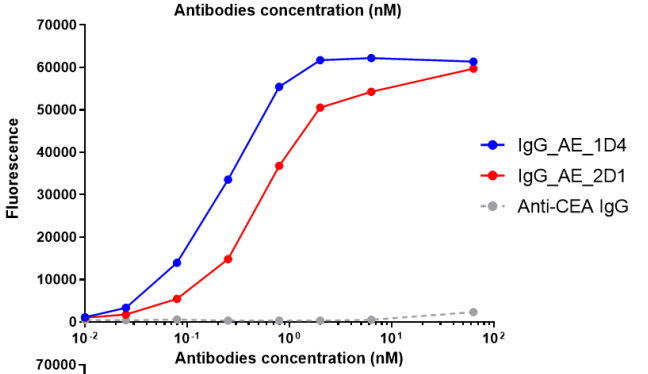

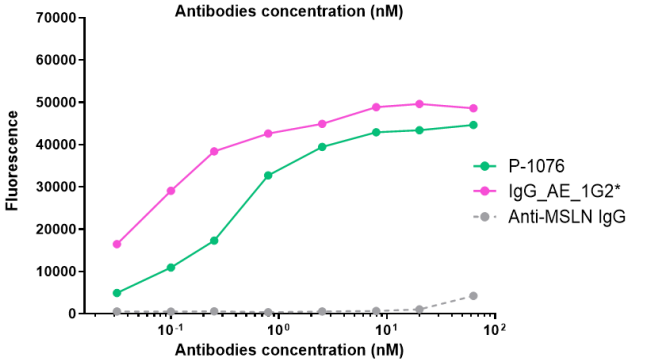

Sandwich / NAMPT-biot

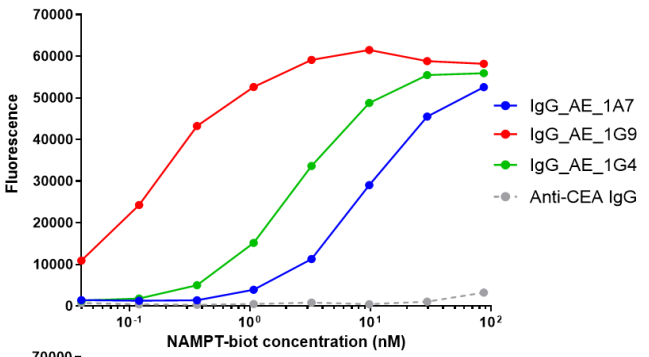

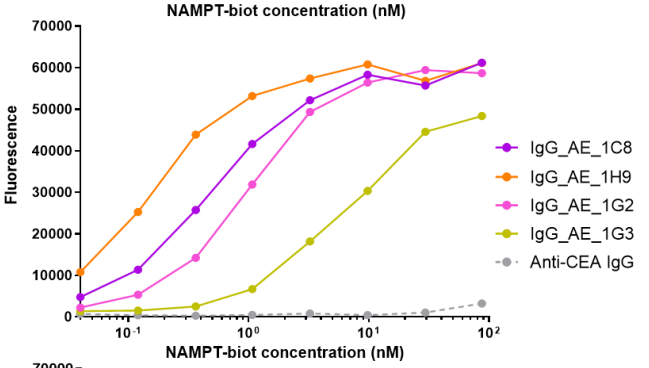

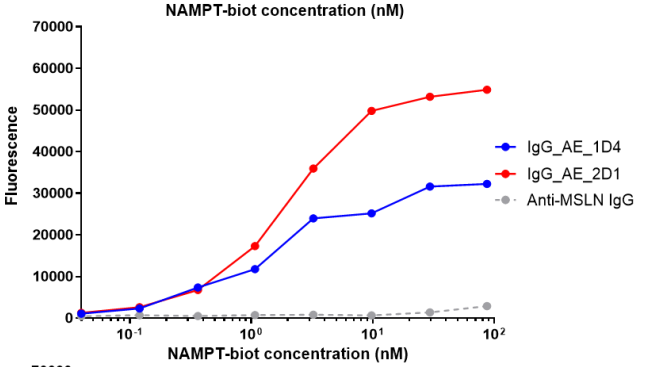

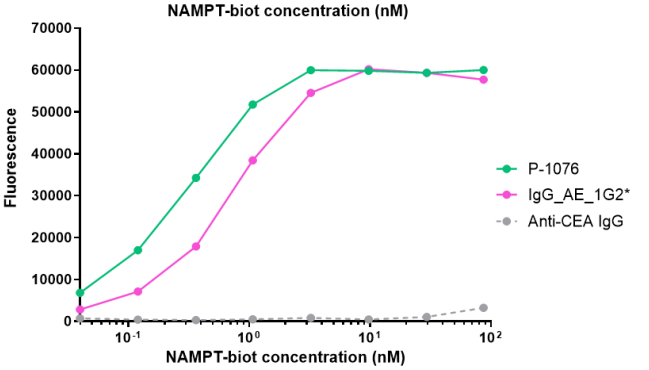

GROUP C

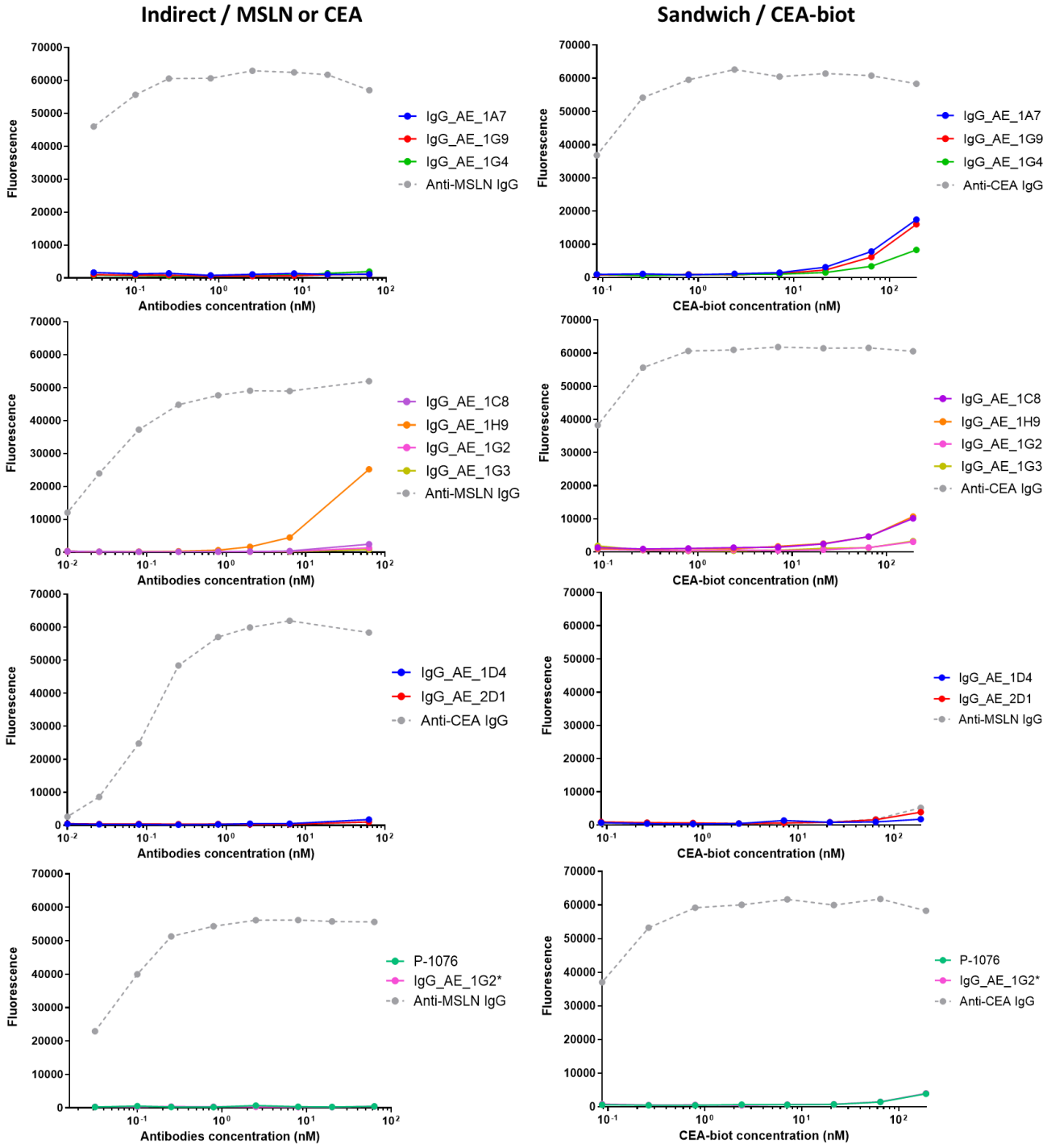

Supplementary Figure S10: Characterization of group C anti-eNAMPT antibody binding by ELISA. The binding of group C antibodies to NAMPT was analyzed by indirect ELISA with a commercial NAMPT protein or by sandwich ELISA with in house NAMPT-biot protein. Maxisorp plates were used for both ELISA assays. IgG_AE_1G2 was tested a second time (*) for comparison with P-1076 benchmark.

Table S1 : EC50s of anti-eNAMPT antibodies. Antibodies were tested in dose response binding experiments with both ELISA configurations. Of the 54 IgGs tested, four were not specific to NAMPT and therefore not included in the present table. The EC50s were calculated from binding curves of Figs. S6, 8 and 10 using a nonlinear regression on GraphPad (equation: log(agonist) vs. response -- variable slope). Legend: - , no binding (fluorescence signal below 10 000); R, residual binding (even at the highest concentrations the binding is weak).

IgG Name	Indirect ELISA		Sandwich ELISA	
	NAMPT (EC50 in nM)	Irrelevant protein	NAMPT-biot (EC50 in nM)	Irrelevant protein-biot
Profile A – Indirect ELISA				
IgG_AE_1G1	0.08	-	R	R
IgG_AE_1G5	0.05	-	R	-
IgG_AE_1G6	0.06	-	R	-
IgG_AE_1H7	0.5	-	R	-
IgG_AE_1C9	0.08	-	R	-
IgG_AE_1A11	0.06	-	R	-
IgG_AE_1A10	0.4	-	-	-
IgG_AE_1A2	0.04	-	R	R
IgG_AE_1A9	0.03	-	R	-
IgG_AE_1D8	0.02	-	R	-
IgG_AE_1D6	0.4	-	-	-
IgG_AE_1E7	0.2	-	-	-
IgG_AE_1D2	0.04	-	R	-
IgG_AE_1A6	0.3	-	R	-
IgG_AE_1F7	2	-	R	-
Profile B – Sandwich ELISA				
IgG_AE_1E3	-	R	1	-
IgG_AE_1B6	-	-	8	-
IgG_AE_1F2	-	R	0.5	-
IgG_AE_1A4	-	-	0.3	-
IgG_AE_1C2	R	R	0.2	-
IgG_AE_1C4	-	-	3	-
IgG_AE_1D1	-	-	3	-
IgG_AE_1E1	-	-	0.3	-
IgG_AE_2H5	-	-	4	-
IgG_AE_1B7	-	-	1.7	-
IgG_AE_2G4	R	-	0.5	-
IgG_AE_1H3	-	-	0.6	-

IgG_AE_1F6	-	-	1.4	-
IgG_AE_1F4	-	-	1	-
IgG_AE_2F2	-	-	0.8	-
IgG_AE_1B10	R	-	0.5	-
IgG_AE_1G8	R	-	0.7	-
IgG_AE_2D2	R	-	0.9	-
IgG_AE_2E3	-	-	0.5	-
IgG_AE_1D10	R	-	0.6	-
IgG_AE_1B1	R	-	0.8	-
IgG_AE_1D3	R	-	1	-
IgG_AE_2E1	R	-	0.5	-
IgG_AE_2G1	R	-	0.5	-
IgG_AE_1A1	-	-	0.6	-
IgG_AE_2A9	R	-	2.2	-
Profile C – Indirect and sandwich ELISA				
IgG_AE_1A7	0.3	-	9	R
IgG_AE_1G4	0.2	-	3	-
IgG_AE_1G9	0.08	-	0.2	R
IgG_AE_1C8	6	-	0.5	R
IgG_AE_1H9	0.03	R	0.2	R
IgG_AE_1G2	0.02/0.01*	-	0.98/0.7*	-
IgG_AE_1G3	3	-	7	-
IgG_AE_1D4	0.2	-	5	-
IgG_AE_2D1	0.6	-	2	-
P-1076	0.4	-	0.3	-

NAMPT

MSLN

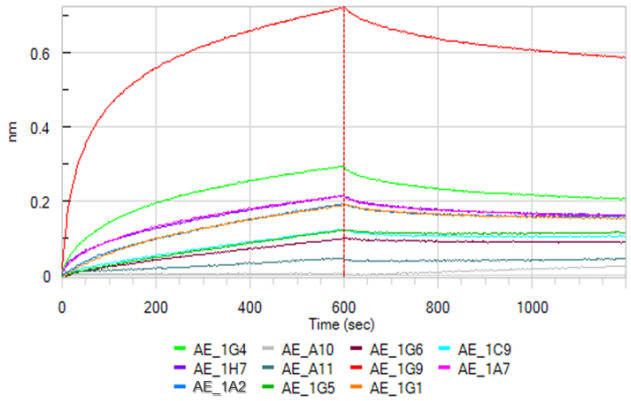
nm
Time (sec)
AE_1G4
AE_A10
AE_1G6
AE_1C9
AE_1H7
AE_A11
AE_1G9
AE_1A7
AE_1A2
AE_1G5
AE_1G1

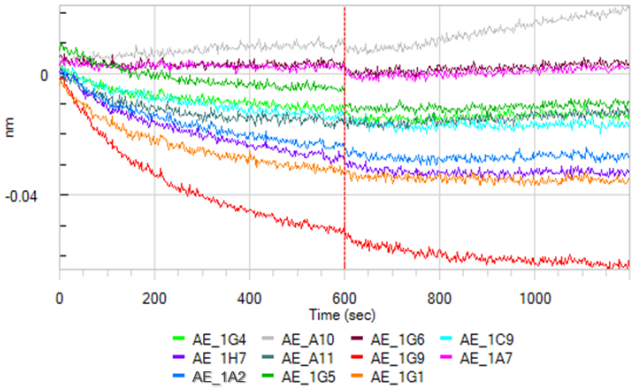
nm
Time (sec)
AE_1G4
AE_A10
AE_1G6
AE_1C9
AE_1H7
AE_A11
AE_1G9
AE_1A7
AE_1A2
AE_1G5
AE_1G1

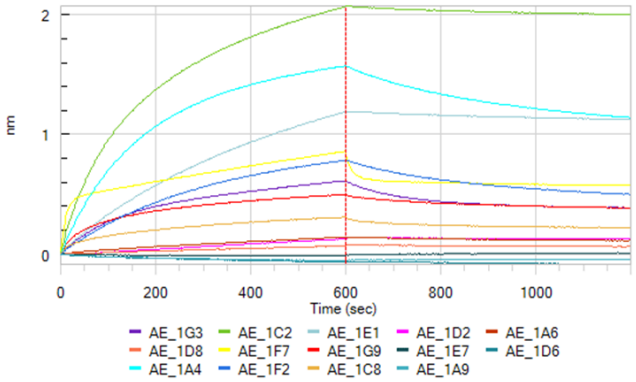
nm
Time (sec)
AE_1G3
AE_1C2
AE_1E1
AE_1D2
AE_1A6
AE_1D8
AE_1F7
AE_1G9
AE_1E7
AE_1D6
AE_1A4
AE_1F2
AE_1C8
AE_1A9

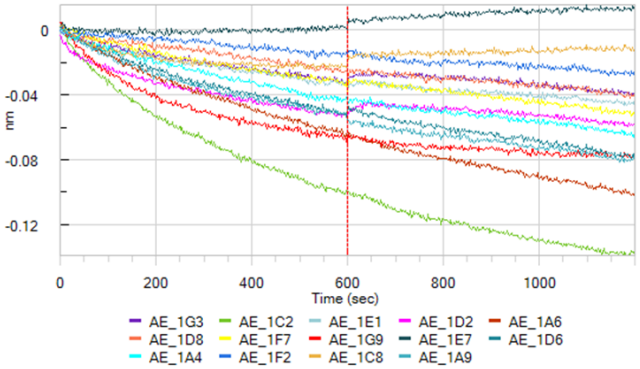
nm
Time (sec)
AE_1G3
AE_1C2
AE_1E1
AE_1D2
AE_1A6
AE_1D8
AE_1F7
AE_1G9
AE_1E7
AE_1D6
AE_1A4
AE_1F2
AE_1C8
AE_1A9

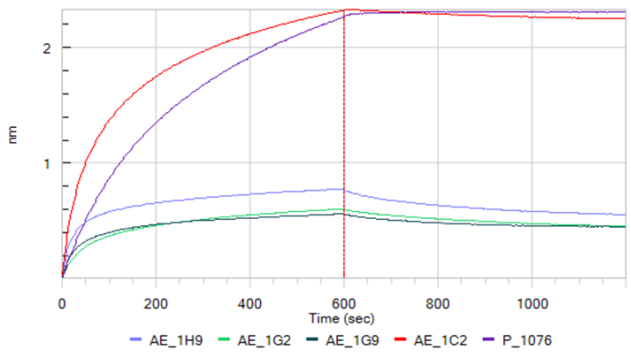
nm
Time (sec)
AE_1H9
AE_1G2
AE_1G9
AE_1C2
P_1076

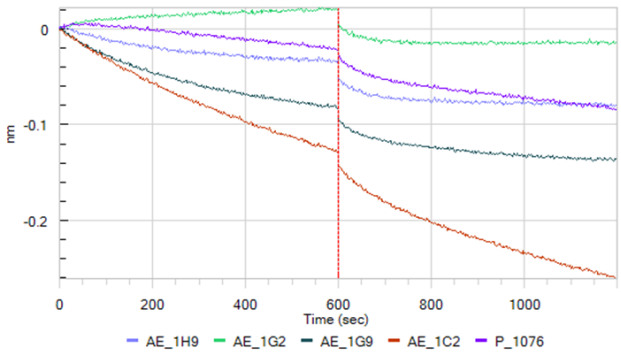
nm
Time (sec)
AE_1H9
AE_1G2
AE_1G9
AE_1C2
P_1076

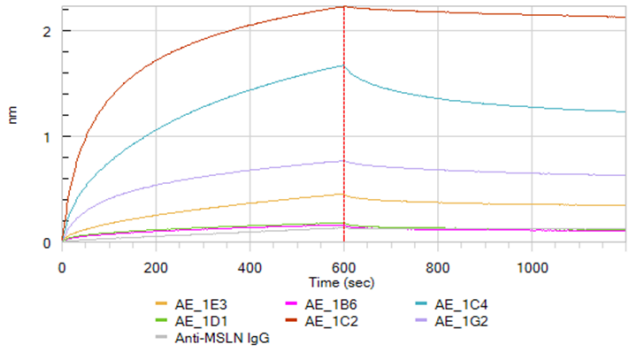
nm
Time (sec)
AE_1E3
AE_1B6
AE_1C4
AE_1D1
AE_1C2
AE_1G2
Anti-MSLN IgG

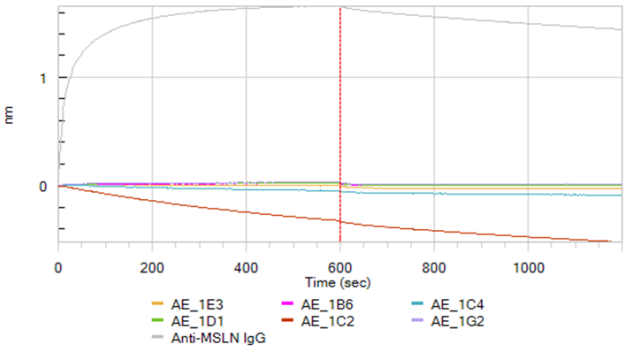
nm
Time (sec)
AE_1E3
AE_1B6
AE_1C4
AE_1D1
AE_1C2
AE_1G2
Anti-MSLN IgG

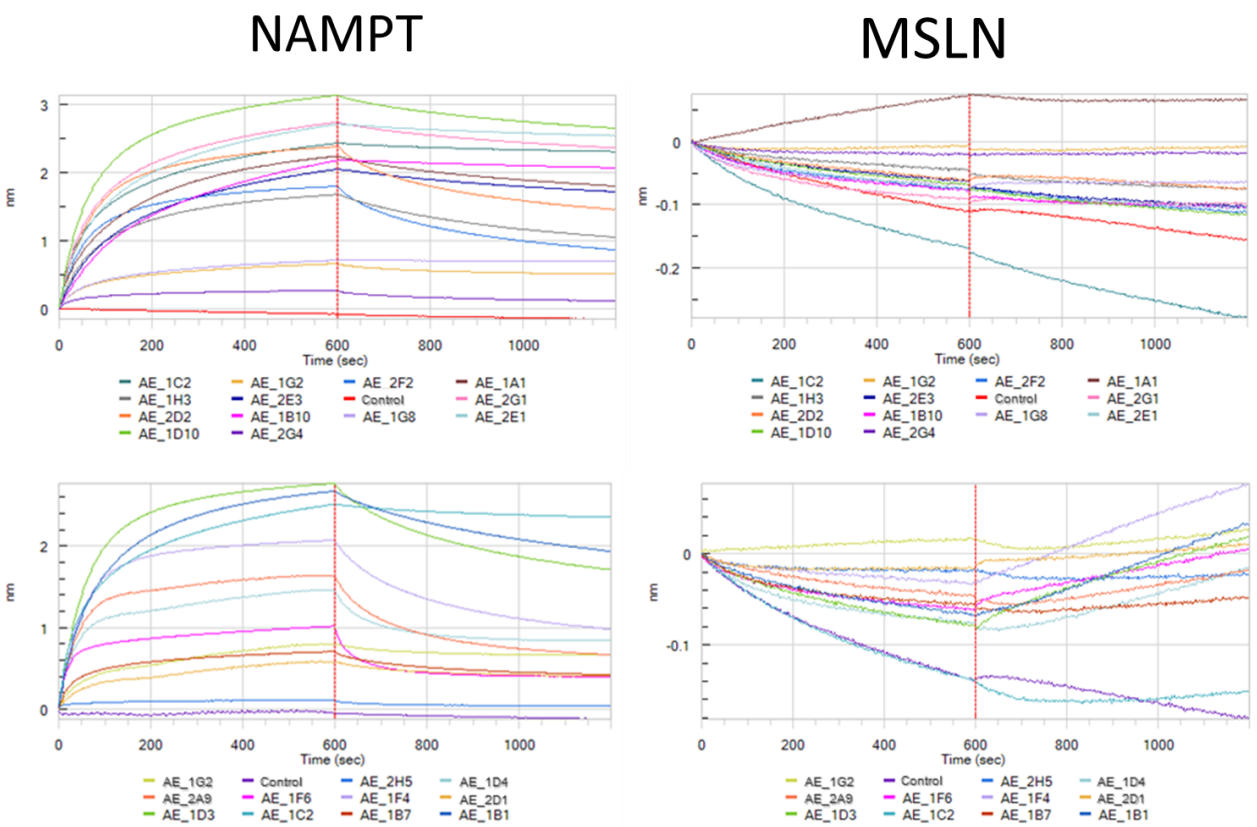

Supplementary Figure S11: Characterization of anti-eNAMPT mAbs by bio-layer interferometry analysis. Association and dissociation of NAMPT protein (150nM) to anti-eNAMPT mAbs were evaluated using Octet instrument (ForteBio). All antibodies, except those previously eliminated with ELISA analysis, were tested once.

- **Epitope binning on NAMPT**

A)

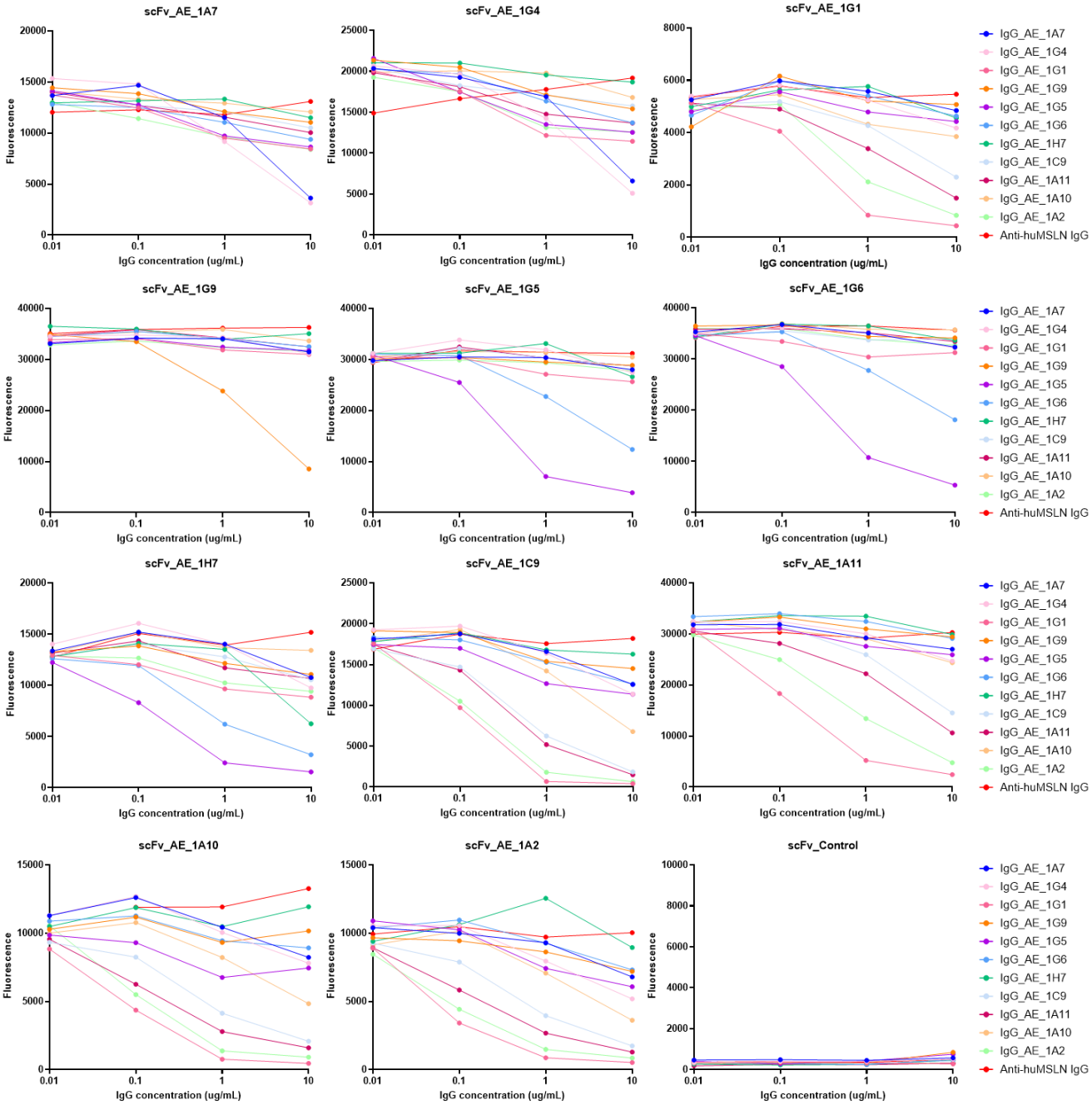

- **Epitope binning on NAMPT**

B)

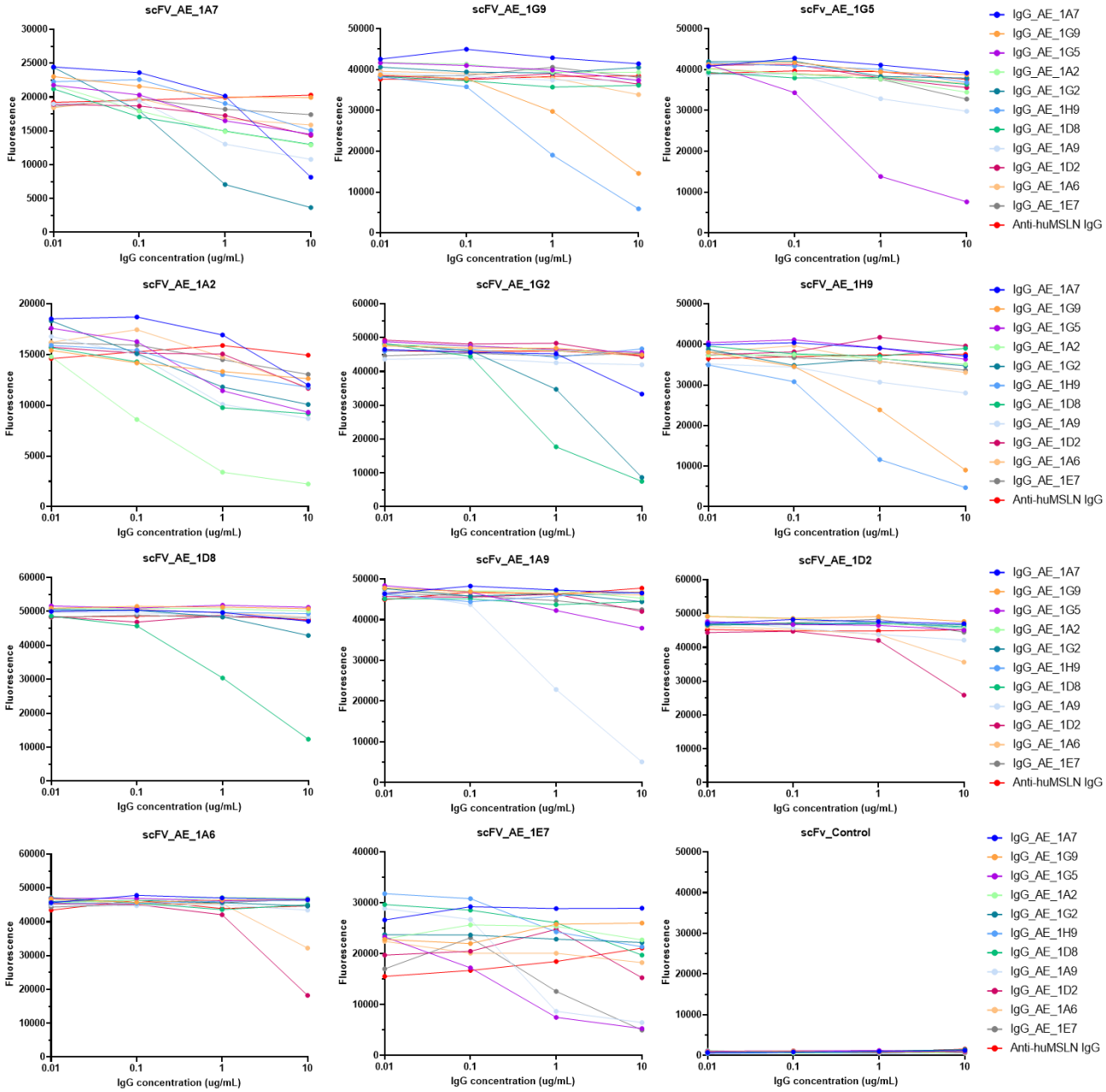

- **Epitope binning on NAMPT**

C)

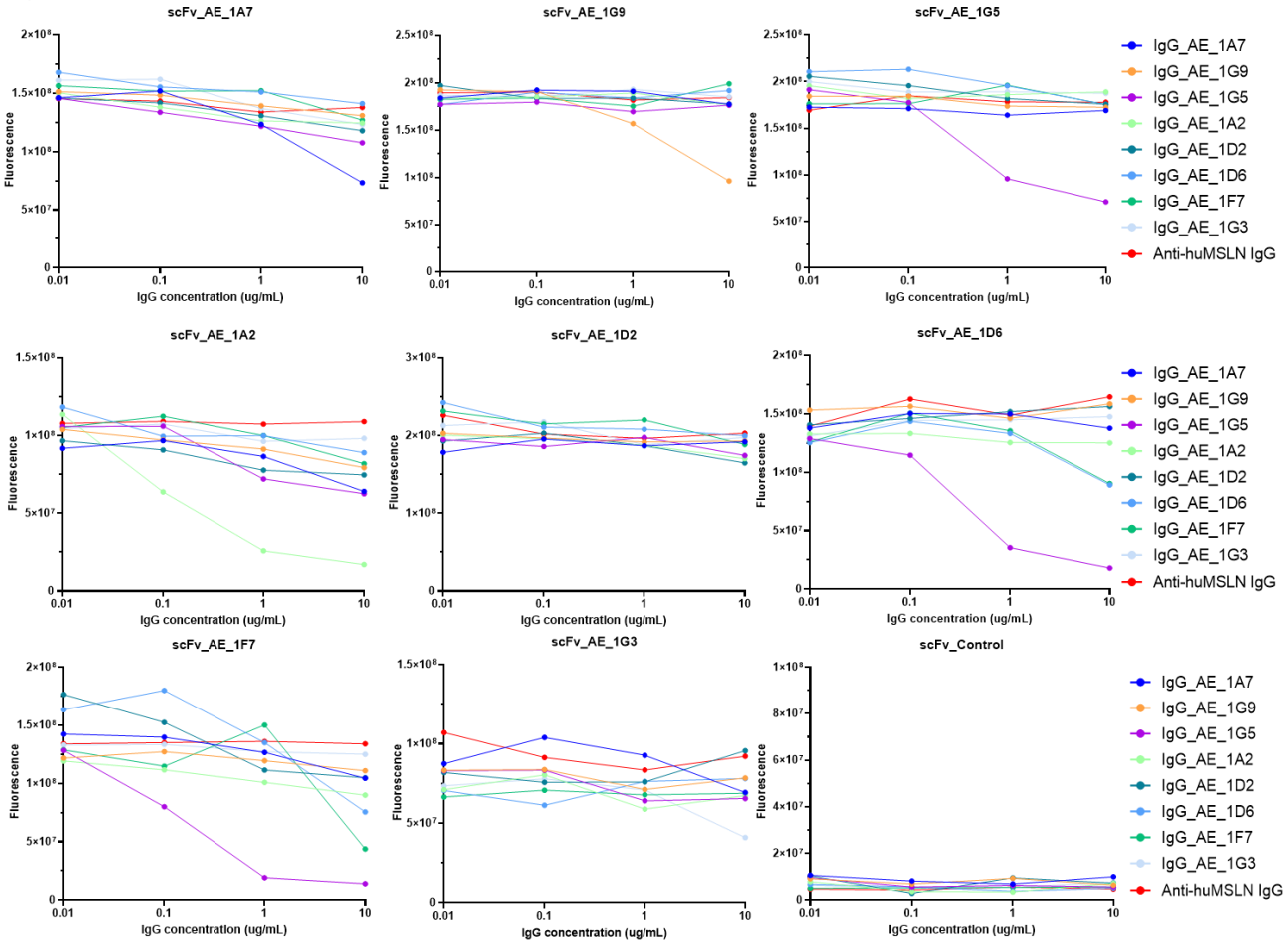

Supplementary Figure S12: Sorting of the anti-eNAMPT antibodies into epitope bin using scFv VS IgG competitive ELISAs. (A-C) Maxisorp plates were coated with commercial NAMPT protein and incubated with increasing concentrations of anti-eNAMPT mAbs (0.01 to 10µg/mL) and a neat periplasmic preparation of scFv. C-myc-tagged scFvs were then detected with a mouse anti-c-myc tag antibody and an anti-mouse IgG Fcγ-HRP antibody. Three individual experiments are presented in **(A)**, **(B)** and **(C)**.

- **Epitope binning on NAMPT-biot**

A)

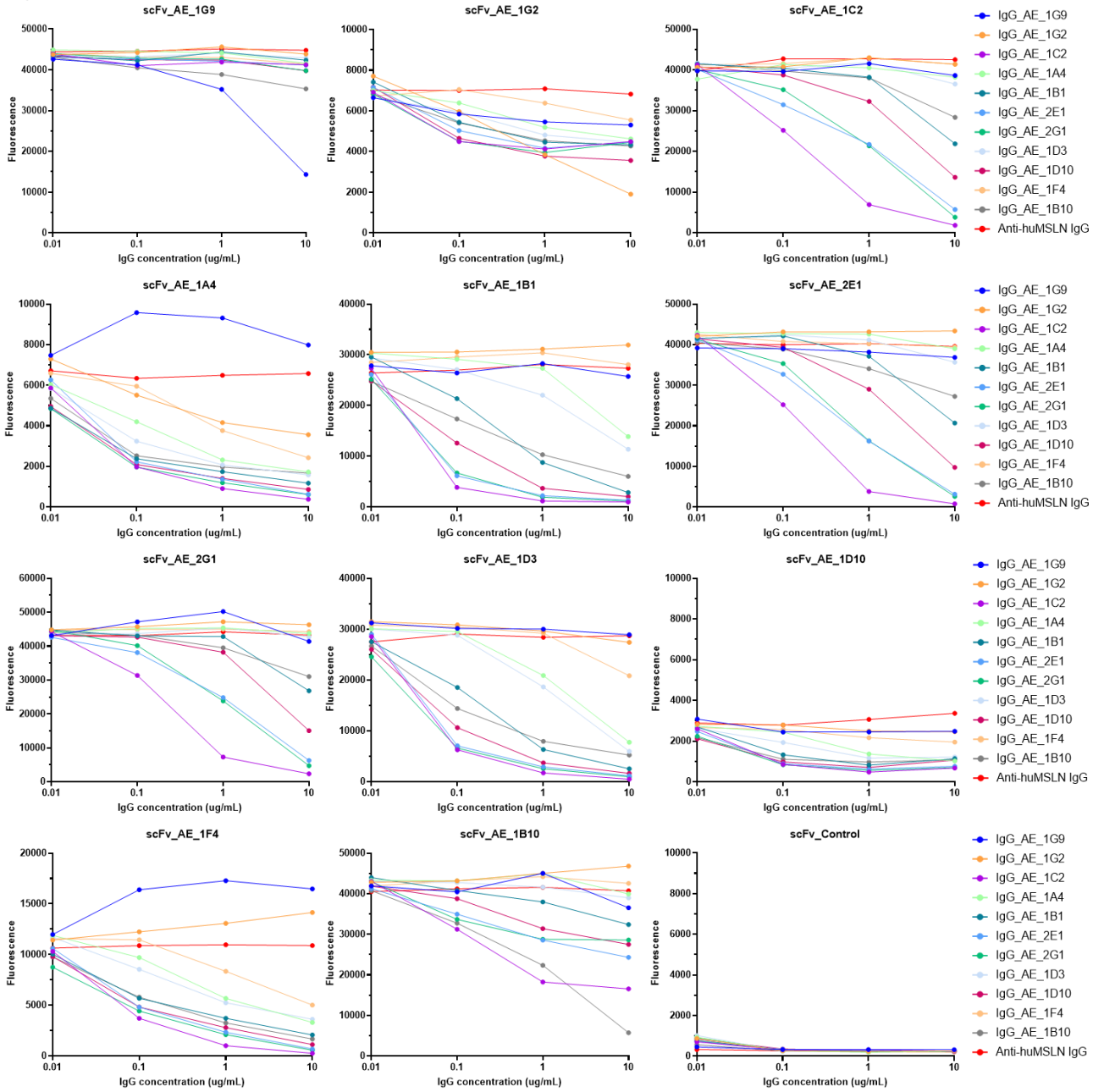

- **Epitope binning on NAMPT-biot**

B)

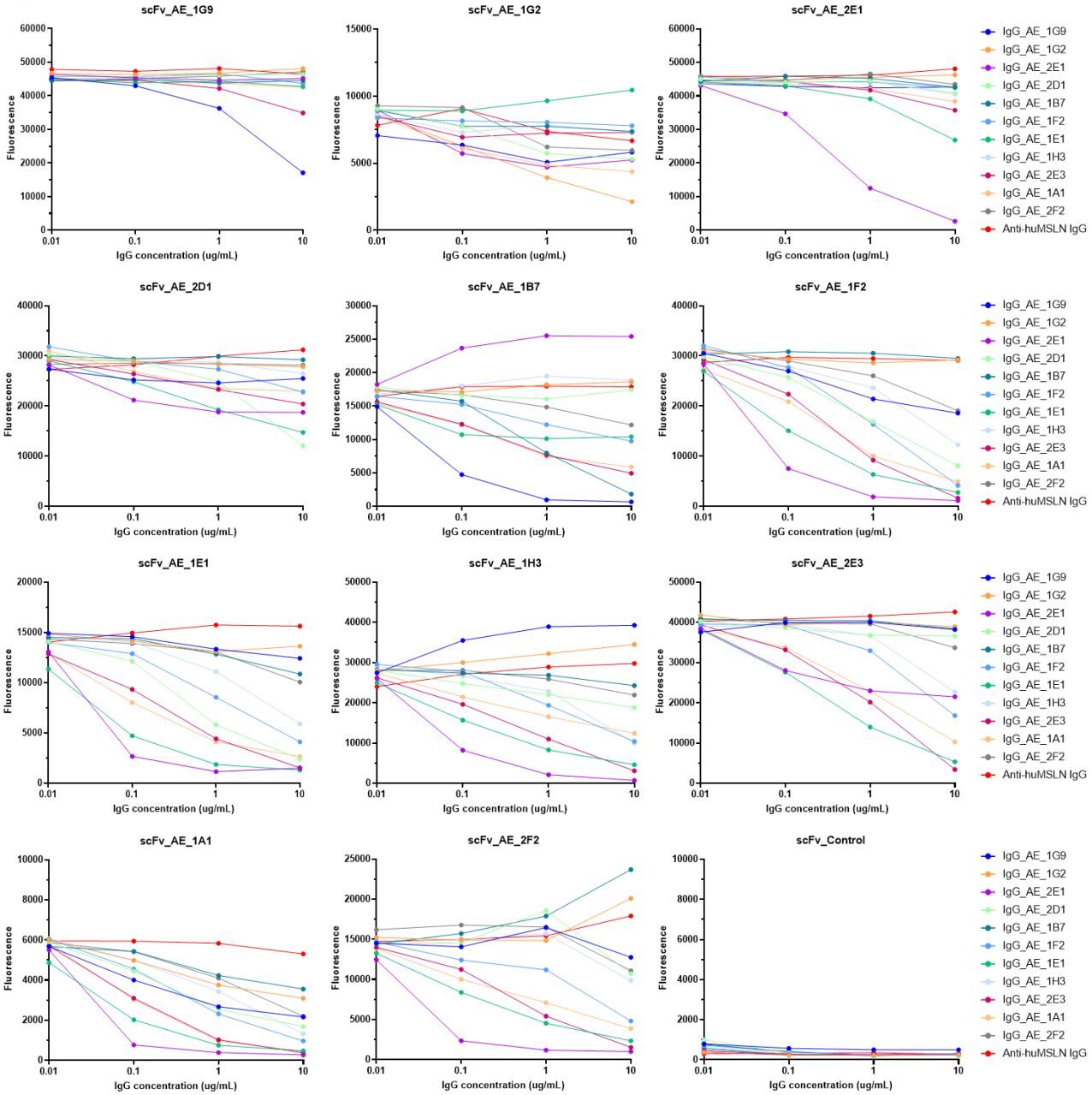

Supplementary Figure S13: Sorting of the anti-eNAMPT antibodies into epitope bin using scFv VS IgG competitive ELISAs. **(A-B)** Streptawell plates were coated with in house NAMPT-biot protein and incubated with increasing concentrations of anti-eNAMPT mAbs (0.01 to 10µg/mL) and a neat periplasmic preparation of scFv. C-myc-tagged scFvs were then detected with a mouse anti-c-myc tag antibody and an anti-mouse IgG Fcγ-HRP antibody. Two individual experiments are presented in **(A)** and **(B)**.

- **Epitope binning on NAMPT (Maxisorp plate)**

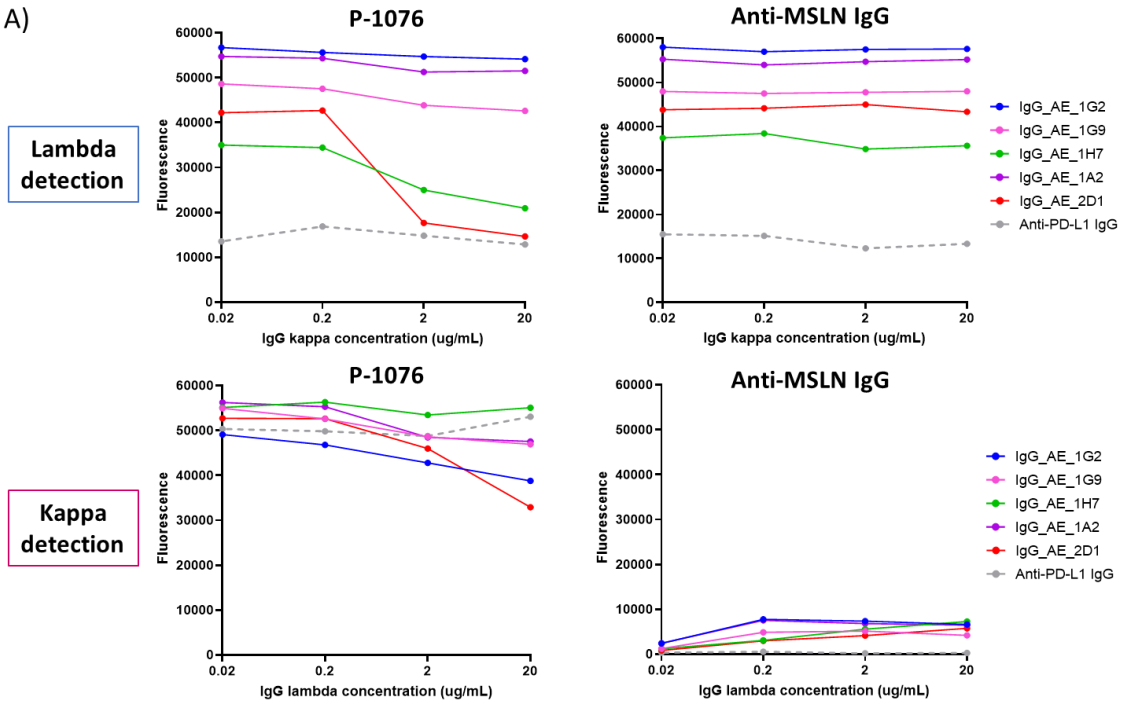

- **Epitope binning on NAMPT-biot (Streptawell plate)**

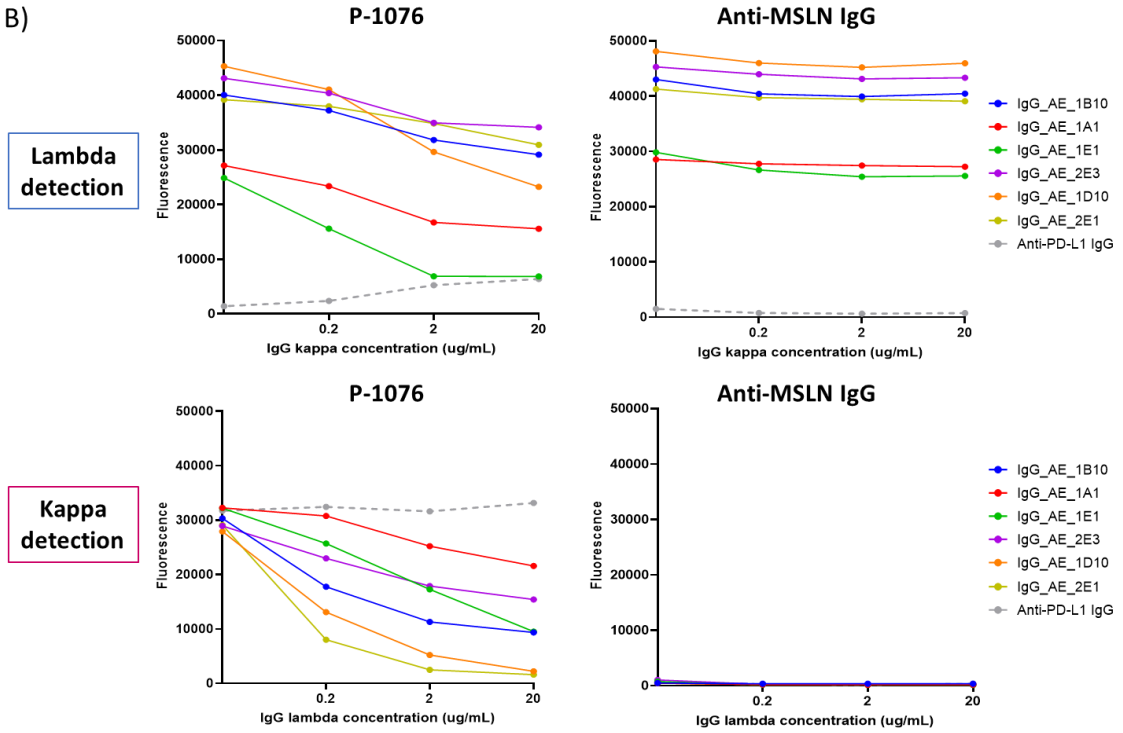

Supplementary Figure S14: P-1076 benchmark epitope bin determination using IgG kappa VS IgG lambda competitive ELISAs. (A-B) NAMPT-coated maxisorp plates **(A)** or NAMPT-biot-coated streptawell plates **(B)** were incubated with increasing concentrations of anti-eNAMPT mAbs (lambda, competitor A) and 0.1µg/mL of P-1076 (kappa, competitor B) in one configuration and with increasing concentrations of P-1076 (kappa, competitor A) and 0.1µg/mL of anti-eNAMPT mAbs (lambda, competitor B) in the reverse configuration. Competitor B antibodies were then detected with an anti-human λ light chain or anti-human κ light chain antibody coupled to HRP according to their isotype.

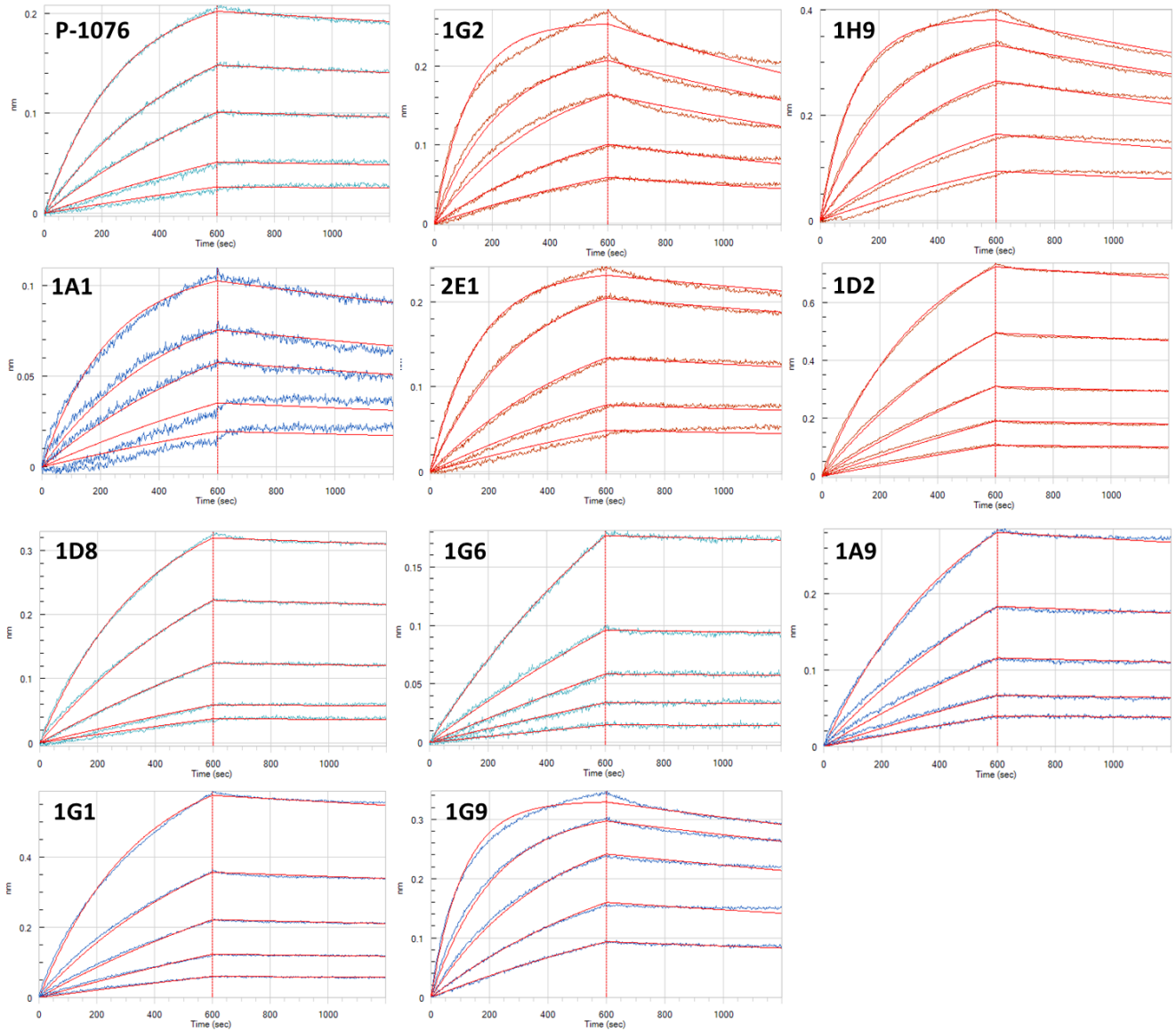

IgG	P-1076	IgG_AE_ 1G2	IgG_AE_ 1G9	IgG_AE_ 1H9	IgG_AE_ 1A1	IgG_AE_ 2E1	IgG_AE_ 1D2	IgG_AE_ 1D8	IgG_AE_ 1G6	IgG_AE_ 1A9	IgG_AE_ 1G1
KD (nM)	0.8±0.43	2.7±0.28	0.7±0.14	1.0±0.20	2.6±0.09	0.5±0.05	19.1±0.95	9.3±2.34	7.9±2.3	24.7±0.2	4.4±0.04

Supplementary Figure S15: Characterization of anti-eNAMPT mAbs by bio-layer interferometry analysis. Affinity was measured using bio-layer interferometry (Octet, Forte Bio) and is shown as the KD ± SD. Results are representative of two independent experiments.

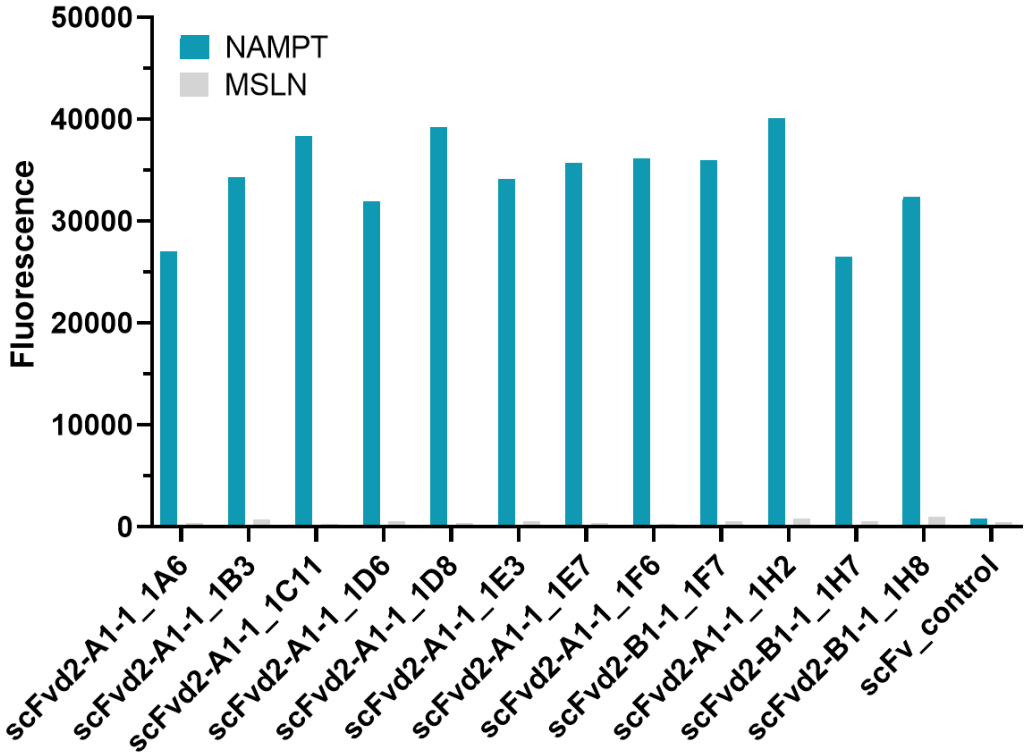

Supplementary Figure S16: Example of LO screening results. scFvs binding to commercial NAMPT protein or MSLN protein was measured by ELISA analysis.

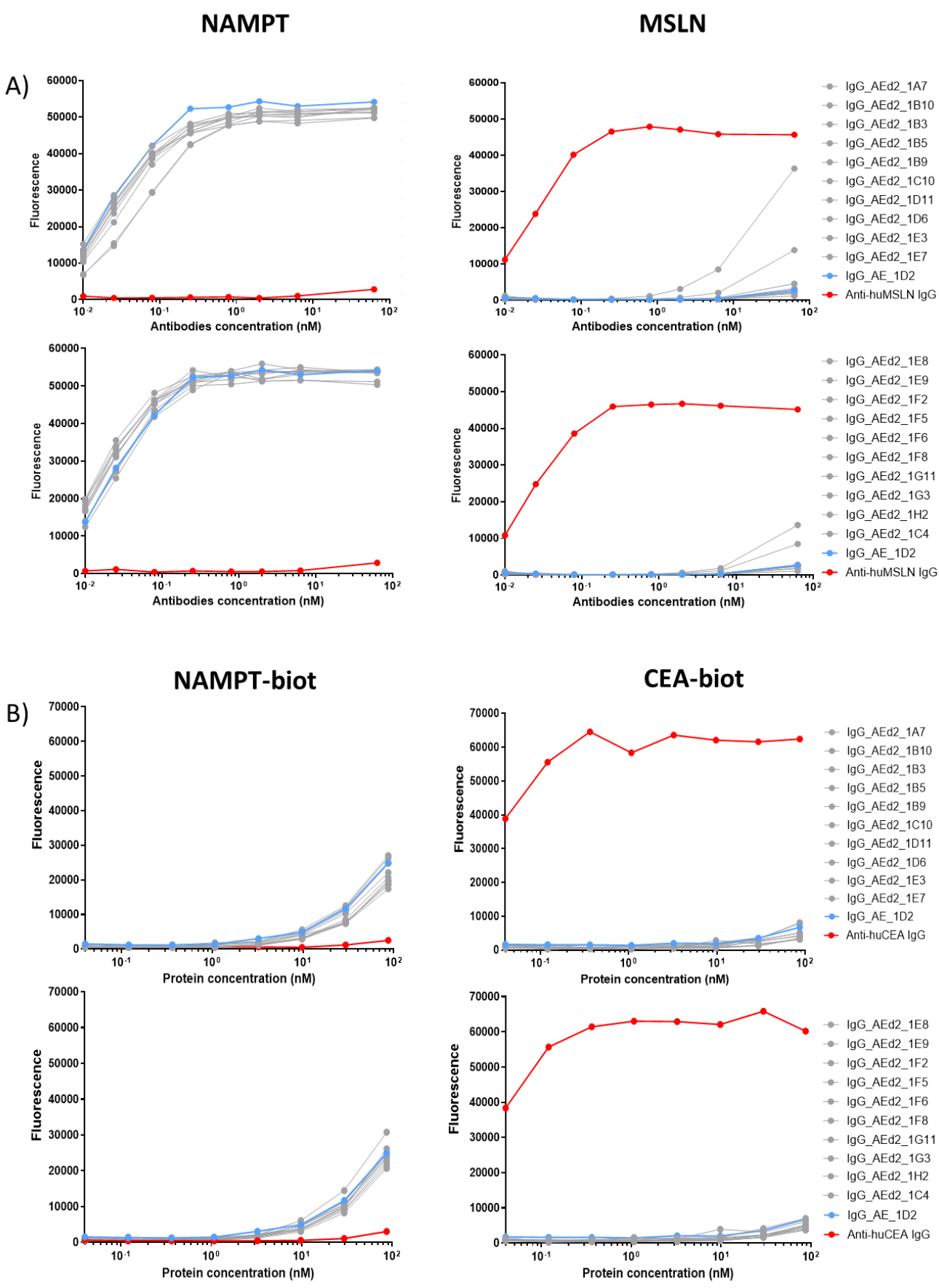
NAMPT
MSLN
A)
Fluorescence
Antibodies concentration (nM)
IgG_AEd2_1A7
IgG_AEd2_1B10
IgG_AEd2_1B3
IgG_AEd2_1B5
IgG_AEd2_1B9
IgG_AEd2_1C10
IgG_AEd2_1D11
IgG_AEd2_1D6
IgG_AEd2_1E3
IgG_AEd2_1E7
IgG_AE_1D2
Anti-huMSLN IgG
IgG_AEd2_1E8
IgG_AEd2_1E9
IgG_AEd2_1F2
IgG_AEd2_1F5
IgG_AEd2_1F6
IgG_AEd2_1F8
IgG_AEd2_1G11
IgG_AEd2_1G3
IgG_AEd2_1H2
IgG_AEd2_1C4
NAMPT-biot
CEA-biot
B)
Protein concentration (nM)
IgG_AEd2_1A7
IgG_AEd2_1B10
IgG_AEd2_1B3
IgG_AEd2_1B5
IgG_AEd2_1B9
IgG_AEd2_1C10
IgG_AEd2_1D11
IgG_AEd2_1D6
IgG_AEd2_1E3
IgG_AEd2_1E7
IgG_AE_1D2
Anti-huCEA IgG
IgG_AEd2_1E8
IgG_AEd2_1E9
IgG_AEd2_1F2
IgG_AEd2_1F5
IgG_AEd2_1F6
IgG_AEd2_1F8
IgG_AEd2_1G11
IgG_AEd2_1G3
IgG_AEd2_1H2
IgG_AEd2_1C4

C)

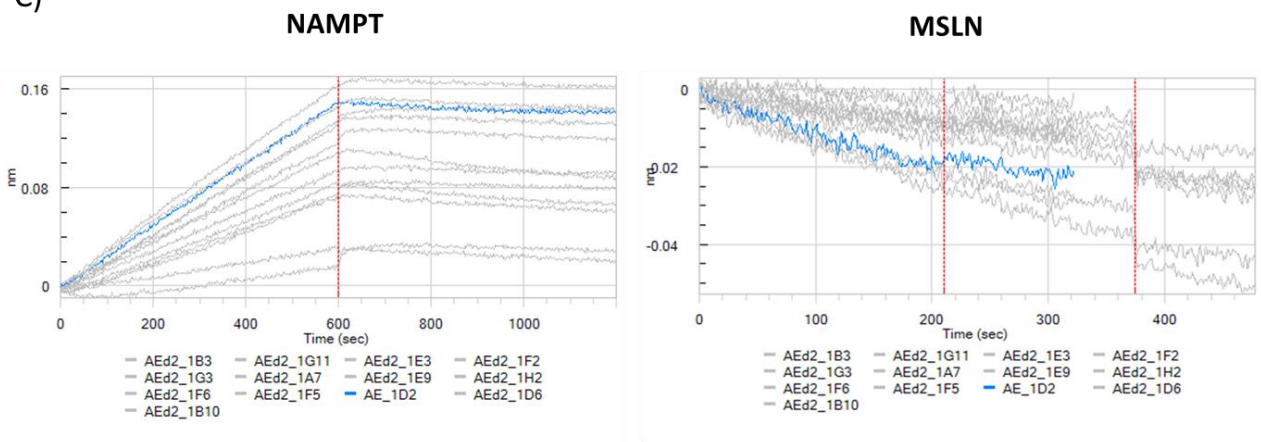

Supplementary Figure S17: Characterization of anti-eNAMPT antibodies issued from LO. (A-B) The binding of LO antibodies to NAMPT was analyzed by indirect ELISA with a commercial NAMPT protein **(A)** or by sandwich ELISA with in house NAMPT-biot protein **(B).** The LO antibodies were tested once with both ELISA configurations using maxisorp plates. **(C)** Association and dissociation of NAMPT protein (150nM) to anti-eNAMPT mAbs was evaluated using Octet instrument (ForteBio).

GROUP B

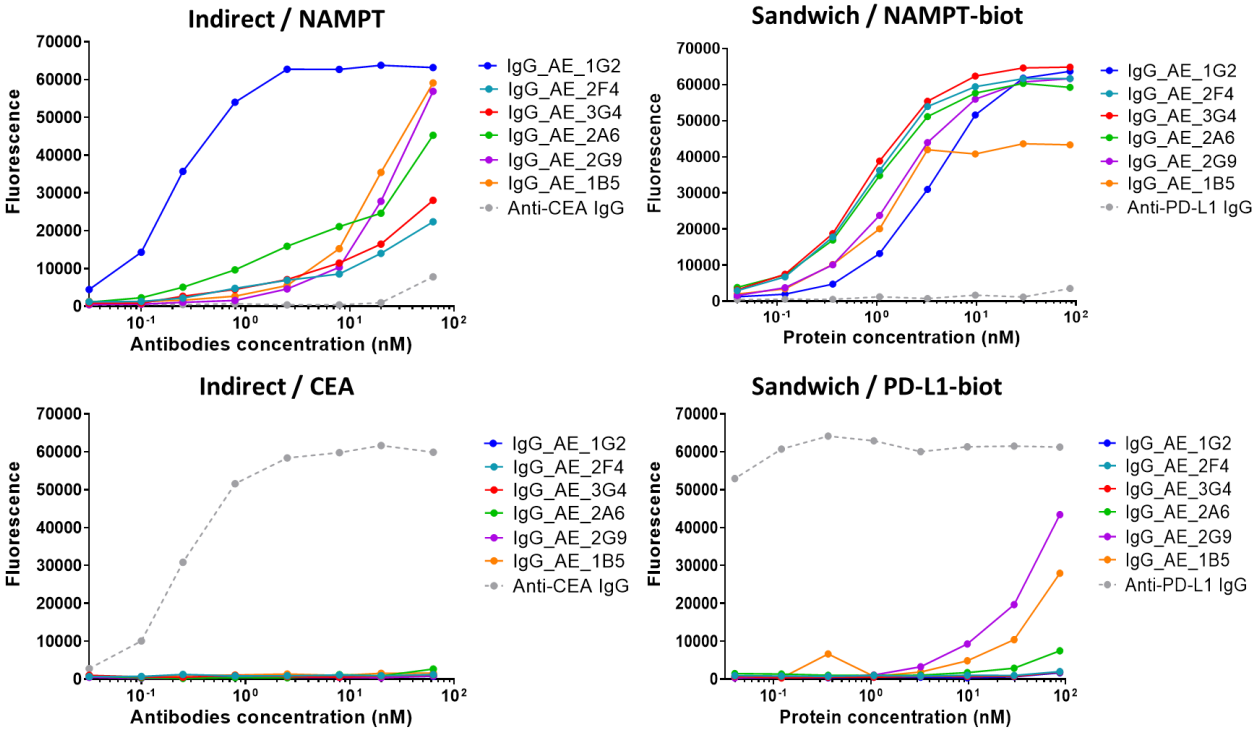

GROUP C

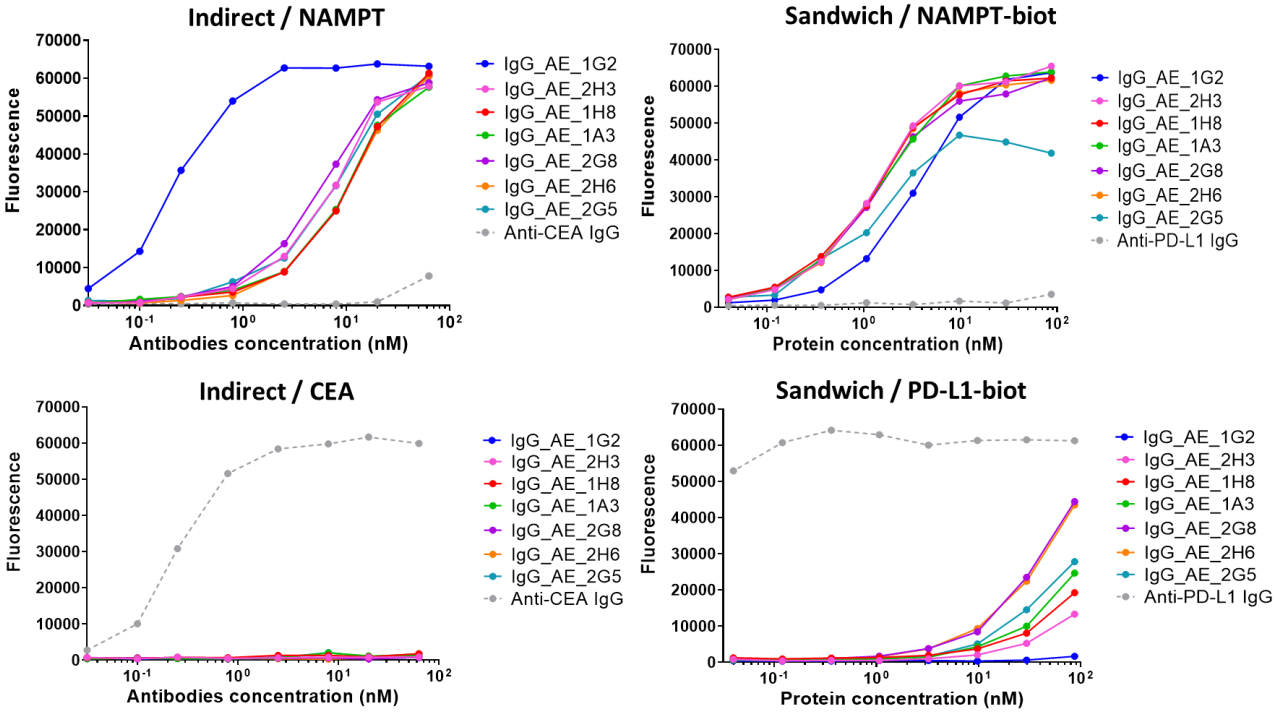

Supplementary Figure S18: Characterization of anti-eNAMPT antibodies issued from RO. The binding of RO antibodies to NAMPT was analyzed by indirect ELISA with a commercial NAMPT protein or by sandwich ELISA with in house NAMPT-biot protein. According to their binding characteristics, the mAbs were categorized into group B or C. A non-RO antibody, IgG_AE_1G2, was used as reference. Maxisorp plates were used for both ELISA assays.

Table S2: EC50s of anti-eNAMPT antibodies derived from RO. Antibodies were tested in dose response binding experiments once in both ELISA configurations. Of the 12 RO IgGs tested, one was not specific to NAMPT and therefore not included in the present table. The EC50s were calculated from binding curves on Fig. S18 using a nonlinear regression on GraphPad (equation: log(agonist) vs. response -- variable slope). Legend: - , no binding (fluorescence signal below 10 000); R, residual binding (even at the highest concentrations the binding is weak).

IgG Name	Indirect ELISA		Sandwich ELISA	
	NAMPT (EC50 in nM)	Irrelevant protein	NAMPT-biot (EC50 in nM)	Irrelevant protein-biot
Profile B - Sandwich				
IgG_AE_2F4	R	-	0.8	-
IgG_AE_3G4	R	-	0.8	-
IgG_AE_2A6	R	-	0.9	-
IgG_AE_2G9	R	-	1.6	R
IgG_AE_1B5	R		1.1	R
Profile C - Indirect and sandwich				
IgG_AE_2H3	7	-	1.3	R
IgG_AE_1H8	11	-	1.3	R
IgG_AE_1A3	10	-	1.4	R
IgG_AE_2G8	7	-	1.3	R
IgG_AE_2H6	11	-	1.3	R
IgG_AE_2G5	9	-	1.2	R

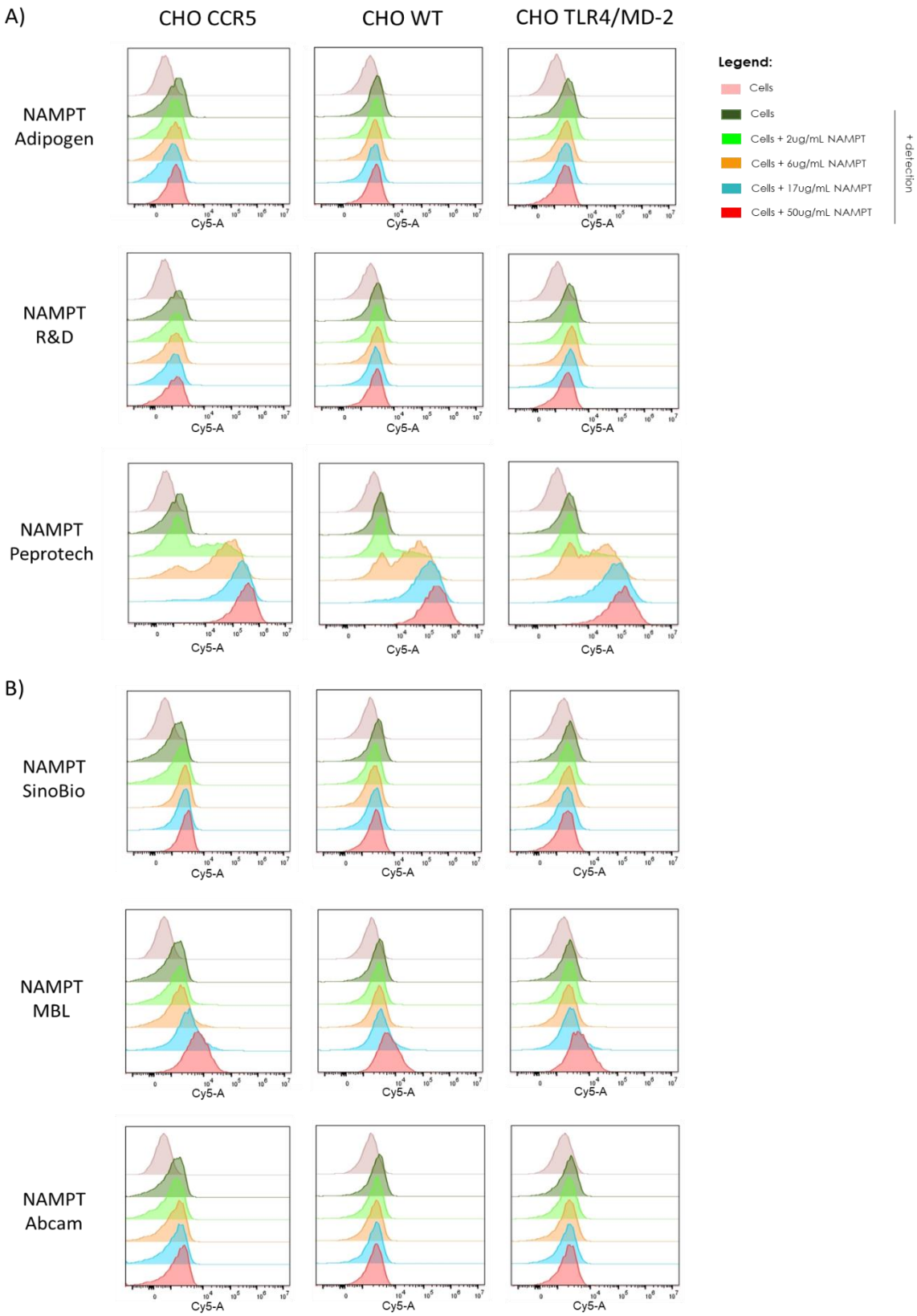

Supplementary Figure S19: eNAMPT binding to CHO-CCR5 and CHO-TLR4/MD-2 cells by flow cytometry. (A-B) Increasing concentrations of NAMPT proteins (2-50ug/mL) were incubated for two hours with CHO-CCR5 , CHO-TLR4/MD-2 or CHO-WT cells. NAMPT proteins were detected with a biotinylated anti-NAMPT antibody (R&D) and streptavidin coupled to cy5. Two individual experiments are presented in **(A)** and **(B)**. The histogram profiles obtained with 50ug/mL of NAMPT are presented in Fig. 19.

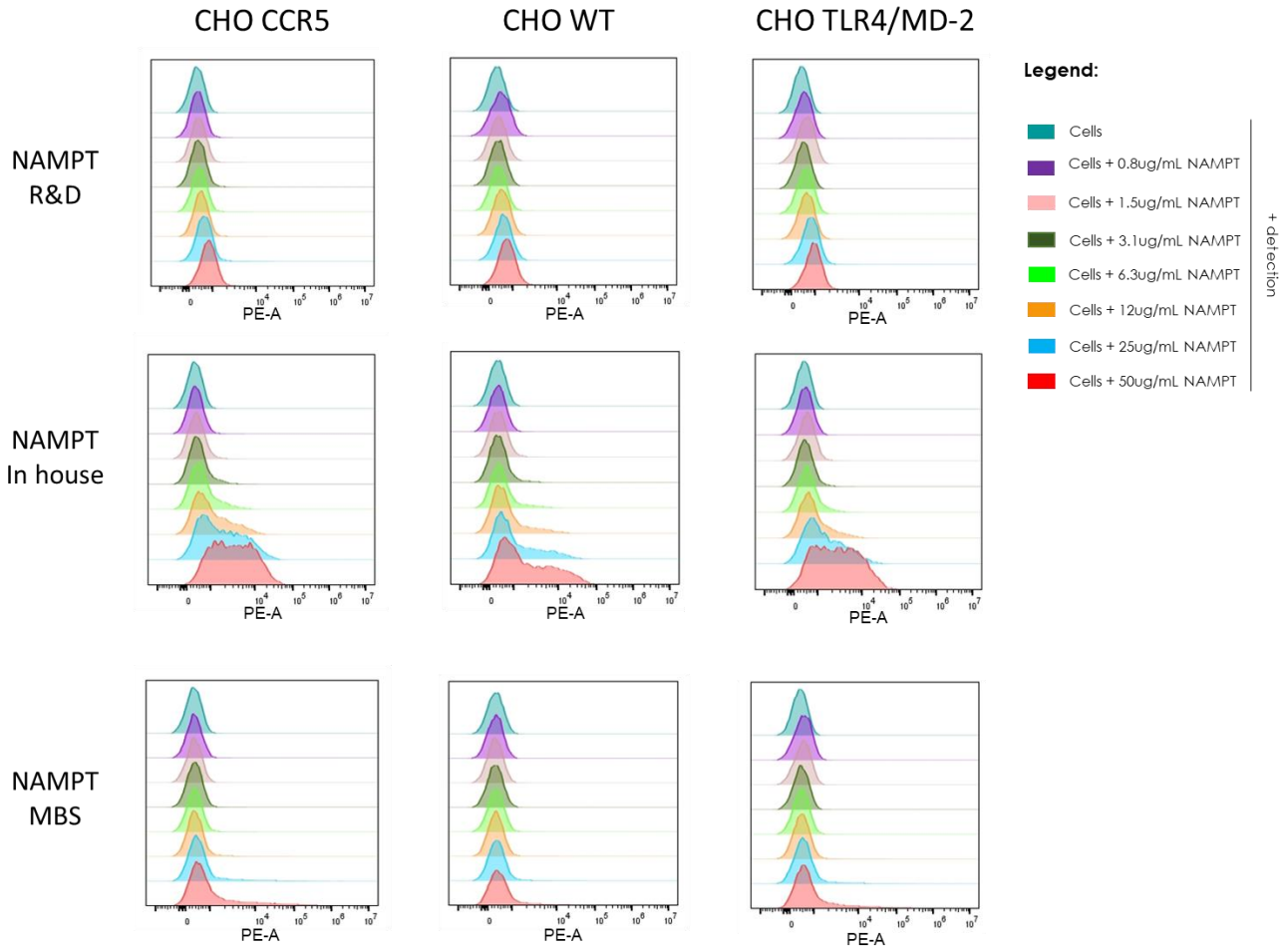

Supplementary Figure S20: eNAMPT binding to CHO-CCR5 and CHO-TLR4/MD-2 cells detected with Adipogen anti-NAMPT mAb by flow cytometry. Increasing concentrations of NAMPT proteins (0.8-50ug/mL) were incubated for two hours with CHO-CCR5, CHO-TLR4/MD-2 or CHO-WT cells. NAMPT proteins were then detected with a mouse anti-NAMPT mAb (Adipogen), in turn detected with an anti-mouse IgG antibody coupled to PE.

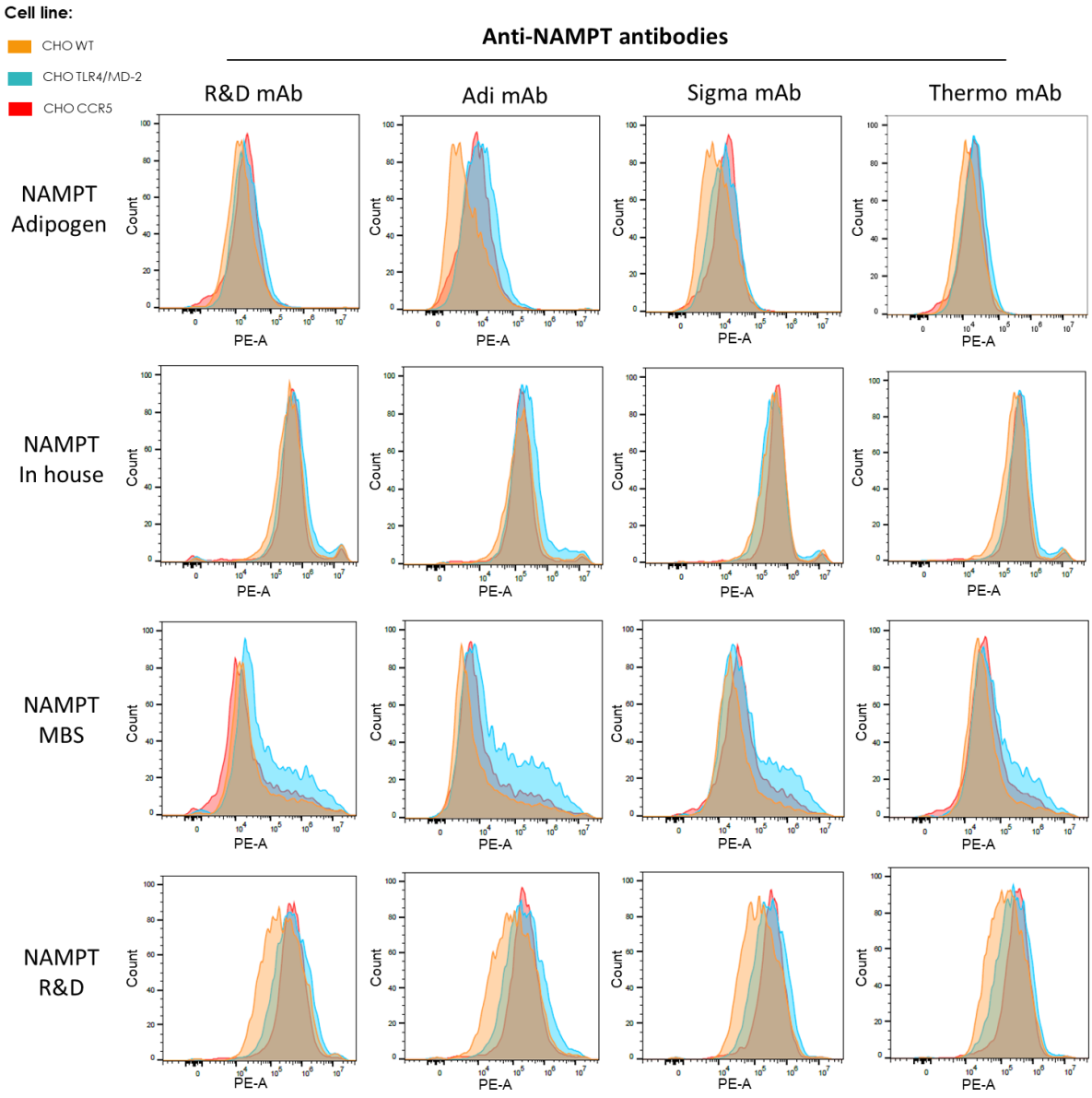

Supplementary Figure S21: eNAMPT binding to CHO-CCR5 and CHO-TLR4/MD-2 cells assessed with different detections by flow cytometry. NAMPT proteins (50ug/mL) were incubated for two hours with CHO-CCR5, CHO-TLR4/MD-2 or CHO-WT cells. NAMPT proteins were then detected with mouse or rat anti-NAMPT antibodies (R&D; Adi, Adipogen; Sigma; Thermo, ThermoFisher Scientific), in turn detected with anti-mouse IgG or anti-rat IgG antibodies coupled to PE.

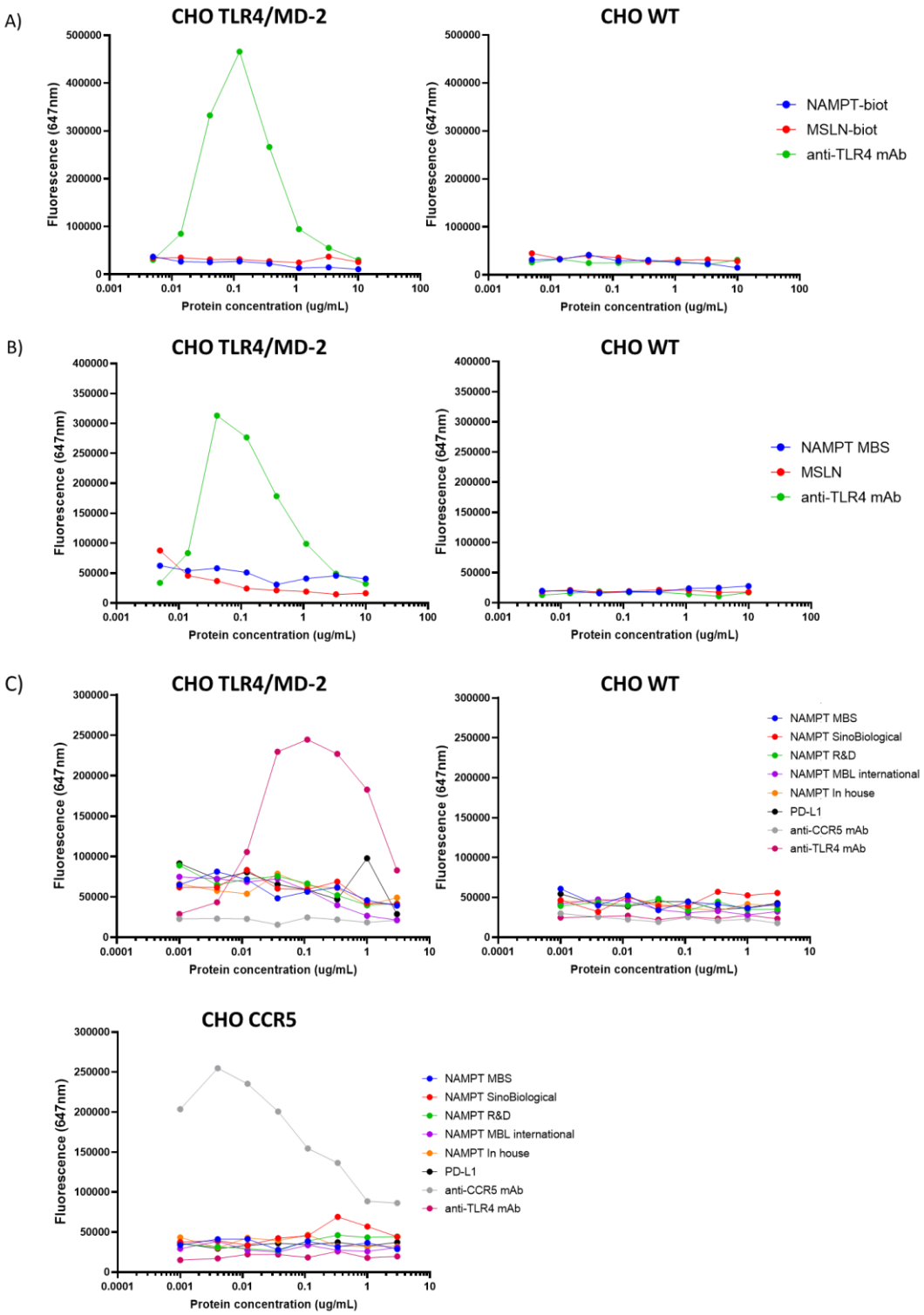

Supplementary Figure S22: eNAMPT binding to CHO-CCR5 and CHO-TLR4/MD-2 cells analyzed with CellInsight™ CX5 HCS imaging platform. (A-C) Increasing concentrations of NAMPT proteins were incubated for three hours with CHO-CCR5, CHO-TLR4/MD-2 or CHO-WT cells. NAMPT proteins were then detected with streptavidin coupled to Cy5 **(A)** or with an anti-PentaHis mAb coupled to AF647 **(B-C).** Cells were also incubated with anti-TLR4 and anti-CCR5 mAbs, detected with an anti-mouse IgG Fcγ antibody coupled to AF647, to control the correct expression of the receptors.

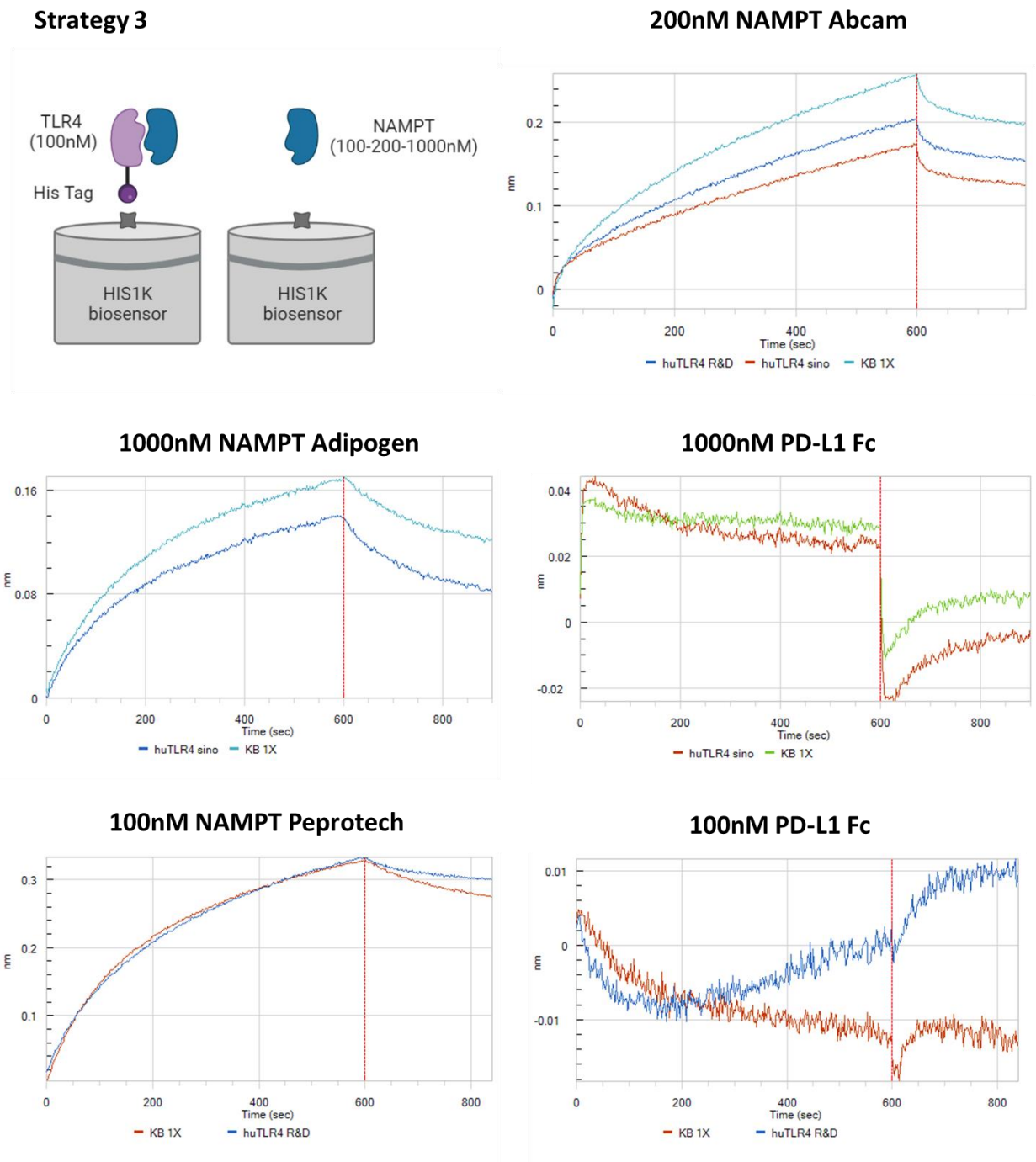

Supplementary Figure S23: eNAMPT binding to TLR4 analyzed with bio-layer interferometry using HIS1K biosensors. His-tagged TLR4 proteins (R&D and SinoBiological, Sino) were loaded onto HIS1K biosensors and incubated for 600sec with NAMPT or PD-L1-Fc proteins (100, 200 or 1000nM). TLR4 proteins were then incubated with KB 1X buffer to allow NAMPT or PD-L1-Fc dissociation.

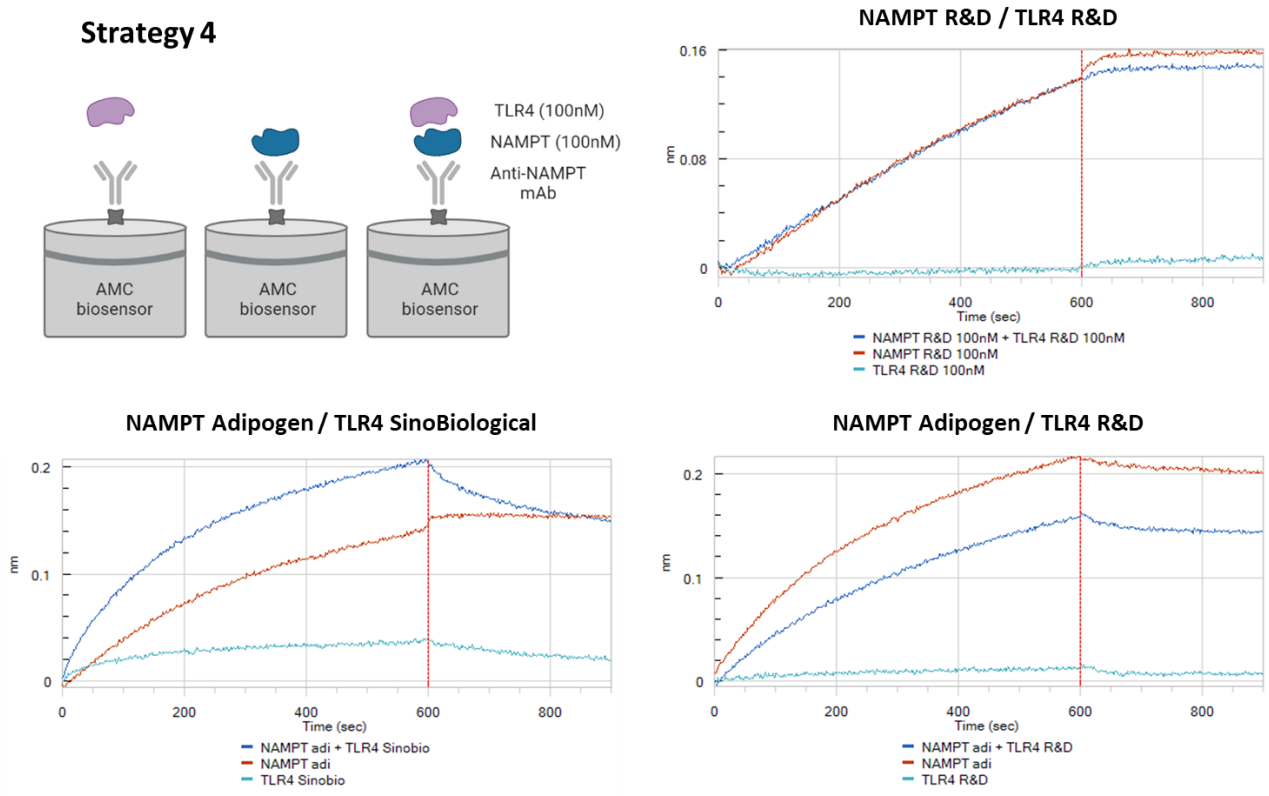

Supplementary Figure S24: TLR4 binding to eNAMPT analyzed with bio-layer interferometry using AMC biosensors. An anti-NAMPT mAb was loaded to AMC biosensors and incubated for 600sec with NAMPT (100nM), TLR4 (100nM) or a mix of NAMPT-TLR4 proteins (both at 100nM). The anti-NAMPT pAb was then incubated with KB 1X buffer to allow protein dissociation.

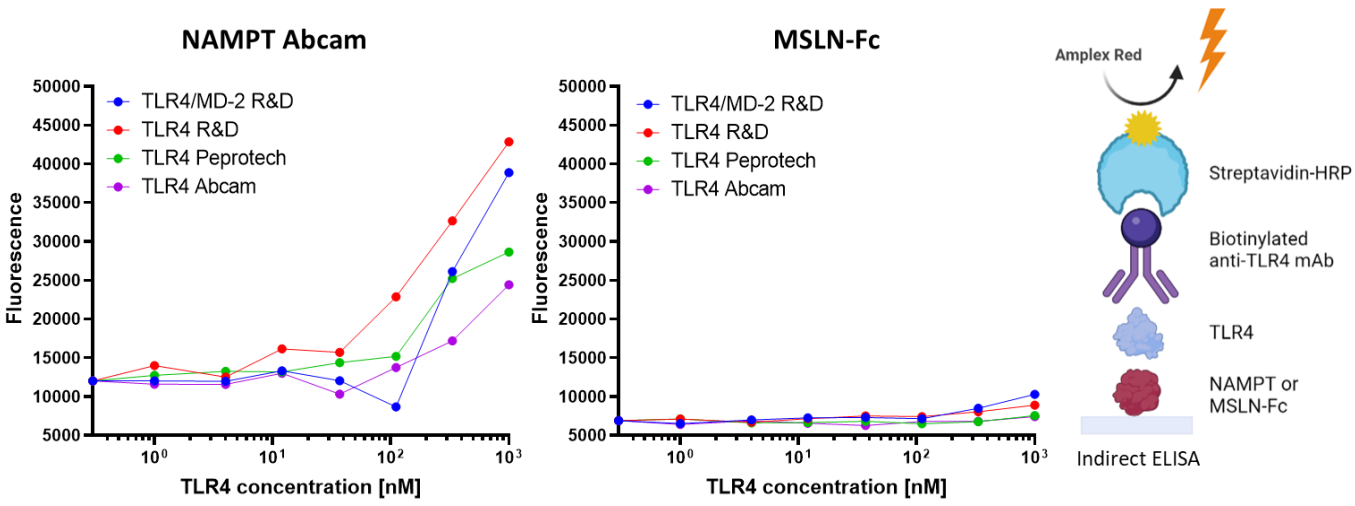

Supplementary Figure S25: TLR4 binds to eNAMPT in the presence of MD-2 in indirect ELISA. Maxisorp plates were coated with 60nM of NAMPT or MSLN-Fc (negative control) and incubated with increasing concentrations of TLR4 or TLR4/MD-2. Recombinant TLR4 proteins were then detected with a biotinylated anti-TLR4 antibody (Biolegend) and streptavidin coupled to HRP. TLR4/MD-2 and NAMPT binding results are representative of two independent experiments.

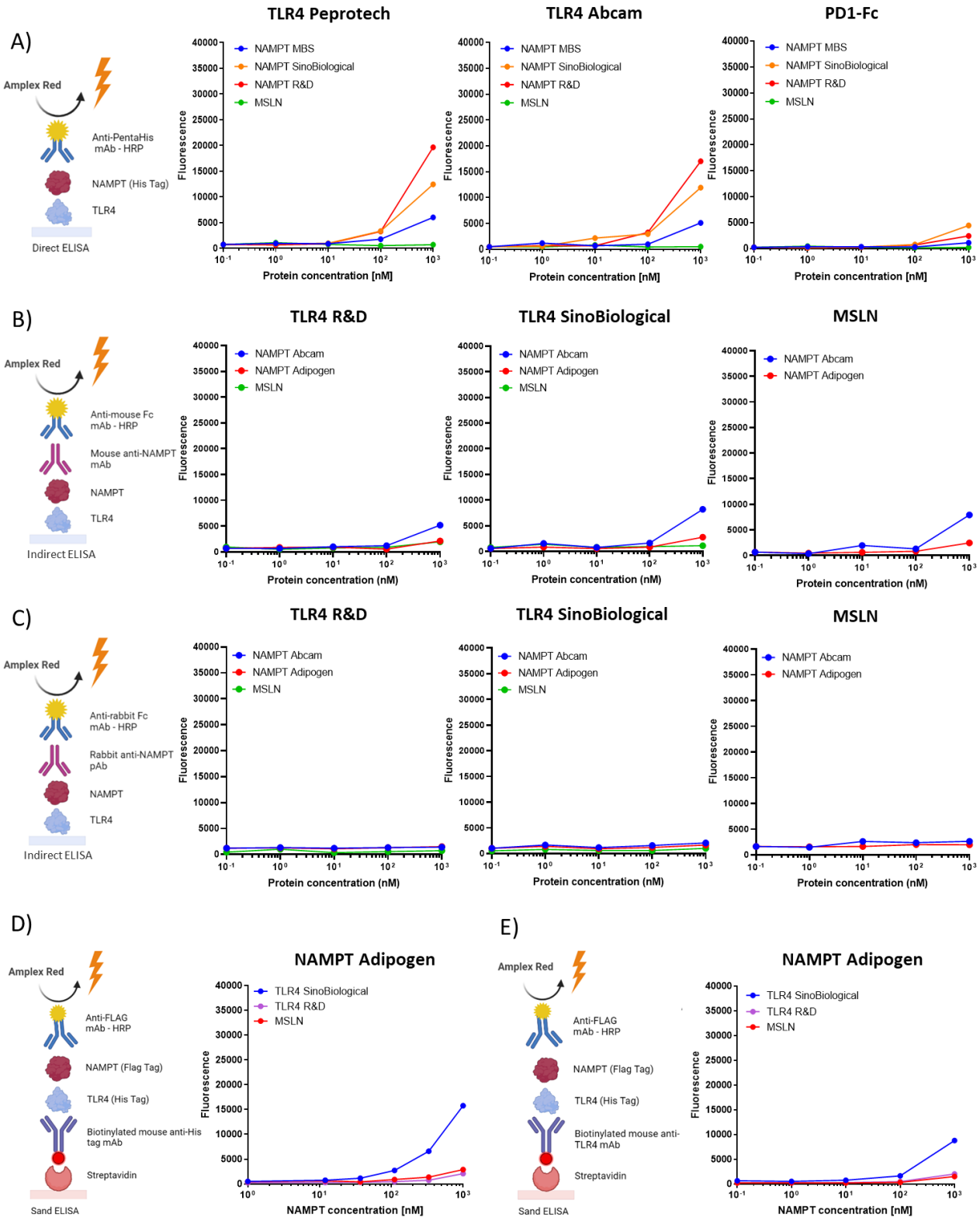

Supplementary Figure S26: eNAMPT did no bind TLR4 in the reverse ELISA configuration and in sandwich ELISAs. (A-C) TLR4 proteins were immobilized on a maxisorp plate and incubated with increasing concentrations of NAMPT proteins. NAMPT proteins were then detected with an anti-PentaHis Tag antibody coupled to HRP **(A)**, or with anti-NAMPT antibodies in turn detected with anti-mouse Fc or anti-rabbit Fc antibodies coupled to HRP **(B-C)**. **(D-E)** Biotinylated anti-HisTag **(D)** and anti-TLR4 **(E)** antibodies-coated streptawell plates were incubated with TLR4 proteins and increasing concentrations of NAMPT protein (Adipogen). FLAG-tagged NAMPT protein was then detected with an anti-FLAG tag antibody coupled to HRP.

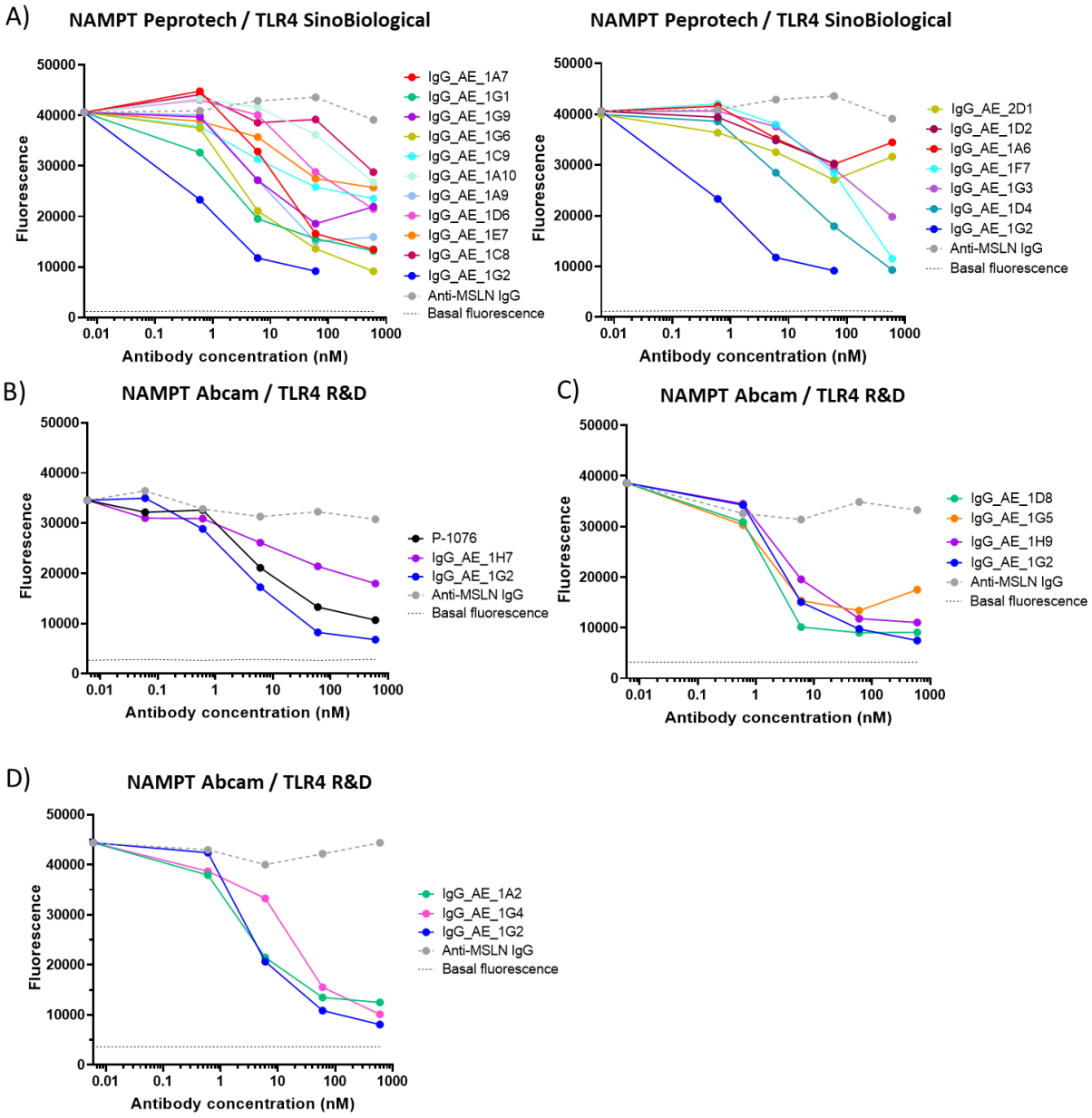

Supplementary Figure S27: Blocking binding of TLR4 to eNAMPT with anti-eNAMPT antibodies. (A-D) Maxisorp plates were coated with 60nM NAMPT protein and incubated with increasing concentrations of anti-eNAMPT mAbs and a fixed concentration of TLR4. His-tagged TLR4 was then detected with an anti-PentaHis tag antibody coupled to HRP. Four independent experiments are presented in **(A)**, **(B)**, **(C)**, and **(D)**.

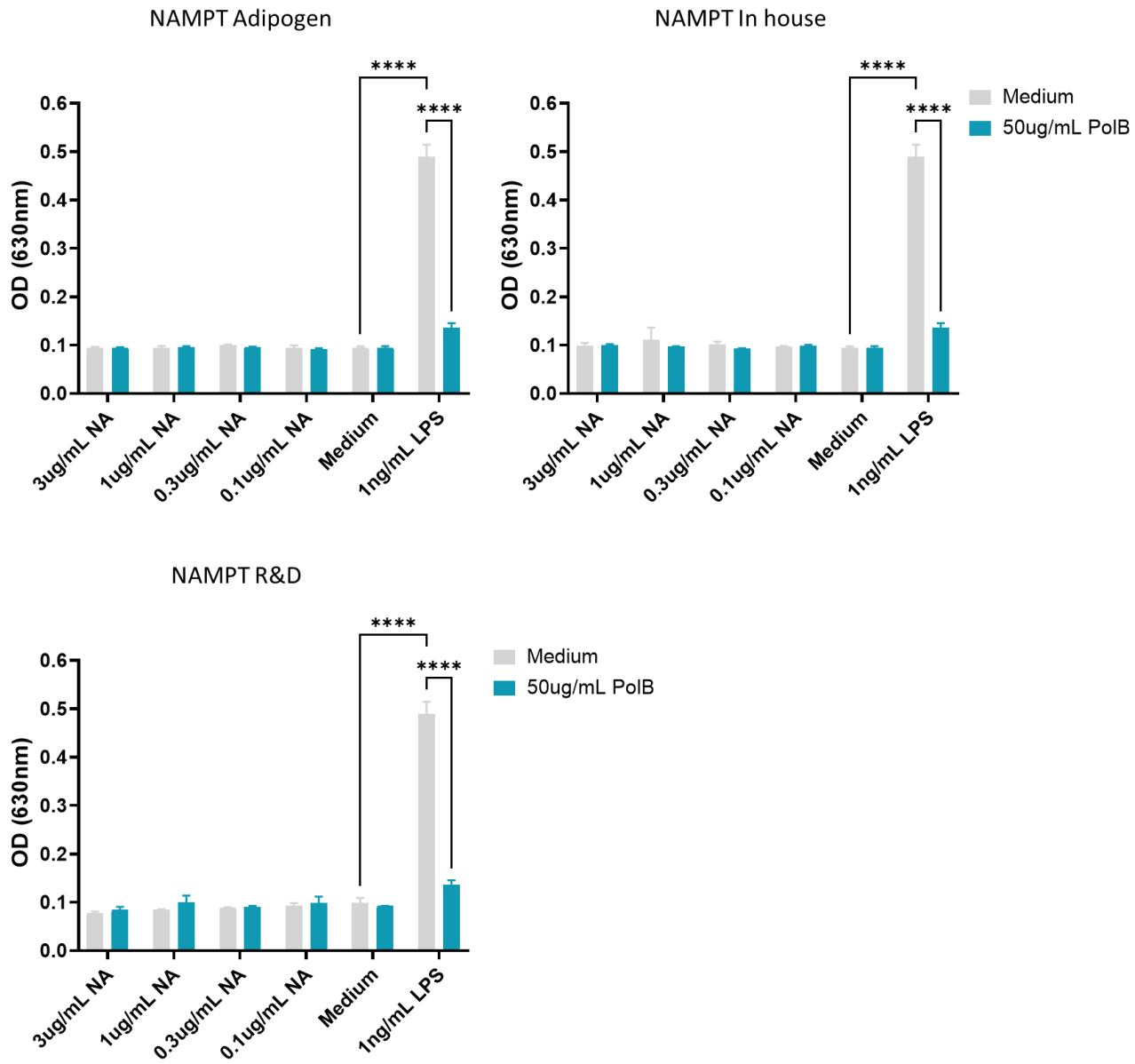

Supplementary Figure S28: NF-kB pathway induction in THP1-Blue-CD14 reporter cells. THP1-Blue-CD14 cells were stimulated with NAMPT proteins (NA, 0.1-3 ug/mL) or with LPS (1ng/mL), preincubated or not with polymyxin B (PolB, 50ug/mL) as indicated. NF-kB activation was quantified by determining the activity of SEAP using QUANTI-Blue™ detection reagent. Results are representative of two independent experiments and are represented as mean OD ± SD of three replicates. *, $p < 0.05$; **, $p < 0.01$; ***, $p < 0.001$; ****, $p < 0.0001$; ns, not statistically significant; were obtained using a two-way ANOVA with Tukey's multiple comparisons test.

8. List of abbreviations

aa: amino acids
ACh: acetylcholine
AMI: acute myocardial infarction
ADC: antibody-drug-conjugate
ADCC: antibody-dependent cell-mediated cytotoxicity
ADCP: antibody-dependent cellular phagocytosis
AKT: protein kinase B
ALI: acute lung injury
Ang: angiogenin
ARDS: acute respiratory distress syndrome
AUC: area under curve
BAL: bronchoalveolar lavage
BLI: bio-layer interferometry
BMI: body mass index
BSA: bovine serum albumin
CAT: catalase
CCL: chemokine (C-C motif) ligand
CCR5: CC-chemokine receptor type 5
CD: cluster of differentiation
CD: crohn's disease
CDC: complement-dependent cytotoxicity
cdk2: cyclin-dependent kinase 2
CDRs: complementarity-determining regions
CH: heavy chain's constant region
CL: light chain's constant region
CLL: chronic lymphocytic leukemia
CRC: colorectal cancer
CRP: c-reactive protein
csDMARDs: conventional synthetic disease modifying antirheumatic drugs
CTCL: cutaneous T-cell lymphoma
CTX-II: c-terminal cross-linked telopeptide of type II collagen
DAS28 : disease activity score 28
DMEM: Dulbecco's Modified Eagle's Medium
DNBS: dinitrobenzene sulfonic acid
DSS: dextran sulfate sodium
ECM: extracellular matrix
E.Coli: *Escherichia coli*
ECL: enhanced chemiluminescence
ELISA: enzyme-linked immunosorbent assay
EMT: epithelial-to-mesenchymal transition
eNAMPT: extracellular nicotinamide phosphoribosyltransferase
EPC: endothelial progenitor cells
ER: endoplasmic reticulum
ERK 1/2: extracellular signal-regulated kinase 1/2
ESR: erythrocyte sedimentation rate
EVs: extracellular vesicles

Fab: antigen-binding fragment
Fc: crystallizable fragment
FcγR: Fc gamma receptors
FcRn: neonatal Fc receptor
FDA: Food and Drug Administration
FFA: free fatty acid
FGF-2: fibroblast growth factor 2
FK866: (E)-N-[4-(1-benzoylpiperidin-4-yl)butyl]-3-(pyridin-3-yl) acrylamide
FMD: flow-mediated vasodilatation
FRD: fructose-rich diet
Kc: keratinocyte-derived chemokine
GAGs: sulfated glycosaminoglycans
GPCR: G protein-coupled receptor
GSIS: glucose-stimulated insulin secretion
GSM: gray-scale median
HAMA: human anti-murine antibodies
HCC: hepatocellular carcinoma
HFD: high-fat diet
HbA_{1c}: hemoglobin A1c
HIV: human immunodeficiency virus
HOMA-IR: homeostasis model assessment of insulin resistance
HPAEC: human pulmonary artery endothelial cells
HUVEC: human umbilical endothelial cells
IBD: inflammatory bowel disease
ICAM-1: intercellular adhesion molecule 1
IDO: indoleamine 2,3-dioxygenase
IFNγ: interferon gamma
Ig: immunoglobulins
IGF-1: insulin like growth factor-1
IL: interleukin
IMT: intima-media thickness
iNAMPT: intracellular nicotinamide phosphoribosyltransferase
iNOS: nitric oxide synthase
IPTG: isopropyl-β-d-thiogalactopyranoside
IR: insulin receptor
IRFs: interferon regulatory factors
IRS: insulin receptor substrate
JAK: janus kinase
KB: kinetic buffer
LBP: LPS binding protein
LDH: lactate dehydrogenase
LO: lead optimization
LPS: lipopolysaccharide
LRR: leucine-rich repeats
mAb: monoclonal antibody
MAC: Membrane Attack Complex
MAPK: mitogen-activated protein kinase
MCP-1: monocyte chemoattractant protein-1

MD-2: myeloid differentiation factor-2
MMP: matrix metalloproteinase
mTOR: mammalian target of rapamycin
MyD88: myeloid differentiation factor 88
NA: nicotinic acid
NAD: nicotinamide adenine dinucleotide
NADS: NAD+ synthetase
NAM: nicotinamide
NAMN: nicotinic acid mononucleotide
NAMPTi: NAMPT inhibitor
NAMPT: nicotinamide phosphoribosyltransferase
NAPRT: nicotinic acid phosphoribosyltransferase
NF-kB: nuclear factor kappa-light-chain-enhancer of activated B cells
NFR2: nuclear factor-erythroid 2 related factor 2
NGF: nerve growth factor
NK: natural killer
NLC: nurse-like cells
NLRP3: NLR family pyrin domain containing 3
nM: nanomolar
NMN: nicotinamide mononucleotide
NMNAT: nicotinamide mononucleotide adenylyltransferase
Nocht1: neurogenic locus notch homolog protein 1
Nox2: NADPH oxidase 2
OA: osteoarthritis
OASFs: OA synovial fibroblasts
OD: optical density
ox-LDL: oxidized low-density lipoprotein
PAK4: P21-activated kinase 4
PAMP: pathogen-associated molecular pattern
PARP: poly(ADP-ribose) polymerase
PBEF: pre-B-cell colony enhancing factor
PBMCs: peripheral blood mononuclear cells
PBS: Phosphate-Buffered Saline
PCa: prostate cancer
PCR: polymerase chain reaction
PEC: peritoneal macrophage
PGE2: prostaglandin E2
PI3K: phosphatidylinositol 3-kinase
PLC-γ: phospholipase C-γ
PMN: polymorphonuclear leucocyte
PROTAC: PROteolysis-TArgeting Chimera
PRPP: 5’-phosphoribosyl-1-pyrophosphate
PRR: pattern recognition receptor family
PVDF: polyvinylidene fluoride
RA: rheumatoid arthritis
RASFs: RA synovial fibroblasts
RILF: radiation-induced lung fibrosis
RO: round optimization

ROC: receiver operating characteristic
ROCK: rho-associated protein kinase
RT-qPCR: quantitative reverse transcription polymerase chain reaction
SCF: stem cell factor
scFv: single-chain variable fragment
SCID: severe combined immunodeficiency
SDF-1: stromal-derived factor 1
SEAP: secreted embryonic alkaline phosphatase
SF: synovial fluid
SIRT: sirtuin
SOD-2: superoxide dismutase
SPR: surface plasmon resonance
SR-A: scavenger receptor
SRB: sulforhodamine B
STAT: signal transducer and activator of transcription
T1DM: type 1 diabetes mellitus
T2DM: type 2 diabetes mellitus
TAA: tumor-associated antigens
TCA: trichloroacetic acid
TDO: tryptophan 2,3-dioxygenase
TEA: triethylamine
TER: transendothelial electrical resistance
TGF-β: transforming growth factor β
TIR: toll/interleukin-1 receptor-like
TLR: toll-like receptor
TNF-α: tumor necrosis factor-α
TME: tumor microenvironment
TRIF: TIR-domain-containing adapter inducing interferon-β
TXAS: thromboxane synthase
TYMS: thymidylate synthase
UC: ulcerative colitis
VCAM-1: vascular cell adhesion protein 1
VSMC: vascular smooth muscle cell
VEGF: vascular endothelial growth factor
VH: heavy chain's variable region
VILI: ventilator-induced lung injury
VL: light chain's variable region
WAT: white adipose tissue
WBC: white blood cell
ZO: zonula occludens

9. References

[1] F. Carbone *et al.*, "Regulation and Function of Extracellular Nicotinamide Phosphoribosyltransferase/Visfatin," *Compr Physiol*, vol. 7, no. 2, Art. no. 2, 16 2017, doi: 10.1002/cphy.c160029.

[2] V. Audrito and S. Deaglio, "NAMPT and NAPRT: Two Metabolic Enzymes With Key Roles in Inflammation," *Frontiers in Oncology*, vol. 10, p. 17, 2020.

[3] B. Samal, Y. Sun, G. Stearns, C. Xie, S. Suggs, and I. McNiece, "Cloning and characterization of the cDNA encoding a novel human pre-B-cell colony-enhancing factor," *Mol Cell Biol*, vol. 14, no. 2, pp. 1431–1437, Feb. 1994, doi: 10.1128/mcb.14.2.1431-1437.1994.

[4] S. Ognjanovic, S. Bao, S. Yamamoto, J. Garibay-Tupas, B. Samal, and G. Bryant-Greenwood, "Genomic organization of the gene coding for human pre-B-cell colony enhancing factor and expression in human fetal membranes," *Journal of Molecular Endocrinology*, vol. 26, no. 2, pp. 107–117, Apr. 2001, doi: 10.1677/jme.0.0260107.

[5] A. Lucena-Cacace, M. Umeda, L. E. Navas, and A. Carnero, "NAMPT as a Dedifferentiation-Inducer Gene: NAD+ as Core Axis for Glioma Cancer Stem-Like Cells Maintenance," *Front. Oncol.*, vol. 9, p. 292, May 2019, doi: 10.3389/fonc.2019.00292.

[6] A. Garten, S. Schuster, M. Penke, T. Gorski, T. de Giorgis, and W. Kiess, "Physiological and pathophysiological roles of NAMPT and NAD metabolism," *Nat Rev Endocrinol*, vol. 11, no. 9, pp. 535–546, Sep. 2015, doi: 10.1038/nrendo.2015.117.

[7] H. Chen *et al.*, "Gene organization, alternate splicing and expression pattern of porcine visfatin gene," *Domestic Animal Endocrinology*, vol. 32, no. 3, pp. 235–245, Apr. 2007, doi: 10.1016/j.domaniend.2006.03.004.

[8] J. R. Revollo *et al.*, "Nampt/PBEF/Visfatin Regulates Insulin Secretion in β Cells as a Systemic NAD Biosynthetic Enzyme," *Cell Metabolism*, vol. 6, no. 5, pp. 363–375, Nov. 2007, doi: 10.1016/j.cmet.2007.09.003.

[9] M.-K. Kim *et al.*, "Crystal Structure of Visfatin/Pre-B Cell Colony-enhancing Factor 1/Nicotinamide Phosphoribosyltransferase, Free and in Complex with the Anti-cancer Agent FK-866," *Journal of Molecular Biology*, vol. 362, no. 1, pp. 66–77, Sep. 2006, doi: 10.1016/j.jmb.2006.06.082.

[10] A. A. Grolla, C. Travelli, A. A. Genazzani, and J. K. Sethi, "Extracellular nicotinamide phosphoribosyltransferase, a new cancer metabokine," *Br. J. Pharmacol.*, vol. 173, no. 14, Art. no. 14, 2016, doi: 10.1111/bph.13505.

[11] T. Kitani, S. Okuno, and H. Fujisawa, "Growth phase-dependent changes in the subcellular localization of pre-B-cell colony-enhancing factor [1]," *FEBS Letters*, vol. 544, no. 1–3, pp. 74–78, Jun. 2003, doi: 10.1016/S0014-5793(03)00476-9.

[12] P. Svoboda *et al.*, "Nuclear transport of nicotinamide phosphoribosyltransferase is cell cycle–dependent in mammalian cells, and its inhibition slows cell growth," *Journal of Biological Chemistry*, vol. 294, no. 22, pp. 8676–8689, May 2019, doi: 10.1074/jbc.RA118.003505.

[13] X. Wang *et al.*, "Subcellular NAMPT-mediated NAD $^+$ salvage pathways and their roles in bioenergetics and neuronal protection after ischemic injury," *J. Neurochem.*, vol. 151, no. 6, pp. 732–748, Dec. 2019, doi: 10.1111/jnc.14878.

[14] M. Pittelli *et al.*, "Inhibition of Nicotinamide Phosphoribosyltransferase," *Journal of Biological Chemistry*, vol. 285, no. 44, pp. 34106–34114, Oct. 2010, doi: 10.1074/jbc.M110.136739.

[15] H. Yang *et al.*, "Nutrient-Sensitive Mitochondrial NAD+ Levels Dictate Cell Survival," *Cell*, vol. 130, no. 6, pp. 1095–1107, Sep. 2007, doi: 10.1016/j.cell.2007.07.035.

[16] M. Yoshida *et al.*, "Extracellular Vesicle-Contained eNAMPT Delays Aging and Extends Lifespan in Mice," *Cell Metab.*, vol. 30, no. 2, pp. 329-342.e5, Aug. 2019, doi: 10.1016/j.cmet.2019.05.015.

[17] Y. Lu *et al.*, "Nicotinamide phosphoribosyltransferase secreted from microglia *via* exosome during ischemic injury," *J. Neurochem.*, vol. 150, no. 6, pp. 723–737, Sep. 2019, doi: 10.1111/jnc.14811.
[18] A. Garten *et al.*, "Nicotinamide phosphoribosyltransferase (NAMPT/PBEF/visfatin) is constitutively released from human hepatocytes," *Biochemical and Biophysical Research Communications*, vol. 391, no. 1, pp. 376–381, Jan. 2010, doi: 10.1016/j.bbrc.2009.11.066.
[19] M. Tanaka *et al.*, "Visfatin is released from 3T3-L1 adipocytes via a non-classical pathway," *Biochemical and Biophysical Research Communications*, vol. 359, no. 2, pp. 194–201, Jul. 2007, doi: 10.1016/j.bbrc.2007.05.096.
[20] M. J. Yoon *et al.*, "SIRT1-Mediated eNAMPT Secretion from Adipose Tissue Regulates Hypothalamic NAD+ and Function in Mice," *Cell Metabolism*, vol. 21, no. 5, pp. 706–717, May 2015, doi: 10.1016/j.cmet.2015.04.002.
[21] G. Sociali *et al.*, "SIRT6 deacetylase activity regulates NAMPT activity and NAD(P)(H) pools in cancer cells," *FASEB j.*, vol. 33, no. 3, pp. 3704–3717, Mar. 2019, doi: 10.1096/fj.201800321R.
[22] M. S. Ghanem, F. Monacelli, and A. Nencioni, "Advances in NAD-Lowering Agents for Cancer Treatment," *Nutrients*, vol. 13, no. 5, p. 1665, May 2021, doi: 10.3390/nu13051665.
[23] A. J. Covarrubias, R. Perrone, A. Grozio, and E. Verdin, "NAD+ metabolism and its roles in cellular processes during ageing," *Nat Rev Mol Cell Biol*, vol. 22, no. 2, Art. no. 2, Feb. 2021, doi: 10.1038/s41580-020-00313-x.
[24] A. Fukuhara *et al.*, "Visfatin: a protein secreted by visceral fat that mimics the effects of insulin," *Science*, vol. 307, no. 5708, pp. 426–430, Jan. 2005, doi: 10.1126/science.1097243.
[25] A. Fukuhara *et al.*, "Retraction," *Science*, vol. 318, no. 5850, p. 565, Oct. 2007, doi: 10.1126/science.318.5850.565b.
[26] S. M. Camp *et al.*, "Unique Toll-Like Receptor 4 Activation by NAMPT/PBEF Induces NFκB Signaling and Inflammatory Lung Injury," *Sci Rep*, vol. 5, p. 13135, Aug. 2015, doi: 10.1038/srep13135.
[27] R. Van den Bergh *et al.*, "Monocytes contribute to differential immune pressure on R5 versus X4 HIV through the adipocytokine visfatin/NAMPT," *PLoS ONE*, vol. 7, no. 4, Art. no. 4, 2012, doi: 10.1371/journal.pone.0035074.
[28] M. Oppermann, "Chemokine receptor CCR5: insights into structure, function, and regulation," *Cellular Signalling*, vol. 16, no. 11, pp. 1201–1210, Nov. 2004, doi: 10.1016/j.cellsig.2004.04.007.
[29] X. Jiao *et al.*, "Recent Advances targeting CCR5 for Cancer and its Role in Immuno-Oncology," *Cancer Res*, vol. 79, no. 19, pp. 4801–4807, Oct. 2019, doi: 10.1158/0008-5472.CAN-19-1167.
[30] M. B. Kim, K. E. Giesler, Y. A. Tahirovic, V. M. Truax, D. C. Liotta, and L. J. Wilson, "CCR5 receptor antagonists in preclinical to phase II clinical development for treatment of HIV," *Expert Opin Investig Drugs*, vol. 25, no. 12, pp. 1377–1392, Dec. 2016, doi: 10.1080/13543784.2016.1254615.
[31] D. Aldinucci, C. Borghese, and N. Casagrande, "The CCL5/CCR5 Axis in Cancer Progression," *Cancers (Basel)*, vol. 12, no. 7, p. 1765, Jul. 2020, doi: 10.3390/cancers12071765.
[32] I. Scurci, E. Martins, and O. Hartley, "CCR5: Established paradigms and new frontiers for a 'celebrity' chemokine receptor," *Cytokine*, vol. 109, pp. 81–93, Sep. 2018, doi: 10.1016/j.cyto.2018.02.018.
[33] Y. Wu and A. Yoder, "Chemokine coreceptor signaling in HIV-1 infection and pathogenesis," *PLoS Pathog*, vol. 5, no. 12, p. e1000520, Dec. 2009, doi: 10.1371/journal.ppat.1000520.
[34] P. Isaikina *et al.*, "Structural basis of the activation of the CC chemokine receptor 5 by a chemokine agonist," *Sci Adv*, vol. 7, no. 25, p. eabg8685, Jun. 2021, doi: 10.1126/sciadv.abg8685.
[35] C. Vaure and Y. Liu, "A Comparative Review of Toll-Like Receptor 4 Expression and Functionality in Different Animal Species," *Front. Immunol.*, vol. 5, Jul. 2014, doi: 10.3389/fimmu.2014.00316.

[36] W. S. Bowen, S. K. Gandhapudi, J. P. Kolb, and T. C. Mitchell, “Immunopharmacology of Lipid A Mimetics,” in *Advances in Pharmacology*, vol. 66, Elsevier, 2013, pp. 81–128. doi: 10.1016/B978-0-12-404717-4.00003-2.
[37] J. L. Adams, K. J. Duffy, M. L. Moore, and J. Yang, “Cancer Immunotherapy—An Emerging Field That Bridges Oncology and Immunology Research,” in *Comprehensive Medicinal Chemistry III*, Elsevier, 2017, pp. 357–394. doi: 10.1016/B978-0-12-409547-2.12400-X.
[38] B. S. Park and J.-O. Lee, “Recognition of lipopolysaccharide pattern by TLR4 complexes,” *Exp Mol Med*, vol. 45, no. 12, pp. e66–e66, Dec. 2013, doi: 10.1038/emm.2013.97.
[39] Y.-C. Lu, W.-C. Yeh, and P. S. Ohashi, “LPS/TLR4 signal transduction pathway,” *Cytokine*, vol. 42, no. 2, pp. 145–151, May 2008, doi: 10.1016/j.cyto.2008.01.006.
[40] M. Dalamaga, G. S. Christodoulatos, and C. S. Mantzoros, “The role of extracellular and intracellular Nicotinamide phosphoribosyl-transferase in cancer: Diagnostic and therapeutic perspectives and challenges,” *Metabolism*, vol. 82, pp. 72–87, May 2018, doi: 10.1016/j.metabol.2018.01.001.
[41] D. Hanahan, “Hallmarks of Cancer: New Dimensions,” *Cancer Discovery*, vol. 12, no. 1, pp. 31–46, Jan. 2022, doi: 10.1158/2159-8290.CD-21-1059.
[42] A. K. Abbas, A. H. Lichtman, S. Pillai, D. L. Baker, and A. Baker, *Cellular and molecular immunology*, Ninth edition. Philadelphia, PA: Elsevier, 2018.
[43] D. N. Forthal, “Functions of Antibodies,” *Microbiol Spectr*, vol. 2, no. 4, pp. 1–17, Aug. 2014.
[44] G. Köhler and C. Milstein, “Continuous cultures of fused cells secreting antibody of predefined specificity,” *Nature*, vol. 256, no. 5517, pp. 495–497, Aug. 1975, doi: 10.1038/256495a0.
[45] M. S. Castelli, P. McGonigle, and P. J. Hornby, “The pharmacology and therapeutic applications of monoclonal antibodies,” *Pharmacology Res & Perspec*, vol. 7, no. 6, Dec. 2019, doi: 10.1002/prp2.535.
[46] L. M. Weiner, R. Surana, and S. Wang, “Monoclonal antibodies: versatile platforms for cancer immunotherapy,” *Nat Rev Immunol*, vol. 10, no. 5, pp. 317–327, May 2010, doi: 10.1038/nri2744.
[47] G. Vidarsson, G. Dekkers, and T. Rispens, “IgG Subclasses and Allotypes: From Structure to Effector Functions,” *Front. Immunol.*, vol. 5, Oct. 2014, doi: 10.3389/fimmu.2014.00520.
[48] L. L. Lu, T. J. Suscovich, S. M. Fortune, and G. Alter, “Beyond binding: antibody effector functions in infectious diseases,” *Nat Rev Immunol*, vol. 18, no. 1, Art. no. 1, Jan. 2018, doi: 10.1038/nri.2017.106.
[49] J. B. Adlersberg, “The immunoglobulin hinge (Interdomain) region,” *La Ricerca in Clin. Lab.*, vol. 6, no. 3, p. 191, Jul. 1976, doi: 10.1007/BF02899970.
[50] H. W. Schroeder and L. Cavacini, “Structure and function of immunoglobulins,” *Journal of Allergy and Clinical Immunology*, vol. 125, no. 2, pp. S41–S52, Feb. 2010, doi: 10.1016/j.jaci.2009.09.046.
[51] M. L. Chiu, D. R. Goulet, A. Teplyakov, and G. L. Gilliland, “Antibody Structure and Function: The Basis for Engineering Therapeutics,” *Antibodies*, vol. 8, no. 4, p. 55, Dec. 2019, doi: 10.3390/antib8040055.
[52] D. K. Challa, R. Velmurugan, R. J. Ober, and E. Sally Ward, “FcRn: From Molecular Interactions to Regulation of IgG Pharmacokinetics and Functions,” in *Fc Receptors*, vol. 382, M. Daeron and F. Nimmerjahn, Eds. Cham: Springer International Publishing, 2014, pp. 249–272. doi: 10.1007/978-3-319-07911-0_12.
[53] P. N. Nesargikar, B. Spiller, and R. Chavez, “The complement system: history, pathways, cascade and inhibitors,” *Eur J Microbiol Immunol (Bp)*, vol. 2, no. 2, pp. 103–111, Jun. 2012, doi: 10.1556/EuJMI.2.2012.2.2.
[54] F. Nimmerjahn and J. V. Ravetch, “Fcγ receptors as regulators of immune responses,” *Nat Rev Immunol*, vol. 8, no. 1, Art. no. 1, Jan. 2008, doi: 10.1038/nri2206.

[55] K. R. Patel, J. T. Roberts, and A. W. Barb, “Multiple Variables at the Leukocyte Cell Surface Impact Fc γ Receptor-Dependent Mechanisms,” *Front Immunol*, vol. 10, p. 223, Feb. 2019, doi: 10.3389/fimmu.2019.00223.
[56] J. M. Hayes, M. R. Wormald, P. M. Rudd, and G. P. Davey, “Fc gamma receptors: glycobiology and therapeutic prospects,” *J Inflamm Res*, vol. 9, pp. 209–219, Nov. 2016, doi: 10.2147/JIR.S121233.
[57] E. A. van Erp, W. Luytjes, G. Ferwerda, and P. B. van Kasteren, “Fc-Mediated Antibody Effector Functions During Respiratory Syncytial Virus Infection and Disease,” *Front Immunol*, vol. 10, p. 548, Mar. 2019, doi: 10.3389/fimmu.2019.00548.
[58] V. R. Gómez Román, J. C. Murray, and L. M. Weiner, “Chapter 1 - Antibody-Dependent Cellular Cytotoxicity (ADCC),” in *Antibody Fc*, M. E. Ackerman and F. Nimmerjahn, Eds. Boston: Academic Press, 2014, pp. 1–27. doi: 10.1016/B978-0-12-394802-1.00001-7.
[59] M. Z. Tay, K. Wiehe, and J. Pollara, “Antibody-Dependent Cellular Phagocytosis in Antiviral Immune Responses,” *Front Immunol*, vol. 10, p. 332, 2019, doi: 10.3389/fimmu.2019.00332.
[60] A. Musolino *et al.*, “Role of Fcγ receptors in HER2-targeted breast cancer therapy,” *J Immunother Cancer*, vol. 10, no. 1, p. e003171, Jan. 2022, doi: 10.1136/jitc-2021-003171.
[61] J. Yu, Y. Song, and W. Tian, “How to select IgG subclasses in developing anti-tumor therapeutic antibodies,” *Journal of Hematology & Oncology*, vol. 13, no. 1, p. 45, May 2020, doi: 10.1186/s13045-020-00876-4.
[62] J. C. Almagro, T. R. Daniels-Wells, S. M. Perez-Tapia, and M. L. Penichet, “Progress and Challenges in the Design and Clinical Development of Antibodies for Cancer Therapy,” *Front. Immunol.*, vol. 8, p. 1751, Jan. 2018, doi: 10.3389/fimmu.2017.01751.
[63] J. Z. Moraes *et al.*, “Hybridoma technology: is it still useful?,” *Curr Res Immunol*, vol. 2, pp. 32–40, Mar. 2021, doi: 10.1016/j.crimmu.2021.03.002.
[64] J. K. H. Liu, “The history of monoclonal antibody development – Progress, remaining challenges and future innovations,” *Ann Med Surg (Lond)*, vol. 3, no. 4, pp. 113–116, Sep. 2014, doi: 10.1016/j.amsu.2014.09.001.
[65] S. Mitra and P. C. Tomar, “Hybridoma technology; advancements, clinical significance, and future aspects,” *J Genet Eng Biotechnol*, vol. 19, p. 159, Oct. 2021, doi: 10.1186/s43141-021-00264-6.
[66] R.-M. Lu *et al.*, “Development of therapeutic antibodies for the treatment of diseases,” *J Biomed Sci*, vol. 27, no. 1, p. 1, Dec. 2020, doi: 10.1186/s12929-019-0592-z.
[67] H. Watier and J. M. Reichert, “Evolution of Antibody Therapeutics,” in *Methods and Principles in Medicinal Chemistry*, T. Vaughan, J. Osbourn, and B. Jallal, Eds. Weinheim, Germany: Wiley-VCH Verlag GmbH & Co. KGaA, 2017, pp. 25–49. doi: 10.1002/9783527699124.ch2.
[68] F. A. Harding, M. M. Stickler, J. Razo, and R. B. DuBridge, “The immunogenicity of humanized and fully human antibodies,” *MAbs*, vol. 2, no. 3, pp. 256–265, 2010.
[69] J. Bazan, I. Całkosiński, and A. Gamian, “Phage display—A powerful technique for immunotherapy,” *Hum Vaccin Immunother*, vol. 8, no. 12, pp. 1817–1828, Dec. 2012, doi: 10.4161/hv.21703.
[70] S. Z. B. Mahdavi *et al.*, “An overview on display systems (phage, bacterial, and yeast display) for production of anticancer antibodies; advantages and disadvantages,” *International Journal of Biological Macromolecules*, vol. 208, pp. 421–442, May 2022, doi: 10.1016/j.ijbiomac.2022.03.113.
[71] M. A. Alfaleh *et al.*, “Phage Display Derived Monoclonal Antibodies: From Bench to Bedside,” *Front. Immunol.*, vol. 11, p. 1986, Aug. 2020, doi: 10.3389/fimmu.2020.01986.
[72] W. Jaroszewicz, J. Morcinek-Orłowska, K. Pierzynowska, L. Gaffke, and G. Węgrzyn, “Phage display and other peptide display technologies,” *FEMS Microbiology Reviews*, vol. 46, no. 2, p. fuab052, Mar. 2022, doi: 10.1093/femsre/fuab052.

[73] J. McCafferty, A. D. Griffiths, G. Winter, and D. J. Chiswell, “Phage antibodies: filamentous phage displaying antibody variable domains,” *Nature*, vol. 348, no. 6301, pp. 552–554, Dec. 1990, doi: 10.1038/348552a0.
[74] L. Ledsgaard *et al.*, “Advances in antibody phage display technology,” *Drug Discovery Today*, May 2022, doi: 10.1016/j.drudis.2022.05.002.
[75] J. C. Almagro, M. Pedraza-Escalona, H. I. Arrieta, and S. M. Pérez-Tapia, “Phage Display Libraries for Antibody Therapeutic Discovery and Development,” *Antibodies*, vol. 8, no. 3, Art. no. 3, Sep. 2019, doi: 10.3390/antib8030044.
[76] S. Bashir and J. Paeshuyse, “Construction of Antibody Phage Libraries and Their Application in Veterinary Immunovirology,” *Antibodies (Basel)*, vol. 9, no. 2, p. 21, Jun. 2020, doi: 10.3390/antib9020021.
[77] K. D. R. Roth *et al.*, “Developing Recombinant Antibodies by Phage Display Against Infectious Diseases and Toxins for Diagnostics and Therapy,” *Front. Cell. Infect. Microbiol.*, vol. 11, p. 697876, Jul. 2021, doi: 10.3389/fcimb.2021.697876.
[78] M. Hasmann and I. Schemainda, “FK866, a highly specific noncompetitive inhibitor of nicotinamide phosphoribosyltransferase, represents a novel mechanism for induction of tumor cell apoptosis,” *Cancer Res*, vol. 63, no. 21, pp. 7436–7442, Nov. 2003.
[79] U. Galli, G. Colombo, C. Travelli, G. C. Tron, A. A. Genazzani, and A. A. Grolla, “Recent Advances in NAMPT Inhibitors: A Novel Immunotherapic Strategy,” *Front. Pharmacol.*, vol. 11, p. 656, May 2020, doi: 10.3389/fphar.2020.00656.
[80] J. A. Khan, X. Tao, and L. Tong, “Molecular basis for the inhibition of human NMPRTase, a novel target for anticancer agents,” *Nat Struct Mol Biol*, vol. 13, no. 7, pp. 582–588, Jul. 2006, doi: 10.1038/nsmb1105.
[81] P. J. Hjarnaa *et al.*, “CHS 828, a novel pyridyl cyanoguanidine with potent antitumor activity in vitro and in vivo,” *Cancer Res*, vol. 59, no. 22, pp. 5751–5757, Nov. 1999.
[82] U. H. Olesen *et al.*, “Anticancer agent CHS-828 inhibits cellular synthesis of NAD,” *Biochem Biophys Res Commun*, vol. 367, no. 4, pp. 799–804, Mar. 2008, doi: 10.1016/j.bbrc.2008.01.019.
[83] Y. Wei, H. Xiang, and W. Zhang, “Review of various NAMPT inhibitors for the treatment of cancer,” *Front. Pharmacol.*, vol. 13, p. 970553, Sep. 2022, doi: 10.3389/fphar.2022.970553.
[84] Y. Ogino, A. Sato, F. Uchiumi, and S.-I. Tanuma, “Cross resistance to diverse anticancer nicotinamide phosphoribosyltransferase inhibitors induced by FK866 treatment,” *Oncotarget*, vol. 9, no. 23, pp. 16451–16461, Mar. 2018, doi: 10.18632/oncotarget.24731.
[85] A. S. Karpov *et al.*, “Nicotinamide Phosphoribosyltransferase Inhibitor as a Novel Payload for Antibody–Drug Conjugates,” *ACS Med. Chem. Lett.*, vol. 9, no. 8, pp. 838–842, Aug. 2018, doi: 10.1021/acsmedchemlett.8b00254.
[86] R. V. J. Chari, “Expanding the Reach of Antibody–Drug Conjugates,” *ACS Med. Chem. Lett.*, vol. 7, no. 11, pp. 974–976, Nov. 2016, doi: 10.1021/acsmedchemlett.6b00312.
[87] C. S. Neumann *et al.*, “Targeted Delivery of Cytotoxic NAMPT Inhibitors Using Antibody–Drug Conjugates,” *Molecular Cancer Therapeutics*, vol. 17, no. 12, pp. 2633–2642, Dec. 2018, doi: 10.1158/1535-7163.MCT-18-0643.
[88] N. Böhnke *et al.*, “A Novel NAMPT Inhibitor-Based Antibody–Drug Conjugate Payload Class for Cancer Therapy,” *Bioconjugate Chem.*, vol. 33, no. 6, pp. 1210–1221, Jun. 2022, doi: 10.1021/acs.bioconjchem.2c00178.
[89] L. E. Navas and A. Carnero, “Nicotinamide Adenine Dinucleotide (NAD) Metabolism as a Relevant Target in Cancer,” *Cells*, vol. 11, no. 17, p. 2627, Aug. 2022, doi: 10.3390/cells11172627.
[90] X. Zhu *et al.*, “Addressing the Enzyme-independent tumor-promoting function of NAMPT via PROTAC-mediated degradation,” *Cell Chem Biol*, vol. 29, no. 11, pp. 1616-1629.e12, Nov. 2022, doi: 10.1016/j.chembiol.2022.10.007.

[91] Y. Wu, C. Pu, Y. Fu, G. Dong, M. Huang, and C. Sheng, “NAMPT-targeting PROTAC promotes antitumor immunity via suppressing myeloid-derived suppressor cell expansion,” *Acta Pharmaceutica Sinica B*, vol. 12, no. 6, pp. 2859–2868, Jun. 2022, doi: 10.1016/j.apsb.2021.12.017.
[92] S. Khan *et al.*, “PROteolysis TArgeting Chimeras (PROTACs) as emerging anticancer therapeutics,” *Oncogene*, vol. 39, no. 26, pp. 4909–4924, Jun. 2020, doi: 10.1038/s41388-020-1336-y.
[93] M. Gasparrini and V. Audrito, “NAMPT: A critical driver and therapeutic target for cancer,” *The International Journal of Biochemistry & Cell Biology*, vol. 145, p. 106189, Apr. 2022, doi: 10.1016/j.biocel.2022.106189.
[94] V. B. Pillai *et al.*, “Nampt secreted from cardiomyocytes promotes development of cardiac hypertrophy and adverse ventricular remodeling,” *American Journal of Physiology-Heart and Circulatory Physiology*, vol. 304, no. 3, pp. H415–H426, Feb. 2013, doi: 10.1152/ajpheart.00468.2012.
[95] V. Audrito *et al.*, “Extracellular nicotinamide phosphoribosyltransferase (NAMPT) promotes M2 macrophage polarization in chronic lymphocytic leukemia,” *Blood*, vol. 125, no. 1, pp. 111–123, Jan. 2015, doi: 10.1182/blood-2014-07-589069.
[96] G. Colombo *et al.*, “Neutralization of extracellular NAMPT (nicotinamide phosphoribosyltransferase) ameliorates experimental murine colitis,” *J Mol Med*, vol. 98, no. 4, pp. 595–612, Apr. 2020, doi: 10.1007/s00109-020-01892-0.
[97] H. Quijada *et al.*, “Endothelial eNAMPT Amplifies Preclinical Acute Lung Injury: Efficacy of an eNAMPT-Neutralising mAb,” *Eur Respir J*, Nov. 2020, doi: 10.1183/13993003.02536-2020.
[98] B. L. Sun *et al.*, “A Humanized Monoclonal Antibody Targeting Extracellular Nicotinamide Phosphoribosyltransferase Prevents Aggressive Prostate Cancer Progression,” *Pharmaceuticals*, vol. 14, no. 12, p. 1322, Dec. 2021, doi: 10.3390/ph14121322.
[99] T. Liu *et al.*, “Visfatin Mediates SCLC Cells Migration across Brain Endothelial Cells through Upregulation of CCL2,” *IJMS*, vol. 16, no. 12, pp. 11439–11451, May 2015, doi: 10.3390/ijms160511439.
[100] L. Xiao, Y. Mao, Z. Tong, Y. Zhao, H. Hong, and F. Wang, “Radiation exposure triggers the malignancy of non-small cell lung cancer cells through the activation of visfatin/Snail signaling,” *Oncol Rep*, vol. 45, no. 3, pp. 1153–1161, Mar. 2021, doi: 10.3892/or.2021.7929.
[101] J. Kieswich, S. R. Sayers, M. F. Silvestre, S. M. Harwood, M. M. Yaqoob, and P. W. Caton, “Monomeric eNAMPT in the development of experimental diabetes in mice: a potential target for type 2 diabetes treatment,” *Diabetologia*, vol. 59, no. 11, pp. 2477–2486, Nov. 2016, doi: 10.1007/s00125-016-4076-3.
[102] J. G. N. Garcia and D. Maccann, “Anti-Nampt Antibodies and Uses Thereof,” Feb. 11, 2021 Accessed: Aug. 10, 2022. [Online]. Available: https://patentscope.wipo.int/search/en/detail.jsf?docId=WO2021026508
[103] T. Bermudez *et al.*, “eNAMPT neutralization reduces preclinical ARDS severity via rectified NFkB and Akt/mTORC2 signaling,” *Sci Rep*, vol. 12, no. 1, p. 696, Dec. 2022, doi: 10.1038/s41598-021-04444-9.
[104] S. Sammani *et al.*, “eNAMPT Neutralization Preserves Lung Fluid Balance and Reduces Acute Renal Injury in Porcine Sepsis/VILI-Induced Inflammatory Lung Injury,” *Front. Physiol.*, vol. 13, p. 916159, Jun. 2022, doi: 10.3389/fphys.2022.916159.
[105] M. Ahmed *et al.*, “Endothelial eNAMPT drives EndMT and preclinical PH: rescue by an eNAMPT-neutralizing mAb,” *Pulm Circ*, vol. 11, no. 4, p. 204589402110597, Oct. 2021, doi: 10.1177/20458940211059712.
[106] A. N. Garcia *et al.*, “eNAMPT Is a Novel Damage-associated Molecular Pattern Protein That Contributes to the Severity of Radiation-induced Lung Fibrosis,” *Am J Respir Cell Mol Biol*, vol. 66, no. 5, pp. 497–509, May 2022, doi: 10.1165/rcmb.2021-0357OC.

[107] G. Colombo, C. Travelli, C. Porta, and A. A. Genazzani, “Extracellular nicotinamide phosphoribosyltransferase boosts IFNγ-induced macrophage polarization independently of TLR4,” *iScience*, vol. 25, no. 4, p. 104147, Apr. 2022, doi: 10.1016/j.isci.2022.104147.
[108] D. Soncini *et al.*, “Nicotinamide Phosphoribosyltransferase Promotes Epithelial-to-Mesenchymal Transition as a Soluble Factor Independent of Its Enzymatic Activity,” *J Biol Chem*, vol. 289, no. 49, pp. 34189–34204, Dec. 2014, doi: 10.1074/jbc.M114.594721.
[109] Y. Li *et al.*, “Extracellular Nampt Promotes Macrophage Survival via a Nonenzymatic Interleukin-6/STAT3 Signaling Mechanism,” *Journal of Biological Chemistry*, vol. 283, no. 50, pp. 34833–34843, Dec. 2008, doi: 10.1074/jbc.M805866200.
[110] G. Magistrelli *et al.*, “Rapid, simple and high yield production of recombinant proteins in mammalian cells using a versatile episomal system,” *Protein Expr Purif*, vol. 72, no. 2, pp. 209–216, Aug. 2010, doi: 10.1016/j.pep.2010.04.007.
[111] J. Garcia and M. Ahmed, “Single Nucleotide Polymorphisms and Treatment of Inflammatory Conditions,” Feb. 10, 2022 Accessed: Jul. 22, 2022. [Online]. Available: https://patentscope.wipo.int/search/en/detail.jsf?docId=WO2022032135&docAn=US2021045005
[112] U. Ravn *et al.*, “By-passing in vitro screening—next generation sequencing technologies applied to antibody display and in silico candidate selection,” *Nucleic Acids Res*, vol. 38, no. 21, p. e193, Nov. 2010, doi: 10.1093/nar/gkq789.
[113] N. Fischer *et al.*, “Exploiting light chains for the scalable generation and platform purification of native human bispecific IgG,” *Nat Commun*, vol. 6, no. 1, p. 6113, May 2015, doi: 10.1038/ncomms7113.
[114] M. Gasparrini *et al.*, “Molecular insights into the interaction between human nicotinamide phosphoribosyltransferase and Toll-like receptor 4,” *Journal of Biological Chemistry*, vol. 298, no. 3, p. 101669, Mar. 2022, doi: 10.1016/j.jbc.2022.101669.
[115] S. Torretta *et al.*, “The Cytokine Nicotinamide Phosphoribosyltransferase (eNAMPT; PBEF; Visfatin) Acts as a Natural Antagonist of C-C Chemokine Receptor Type 5 (CCR5),” *Cells*, vol. 9, no. 2, Art. no. 2, Feb. 2020, doi: 10.3390/cells9020496.
[116] A. Managò *et al.*, “Extracellular nicotinate phosphoribosyltransferase binds Toll like receptor 4 and mediates inflammation,” *Nature Communications*, vol. 10, no. 1, Art. no. 1, Sep. 2019, doi: 10.1038/s41467-019-12055-2.
[117] M. R. Yun, J. M. Seo, and H. Y. Park, “Visfatin contributes to the differentiation of monocytes into macrophages through the differential regulation of inflammatory cytokines in THP-1 cells,” *Cellular Signalling*, vol. 26, no. 4, Art. no. 4, Apr. 2014, doi: 10.1016/j.cellsig.2013.12.010.
[118] H.-J. Park *et al.*, “Visfatin promotes cell and tumor growth by upregulating Notch1 in breast cancer,” *Oncotarget*, vol. 5, no. 13, Art. no. 13, Jul. 2014, doi: 10.18632/oncotarget.2086.
[119] Z. Gholinejad *et al.*, “Extracellular NAMPT/Visfatin induces proliferation through ERK1/2 and AKT and inhibits apoptosis in breast cancer cells,” *Peptides*, vol. 92, pp. 9–15, Jun. 2017, doi: 10.1016/j.peptides.2017.04.007.
[120] A. C. Hung *et al.*, “Extracellular Visfatin-Promoted Malignant Behavior in Breast Cancer Is Mediated Through c-Abl and STAT3 Activation,” *Clinical Cancer Research*, vol. 22, no. 17, pp. 4478–4490, Sep. 2016, doi: 10.1158/1078-0432.CCR-15-2704.
[121] S. C. Taylor, L. K. Rosselli-Murai, B. Crobeddu, and I. Plante, “A critical path to producing high quality, reproducible data from quantitative western blot experiments,” *Sci Rep*, vol. 12, no. 1, p. 17599, Oct. 2022, doi: 10.1038/s41598-022-22294-x.
[122] L. Pillai-Kastoori, A. R. Schutz-Geschwender, and J. A. Harford, “A systematic approach to quantitative Western blot analysis,” *Analytical Biochemistry*, vol. 593, p. 113608, Mar. 2020, doi: 10.1016/j.ab.2020.113608.

[123] D. M. O'Hara *et al.*, "Ligand Binding Assays in the 21st Century Laboratory: Recommendations for Characterization and Supply of Critical Reagents," *AAPS J*, vol. 14, no. 2, pp. 316–328, Mar. 2012, doi: 10.1208/s12248-012-9334-9.
[124] L. A. A. de Jong, D. R. A. Uges, J. P. Franke, and R. Bischoff, "Receptor–ligand binding assays: Technologies and Applications," *Journal of Chromatography B*, vol. 829, no. 1–2, pp. 1–25, Dec. 2005, doi: 10.1016/j.jchromb.2005.10.002.
[125] C. Zhang *et al.*, "ATF4 is directly recruited by TLR4 signaling and positively regulates TLR4-trigged cytokine production in human monocytes," *Cell Mol Immunol*, vol. 10, no. 1, pp. 84–94, Jan. 2013, doi: 10.1038/cmi.2012.57.
[126] S. T. Patel *et al.*, "A novel role for the adipokine visfatin/pre-B cell colony-enhancing factor 1 in prostate carcinogenesis," *Peptides*, vol. 31, no. 1, pp. 51–57, Jan. 2010, doi: 10.1016/j.peptides.2009.10.001.
[127] K. Behrouzfar, M. Alaee, M. Nourbakhsh, Z. Gholinejad, and A. Golestani, "Extracellular NAMPT/visfatin causes p53 deacetylation via NAD production and SIRT1 activation in breast cancer cells," *Cell Biochem Funct*, vol. 35, no. 6, pp. 327–333, Aug. 2017, doi: 10.1002/cbf.3279.
[128] Y.-F. Chiang, H.-Y. Chen, K.-C. Huang, P.-H. Lin, and S.-M. Hsia, "Dietary Antioxidant Trans-Cinnamaldehyde Reduced Visfatin-Induced Breast Cancer Progression: In Vivo and In Vitro Study," *Antioxidants*, vol. 8, no. 12, p. 625, Dec. 2019, doi: 10.3390/antiox8120625.
[129] S.-R. Kim *et al.*, "Visfatin promotes angiogenesis by activation of extracellular signal-regulated kinase 1/2," *Biochem. Biophys. Res. Commun.*, vol. 357, no. 1, pp. 150–156, May 2007, doi: 10.1016/j.bbrc.2007.03.105.
[130] R. Adya, B. K. Tan, A. Punn, J. Chen, and H. S. Randeva, "Visfatin induces human endothelial VEGF and MMP-2/9 production via MAPK and PI3K/Akt signalling pathways: novel insights into visfatin-induced angiogenesis," *Cardiovascular Research*, vol. 78, no. 2, Art. no. 2, May 2008, doi: 10.1093/cvr/cvm111.
[131] J. Xiao *et al.*, "Involvement of dimethylarginine dimethylaminohydrolase-2 in visfatin-enhanced angiogenic function of endothelial cells," *Diabetes Metab. Res. Rev.*, vol. 25, no. 3, pp. 242–249, Mar. 2009, doi: 10.1002/dmrr.939.
[132] A. Dakroub *et al.*, "Visfatin: An emerging adipocytokine bridging the gap in the evolution of cardiovascular diseases," *Journal Cellular Physiology*, vol. 236, no. 9, pp. 6282–6296, Sep. 2021, doi: 10.1002/jcp.30345.
[133] S.-R. Kim *et al.*, "Upregulation of thromboxane synthase mediates visfatin-induced interleukin-8 expression and angiogenic activity in endothelial cells," *Biochemical and Biophysical Research Communications*, vol. 418, no. 4, pp. 662–668, Feb. 2012, doi: 10.1016/j.bbrc.2012.01.072.
[134] J.-Y. Kim *et al.*, "Visfatin through STAT3 activation enhances IL-6 expression that promotes endothelial angiogenesis," *Biochimica et Biophysica Acta (BBA) - Molecular Cell Research*, vol. 1793, no. 11, pp. 1759–1767, Nov. 2009, doi: 10.1016/j.bbamcr.2009.09.006.
[135] C. Miethe, M. Zamora, L. Torres, K. G. Raign, C. J. Groll, and R. S. Price, "Characterizing the differential physiological effects of adipocytokines visfatin and resistin in liver cancer cells," *Hormone Molecular Biology and Clinical Investigation*, vol. 38, no. 2, May 2019, doi: 10.1515/hmbci-2018-0068.
[136] Wang, "Visfatin/PBEF/Nampt induces EMMPRIN and MMP-9 production in macrophages via the NAMPT-MAPK (p38, ERK1/2)-NF-κB signaling pathway," *Int J Mol Med*, vol. 27, no. 4, Apr. 2011, doi: 10.3892/ijmm.2011.621.
[137] B. Li *et al.*, "Visfatin Destabilizes Atherosclerotic Plaques in Apolipoprotein E–Deficient Mice," *PLoS ONE*, vol. 11, no. 2, p. e0148273, Feb. 2016, doi: 10.1371/journal.pone.0148273.
[138] R. Adya, B. K. Tan, J. Chen, and H. S. Randeva, "Nuclear Factor-κB Induction by Visfatin in Human Vascular Endothelial Cells," *Diabetes Care*, vol. 31, no. 4, pp. 758–760, Apr. 2008, doi: 10.2337/dc07-1544.

[139] G. Wang *et al.*, “Visfatin Triggers the Cell Motility of Non-Small Cell Lung Cancer via Up-Regulation of Matrix Metalloproteinases,” *Basic Clin. Pharmacol. Toxicol.*, vol. 119, no. 6, pp. 548–554, Dec. 2016, doi: 10.1111/bcpt.12623.
[140] B. L. Sun *et al.*, “Role of secreted extracellular nicotinamide phosphoribosyltransferase (eNAMPT) in prostate cancer progression: Novel biomarker and therapeutic target,” *EBioMedicine*, vol. 61, p. 103059, Nov. 2020, doi: 10.1016/j.ebiom.2020.103059.
[141] J.-S. Kim *et al.*, “Colon-Targeted eNAMPT-Specific Peptide Systems for Treatment of DSS-Induced Acute and Chronic Colitis in Mouse,” *Antioxidants*, vol. 11, no. 12, p. 2376, Nov. 2022, doi: 10.3390/antiox11122376.
[142] J. G. N. Garcia, “Compositions and methods for treating pulmonary arterial hypertension,” WO2018191747A1, Oct. 18, 2018 Accessed: Jul. 15, 2022. [Online]. Available: https://patents.google.com/patent/WO2018191747A1/en
[143] A. N. Garcia *et al.*, “Involvement of eNAMPT/TLR4 signaling in murine radiation pneumonitis: protection by eNAMPT neutralization,” *Translational Research*, p. S1931524421001419, Jun. 2021, doi: 10.1016/j.trsl.2021.06.002.